Imperial College London
Department of Civil and Environmental Engineering

Flow Estimation and Fault Diagnosis for Automatic Control Valves in Water Supply Networks

Jiramate Changklom

Submitted in part fulfilment of the requirements for the degree of
Doctor of Philosophy in Civil and Environmental Engineering of
Imperial College London, August 2018

Acknowledgements

I would like to thank the sponsor of my research, The Royal Thai Government. I would like to thank my supervisor, Dr Ivan Stoianov for supporting me throughout. I would like to thank Cla-Val for providing laboratory resources and accommodation during the whole period of the experiments. I would like to thank my colleagues for all the useful technical guidance, in particular, Edo Abraham and Filippo Pecci. I would like to thank Titinun Suannun for endless emotional support. I would like to thank my parents for financial support and encouragement.

Finally, I would like to thank all friends for keeping me sane.

Declaration of Originality

I declare that all work in this thesis is my own. Any referenced work is credited.

Copyright Declaration

Abstract

Dynamic adaptability of water supply networks (WSNs) in terms of connectivity and hydraulic conditions is essential for their operation as there are increasing demands on serviceability (leakage, water quality, incident management and fire flow), resilience and cost efficiency. A common approach to achieve multiple control functions throughout networks is to employ automatic control valves (ACVs).

Advances in low-powered electronics and micro-actuators enable a wide range of novel control methods in WSNs, including the flow-based pressure control (or flow modulation control (FM)). The implementation of FM schemes has been steadily increasing as it has a major advantage of a closed-loop (feedback) control by utilising measurements to define the flow-pressure control profile. The performance of the FM scheme relies on continuous and accurate flow measurements. Hence, to achieve robust control in WSNs, high-level reliability of the control solution is required. Herein, two methods for the reliable operation of ACVs are investigated, namely (i) Flow estimation and (ii) Fault detection and diagnosis.

A novel flow estimation method for diaphragm-actuated globe valves has been developed and experimentally investigated. The method utilises three pressure measurements, namely the valve inlet pressure, the valve outlet pressure and the control chamber pressure (*the 3P flow estimation method*). The method relies upon the accurate computation of the valve stem position, the measured pressure differential across the valve and the flow coefficients of the valve *(C_v, K_v)*. The developed valve stem position estimation model results in multiple solutions. Advances in signal processing are combined with a machine learning technique (support vector machine) to distinguish the correct solution. The proposed 3P method is compared with a method which uses sensor measurements of the valve stem position (*the 2P&Pos method*), and its performance validated against measurements from an electromagnetic flowmeter. The uncertainty bounds of the flow estimation methods are also derived.

For fault diagnosis, methods for early fault detection and diagnosis (FDD) are investigated. Potential faults are categorised, and residuals and feature variables are defined to detect a fault and diagnose its likely cause. Experimental data have been generated and utilised from controlled laboratory conditions, from an operational network and also from a numerical simulation. The performance of the proposed schemes has been validated.

Contents

List of Tables

List of Figures

Chapter 1

Introduction

1.1 Motivation and objectives

Dynamic pressure management is an increasingly important operational practice in water supply networks (WSNs), as it enables a significant reduction in leakage, demand and pipe failures. Dynamic pressure management includes pump control, valve control or their combined implementation (Thornton, 2003) in order to continuously maintain optimal and quasi-steady state operational conditions. Hydraulically actuated globe-diaphragm control valves are commonly used for dynamic pressure management.

WSNs in the UK have been divided into sectors called district metered areas (DMAs) to manage leakage and pressure. In some regions, the DMA is referred to as pressure managed areas (PMAs). Pressure in DMAs is regulated by pressure control valves installed at the entry point(s) of a sector. A novel concept of dynamically adaptive WSNs has been pioneered at the Infrasense Labs, Imperial College London (Wright et al., 2014). It includes the periodic aggregation and segregation of DMAs as electro-hydraulically actuated inlet control valves and boundary control valves are installed and remotely operated. The main advantages of the dynamically adaptive WSNs are to increase the network's resilience to failure and to reduce frictional energy losses as the network redundancy is increased. As a consequence, the number of control valves in WSNs is expected to increase significantly in order to facilitate a greater controllability of

water distribution systems both in terms of topological connectivity and dynamic pressure management, both of which could significantly increase the resilience of networks and improve incident management. The scalable adoption and operation of this process would depend on many factors, one of which is the reliability and redundancy in the estimation of key control variables such as flow.

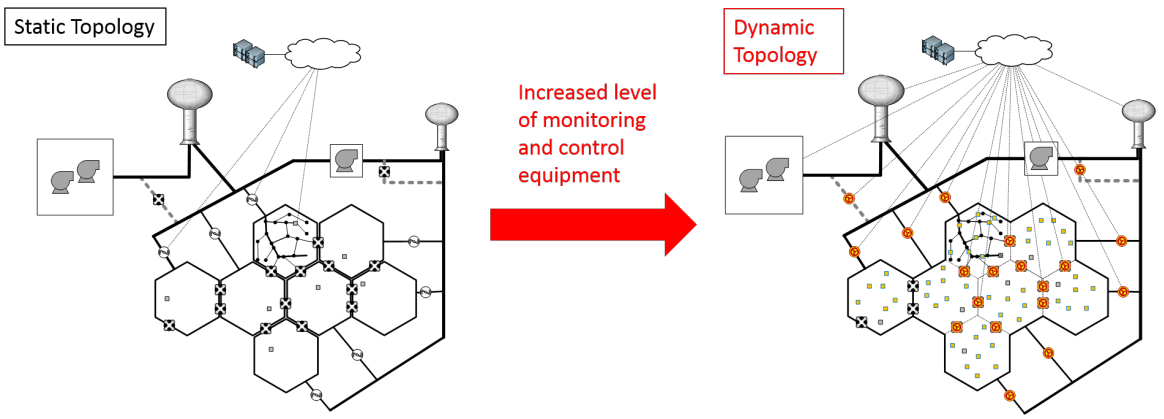

Figure 1.1: Sectorisation of WSNs with dynamically adaptive topology; Inlet boundary valves and kept shut boundary valves (on the left) are replaced with automatic control valves (on the right).

A control valve is a hydro-mechanical device consisting of a globe-diaphragm valve with a hydraulic control loop. The control loop consists of a fixed orifice, needle valves, and a pilot valve. An opening of the control valve is hydraulically regulated by the control loop. The control valve is essentially a variable size orifice that modifies energy losses based on specific hydraulic requirements. Examples of control valves are pressure reducing valves (PRVs), pressure sustaining valves and flow control valves. PRV is the most commonly used control valve in WSNs. It maintains a set pressure downstream of the valve (P_{out}) irrespective of the variations in the upstream pressure (P_{up}) and flow (as far as $P_{up} > P_{out}$).

Advances in low power electronics and micro-actuators have transformed the control of PRVs. Electro-hydraulically actuated PRVs, which require little power and DC voltage supply, enable a wide range of novel control methods in WSNs. Pressure control methods include a time-based modulation, a flow-based modulation (FM) and a node-based modulation. The FM method of control is becoming increasingly popular (Vicente et al., 2016) as it offers a major advantage of feedback control based on the hydraulic conditions within the network (Prescott et al.,

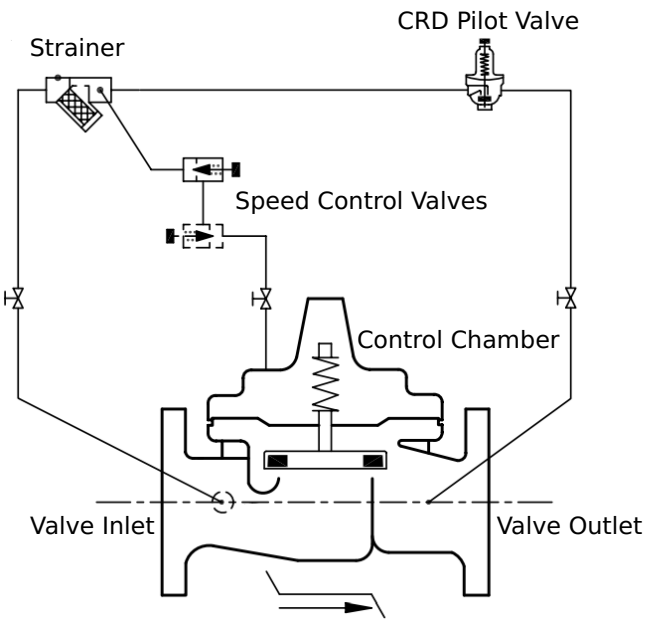

Figure 1.2: A diagram of Pressure Reducing Valve (PRV) (adapted from www.cla-val.co.uk)

2003, Ulanicki et al., 2000, Wright et al., 2015). The FM control method adjusts the outlet pressure setting of the valve according to locally measured flow in order to maintain a constant minimum allowable pressure at a hydraulically critical point in a network. Consequently, it requires reliable and accurate flow data from a locally installed flow meter. In the case of a flow-meter failure (a zero flow reading), the pilot valve setting enters a fail-safe mode of fixed outlet pressure. This pressure target could be significantly higher than the operating pressure under flow modulation. This fail-safe model might result in significant pressure variations that cause pipe failures and discolouration. With a redundant flow estimation, the FM control mode can be maintained within an error bound of the FM curve. Therefore, a redundant flow estimation from surrogate measurements can maintain the reliability of the FM control scheme. A modelling framework for the robust flow estimation problem is needed to achieve this operational goal.

Furthermore, the same mathematical modelling framework, which combines physical-based and data-driven modelling methods, could be extended and utilised for the fault detection and diagnosis of the pressure control valves. Since control valves operate under a wide range of flow conditions, faults can have a major impact on the operation of a water supply network. Undesirable hydraulic conditions that include high average pressure and pressure variations or

hydraulic instabilities may also result in pipe failures and discolouration. If faults (abrupt, incipient or intermittent) are detected in real time, the undesirable impact on the hydraulic conditions in a network can be promptly rectified. In addition, the continuous fault detection aims to enable condition-based maintenance in order to replace the current practice of inefficient and costly time-based maintenance, which becomes cost prohibitive as the number of automatic control valves increases. The fault diagnosis aims to both detect and identify the source of faults in order to trigger the condition-based maintenance.

Currently, there is no robust modelling framework for globe-diaphragm automatic control valves that can accommodate both the redundant flow estimation and continuous fault detection and diagnosis. A rigorous investigation of robust modelling approaches for automatic control valves is needed to fulfil these research and operational gaps. The proposed modelling framework also investigates the applicability of various monitoring strategies both in terms of acquired variables (e.g. pressure and stem position) and their sampling (data acquisition) rates.

1.2 Research aim and objectives

The overall goal of this research programme is to formulate, develop and validate an integral modelling framework for both the redundant flow estimation, and continuous fault detection and diagnosis of diaphragm-actuated globe control valves. This modelling framework combines physical-based modelling with data-driven methods. It also provides a unified design environment for both the control algorithms and components of the considered control valves. The flow estimation will utilise either three pressure sensors (3P) or two pressure sensors and a stem position sensor (2P&Pos).

The specific objectives for the flow estimation problem include:

1. Review the principles of fluid control in hydraulic circuitry, types of control valves and control valves modelling approaches. Investigate and perform simulation for existing models of control valves.

2. Develop and investigate control valve models for the robust flow estimation problem.

3. Acquire experimental data to train, validate and test the developed models.

4. Analyse methods to identify the robust (and correct) solution of the flow estimation problem.

5. Design and execute an experimental programme to validate the performance of the developed flow estimation method in an operational water supply network.

The specific objectives for the fault detection and diagnosis problem include:

1. Review common faults and failure modes of control valves, and investigate experimental data describing these faults.

2. Carry out simulations of faults by applying the developed flow estimation model.

3. Design and execute an experimental programme to support the development of the fault detection and diagnosis method. Replicate common failure modes through these experiments.

4. Develop a fault detection and diagnosis method by engineering and extracting fault features from continuous signal measurements. Signals during fault conditions will be compared with signals during normal conditions for the feature engineering process.

5. Validate and test the developed fault detection and diagnosis method.

Chapter 2

Literature Review

This chapter aims to highlight the importance of automatic control valves (ACVs) modelling in WSNs, established throughout previous studies. An ACV is a key device for pressure management, which is an efficient scheme with multiple benefits for WSNs. Development of technologies on ACVs, allowing them to perform advanced control modes, is discussed in this chapter. With flexible control functions, the number of ACVs is expected to increase significantly. Hence, the review illustrates a research gap in accurate ACV modelling to improve engineering reliability, which can be demonstrated through tasks such as flow estimation and fault detection and diagnosis.

2.1 Pressure management in WSNs

In the last decade, pressure management (PM) in WSNs has been steadily implemented in many systems around the world. PM schemes explore the balance between low operating pressure that reduces leakage and minimum operating pressure that is sufficient to meet serviceability requirements (e.g. in the UK, these are imposed by the Water Services Regulation Authority (or Ofwat)). PM is critical to the operation of water supply networks as it is directly related to reduction of leakage, probability of pipe failures and consumption rates (Lambert, 2000). To quantify those benefits, operators and researchers have been trying to determine a relationship

between pressure and reduction rate, burst rate and consumption. The progress is summarised as follows:

- **Leakage Reduction**: Since it is difficult to derive an analytical relationship between pressure and leakage rate, some research established relationships for particular case studies with different physical factors; Lambert (2000) and Thornton (2003) suggested that the most practical relationship between leakage rate and pressure is a power relationship relating a change in leakage rate to a change in overall pressure, $L_0/L_1 = (P_0/P_1)^{N1}$. Analyses of over 100 field tests on sections of WSNs found that $N1$ is between 0.5 and 1.5 (Thornton and Lambert, 2005). Later studies by Lambert and Fantozzi (2009) illustrated that $N1$ depends on the rigidity and flexibility of pipes and $N1$ may vary for the same leak orifice. van Zyl and Clayton (2007) found that leakage types and pipe materials are important factors to be included in the relationship. Greyvenstein and van Zyl (2007) and Guo et al. (2013) modelled the relationship between leakage from cracked pipes and pressure with other physical parameters such as crack shape, crack size and pipe depth.

- **Burst Rate Reduction**: Some statistics-based methods and data-driven models suggest that pressure is related to bursts frequency. Shirzad et al. (2014) found that average hydraulic pressure is an essential parameter to predict burst rate. Thornton and Lambert (2005) used the same exponent formula to the leakage for burst rate and the power factor is now $N2$. $N2$ was found to be in a wide range between 0.5 and 6.5. It was suggested that different factors such as pipe materials and ageing significantly affect N2. Different hydraulic assumptions and pipe materials are categorised to find a more precise N2 (Lambert and Thornton, 2012)

- **Reduction in Demand**: It is believed that pressure reduction can also reduce consumption because some types of water consumption are pressure-dependent. Using the previous power relation ($N3$ in this case), Lambert and Fantozzi (2009), found a statistically meaningful value of $N3$ for only outdoor consumption rate to be 0.4-0.5. This suggests that outdoor consumption rate is pressure-dependent. In addition, a reduction in water consumption was also observed in Wright et al. (2015), where an experimental

programme was carried out to validate advanced pressure reduction schemes.

Both field test data and experimental data have been analysed to emphasise the importance of pressure management. Over the last decade, practical approaches in PM have been developed. While many advanced control schemes have been established, they depend on the performance and reliability, which requires condition-based maintenance, of pressure control valves.

2.2 Automatic control valves in WSNs

Figure 2.1 shows the application of automatic control valves in WSNs.

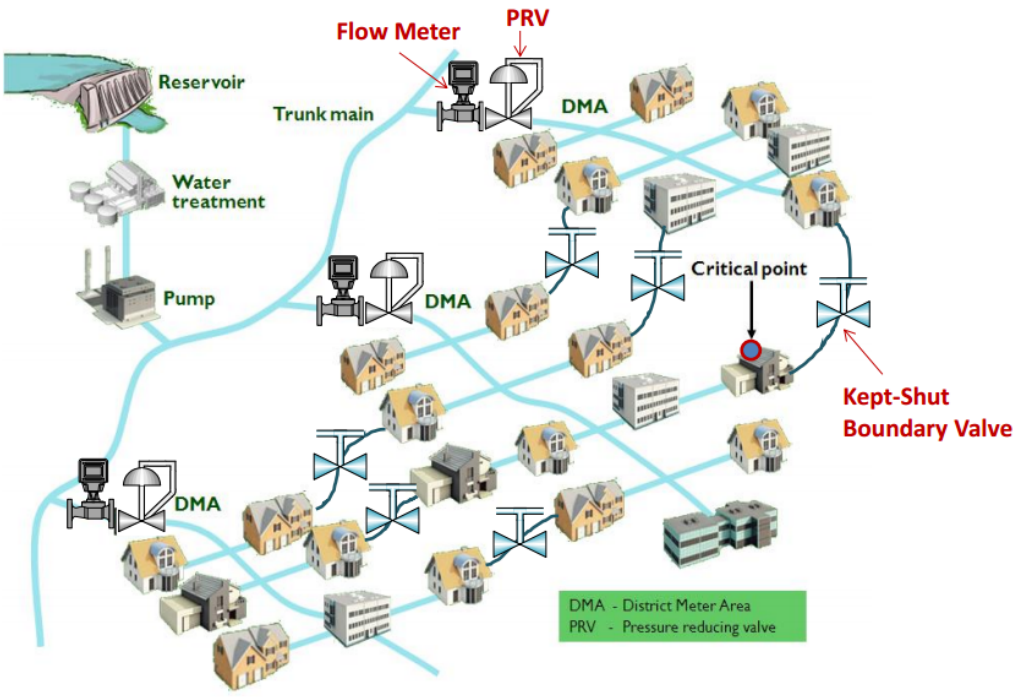

Figure 2.1: A depiction of pressure control valves in WSNs

In WSNs, automatic control valves are commonly used to control pressure or/and flow. The most commonly used automatic control valves in WSNs are the pressure reducing valves (PRVs). PRVs in WSNs are categorised into 4 types depending on their outlet pressure regime, control mechanism and actuation (Ratcliffe, 1986). The four types are:

1. Constant outlet pressure, spring-loaded diaphragm valve.

2. Constant outlet pressure, controlled by a spring-loaded external pilot valve. This is also known as fixed-outlet pressure PRV.

3. Flow-modulated outlet pressure, controlled by a spring-loaded and diaphragm-modulated external pilot valve.

4. Flow-modulated outlet pressure, controlled by an electronically actuated pilot valve.

Type 3 and type 4 PRVs are a modification of type 2 PRV with a pilot valve with an extra chamber, and with an electronic pilot valve, respectively. Automatic control valves controlled by an external pilot valve (Type 2, 3 and 4) are popular among the water industry because they require lower force to operate the control setting compared to type 1. This research focuses mainly on the diaphragm-actuated globe valve with a pilot valve, which is mostly used for automatic control valves in WSNs (PRV type 2, 3 and 4).

2.2.1 Principle of operation of hydraulically-actuated diaphragm-operated globe valves as various types of automatic control valves

An automatic control valve consists of two parts, the valve body and the hydraulic control circuit (control loop). The type of automatic control valves depends on the hydraulic control circuits. Herein, the principles of operation of each automatic control valve type are described. Most automatic control valves in WSNs are pressure control valves.

Pressure reducing valve (PRV)

In WSNs, the PRV is the most widely used control valve as it is necessary to control the pressure at the inlet(s) of a DMA or PMA. Sometimes, pressure control valves generally refer to pressure reducing valves. Figure 2.2 shows a typical fixed outlet PRV used in WSNs. The pilot valve, the strainer and the speed control valve are labelled. The PRV consists of the

main valve body, A, and the hydraulic control loop. The working principles of a PRV in WSNs are similar to those of a pressure regulator used for other fluid systems. In a typical pressure regulator (single stage), the outlet pressure acting on a large diaphragm is balanced with the handle initial displacement; therefore, a large force is required to adjust the setting of the valve. To control pressure in WSNs, a valve with an external pilot valve is more commonly used as a PRV because a small force is sufficient to adjust the control setting, i.e set pressure in this case. This small force is the operating force for adjustment, and not to be confused with the actuating force due to pressure. The controllability with small adjustment force on the pilot valve facilitates the advanced PRV with flow-modulated control or time-modulated control. The pilot valve, B, provides a control setting of the PRV. It can be adjusted to give a different fixed outlet pressure. The speed control valve (SCV), C, provides different discharge characteristics for the pilot system based on the flow direction. Consequently, the oscillatory movement of the valve stem is minimised. A strainer, D, blocks unwanted particles in the control loop. It also provides a fixed orifice to reduce the pressure in the control chamber that controls the opening of the main valve to facilitate the discharge from the control chamber.

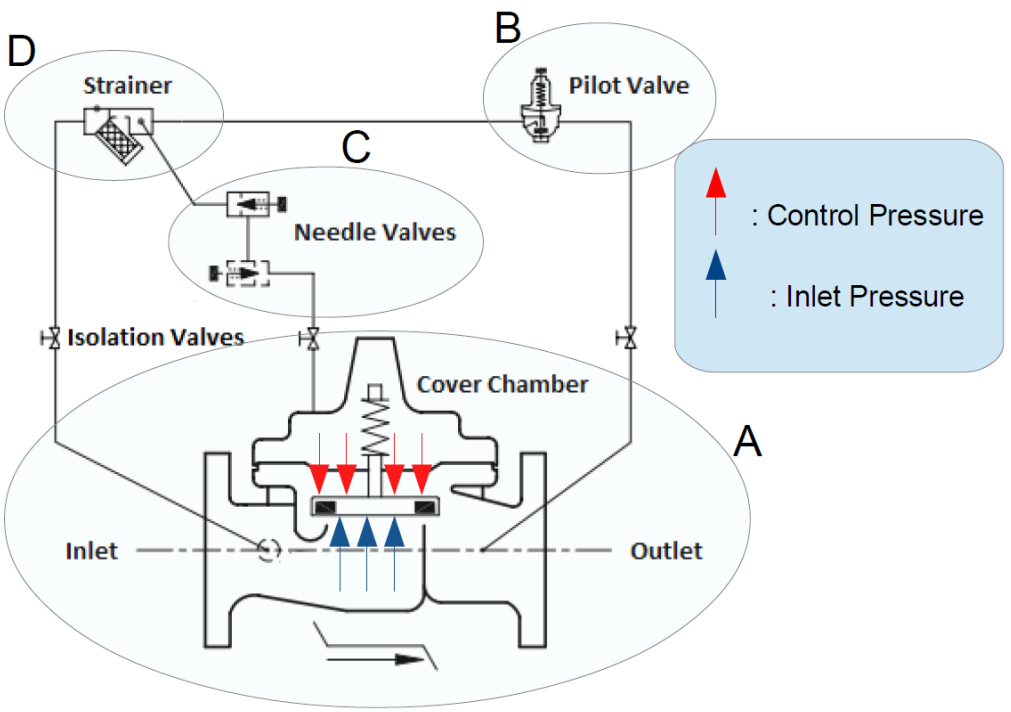

Figure 2.2: A PRV used in a water supply network (Modified from www.cla-val.co.uk)

The PRV automatically reduces a higher inlet pressure to a steady lower downstream pressure

regardless of changing flow rate and varying inlet pressure. The outlet pressure (downstream pressure) can be accurately controlled to a pre-determined limit. To control the outlet pressure of the PRV, the outlet pressure is balanced with the pilot valve setting at the pilot valve diaphragm. The pilot valve setting hence provides the set pressure (pre-determined pressure).

If the outlet pressure drops below the pressure setting of the control pilot, the pilot valve seat will open wider. As a consequence, water from the control chamber is discharged into the control loop, causing the main valve to lift up. When the main valve lifts up, it generates a lower pressure loss at the main valve; therefore, the outlet pressure increases until the pressure is balanced with the pilot valve setting again. On the other hand, if the outlet pressure exceeds the set pressure, the pilot valve will close and recharge water into the control chamber. As a result, the main valve will close, causing a higher pressure loss and hence a lower outlet pressure.

The equilibrium of the PRV is reached when the pilot valve spring force is balanced with the outlet pressure. The outlet pressure can be controlled by simply adjusting the pilot valve spring initial position. To achieve a more advanced control over the PRV, electronic controllers to control the pilot valve have been developed. Those controllers receive flow signals, or time signals in order to adjust the pilot valve setting. Furthermore, the pilot valve itself has been developed to be more robust and to be compatible with those electronic controllers.

Pressure sustaining valve (PSV)

The PSV maintains constant upstream pressure to the valve (valve inlet pressure). In WSNs, a PSV is installed in a line between two zones, typically between a zone with high pressure (upper zone) and a zone with low pressure but high demand. The PSV helps to prevent all the flows from going to the area of heavy demand (the so-called “robbing"). The PSV can also be implemented to be a pressure relief valve. A diagram of a PSV is shown in Figure 2.3a.

The control circuit of the PSV is similar to that of the PRV, except that the PSV has a pilot valve with an extra chamber above the diaphragm that bypasses the inlet. Therefore, the pilot

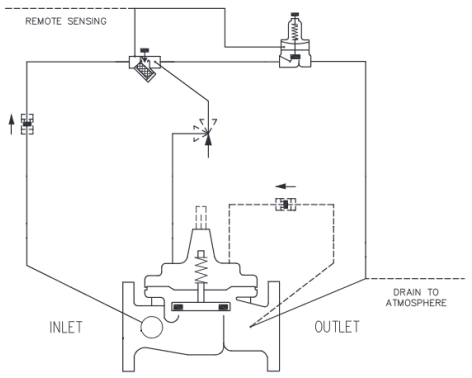

(a) A diagram of pressure sustainig valve

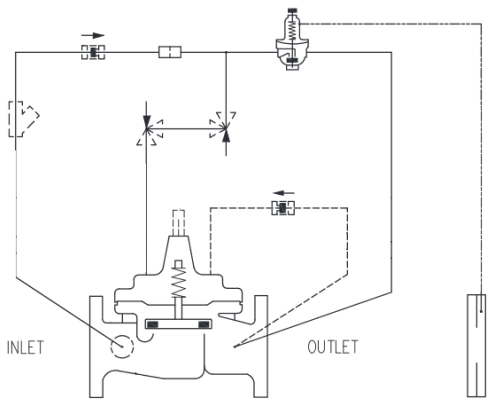

(b) A diagram of flow control valve

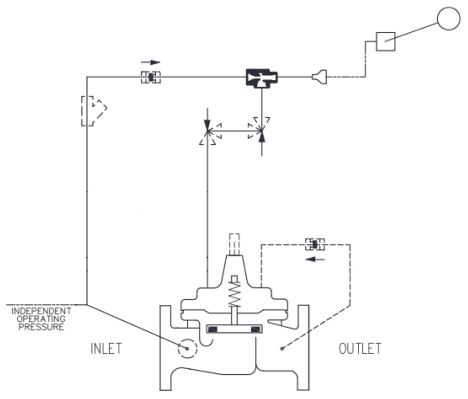

(c) A diagram of level control valve

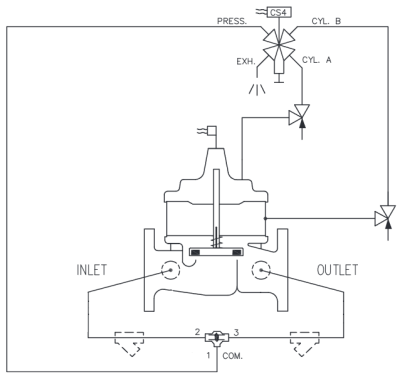

(d) A diagram of booster pump control valve

Figure 2.3: Diagrams of four commonly used ACVs, which are pressure sustaining valve, flow control valve, level control valve and booster pump control valve (taken with permission from www.cla-val.com)

valve acts on the valve upstream to provide a feedback control. If the valve inlet pressure is higher than the set pressure, the pilot valve will open and discharge water from the control chamber. Consequently, the main valve opens to provide less pressure loss and reduces upstream pressure. If the valve inlet pressure is lower than the set pressure, the pilot valve will close and recharge water into the control chamber. The main valve closes to provide more pressure loss and to increase upstream pressure.

For pressure relief application, a PSV is installed next to a pump and in a separate branch to the main supply because a pump start-up or shutdown can generate a pressure surge to networks. In this case, the SCV of the PSV is set such that the valve opens fast and closes slowly. With this setting, the PSV can dissipate an excessive pressure surge to a safe location

and does not generate an additional surge.

Flow control valve (FCV)

The FCV controls flow rate to a system such as a reservoir or industrial users. A diagram of an FCV is shown in Figure 2.3b. The FCV maintains the flow rate to a pre-set value, regardless of pressure. Upstream and/or downstream pressure will be affected by the valve response to control flow. An FCV control circuit is also similar to the PRV, except that the pilot valve has an extra chamber connected to an orifice plate further downstream to the valve. This extra chamber is above the pilot valve diaphragm. Therefore, the opening of the pilot valve will respond to the differential between the valve outlet pressure and the pressure after the orifice. If flow rate is below the set value, differential pressure will decrease, causing the pilot valve to open. Water is then drawn from the control chamber. The valve will open up to allow more flow. On the other hand, if flow rate is above the set value, differential pressure will increase, causing the pilot valve to close. Water is then pushed into the control chamber. The valve will close to restrict flow.

Level control valve

Level control application normally serves to control the level of water in a reservoir. A diagram of a level control valve is shown in Figure 2.3c. The control circuit consists of a variable orifice that connects the valve control chamber to the atmosphere. A floating object is connected to the orifice mechanically. Any changes in water level will affect the floating object, the orifice size and subsequently the opening of the control valve.

Booster pump control valve

This control valve aims to eliminate surges generated by the switch-on/off of the pump. A diagram of a booster pump control valve is shown in Figure 2.3d. The valve is installed next to the pump. The control circuit consists of a four-way solenoid valve connected to the control

chamber and two-speed control valves. The solenoid valve can either allow flow into the control chamber or discharge flow from the control chamber. The solenoid valve receives signals directly from the pump switching signal. The pump starts against a closed valve. When the pump is signalled to turn on, the solenoid valve is energised and the valve begins to open slowly. When the pump is signalled to shut off, the solenoid valve is de-energised and the valve begins to close slowly.

2.3 Technologies on pressure control valves

Various forms of controllability are challenging for pressure control valves, especially the PRV. Advanced control techniques have been developed, allowing a variety of pressure control schemes in WSNs. The techniques are usually referred to as Advanced Pressure Control (APC) methods (Charalambous and Kanellopoulou, 2010, Vicente et al., 2016). Electronic pilot valves have been developed to facilitate the control methods. The introduction of electronic controllers to control the PRV pilot valve has been a significant advance in PM. This section highlights APC methods and technologies on electronic pilot valves.

2.3.1 Advanced Pressure Control (APC) methods

- **Fixed Outlet mode** The most common control of a PRV is the fixed outlet PRV because it provides a constant outlet pressure which is adequate to manage pressure for each DMA, and it is low cost. This mode is achieved by keeping a constant setting of the pilot valve and does not require additional controllers.

- **Time Modulated mode (TM)** A timer device is connected to the pilot valve. The device can change the pilot valve setting at different times of a day. It is suitable for a repetitive demand profile that changes on a daily basis. Some researchers have been developing algorithms to improve the performance of TM (Ulanicki et al., 2000, 2008).

- **Flow Modulated mode (FM)** The FM controller is a real-time controller and is a

closed-loop controller. It sets the targeted pressure according to the demand profile. Hence, it requires signals from a flowmeter. The FM scheme keeps high set pressure during high demand to satisfy the minimum pressure requirement at the critical point (the area that receives the lowest supplied pressure) and minimises pressure during low demand to minimise leakage. Although the FM controller is much more complex than the TM, it provides a more flexible control solution. Normally, users can set the flow modulation curve (flow-pressure profile), and then the controller will adjust the pilot valve setting according to the curve. The curve is sometimes called the control profile. The FM scheme has been widely used in the last decade (Charalambous and Kanellopoulou, 2010, Wyeth and Chalk, 2012).There are two main focuses in the literature on FM. The first type is to find control algorithms to be associated with the FM controller, as, for example, in Li et al. (2010), whereas the second focuses on how to generate the flow modulation curve, such that it minimises overall leakage in the system (Abdelmeguid and Ulanicki, 2010).

- **Remote Node Based Modulated mode (RNM)** The RMN controller is a data-based real-time controller. It receives measurement signals from a specific node and determines the pilot valve setting. The specific node is usually a critical point. Some companies have already provided this type of controllers in the market. Beyond the real-time control based on the data received from the node, machine learning techniques have been implemented to update the control profile (Burrows, 2010, HWM, 2011). Many control algorithms based on the feedback from the critical point have been proposed. (Campisano et al., 2012, Creaco and Franchini, 2013, Nicolini and Zovatto, 2009, Sanz et al., 2012).

- **Position Control mode** Instead of controlling the pilot valve setting, which can control the set pressure, the position controller controls the opening of the main valve straight away. The exact valve stem position is then achieved. The controller is designed such that the exact head loss coefficient (has a relationship with the valve opening) can be obtained. This allows other parameters to be controlled, i.e. head loss coefficients and flow in some cases, in addition to the outlet pressure. It has already been used for a specific task such as tank filling. (Cla-Val, 2015)

2.3.2 Pilot Valve Innovation

Various types of pilot valves have been developed to work together with advanced controllers. Due to the limited power supply in WSNs, it is challenging to develop pilot valves with low-energy actuators. The advanced pilot valves adjust the setting following the command signal from the controllers and consume low energy to actuate.

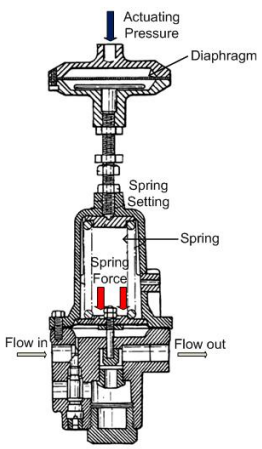

(a) Wessex pilot valve

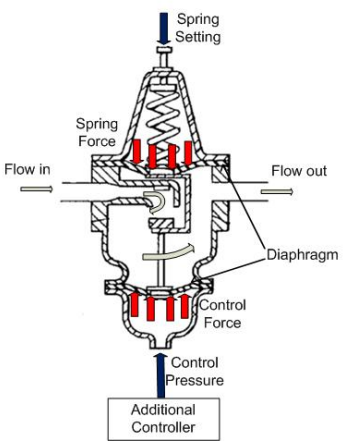

(b) Technolog pilot valve

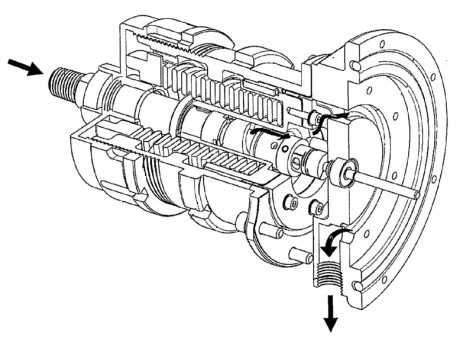

(c) i2O pilot valve

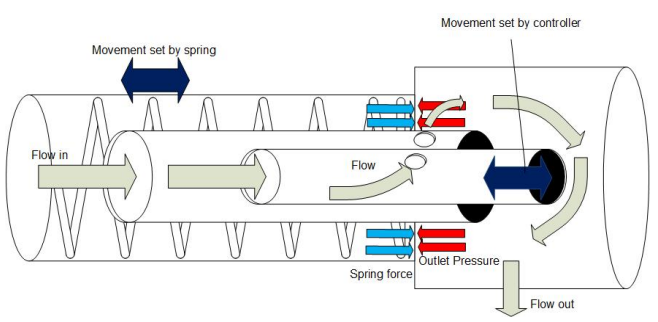

(d) i2O pilot valve (diagram)

Figure 2.4: Examples of pilot valves for ACVs. All of these pilots are compatible with APCs.

- **Wessex Pilot Valve** Sotoudeh (2000) from Wessex Electronics Consultants Limited, GB, has introduced an additional control to a conventional pilot valve (Figure 2.4a). This pilot valve enables a dual setting for the outlet pressure. The pilot valve comprises 2 chambers: a control chamber and a bias chamber. A bias chamber containing a hydraulic actuator (diaphragm) is added on top of the control chamber. A disc-shaped flange is placed inside the bias chamber below the diaphragm, and it is connected to the spring stopper using the push rod. When the actuator is actuated, the flange hits the bottom of the bias chamber, causing the high setting pressure of the pilot valve. On the other hand, if the actuator is not actuated, the flange moves upward until it hits the diaphragm, causing the low-pressure setting of the pilot valve. Typically, a three-way ball valve, connected to the inlet part, is placed above the bias chamber. It can be switched on and off to activate the high-set pressure or low-set pressure.

- **Technolog Pilot Valve** Yonnet (2004) from Technolog Limited, GB, has proposed a dual chamber pilot valve (Figure 2.4b). A bias chamber is added to the bottom of a conventional pilot valve. A diaphragm is used to separate the bias chamber and the control chamber. The spring on top of the pilot valve is attached to another diaphragm at the top of the control chamber. The upper diaphragm is manually adjusted and the lower diaphragm moves according to the control pressure. A control fluid is fed into the bottom chamber. By controlling the pressure of the control fluid, different settings of the pilot valve can be achieved. This task requires an additional controller.

- **i2O Pilot Valve** Heron and Burrows (2010) from i2O Water Limited, GB, has invented a more complicated motor-driven pilot valve (Figure 2.4c and 2.4d). The pilot valve is designed such that it can communicate directly with a multi-function controller. It comprises two valve members. These two members have a cylindrical shape; one is inside the other one. The two cylinders allow telescopic motions. There is a flow aperture between the members. The aperture size can be determined by the relative movement of the members. The first valve member is attached to a spring. The spring position can be changed by screwing the outside cap, which will then move the first member. The second member is attached to the adjuster, which is connected to a motor. The motor receives

controlling signals from the additional controller. The i2O additional controller shows an advance in technology in a way that it receives wireless signals from many points in networks. For example, information on inlet flow, local inlet and outlet pressure, and pressure at different points in networks can be received. The controller contains a CPU, memory units and clock, which will allow different forms of controllers, including TM, FM, RNM at the same time.

2.4 Control valve modelling

Two main control valve modelling approaches are considered: (i) the control valve modelling for network simulation and (ii) the detailed control valve modelling for understanding valve behaviours and valve simulation. While the first focuses on a successful incorporation of a control valve model into a network model, the latter focuses on representing the control valve principles by accurate equations. A detailed control valve model tends to be complex and difficult to solve together with network equations. Reviewing both approaches helps to understand control valve behaviours. The gained insight can also facilitate future work when network simulation can include complex equations representing devices.

2.4.1 Control valves modelling for network models

Water supply networks can be modelled into network topology to perform network analysis. The topology consists of nodes and edges. Each node represents a number of properties lumped together and edges represent pipe connection. To analyse a network model, equations representing the mass balance principle and the energy conservation principle are formulated throughout the network. For extended period simulation, a steady-state solution is obtained at each time point.

A network normally consists of a number of control valves, especially PRVs. It is challenging to incorporate PRVs into network models because PRV operation affects the flow rate and

energy equations. The challenge of including PRV in network calculations leads to several research studies on PRV modelling for network simulation. The PRV models can be status-based (Chandrashekar, 1980, Collins, 1980, Gessler, 1981, Jeppson, 1976, Jeppson and Davis, 1976, Zarghamee, 1971) or physical-based (Khezzar et al., 1999, 2001, Piller and Bremond, 2001, Piller and van Zyl, 2014, Rossman, 2000, Simpson, 1999, Todini and Pilati, 1988).

2.4.2 Control valve modelling for accurate representation of valve behaviours

Automatic control valves, especially the pressure control valves, are key devices for pressure management. Detailed mathematical modelling of control valves allows for an investigation of behaviours. Equations governing hydraulic components tend to include non-linear terms, which sometimes make classical mathematical analysis impossible. Accurate models are necessary for computer simulation which will help to gain an understanding of the way the control valve behaves.

Models can also provide a benefit in condition monitoring as they can be matched with actual operating performance and hence deduce conditions and faults (if occur). Potential faults and existing faults can be inserted and simulated. Further applications of models include key variable estimation and design problem support. Prescott and Ulanicki (2003) proposed 4 PRV dynamic models:

- **The Full Phenomenological Model (FPM)** The FPM was derived from fundamental principles. The variables are shown in Figure 2.5. Where h is pressure (hydraulic head), and q is flow at different parts of the valve. Various C_v characteristics at different valve parts are, C_{vm} for the main valve, C_{vfo} for the fixed orifice, C_{vp} for the pilot valve and C_{vnv} for the needle valve (speed control valve). The model consists of equations of motion of the main valve and of the pilot valve, the head loss equations at different parts of the hydraulic circuits, the continuity at the T-junction and a relationship between the control chamber discharge flow and the control chamber volume. Variable f_m and f_p represent damping force

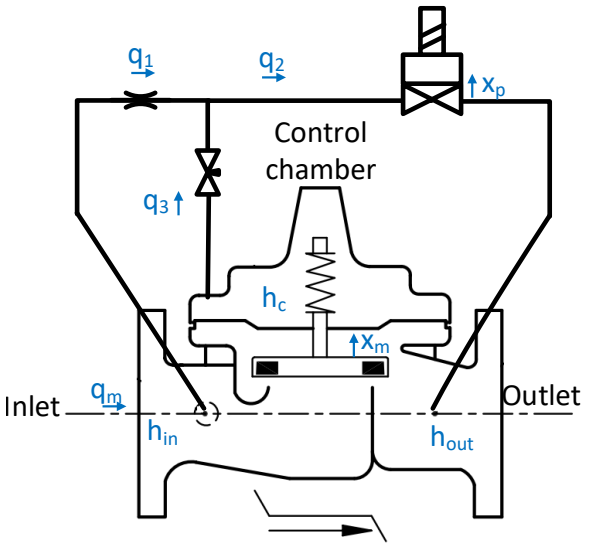

Figure 2.5: A PRV with labelled variables

constants. The Prescott's FPM is:

$$
\begin{gathered}
q_3 = f(x_m)\dot{x}_m \\
m_m\ddot{x}_m = \rho g\left(h_{in}a_1 + h_{out}(a_2 - a_1) - h_c a_2\right) - m_m g - f_m\dot{x}_m + \frac{\rho q_m^2}{a_1} \\
m_p\ddot{x}_p = \rho g h_t a_d - k_{pspr}(x_{sp} - x_p) - m_p g - f_p\dot{x}_p \\
q_1 = C_{vfo}\sqrt{|h_{in} - h_t|}\cdot sgn(h_{in} - h_t) \\
q_2 = C_{vp}(x_p)\sqrt{|h_t - h_{out}|}\cdot sgn(h_t - h_{out}) \\
q_m = C_{vm}(x_m)\sqrt{|h_{in} - h_{out}|}\cdot sgn(h_{in} - h_{out}) \\
q_3 = C_{vnv}\sqrt{|h_c - h_t|}\cdot sgn(h_c - h_t) \\
q_1 + q_3 = q_2
\end{gathered}
\quad , \tag{2.1}
$$

- **The Simplified Phenomenological Model (SPM)** The SPM is obtained by making a quasi-static approximation on the FPM. Consequently, the friction and the inertia terms in equations of motion are neglected. In the hydraulic control circuit, there is no inverse flow

except for control chamber discharge. The SPM is:

$$
\begin{gathered}
q_3 = f(x_m)\dot{x}_m \\
\rho g\left(h_{in}a_1 + h_{out}(a_2 - a_1) - h_c a_2\right) - m_m g + \frac{\rho q_m^2}{a_1} = 0 \\
\rho g h_t a_d - k_{pspr}(x_{sp} - x_p) - m_p g = 0 \\
q_1 = C_{vfo}\sqrt{h_{in} - h_t} \\
q_2 = C_{vp}(x_p)\sqrt{h_t - h_{out}} \\
q_m = C_{vm}(x_m)\sqrt{h_{in} - h_{out}} \\
q_3 = C_{vnv}(x_p)\sqrt{|h_c - h_t|}\cdot sgn(h_c - h_t) \\
q_1 + q_3 = q_2
\end{gathered}
\tag{2.2}
$$

- **The Behavioural Model (BM):** The BM is derived from observation. It is observed that the main valve opens and closes following the exponential function of time. Therefore, the derivative of the main valve position must be proportional to the difference between the desired outlet pressure (h_{set}), and the current outlet pressure (h_{out}). The BM is:

$$
\begin{gathered}
\dot{x}_m = \begin{cases} \alpha_{open}(h_{set} - h_{out}), & \dot{x}_m \geq 0. \\ \alpha_{close}(h_{set} - h_{out}), & \dot{x}_m < 0. \end{cases} \\
q_m = C_{vm}(x_m)\sqrt{h_{in} - h_{out}}
\end{gathered}
\tag{2.3}
$$

- **The Linear Model (LM)** The LM was proposed in Prescott and Ulanicki (2001) by applying a linearlisation method onto the FPM. The model is a system model which includes small parts of networks upstream and downstream to the valve. The small network consists

of an upstream reservoir, an upstream pipe and a downstream pipe. The LM is:

$$\begin{aligned} \dot{x} &= f(\mathbf{x}, \mathbf{y}, \mathbf{u}) \\ g(\mathbf{x}, \mathbf{y}, \mathbf{u}) &= 0 \end{aligned} \tag{2.4}$$

where x is the vector of differentiable variables, y is the vector of algebraic variables, and u is the vector of control inputs, given by:

$$\begin{aligned} \mathbf{x} &= (x_m, y_m, x_p, y_p, Q_1, Q_2)^T \\ \mathbf{y} &= (q_m, q_1, q_2, q_3, h_t, h_c, h_{in}, h_{out}, H_{end})^T \\ \mathbf{u} &= (H_{res}, P_{sp})^T, \end{aligned} \tag{2.5}$$

where all variables have their usual meaning, y_m and y_p are the first derivative of x_m, x_p, respectively. Variables with capital letters represent flows and heads in the small network connected to the PRV, a reservoir and an opened end; H_{res} and H_{end} are the head of the reservoir and of the opened end, respectively; Q_1 and Q_2 are the incoming/outgoing flows. $Q_1 = Q_2$ because of the leakage factor. The first order Taylor's series expansion around the steady state is:

$$\begin{aligned} \dot{x} + \delta\dot{x} &\approx f(\mathbf{x}, \mathbf{y}, \mathbf{u}) + f_x\delta\mathbf{x} + f_y\delta\mathbf{y} + f_u\delta\mathbf{u} \\ 0 &\approx g(\mathbf{x}, \mathbf{y}, \mathbf{u}) + g_x\delta\mathbf{x} + g_y\delta\mathbf{y} + g_u\delta\mathbf{u}. \end{aligned} \tag{2.6}$$

From Equations 2.4 and Equations 2.6, the expression is deduced to be:

$$\delta\dot{x} \approx A\delta\mathbf{x} + B\delta\mathbf{u}, \tag{2.7}$$

where: $A = (f_x - f_y g_y^{-1} g_x)$, and $B = (f_u - f_y g_y^{-1} g_u)$. This equation evolves around its steady state determined by u.

The models have been simulated under various dynamic hydraulic conditions and have been performed in Prescott and Ulanicki (2001) and Prescott and Ulanicki (2003). The FPM was assumed to show the same behaviour as the SPM. The result shows that simulation using the SPM provides similar results to that using the BM. The LM was shown to be similar but did lack some of the dynamic features set by the speed control valve. Further analysis of these models is performed in Chapter 4.

2.5 Control valve model applications: Flow estimation and Fault diagnosis

This section will detail two applications from accurate control valve models– Flow estimation and fault diagnosis.

2.5.1 Flow estimation

The flow (or flow rate) is a key control variable in WSNs. Especially for an implementation of the FM scheme, flow measurement is required to set up a pressure control profile. Flow measurement devices, the flowmeters, may be classified into three general methods depending on how the flow information is extracted (Hardy et al., 1999):

1. **Inferential flowmeters:** An inferential flowmeter normally infers flow rate from other sources of information such as a differential pressure measurement, the inertia force or the generated vorticity. According to the major principles of inference, the inferential flowmeter can utilise the following data:

    - **Differential pressure:** A differential pressure flowmeter contains a flow restriction in different forms. Flow can be calculated from the differential pressure and its discharge coefficient. Examples of this type of devices are the orifice plate, the venturi and the nozzle.

- **Drag force:** A drag-force flowmeter utilises inertia force of flow to determine the flow rate. Examples of this type are a rotameter, a drag body flowmeter and a spring-loaded variable aperture.
- **Vorticity:** A vortex flowmeter consists of a bluff body in the path of the fluid. Disturbances in the flow called vortices are created after the fluid passes through the body. The flow rate is proportional to the frequency at which these vortices alternate sides.

2. **Direct-measurement flowmeters:** The direct-measurement flowmeters directly measure volumetric flow rate or velocity. Examples of this type are the turbine flowmeter and the positive-displacement flowmeter.

3. **Energy-additive flowmeters:** The energy-additive flowmeters impart additional energy such as thermal, acoustic and electric into the system. Effects of those forms of energy, which change according to flow, are monitored.

Since a control valve introduces a constriction on the fluid path, it has a potential to work as a differential pressure flowmeter. The flow rate and the differential pressure are related by a discharge coefficient, C_v. The discharge coefficient, C_v, depends on the restricted cross-sectional area of the flow path.

There has been some research focusing on the possibility of using a control valve for flow measurement. In Atmanand and Konnur (1996), a conventional flow control loop, which consists of a control valve, a flowmeter and a controller is replaced with a new control loop with only a valve and a new controller. In this case, the new controller receives a differential pressure signal and a valve position signal. After flow calculation, the controller provides control signals to the control valve to control flow. Leephakpreeda (2003) proposed a similar method for using signals from a control valve to measure flow for flow control purposes. But a neural network model is used instead of using the C_v characteristic relationship to calculate flow. Choi (2012) developed a flow control system using a butterfly control valve. The analysis includes the characteristics of mechanical frictions and the dynamic interaction between the valve disk and the controller

to improve the accuracy of the control system.

2.5.2 Fault detection and diagnosis for automatic control valve

A fault can be defined as a deviation of characteristic properties of a system from a normal condition. A fault may initiate a malfunction, which is a temporary interruption of a system to perform a function, or a failure, which is a permanent interruption. The failures and malfunctions can be avoided if faults are detected and specified early; therefore, fault detection and diagnosis (FDD) (or fault detection and isolation (FDI)) are vital for technical processes.

In the field of process engineering, FDD is an important problem. As a process plant is usually complex and consists of a large number of process variables, it is difficult for human operators. Most of the body of literature for FDD is in the field of process engineering, but the scope of work can be applied for automatic control valves. A series of work by Venkatasubramanian (Venkatasubramanian, 2003, Venkatasubramanian et al., 2003a,b) provides an intensive review for FDD. Various diagnostic methods are categorised and compared. The authors classified diagnostic methods based on a prior knowledge into three categories: model-based methods, qualitative model-based methods and process history-based methods. The model-based methods generate residuals sensitive to faults using models and measurements. The qualitative mode-based methods utilise the fundamental understanding of a process to infer fault features, whereas the process history-based methods infer fault features from past experience.

In general, a diagnostic system is a series of transformation as shown in Figure 2.6. The measurement space contains physical measurements without a prior knowledge. The prior knowledge about a fault is utilised to obtain a feature, which is a function of measurement. To design a feature, the chosen features have to be indicative of faults and hence are directly related to fault symptoms. Isermann (2011) defined a symptom as a deviation of the feature from its nominal values when a fault exists. In other words, when a fault presents itself, the symptom should present itself, too, if a good feature is designed. Symptoms can be generated from analytical knowledge to produce quantifiable, analytical information (characteristic values) or from heuristic knowledge to produce qualitative information from human experiences.

There are two common methods to obtain features: feature selection and feature extraction. Feature selection selects some measurements and processes them as a feature, whereas feature extraction includes transformation of measurements to obtain some characteristic values (feature variables).

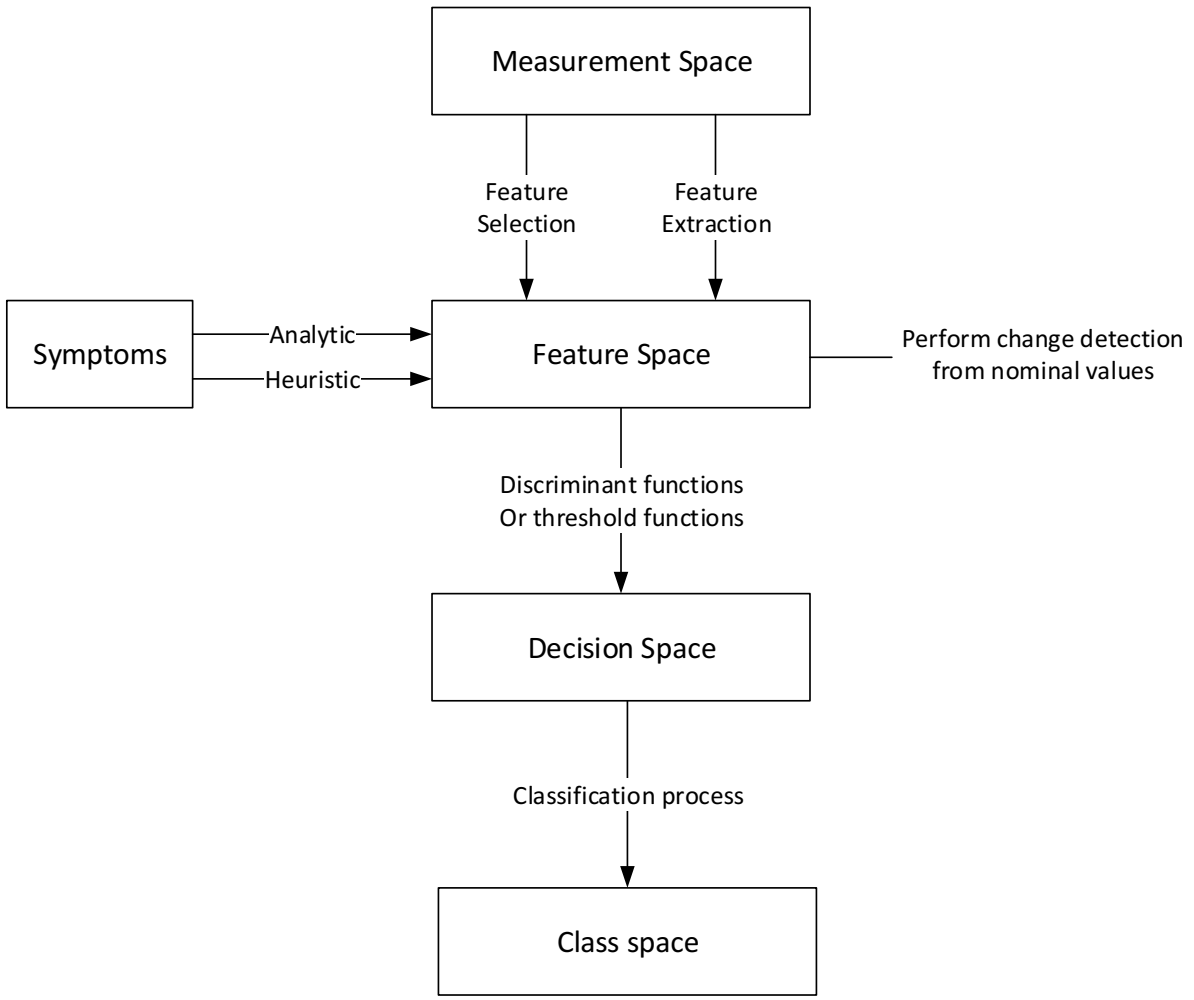

Figure 2.6: A series of transformation for a diagnostic system adapted from Isermann (2011), Venkatasubramanian (2003)

After obtaining feature variables in a feature space, those variables are then transformed to a decision space to aid the decision of diagnosis whether a high enough severity level of fault exists. The transformation function can be, for example, discriminant functions or threshold functions. Finally, the class space is obtained from a final transformation from the decision space through a classification process. Sometimes, the decision space and the class space can be the same space.

Automatic control valves (ACVs) in WSNs control pressure or flow, making it a particular value in certain conditions depending on the setting. The control setting is called "the control profile". It is straightforward to perform fault detection because faults are recognised when ACVs fail to regulate pressure/flow following the control profile. A more challenging task is to diagnose faults from how the measurement deviates from the control profile.

To perform FDD, data indicative of faults are required. The data can be obtained through a real operation of ACVs in networks, through laboratory experiments or through computer simulation. An accurate mathematical model of ACVs is essential to generating data indicative of faults from computer simulation, especially a mechanistic model. A mechanistic model has an advantage that it is derived from physics principles; therefore, faults can be added as changes of physical variables.

2.6 Conclusions

Pressure management in WSNs is increasingly implemented worldwide owing to its many benefits and significance. Automatic control valves (ACVs) are key devices for pressure management and also other control tasks in WSNs. The literature has shown a variety of developmental processes of ACVs on valve types, control algorithms and pilot valves. Innovations in ACVs have made it possible to achieve flexibility on different tasks of ACVs.

As ACVs are becoming an important part of WSNs, there have been some technological advancements in ACV models. The models are mostly a part of network models for network simulation purposes. Studying these models allows ones to better understand ACV operations. However, developing accurate ACV models for flow estimation and fault diagnosis remains a daunting task. Only a few researchers focus on accurate ACV models, which are vital for tasks such as flow estimation and fault diagnosis. Those tasks could be important as they will significantly increase the engineering reliability on ACVs. The ability to deliver reliable ACVs is necessary for current control schemes and could also be useful for more sophisticated control schemes in the future.

Some researchers have already proposed methods of flow estimation through a valve (Atmanand and Konnur, 1996, Choi, 2012, Leephakpreeda, 2003). Those methods rely on a measurement of the flow constriction opening, e.g. a valve stem position for a globe valve or an angle for a butterfly valve. For a diaphragm-actuated globe valve, installation process of sensors to measure the valve stem position requires operational disruption, which might not be feasible at some locations. Therefore, there is a research gap on developing a valve model that can estimate the flow constriction opening, specifically the valve stem position for the diaphragm-actuated globe valve, from surrogate measurement (pressures). The valve stem position estimate will be further used for flow estimation. As the model that supports flow estimation application requires accurate relationships between parameters and variables, it will also support fault detection and diagnosis.

Currently, there is no robust modelling framework for globe-diaphragm pressure control valves that can accommodate both a redundant flow estimation and continuous fault detection and diagnosis. A rigorous investigation of robust modelling approaches for pressure control valves is needed to fulfil these research and operational gaps. Here, the proposed modelling framework will also investigate the applicability of various monitoring strategies, both in terms of acquired variables (e.g. pressure and stem position) and their sampling rates (data acquisition).

Chapter 3

Experimental Programme

This chapter aims to outline experimental settings and procedures, which are necessary for ACV model development. There are three experimental sites (two laboratories and the “Field Lab”) throughout this research. Details of laboratory settings are described. Settings of measurement devices were prepared according to the “standard procedure" for valve C_v measurement (ANSI/ISAâĂŞ75.02.01âĂŞ2008).

3.1 Introduction

Experimental data are essential for the model development process. The data help to investigate the accuracy of existing models and derive data-driven models. Furthermore, continuous data help to monitor the condition of a system. Such data come from carefully designed experimental programmes. This section details the description of laboratories and experimental design to obtain data for different purposes. The main aims for this experimental programme are:

1. To investigate the accuracy of existing control valve models in the literature and to find the limitation of using the existing control models for flow estimation purposes.

2. To derive and validate a more accurate model for flow estimation.

3. To simulate fault conditions and to collect data indicative of faults.

Two experimental rigs have been used to obtain measurements throughout the research– the Imperial College London pipe rig and the Cla-Val HQ, Switzerland pipe rig. The experimental rig at Imperial College London was prepared for the set-up, the test procedures comply with the standard ANSI/ISA-75.02.01-2008, entitled Control Valve Capacity Test Procedures and the experimental rig at Cla-Val HQ already complies with the standard ANSI/ISA-75.02.01-2008.

According to ANSI/ISAâĂŞ75.02.01âĂŞ2008, the following measurements should be acquired:

1. Valve travel (stem position)
2. Upstream pressure ($P1$)
3. Differential pressure (ΔP) across the test section (shown as pressure taps)
4. Volumetric flow rate (Q) (measurement error not exceeding Âś 2 percent of actual value)
5. Fluid inlet temperature ($T1$) (measurement error not exceeding Âś 1 ÂřC [Âś 2 ÂřF])
6. Barometric pressure (measurement error not exceeding Âś 2 percent of actual value)
7. Physical description of test specimens (i.e., type of valve, flow direction, etc.)
8. Physical description of the test system and the test fluid
9. Any deviation from the provisions of this standard.

Figure 3.1 shows the experimental setting of ANSI/ISAâĂŞ75.02.01âĂŞ2008.

The only difference between the laboratory setting and the ANSI/ISAâĂŞ75.02.01âĂŞ2008 is that the fluid temperature and barometric pressure were not continuously measured. The fluid temperature was kept relatively constant throughout the recirculating pipe rig. The pressure transducers were gauge transducers and these were calibrated (zeroed) at the start of each experimental setting and cross-checked every day.

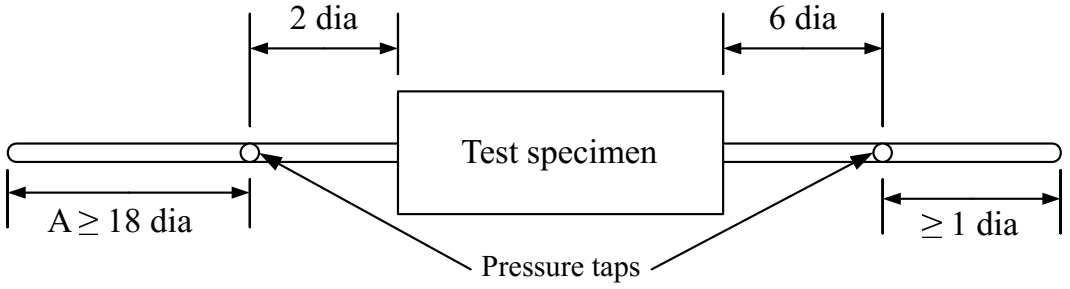

Figure 3.1: A measurement set-up as defined by ANSI/ISAâĂŞ75.02.01âĂŞ2008: “dia” in the diagram is the pipe diameter.

The data acquisition system continuously recorded valve inlet pressure, valve cover chamber pressure, valve outlet pressure, flow from a dedicated electromagnetic flowmeter, valve stem position (opening), “standard-defined" inlet pressure and “standard-defined" outlet pressure. According to ANSI/ISAâĂŞ75.02.01âĂŞ2008, the pressure sensors for measuring the differential pressure across the valve should be placed two (2x) times the nominal valve diameter upstream of the tested valve and six (6x) times the nominal valve diameter downstream of the valve. Such pressure measurements are labelled as “standard" or “standard-defined". However, the flow estimation process would utilise pressure measured at the inlet and outlet of the valve due to physical constraints in operational networks; therefore, the pressure at the inlet and outlet of the valve are measured to compare with the standard measurement. Figure 3.2 shows an experimental set-up diagram with the data acquisition system.

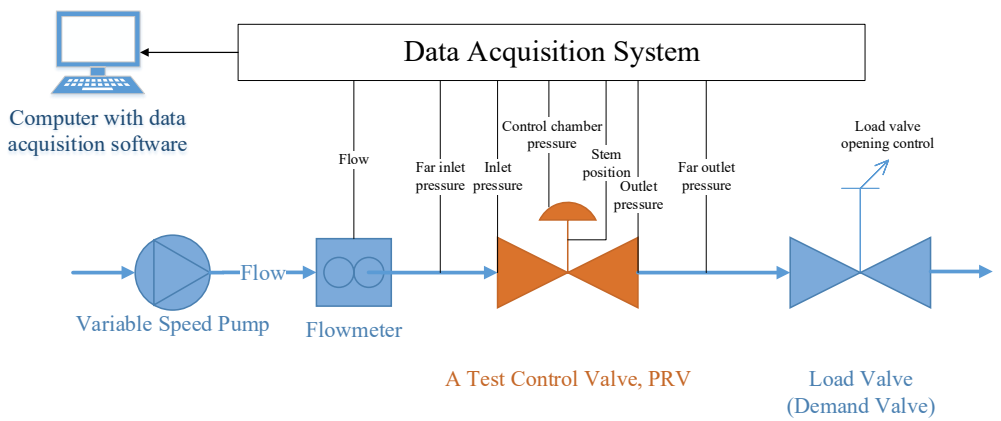

Figure 3.2: A laboratory set-up for the experimental programme

3.2 General description of the laboratories

This section describes the laboratory facilities used throughout this research. Two facilities include the Imperial College Laboratory (InfraSense pipe rig) and the Cla-Val Europe Laboratory.

3.2.1 General description of laboratory 1 (InfraSense pipe rig)

The pipe rig is located in the Hydrodynamics Laboratory, Department of Civil and Environmental Engineering, Imperial College London. The schematic of the rig is shown in Figure 3.3 The rig consists of the main elements as follows:

- **The pipe:** The pipe is 30m in length and 200mm Diameter Nominal (DN200). There is also a DN100 pipe connected parallel to the DN200 pipe downstream with a length of about 5m. It has an outside diameter of 219mm , inside diameter of 202mm , and the thickness of 8.5mm. The material is PVC, class C. According to the product description, the pressure rating is 9 bar or 92 mH2O.

- **The PRV:** The PRV acts as a main control valve in this system. The PRV model is Cla-Val GE DN100.

- **The PRV control panel:** The control elements (control loop) of the PRV were extended and put on the panel to facilitate the operation on different control modes.

- **The variable speed pump:** The pump is located upstream of the pipe rig. It provides inlet pressure to the PRV. The variable speed setting allows a range of inlet pressures. The pump model is Grundfos CRNE 64.

- **The downstream load valve:** The load valve creates different demands through the main control valve. The valve is electronic actuated motorised position control valve (Cla-Val CPC model). The CPC valve is controlled using a 4-20mA input signal.

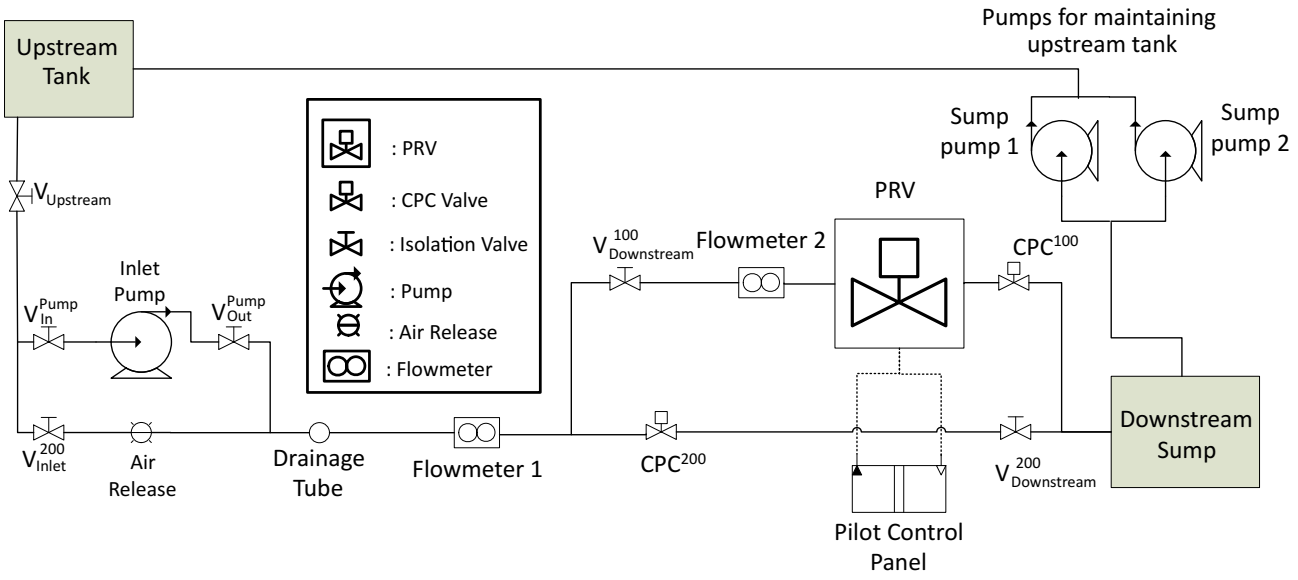

Figure 3.3: Overall InfraSense Pipe System Schematic at Imperial College London

- **The sump and the sump pumps:** There is a sump (a hollow space into which liquid drains) located downtream of the pipe rig and there are two pumps which suck water from the sump to fill the tank.

- **The tank:** The tank is located 3 floors above the ground (approximately 14m).

- **The flowmeters:** There are two electromagnetic flowmeters in the rig– at the DN100 pipe and DN200 pipe. The model is ABB ProcessMaster FEP500.

There are also other devices in the rig such as a few valves for partial isolation of the rig, an air release valve and a drainage tube. The outline of the overall pipeline system is shown in Figure 3.3. There are two ways to operate the system: gravity feed and pump feed. The gravity feed can provide the maximum pressure of 14 mH_2O, which is 1.4 bar and the pump feed can provide the maximum pressure of 66 mH_2O.

The pilot control panel shown in Figure 3.4 is used to operate the main control valve in this system. The control panel consists of a hydraulic control circuit that provides various control options. The control options are operated by opening/closing the small valves at the control panel (labelled as V in Figure 3.4) and the blue electronic box. Three control options are available at the current state of the control panel, as shown below:

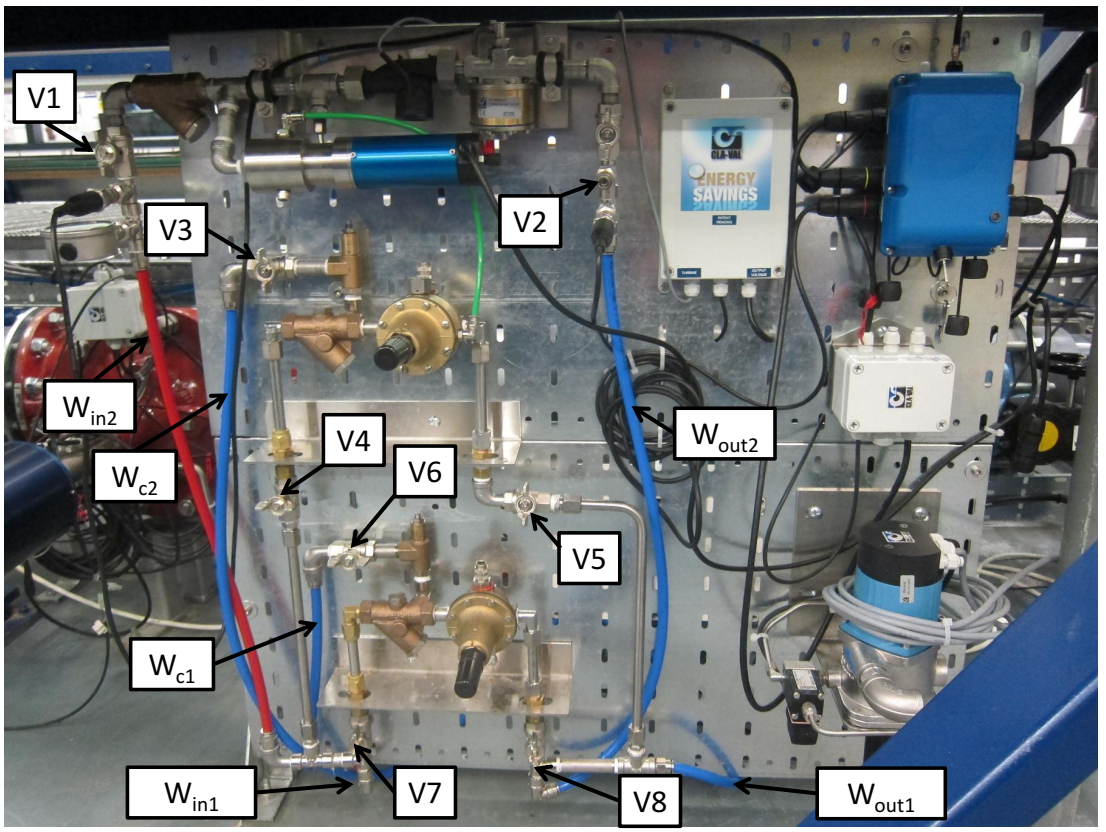

Figure 3.4: Picture of the control panel of the Imperial Rig

1. **The fixed outlet mode:** This control mode has a fixed setting of the CRD pilot valve, the outlet pressure of the PRV is kept relatively fixed regardless of the inlet pressure and flow.

2. **The flow modulation mode:** This control mode utilises an advanced CRD pilot valve, the pilot valve changes its setting according to the flow signal.

3. **The position control mode:** This control mode does not use any of the control circuits on the panel. The control chamber is connected to a motorised needle valve that can pressurise the control chamber to open or close.

3.2.2 General description of laboratory 2 (Cla-Val Europe)

The laboratory at Cla-Val HQ, Switzerland has four pipelines in parallel. The four pipelines have different diameters which are DN50, DN80, DN100 and DN150. As a result, four test valves can be put in the rig at the same time. The end of the four lines is connected to the tank which feeds the pump on the other side to complete the water circulation. The schematic diagram of Cla-Val laboratory is shown in Figure 3.5. The main elements of the rig are:

1. **The pipe:** The pipe material is steel. The pressure rating is much higher than the usual operational pressure.

2. **The pump:** The pump speed can be adjusted precisely up to a step of approximately 20 cmH_2O through a digital controller.

3. **The test valves:** A maximum of four test valves of different sizes can be put in the pipelines at the same time. For the scope of this research, the three test valves are Cla-Val DN80 NGE, Cla-Val DN100 GE and Cla-Val DN150 NGE. Those valves were set as fixed pressure PRVs. The stem position sensors were installed on each test valve.

4. **The load valves:** The load valve is a globe-diaphragm valve. The control chamber is bypassed to the valve outlet via the adjustable variable orifice. The opening of the load valve can be controlled precisely by turning the mechanical gear which will adjust the orifice size.

5. **The flowmeters:** The flowmeter is next to the pump with the DN150 pipe. The flowmeter is the ABB electromagnetic flowmeter, ABB ProcessMaster FEP500 with an accuracy of 0.2% of the measured flow.

To operate the rig, the isolation valves of pipelines that were not relevant to each experiment would be shut. The pump was switched on and adjusted to the preferred inlet pressure. The outlet pressure to a test valve was adjusted through the CRD pilot valve and the flow through each pipeline was adjusted through the load valve.

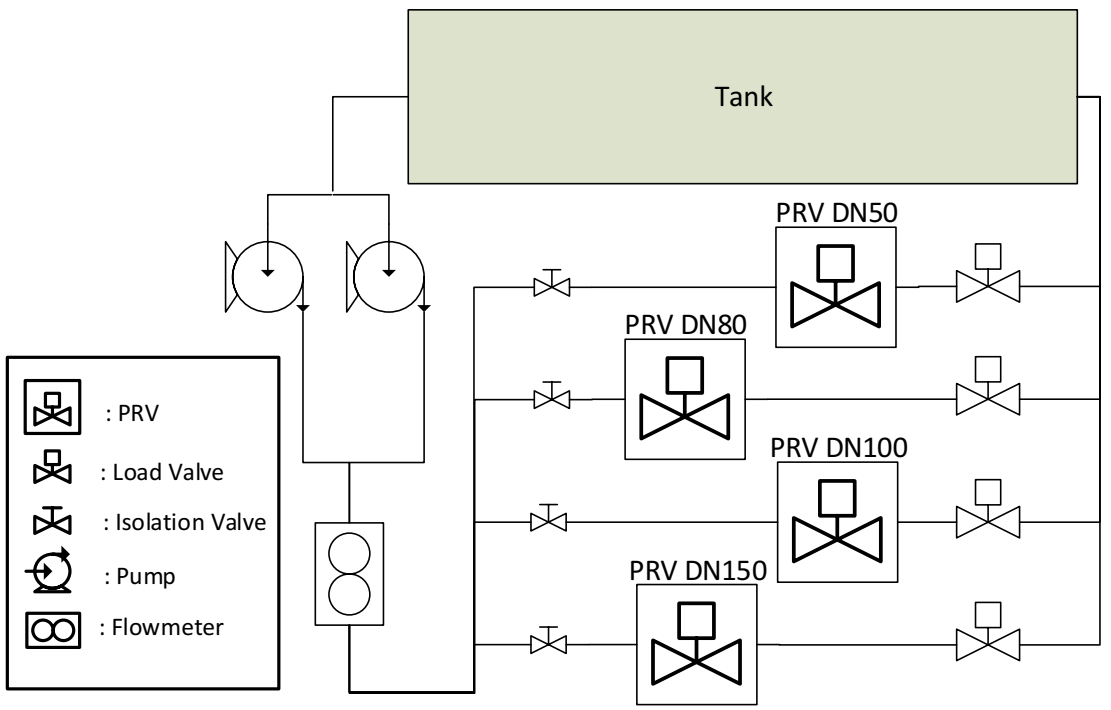

Figure 3.5: Overall Cla-Val Pipe System Schematic Representation at Cla-Val HQ, Switzerland

3.2.3 Data acquisition devices and software

The same set of data acquisition system has been used for the experiments carried out at both laboratories. The data acquisition system consists of:

1. **The software:** The software for data visualisation, analysis and storage is HBM Catman. Calibration of the sensors was also performed and saved into the sensor database of the software.

2. **The pressure sensors:** The pressure transducers are gauge transducers and they were calibrated (zeroed) at the start of each experimental programme and cross-checked every day. The accuracy was 0.1% full scale (20 bar).

3. **The valve stem position sensors:** The sensors are magnetostrictive linear position sensors (BTL6-E500-M0050-PF-S115). They have a repeatability of Âś0.002 % full scale (50mm stroke).

3.3 General description of the “Field Lab"

The “Field Lab” is part of an operational WSN which has approximately 10,000 customers and it is operated by Bristol Water, InfraSense Labs (Imperial College London) and Cla-Val (Wright et al., 2014, 2015). A schematic diagram of the “Field Lab" is shown in Figure 3.6. It contains three PMAs with three FM-based automatic control valves (ACVs) and two boundary control valves (BCVs). All these valves are diaphragm-actuated globe valves with specifically developed pilot control systems; for example, the BCVs allow stem position control in both directions based on the differential pressure. The FM control profiles for the ACVs are shown and include the “fail-safe" settings and error bounds in the FM curves. These bounds are derived from multiple factors such as the deadband of the pilot controller and valve, the hydraulic dynamics of the system and the hydraulic uncertainty associated with the management of pressure within the network close to the minimum regulatory requirement for serviceability.

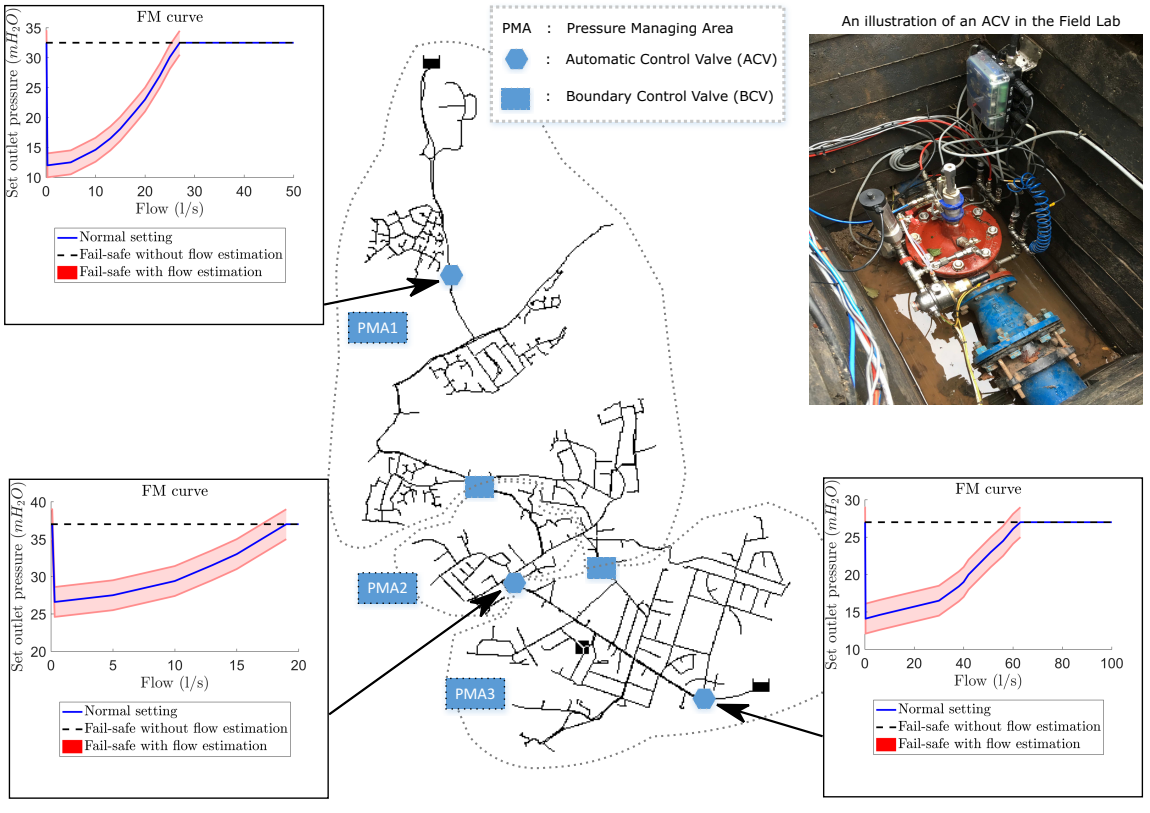

Figure 3.6: An operational network (the “Field Lab”) with three PMAs that utilise flow modulation for pressure control; A set of flow modulation curves for the automatic control valves is also included.

According to Figure 3.6, the top ACV is located at Stoke Lane, Bristol, the middle ACV is

located at Woodland Way, Bristol, and the bottom valve is located at Lodge Causeway, Bristol. Those valves will be referred to as Stoke Lane valve, Woodland Way valve and Lodge Causeway valve, respectively. In terms of valve sizes and types, the Stoke Lane valve is Cla-Val DN100 GE, the Woodland Way valve Cla-Val DN150 GE and Lodge Causeway valve Cla-Val DN100 GE. Throughout this thesis, the stoke Lane valve is referred to as SKL, the Woodland Way valve as WLW and the Lodge Causeway valve LCW. Each ACV is connected to an electromagnetic flow meter, which provides flow measurement for flow-modulated pressure control. An illustration of an ACV in the "Field Lab" is at top-right of Figure 3.6.

Each valve is equipped with three data acquisition devices described below:

1. **Cla-Val device:** This device aimed to collect data for the control purpose. The device is integrated with an electronic pilot valve which provides an advanced outlet pressure control such as flow-based modulation, time-based modulation or node-based modulation. The default mode is FM and the FM control profile can be set online through a website. It is also the only device that receives signals from the valve stem position sensor. It collects all of the 5 valve variables (h_{in}, h_c, h_{out}, x_m and q) at a sampling rate of 1 samples/minute.

2. **Infrasense device:** The Infrasense device was installed to collect high sampling rate data (128 samples/s) at key locations in the "Field Lab", especially at ACVs and BCVs. It aimed to provide a real-time monitoring system of the "Field Lab". This device measures 3 variables which are h_{in}, h_{out} and q.

3. **Inflowmatix device:** Similar to the Infrasense device, the Inflowmatix device was installed for monitoring purpose widely across in the "Field Lab". This device took the high sampling rate measurement of 128 samples/s but store data of 1 samples/s with additional maximum and minimum readings. This device is relatively easy to install where it is required. For flow estimation purposes, this device is used to measure high-resolution control chamber pressure,h_c to improve estimation resolution and outlet pressure h_{out} for synchronisation.

3.4 Experimental design for model validation

3.4.1 Data requirement

Overall the experiment aimed to provide two types of data–the steady-state data and the dynamic-state data. The steady state was obtained when the pressure, flow and the valve stem position were relatively constant for a short period of time. The steady-state data collected for this research were only taken if the measurements were constant for at least 30 seconds. The dynamic state was any period of measurement that was not considered to be a steady state including a transition between two steady states. The steady-state data will be used to validate the existing force balance equation, validate the existing C_v characteristic relationship and train for the proposed force balance equation. The dynamic-state data can be obtained through separate sets of experiments or through the set of experiments aiming for steady-state data, and the steady-state data were taken out. The dynamic-state data were used to validate the proposed force balance equation and to train and validate the classification model to identify the correct solution to the flow estimation.

The experiment was divided into two set-ups. Set-up 1 (or stage 1) aimed to collect steady-state data for the whole operational range of the control valve and set-up 2 (or stage 2) aimed to collect continuous data to mimic the behaviour of the real control valve. Hence, the data from set-up 1 contain various steady-state conditions of certain valve stem positions and the data from set-up 2 contain continuous hydraulic conditions including dynamic states. Figure 3.7 shows an example of real data collected from the lab. Data from set-up 1 and set-up 2 are shown separately. As mentioned above, the experimental set-up 1 after the steady-state data were taken out, is considered to be set-up 2.

In terms of measurement, a typical experiment for set-up 1 includes:

- Acquire data for seven valve variables for each test as shown in Figure 3.2: h_{in}, h_{in}^{std}, h_c, h_{out}, h_{out}^{std}, q and x_m. These correspond to the inlet pressure, standard-defined inlet pressure, control chamber pressure, outlet pressure, standard-defined outlet pressure, flow

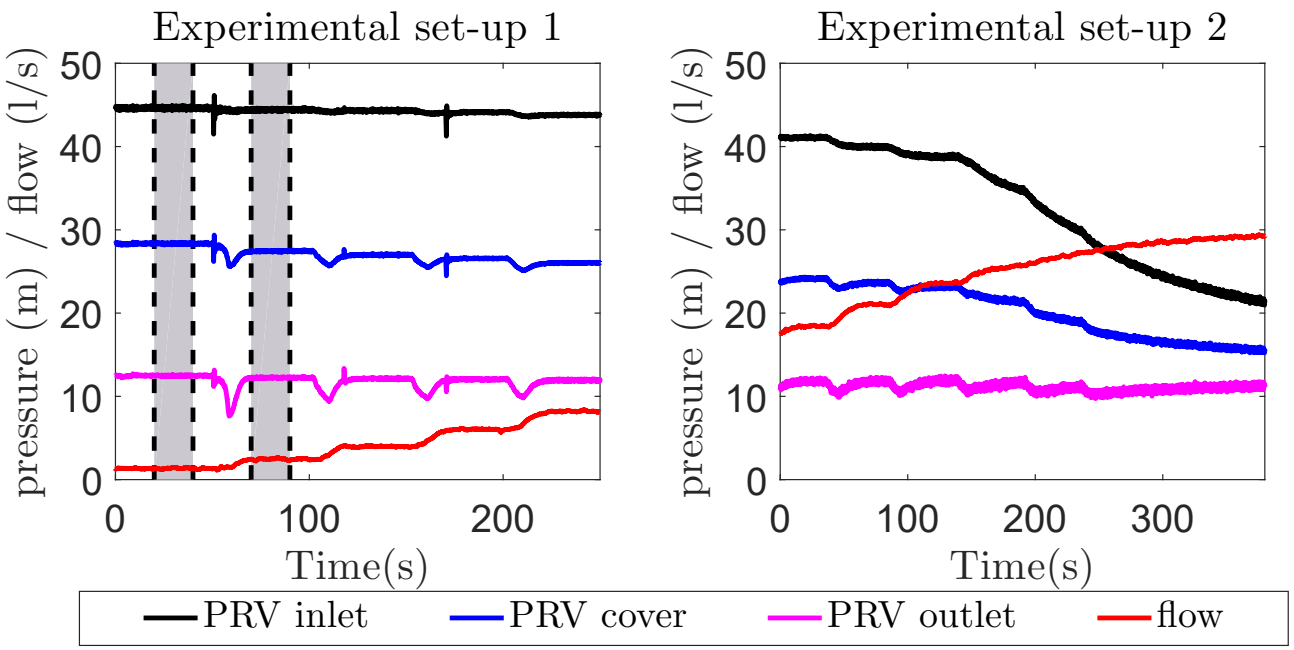

Figure 3.7: Experimental set-up 1 and set-up 2 (or stage 1 and stage 2); In the set-up 1, data from the steady state is highlighted in grey areas.

and valve stem position.

- Acquire data to capture steady-state flow conditions for a period of time (e.g. 30 seconds). Alternatively, the load valve opening will be varied gradually within a pre-defined opening range.

- Each experiment was carried out with constant h_{in} and h_{out}. A set of experiments was designed to include various combinations of h_{in} and h_{out}.

3.4.2 Details of the control procedure for the experimental set-up 1

The procedure for the experimental programme is as follows:

Experiment 1-1:

1. At fixed h_{in}^1 and h_{out}^1, adjust x_m to 2 mm opening, through varying the flow (demand).

2. At the same h_{in}^1 and h_{out}^1, adjust x_m to the next required setting for the valve stem position (e.g. 4 mm).

3. Continue the process of varying x_m through a pre-defined step change (e.g. 2 mm) until it reached the maximum opening of the tested valve.

Experiment 1-2 to experiment 1-N

1. At fixed h_{in}^2 and h_{out}^1, repeat experiment 1-1 until x_m reached the maximum opening.
2. At fixed h_{in}^3 and h_{out}^1, repeat experiment 1-1 until x_m reached the maximum opening.
3. Repeat by changing h_{in} for each experiment until h_{in}^N.

Experiment 2-1 to experiment M-N

1. Repeat experiment 1-1 to 1-N for a new set of outlet pressure h_{out}^2.
2. Repeat until the outlet pressure is h_{out}^M.

Within the proposed experimental procedure, h_{in} was varied by the variable speed pump, as each pump setting had a label V, (V1 to V5). We set valve inlet pressure according to the variable speed pump setting ($h_{in}(V)$). h_{out} was varied by the CRD pilot valve, each pilot valve setting had a label SP, (SP1 to SP5). The valve outlet pressure was set by modifying the CRD setting ($h_{set}(SP)$). x_m was varied by the demand (load) valve. The experimental procedure is graphically presented in Figure 3.8.

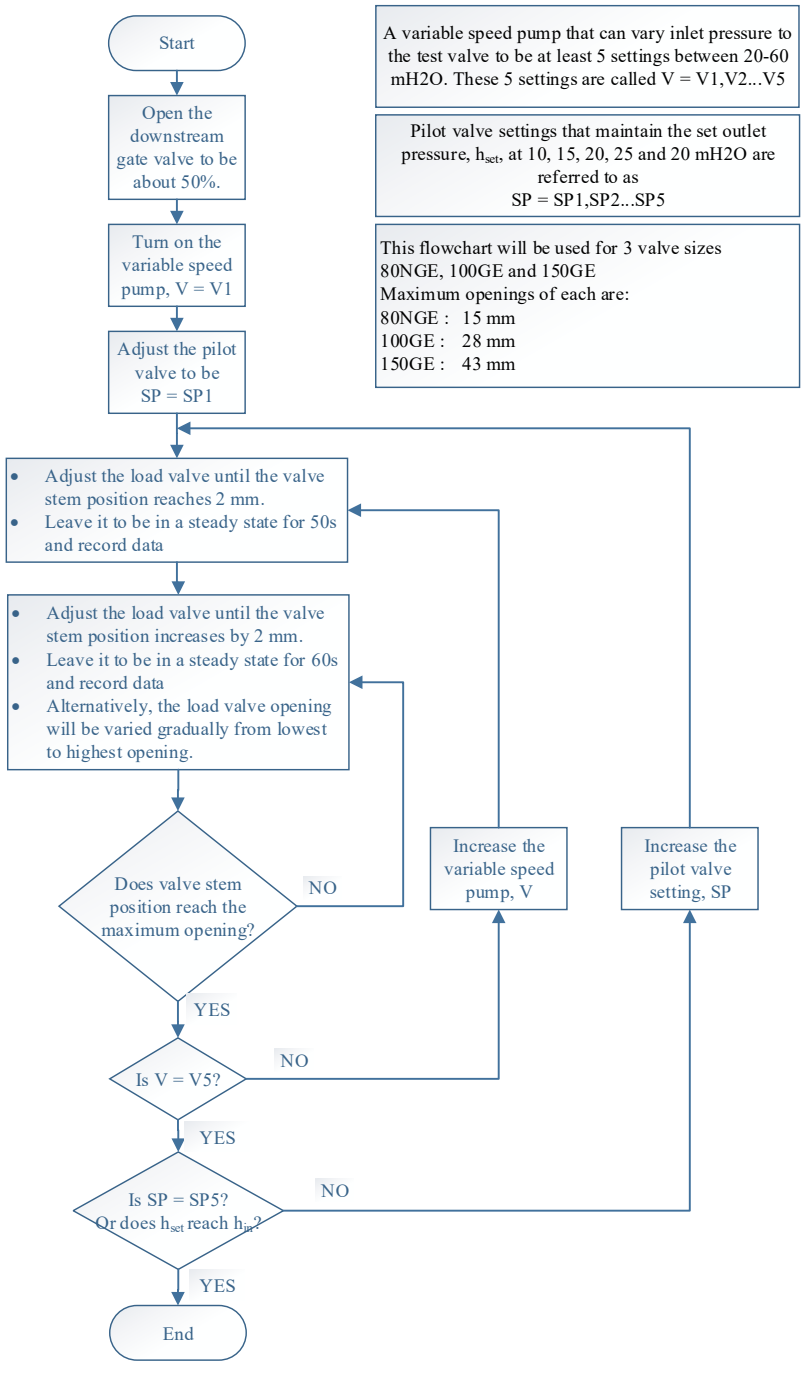

Figure 3.8: A workflow chart indicating the experimental procedure for one valve

Chapter 4

Automatic Control Valves Model Development for Flow Estimation (Part 1: An analysis of existing models)

This chapter investigates existing ACV models and their potential use on flow estimation and fault detection and diagnosis. The existing models are analysed and primarily modified to obtain a steady-state model, which is suitable for flow estimation and will facilitate fault detection and diagnosis. The obtained steady-state model of an ACV for flow estimation comprises 2 equations, which are investigated separately. The accuracy of the obtained steady-state model and its analogous model is assessed and discussed.

4.1 Introduction

A model is a description of a system that supports the understanding of the system's behaviour. Models can be expressed as a set of mathematical formulas, a concept, a computer program or a physical object. In this work, ACV models are sets of mathematical formulas. A good

mathematical model should be consistent with the past behaviour of the system (retrodiction) and also be predictive of the future behaviour, including the behaviour under perturbation (prediction). ACV models here will be developed for the following main objectives: to estimate flow, to assist FDD and to support design problems in future work.

4.2 Investigation of existing ACV models

Two main types of mathematical models of systems are mechanistic model and empirical model. In a mechanistic modelling method (or system analytic), a system is divided into small components, which will then be examined individually. The working principles of each individual part are determined by laws of physics, providing the visibility of a system. All components of a system are then coupled. On the other hand, empirical models are based on direct observation. System behaviours are usually represented as mathematical functional forms based on characteristics. With empirical approaches, the complexity of a model representative of a system can be greatly reduced. While empirical models are easier to handle numerically, they can fail to represent accurately fundamental principles of individual components.

A system model can contain different mechanistic and empirical levels depending on specific objectives of such models. For example, a model that is suitable for real-time simulation might not have enough accuracy for a parameter estimation. A valve model in network simulation might not contain enough details for fault detection and diagnosis problems. In this section, existing ACV models are investigated.

4.2.1 Modification of a selected ACV model to obtain a steady-state model

Four dynamic models of PRVs were presented in Prescott and Ulanicki (2001, 2003) and the models had different levels of mechanistic expressions of the valve. Detailed reviews of those models were presented in Chapter 2. The mechanistic models are preferable because they

support model-based design (Papalambros and Wilde, 2000) and can be used for further fault detection and diagnosis (Watton, 2007). Mechanistic models support those applications because they contain the working principles of individual parts. Using mechanistic models, faults can be simulated by adjusting the ACV parameters at different components and performance of each individual part can be investigated separately.

Two phenomenological models proposed by Prescott and Ulanicki (2003), which are considered mechanistic models, are investigated: The full phenomenological model (FPM) and the simplified phenomenological model (SPM). A major difference between the two models is that the FPM contains differential equations of motion of the main valve and the pilot valve, whereas the SPM contains force balance equations. Experimental and operational data shows that the main valve is under the quasi-static state most of the time. The observation suggests that the quasi-static approximation is a good approximation for the main valve. Under the quasi-static state, terms of inertia are negligible and the force balance equation is sufficient.

There are two additional reasons to suggest that the force balance equation suffices for flow estimation. First of all, the objective is not to achieve a high temporal resolution of flow estimation. Therefore, sudden changes of flow, transients and small oscillation can be ignored. Secondly, the force balance equation equalises forces due to pressures above and below the valve diaphragm. Flow will be estimated using the continuous measurement of pressures at high sampling rates such that pressure transients are captured. Flow estimation reaches its limitation when quasi-static approximation is no longer a good approximation (when continuous transient events occur).

A model modification to obtain the mechanistic steady-state model

The SPM is modified as follows:

1. Since a globe-diaphragm control valve contains a spring at the valve stem inside the control chamber, the force term due to the spring is added into the force balance equation.

2. A proportion of flow into the control loop is taken into account.

The modified SPM is:

$$
\begin{gathered}
q_3 = f(x_m)\dot{x}_m \\
\rho g(h_{in} + h_{out}(a_2 - a_1) - h_c a_2) - m_m g + \frac{\rho q_m^2}{a_1} - k_{mspr}(x_0 + x_m) = 0 \\
k_{pspr}(P_{sp} - x_p) - \rho g h_{out} a_d + m_p g = 0 \\
q_1 = C_{vfo}\sqrt{h_{in} - h_t} \\
q_2 = C_{vp}(x_p)\sqrt{h_t - h_{out}} \\
q_m = C_{vm}(x_m)\sqrt{h_{in} - h_{out}} \\
q_3 = C_{vnv}\sqrt{|h_c - h_t|} \cdot sgn(h_c - h_t) \\
q_1 + q_3 = q_2 \\
q_{tot} = q_m + q_1
\end{gathered}
\tag{4.1}
$$

, where all terms have their usual meanings (See Figure 2.5). For additional variables, k_{mspr} is the main valve spring constant, x_0 is the initial displacement of the main valve spring, and q_{tot} is the total flow across the valve.

A static approximation is applied to the modified SPM. The dynamic term, $\dot{x}_m$, goes to 0. Consequently, the flow between the T-junction and the control chamber, q_3, also equals 0. The steady-state model (SSM) is:

$$\begin{gathered}
\rho g(h_{in} + h_{out}(a_2 - a_1) - h_c a_2) - m_m g + \frac{\rho q_m^2}{a_1} - k_{mspr}(x_0 + x_m) = 0 \\
k_{pspr}(P_{sp} - x_p) - \rho g h_{out} a_d + m_p g = 0 \\
q_m = C_m(x_m)\sqrt{h_{in} - h_{out}} \\
q_b = C_{vfo}\sqrt{h_{in} - h_t} = C_{vp}(x_p)\sqrt{h_t - h_{out}} \\
q_{tot} = q_m + q_b
\end{gathered} \tag{4.2}$$

, where q_b is the flow through the control loop.

4.2.2 Preliminary simulation

Preliminary simulation problem and parameters

To simulate behaviours of the PRV, a problem is formulated that at each point in time, a controlled variable, the outlet pressure, h_{out}, is calculated from the given hydraulic conditions which are the inlet pressure, h_{in}, and flow, q_{tot} and from the control setting, the pilot valve setting, P_{sp}.

For the SSM, sets of non-linear algebraic equations are solved for the following variables: h_{out}, x_m, x_p, h_c and q_m. The model contains 5 equations and 5 unknown variables. The focus is on h_{out}, which should be kept relatively constant at various hydraulic conditions. The incoming hydraulic condition is set by two variables, h_{in} and q_{tot} and the control set by the valve is set by the variable P_{sp}. Therefore, the simulation result is shown as: $\tilde{h}_{out} = \tilde{h}_{out}(h_{in}, q_{tot}, P_{sp})$.

The modified SPM contains a differential equation and hence is a set of differential algebraic equations. In order to discretise a differential equation into an algebraic equation, the research has considered both the backward Euler Method and the forward Euler Method. The backward

Euler method is selected to discretise a differential equation into an algebraic equation. Given a differential equation, $\frac{dy}{dt} = f(t, y)$, the backward Euler Method is defined as follows:

$$y_n = y_{n-1} + h_n f(t_n, y_n). \tag{4.3}$$

In comparison, the Forward Euler Method is written as:

$$y_{n+1} = y_n + h_n f(t_n, y_n). \tag{4.4}$$

Using the backward Euler method, y_n is defined implicitly as it appears at both sides of Equation 4.3.

In order to find y_n, the equation needs to be solved explicitly because y_ns appear at both sides of the equation, whereas, for the forward Euler method, y_n can be expressed as a function of variables at the step n-1.

The forward Euler method has higher chance of having numerical instability compared to the backward Euler method (Butcher, 2008). This instability means that the numerical solution grows very large for equations where the exact solution does not. On the other hand, the backward Euler method introduces an additional algebraic equation at each time step, i.e. to solve for y_n. Therefore, the backward Euler method has a disadvantage due to its computation expense, but it has a better numerical stability as a trade-off.

For the PRV models, it is solved at the same time with other algebraic equations at time step n. The Backward Euler is selected because the system of differential algebraic equations of the PRV can be stiff and computational power is not a problem at this stage.

Borotoulas (2009) carried out sets of experiment on PRV behaviours. The experiments included continuous measurements of h_{in}, h_c, h_{out} and q_{tot}. Preliminarily, the simulation aimed to simulate $\tilde{h}_{out}$ and compare it with the measured h_{out} from sets of experiment carried out by Borotoulas (2009). The valve parameter would be approximated. The approximated valve parameters are shown in Table 4.1.

parameter	value/expression
m_m *and* m_p	0.5 kg and 0.1 kg
a_1, a_2 and a_d	0.0078 m^2, 0.0218 $m^2$and 0.00196 m^2
k_{spr}	70,000 N/m
k_{mspr}	130,000 N/m
ρ	1000 kg/m^3
g	9.8 m/s^2
C_{vfo}	2.9979 $\times 10^{-5}$ $m^{5/2}/s$
C_{vnv}	varies around 0.00011 $m^{5/2}/s$
C_{vm}	$0.02107 - 0.02962e^{-51.1322x_m} + 0.0109e^{-261x_m} - 0.00325e^{-683.17x_m} + 0.0009e^{-399.5x_m}$
C_{vp}	$0.0000753(1 - e^{-1135x_p})$
$f(x_m)$	$3700(0.02732 - x_m)$

Figure 4.1: The parameters used in preliminary simulation

The algorithm used in preliminary simulation

Because all of the control valve models are highly non-linear, an efficient algorithm to solve a non-linear system of equations is required. The Newton method was first considered. For a system of algebraic equations, $\mathbf{g}(\mathbf{x}) = \mathbf{0}$, an iteration obtained is:

$$\mathbf{x}^{\nu+\mathbf{1}} = \mathbf{x}^{\nu} - \left(\frac{\partial \mathbf{g}}{\partial \mathbf{x}}(\mathbf{x}^{\nu})\right)^{-1} \mathbf{g}(\mathbf{x}^{\nu}). \tag{4.5}$$

The step, δ , is defined by the difference between $\mathbf{x}^{\nu+\mathbf{1}}$ and $\mathbf{x}^{\nu}$. The Newton step, δ_n can be found by solving:

$$\left(\frac{\partial \mathbf{g}}{\partial \mathbf{x}}\right) \delta = -\mathbf{g}(\mathbf{x}^{\nu}). \tag{4.6}$$

The inverse of the Jacobian matrix $\mathbf{J}(\mathbf{x}^{\nu}) = \frac{\partial \mathbf{g}}{\partial \mathbf{x}}(\mathbf{x}^{\nu})$ is calculated in each iteration. It is important to note that most algorithms does not solve for this directly. For the PRV models, elements of the solution vector can have a difference in orders of magnitude up to 7 orders. It is often that the Jacobian becomes very large, and the solver struggles to find the solution.

In the Newton method, the Jacobian often tends to be singular and the solution cannot be found. The **Trust-Region Dogleg Algorithm** is capable of solving complex equations. The **Trust-Region** part has an advantage over the conventional Newton method that it can handle a case when the Jacobian is singular and it has a higher robustness when starting far from the

solution. The Trust Region strategy decides whether the new iterated step is better or worse than the previous one by formulating an optimisation sub-problem (Mathworks, 2018).

Instead of solving for the Newton step which can be expensive, the trust region strategy is to define a subproblem from the Newton step equation. The Newton step Equation is to find the root of:

$$\mathbf{M}(\mathbf{x}^{\nu} + \delta) = \mathbf{g}(\mathbf{x}^{\nu}) + \mathbf{J}(\mathbf{x}^{\nu})\delta. \tag{4.7}$$

The subproblem is:

$$\begin{aligned} \min_{\delta} \left\{ m(\delta) = \frac{1}{2}\|\mathbf{M}(\mathbf{x}^{\nu} + \delta)\|_2^2 = \frac{1}{2}\|\mathbf{g}(\mathbf{x}^{\nu}) + \mathbf{J}(\mathbf{x}^{\nu})\delta\|_2^2 \right\} \\ = \min_{\delta} \left\{ \frac{1}{2}\mathbf{g}(\mathbf{x}^{\nu})^{\top}\mathbf{g}(\mathbf{x}^{\nu}) + \delta^{\top}\mathbf{J}(\mathbf{x}^{\nu})\mathbf{g}(\mathbf{x}^{\nu}) + \frac{1}{2}\delta^{\top}\mathbf{J}(\mathbf{x}^{\nu})^{\top}\mathbf{J}(\mathbf{x}^{\nu})\delta \right\}. \end{aligned} \tag{4.8}$$

This subproblem can be solved using the Powell dogleg strategy. The step δ is a combination of the Cauchy step and the Gauss-Newton step. The Cauchy step is:

$$\delta_C = -\alpha\mathbf{J}(\mathbf{x}^{\nu})^{\top}\mathbf{g}(\mathbf{x}^{\nu}) \tag{4.9}$$

and the Gauss-Newton step is to solve:

$$\mathbf{J}(\mathbf{x}^{\nu}) \cdot \delta_{GN} = -\mathbf{g}(\mathbf{x}^{\nu}) \tag{4.10}$$

, which can be calculated using the Gaussian elimination. The step δ is chosen so that:

$$\delta = \delta_C + \lambda(\delta_{GN} - \delta_C) \tag{4.11}$$

, where λ is the largest value in the interval $[0, 1]$ such that $\|\delta\| \leq \Delta$. Therefore, if the Jacobian tends to be singular, δ will tend to be the Cauchy step.

Simulation results

Herein, the simulation was performed through the modified SPM and through the SSM. The modified SPM simulation result is shown in Figure 4.2 and the SSM simulation result is shown in Figure 4.3. The modified SPM successfully represents a slight variation of outlet pressure at various hydraulic conditions. The SSM shows a similar result to the modified SPM, but for each steady state, the simulated pressure is less varied.

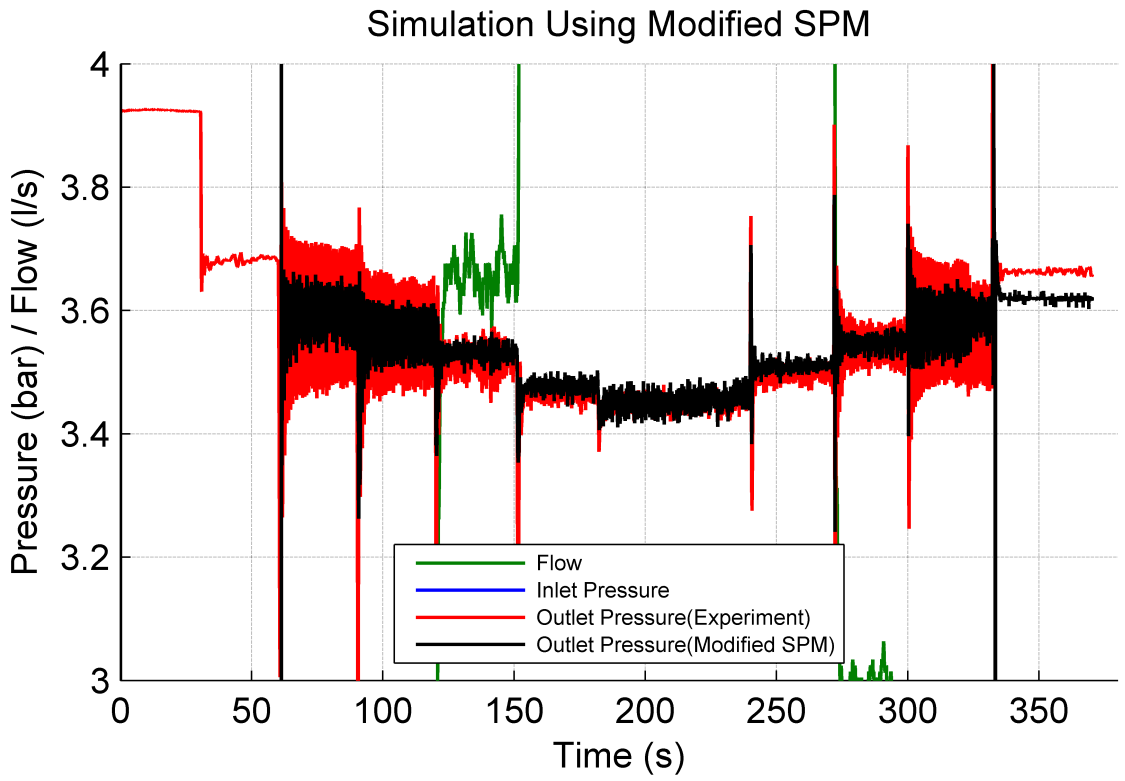

Figure 4.2: Simulation result using the modified SPM model (SPM with the spring term and the bypass flow); Axes have been adjusted to show the same scale of flow and pressure. Inlet pressure and flow are not seen clearly because the figure is zoomed in to focus only on small range of outlet pressure.

In comparison to the simulation results in Figure 4.2 and Figure 4.3, both models well represent variation of the outlet pressure. The only difference is that the modified SPM picks up some dynamic behaviours. The SSM requires less computational resource to solve and these dynamic behaviours are not necessary for the control scheme based on flow estimation (the flow modulation) because the control will be implemented assuming a steady-state condition. Therefore, flow estimation was performed using the SSM.

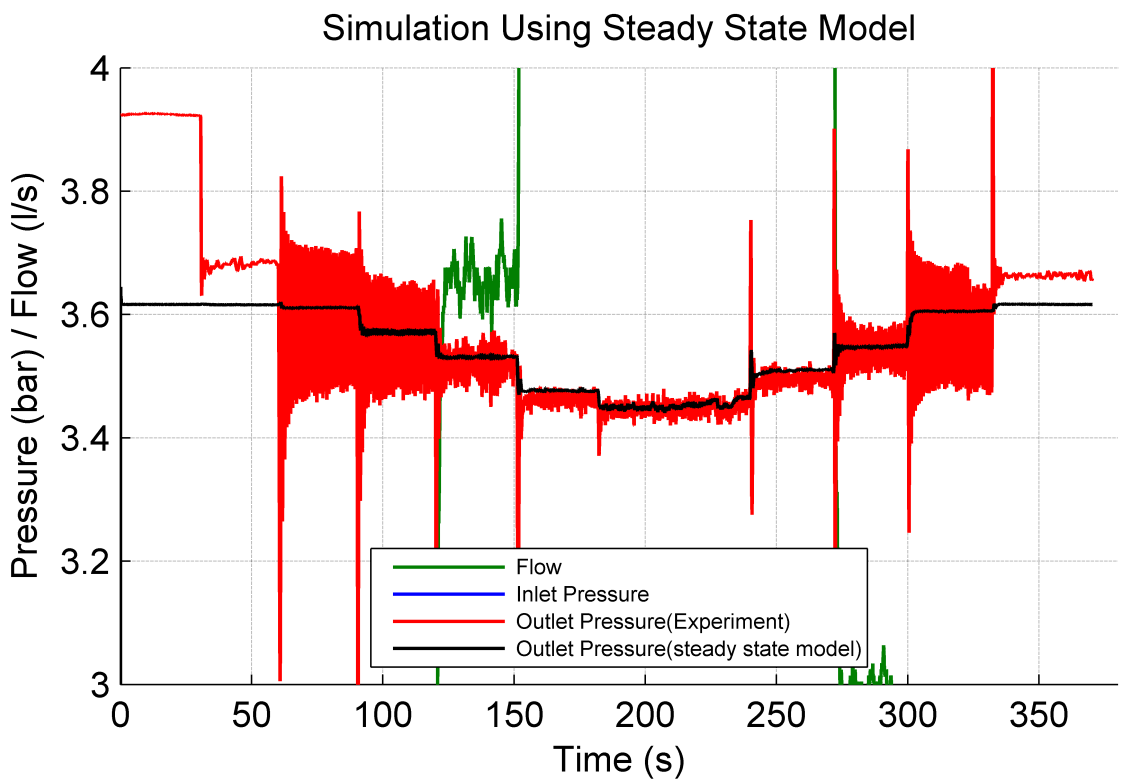

Figure 4.3: Simulation result using the SSM model; Axes have been adjusted to show the same scale of flow and pressure. Inlet pressure and flow are not seen clearly because the figure is zoomed in to focus only on small range of outlet pressure.

The flow estimation simulation problem was formulated in a similar fashion to the outlet pressure simulation. The flow estimate was calculated through the SSM, i.e. $\tilde{q}_m = \tilde{q}_m(h_{in}, h_{out}, P_{sp})$. The simulation result shows that within a steady state where flow is relatively constant, the flow estimate fluctuates significantly (see Figure 4.4). This fluctuation implies high sensitivity of flow to other measured variables. The accuracy is uncertain because all the parameters are estimated and could be totally different from the actual parameters. The preliminary simulation suggests that even with an accurate model relationship, the precision of flow estimation could be limited by the sensitivity of the flow estimate to the measured variables in the relationships. The simulation result also shows that the flow into the control loop is much smaller than the main valve flow. Therefore, in most cases, $q_m \approx q_{tot}$. The accuracy of the SSM equations for flow estimation will be investigated later on.

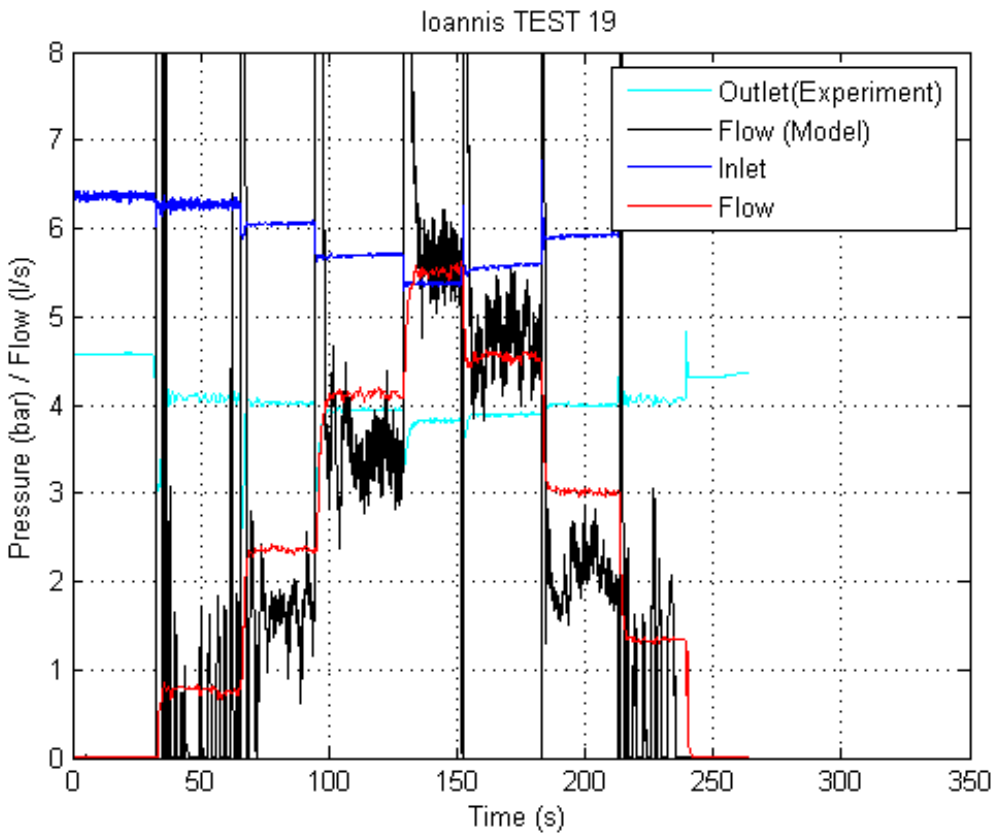

Figure 4.4: An attempt to calculate the flow from inlet pressure, outlet pressure and the pilot valve setting: Axes have been adjusted to show the same scale of flow and pressure.

4.2.3 Flow estimation methodology

Control valve models consist of two parts–the main valve body part and the control loop part of the valve. Equations describing the control loop depend on the function of a control valve. The control loop adjusts the pressure in the control chamber which can be directly measured. The main valve part of the model includes the control chamber pressure and therefore, equations representing the control loop are not necessary for flow estimation. The main valve body part of the SSM is:

$$q_m = C_m(x_m)\sqrt{h_{in} - h_{out}} \tag{4.12a}$$

$$\rho g(h_{in}a_1 + h_{out}(a_2 - a_1) - h_c a_2) - m_m g + \frac{\rho q_m^2}{a_1} - k_{mspr}(x_0 + x_m) = 0. \tag{4.12b}$$

A local valve control requires continuous data for control purposes. Pressure signals inlet and outlet of the control valve must be measured. With mathematical models of control valves,

pressure measurements can be utilised for essential applications. This research focuses on mathematical modelling of control valves for flow estimation using surrogate measures.

The 2P&Pos flow estimation method was performed by solving Equation 4.12a for a flow estimate ($\tilde{q}$), with the given continuous measurements of x_m, h_{in} and h_{out}. For the 3p flow estimation method, Equation and 4.12b and Equation 4.12a, which are coupled, will be solved together for both the position estimate, $\tilde{x}_m$, and the flow estimate, $\tilde{q}_m$, using three pressure measurements (h_{in}, h_c and h_{out}) The accuracy of Equation 4.12a and Equation 4.12b will be investigated separately. The Equation 4.12a will be validated in Section 4.3 and the Equation 4.12b will be validated in Section 4.4.

4.3 The SSM body part model validation part 1, the C_v characteristic equation

4.3.1 The C_v characteristic relationship

The C_v coefficient is a relative measure of a device's efficiency at allowing fluid flow. It relates the differential pressure across the device to the corresponding flow and can be expressed as:

$$C_v = Q\sqrt{\frac{SG}{\Delta P}}, \tag{4.13}$$

where Q is the flow rate, SG is the specific gravity and ΔP is the differential pressure across the device. For the valve case, C_v can be referred to as the flow coefficient, the valve capacity or the valve sizing characteristic depending on units and fields of use. For example, the flow coefficient (also C_v) is defined as the volume (in US gallons) of water at 60Âř F that will flow per minute through a valve with a pressure drop of 1 psi. For the flow factor (K_v), the flow rate is expressed in units of cubic meters per hour, and the pressure in bar.

Since the standard definition of the C_v is not in SI units, to avoid confusion in this work, the

C_v is referred to as the C_v characteristic and will be described with associated units.

The C_v characteristic equation is validated by observing the experimental values of the $C_{vm}(x_m)$, calculated from the pressure drop across and flow through the main valve for a range of openings. The $C_{vm}(x_m)$ is then plotted against the valve opening (or the stem position), x_m. The C_v characteristic is valid if $C_{vm}(x_m)$ values only show a small variation at a particular opening and the data points can be fitted into a curve. This also means that the hysteresis effect of the valve is negligible.

The valve manufacturer (Cla-Val) provides C_v characteristic relationships in a form of polynomial for each valve type, which are derived from experiment. The polynomial is six ordered with the normalised value of the valve opening against the normalised value of the C_v. For each valve type, the manufacturer provides two different maximum C_v values for each valve: the documentation value and the testing lab value. The C_v characteristic relationships from experimental data and relationships provided by the valve manufacturer are compared. Four valves were investigated, which are Cla-Val DN80 NGE, Cla-Val DNN100 GE, Cla-Val DN150 GE and a 2nd Cla-Val DN100 GE. The Cla-Val valves are usually referred to among practitioners as the valve DN size followed by the valve body type (90GE-01(GE) or NGE90-01(NGE)). For example, 100GE means the valve is Cla-Val DN100 GE.

The C_v values used for the comparison were derived from:

1. Cla-Val Documentation polynomial (Cla-Val Cv 1).
2. Cla-Val Testing Lab polynomial (Cla-Val Cv 2).
3. The acquired experimental data and the C_v were calculated using pressure transducers which were installed at the valve (C_v Valve).
4. Experimental data, for which the inlet and outlet pressure was acquired according to the standard ANSI/ISAâĂŞ75.02.01âĂŞ2008 (C_v Standard).

For the 80NGE, measurements were acquired for the full range of valve openings, as this valve size tends to operate across its full range. The 100GE was also investigated across its full stem position range to test its repeatability against experimental data acquired from a 100GE

valve at Imperial College London and a 100GE valve operated in the “Field Lab". With regard to the 150GE and the second 100GE valve, the experimental programme focused upon specific operational pressure and flow conditions according to its typical operational range. These operational ranges were taken from typical operational profiles of the control valves within the “Field Lab". The C_v values of the 80NGE and the 100GE from the experimental programme were normalised with the maximum measured C_v and were compared with the Cla-Val polynomials. The C_v values of all valves measured from the experiment are shown as follows:

1. Cla-Val DN80 NGE (80NGE)

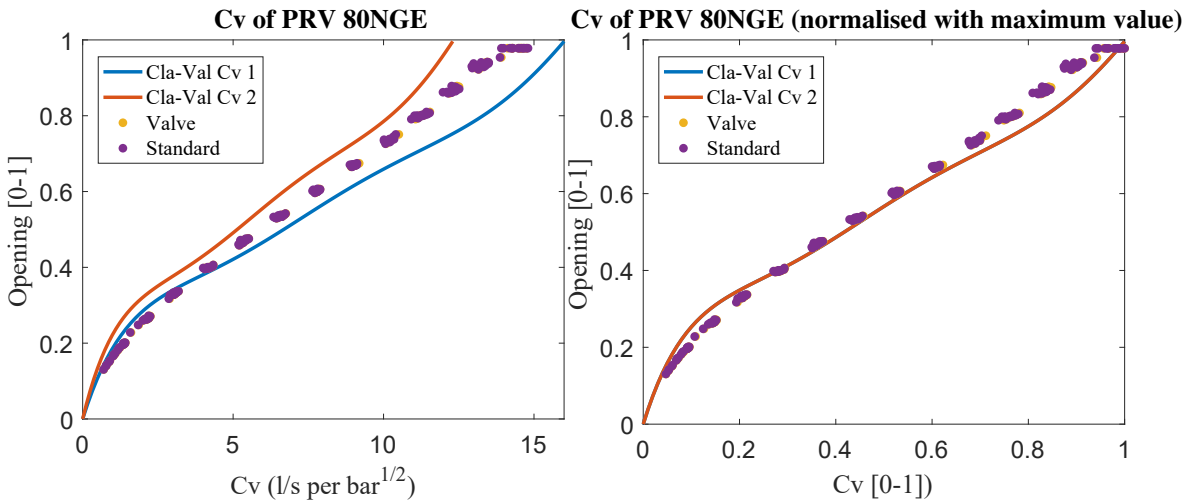

(a) C_v of 80NGE

(b) C_v of 80NGE normalised with the maximum measured Cv

Figure 4.5: A comparison of 80NGE C_v using the acquired experimental data and Cla-Val-provided polynomials

	Cla-Val Documentation	Cla-Val Testing Lab	C_v "Valve"	C_v "Standard"
C_v (l/s per bar^1/2)	16.0	12.3	14.76	14.80

Table 4.1: A comparison of the maximum value of 80NGE C_v

2. Cla-Val DN100 GE (100GE)

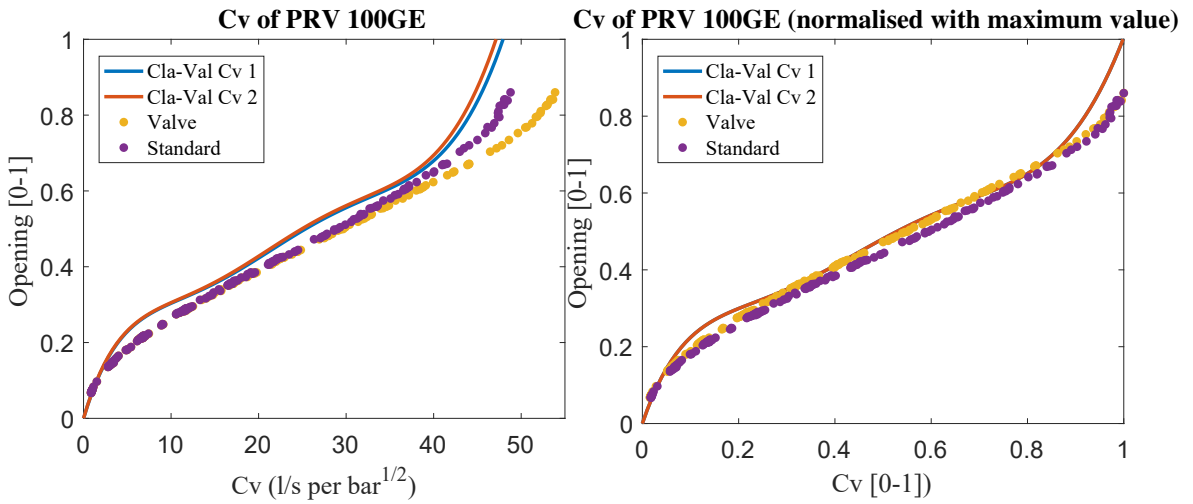

(a) Cv for 100GE

(b) Cv for 100GE normalised with the maximum Cv

Figure 4.6: A comparison of 100GE C_v based on the acquired experimental data and Cla-Val-documented polynomials

	Cla-Val Documentation	Cla-Val Testing Lab	C_v "Valve"	C_v "Standard"
C_v (l/s per bar^1/2)	48.0	47.2	53.87	48.78

Table 4.2: A comparison of the maximum value of 100GE C_v

3. Cla-Val DN150 GE (150GE)

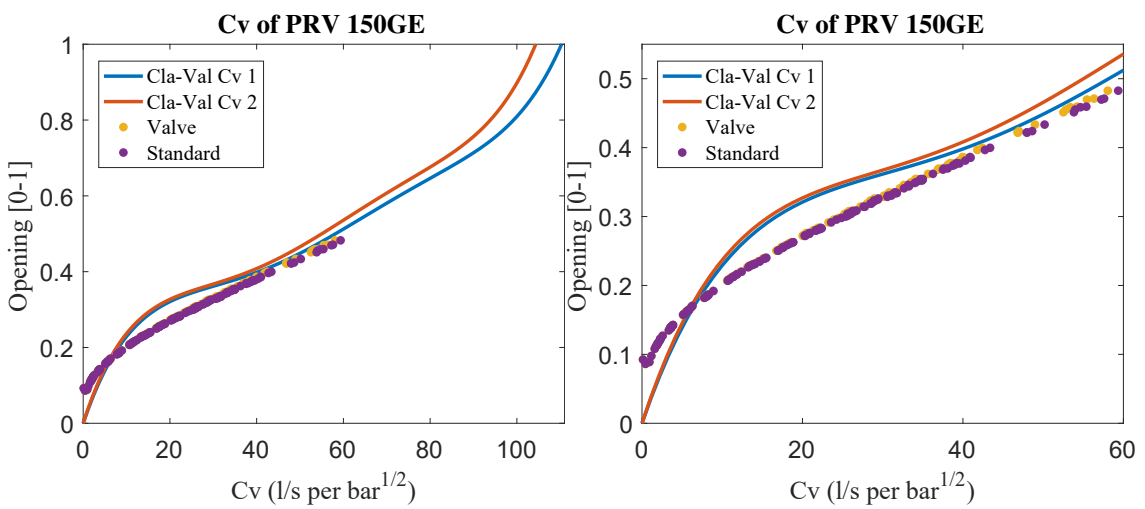

(a) Cv for 150GE

(b) Cv for 150GE, focused at the experimental range

Figure 4.7: A comparison of 150GE C_v between the acquired experimental data and Cla-Val-documented polynomials

4. 2nd Cla-Val DN100 GE (2nd 100GE)

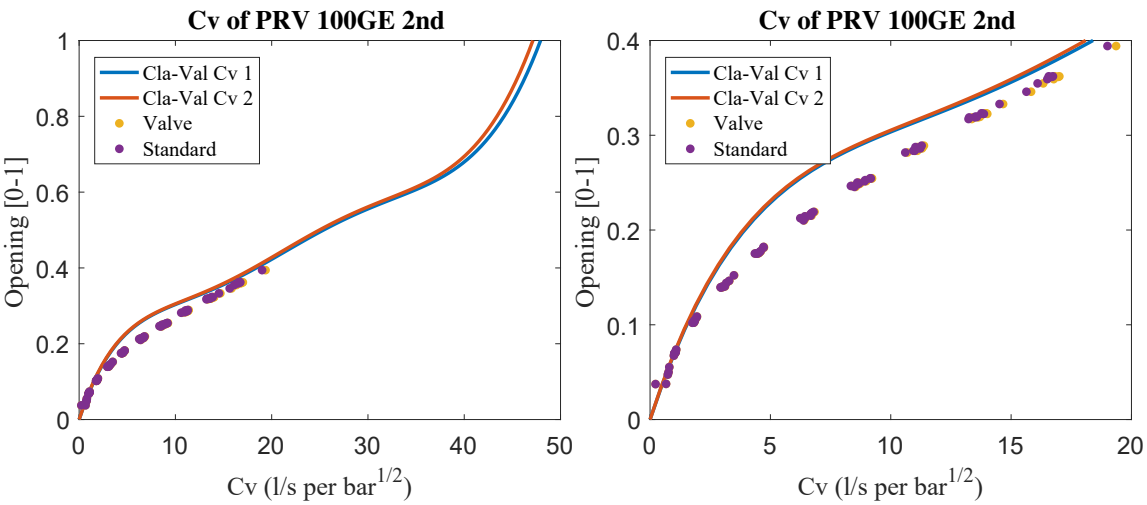

(a) Cv for 2nd 100GE

(b) Cv for 2nd 100GE, a limited experimental range

Figure 4.8: A comparison of Cvs for the second 100GE based on the experimental data and Cla-Val documented polynomials

For all valves, the "C_v valve" values were similar to the "C_v standard". Values of the two C_v started to differ when the valve stem position, and hence the flow, is high. The reason behind this difference is believed to come from the jet flow and cavitation at high flow. Under the jet flow and cavitation conditions, the values of an outlet pressure measured at a valve and measured downstream of the valve are different because the jet and the cavitation implosion causes slightly higher pressure. For the current experimental result of 4 valves, C_v values from both set-ups were identical up to the flow of approximately 30 l/s. In the flow estimation analysis, the differential pressure obtained from the inlet and outlet of the valve, rather than "standard-based" rules, was used to investigate the repeatability and analyse the flow estimation performance.

4.3.2 Repeatability of C_v values of the same valve type (100GE)

Data acquired from four different 100GE valves have been used to investigate the repeatability of C_v in order to assess the impact on the uncertainty of flow estimation. The four valves are: (i) the first 100GE valve tested in Cla-Val HQ, (ii) the second 100GE valve tested in Cla-Val HQ, (iii) the 100GE valve at Imperial College London (Hydrodynamics Laboratory) and (iv) the 100GE valve installed in the "Field Lab" (Stoke Lane). These four valves showed differences in their C_v and also a difference in the C_v polynomials provided by Cla-Val (see Figure 4.9). As an initial interpretation, the discrepancies in C_v between valves of the same model would affect the accuracy of flow estimation, and these are demonstrated in the following section.

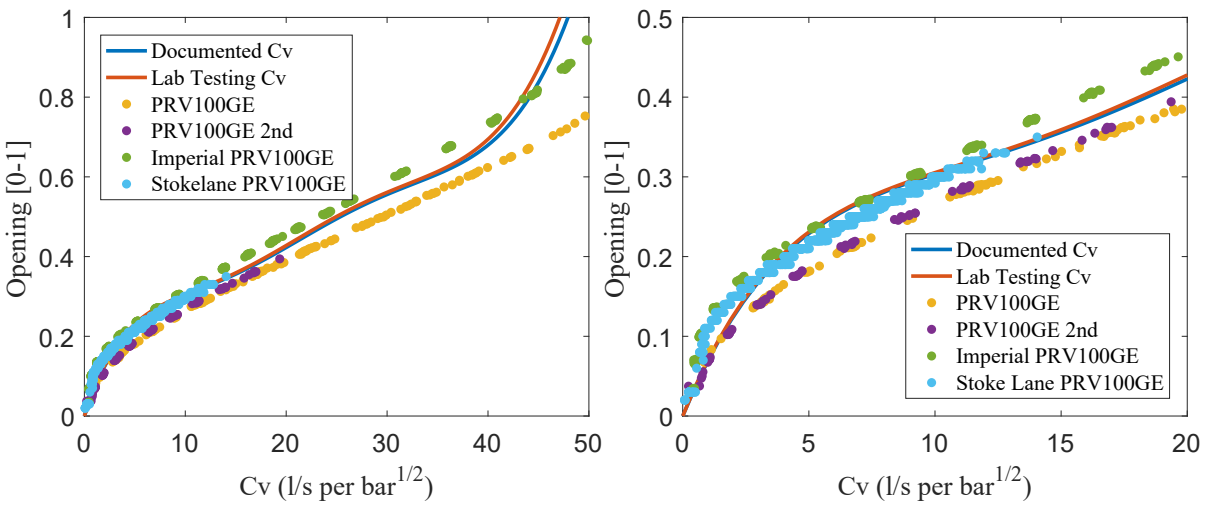

(a) Cv for four 100GE valves

(b) Cv for four 100GE valves. The plotted range is based on the experimental range selected for the 2nd 100GE valve

Figure 4.9: A comparison of Cvs for four 100GE valves based on the acquired experimental data and the provided Cla-Val polynomials

As an initial interpretation, the discrepancies in C_v between valves of the same model would affect the accuracy of flow estimation, and these are demonstrated in the following subsection.

4.3.3 Impacts of C_v uncertainty on flow estimation

It has been shown that the C_v values obtained from the experiment were slightly different from the curves provided by Cla-Val and they also presented a variability between different valves of the same type. Therefore, the C_v curves fitted from the experimental C_v values are slightly different from the C_v curves provided by Cla-Val. This subsection aims to demonstrate the impact of using the experimentally derived C_v and using the manufacturer's provided C_v for flow estimation. The flow estimation considered here is the 2p&pos method utilising measurements of the valve inlet pressure (h_{in}), the outlet pressure (h_{out}), and the valve stem position (x_m). It is important to note that the result shown in this subsection is to validate the feasibility of using the C_v characteristic relationship to perform the flow estimation and not to validate the accuracy of the method (it would be a self-validation since the flow is used to derive the C_v curve and the C_v curve is used to estimate the same flow). Cross-validation of the C_v for flow estimation will be shown later on.

Herein, the flow estimation method utilises both the C_v polynomial provided by Cla-Val and the C_v values that were derived from the acquired experimental data (6-degree polynomials). As the stem-position sensor had the accuracy of 1 µm, the uncertainty in the flow estimation method would depend primarily on the accuracy of the C_v. The 2P&Pos flow estimation results using different C_v curves are shown below:

1. 80NGE

1.1. 80NGE, manufacturer's provided C_v relationships

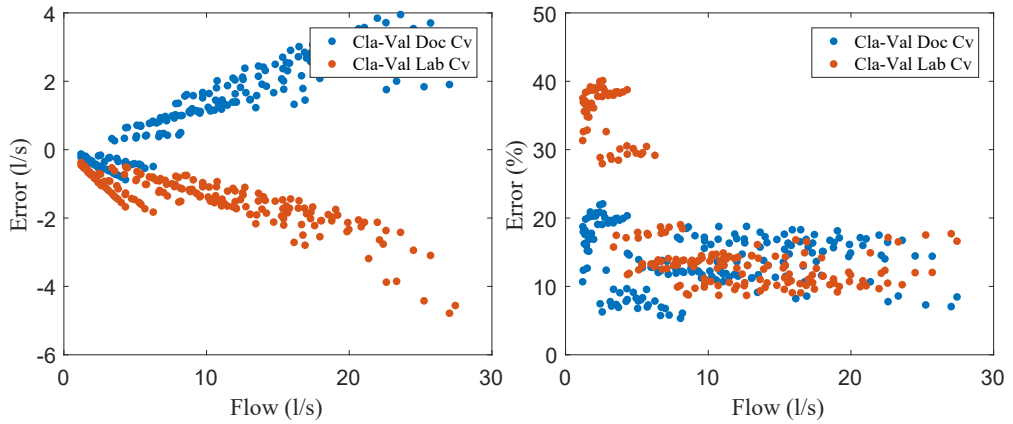

(a) 80NGE absolute error (Cla-Val C_v) (b) 80NGE relative error (Cla-Val C_v)

Figure 4.10: Accuracy of the 80NGE flow estimation through the manufacturer's provided C_v

1.2. 80NGE, derived C_v relationship

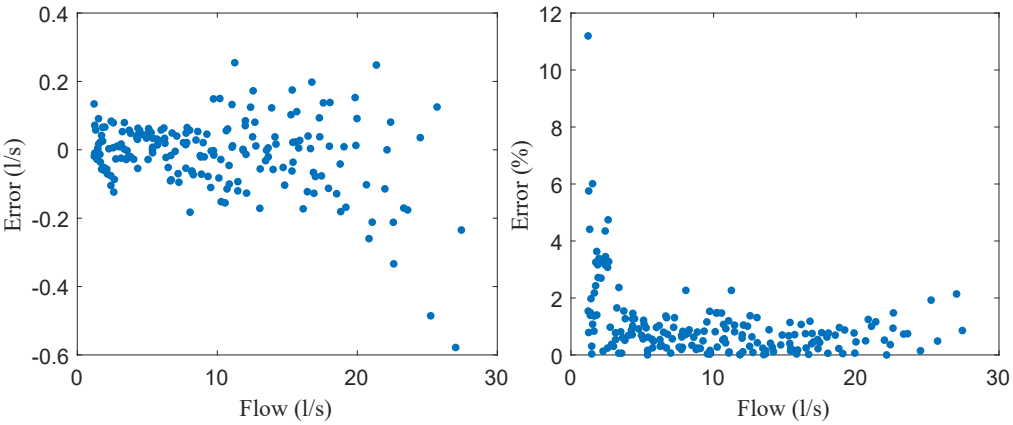

(a) 80NGE absolute error (derived C_v) (b) 80NGE relative error (derived C_v)

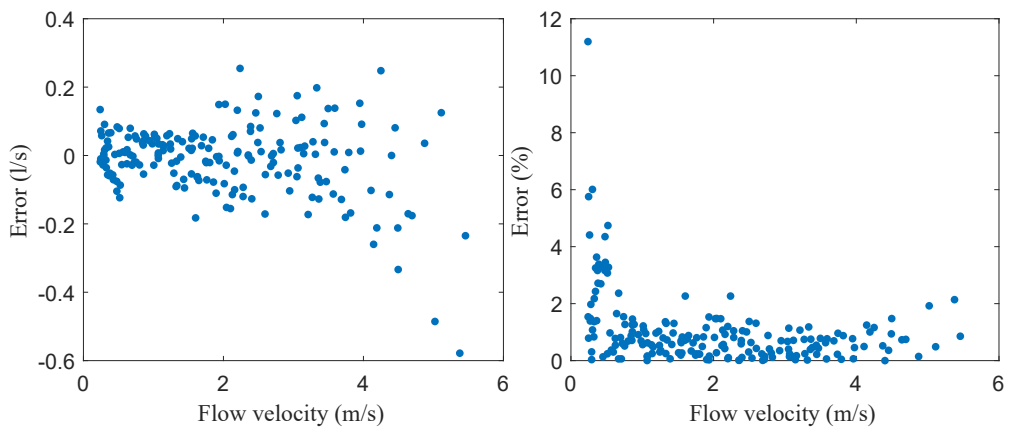

(c) 80NGE absolute error (derived C_v) (d) 80NGE relative error (derived C_v)

Figure 4.11: Accuracy of 80NGE flow estimation through the derived C_v

2. 100GE

2.1. 100GE Cla-Val Cvs

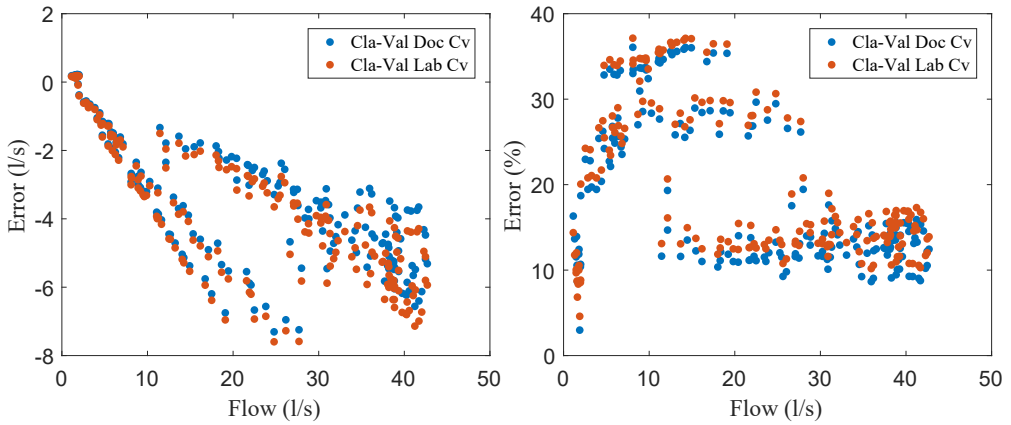

(a) 100GE absolute error (Cla-Val C_v) (b) 100GE relative error (Cla-Val C_v)

Figure 4.12: Accuracy of 100GE flow estimation through the manufacturer's provided C_v

2.2. 100GE derived Cv

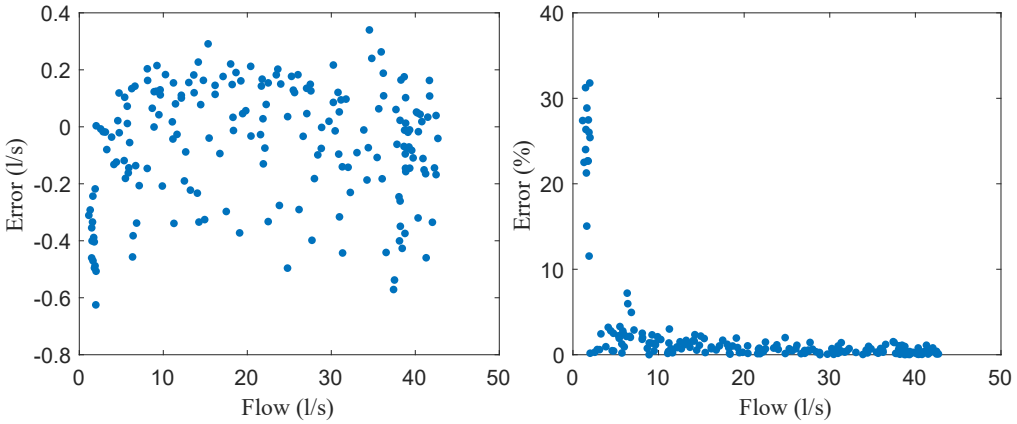

(a) 100GE absolute error (derived C_v) (b) 100GE relative error (derived C_v)

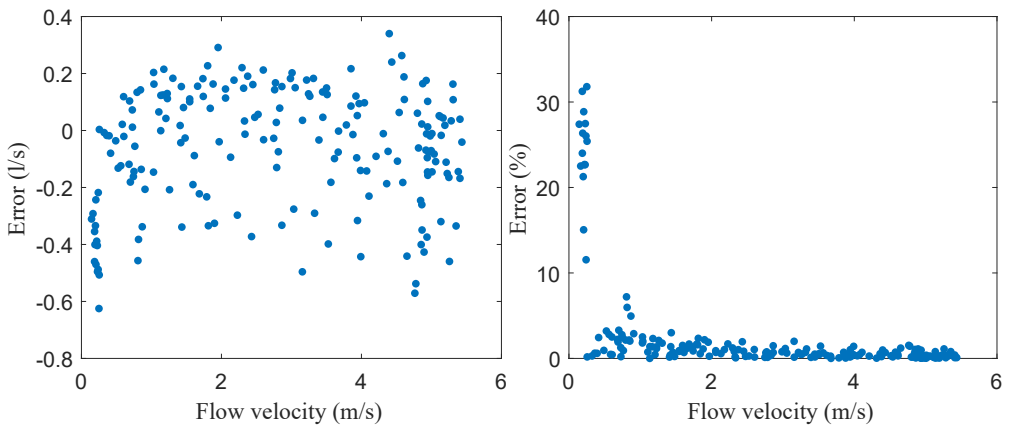

(c) 100GE absolute error (derived C_v) (d) 100GE standard error (derived C_v)

Figure 4.13: Accuracy of the 100GE flow estimation through the derived C_v

3. 150GE

3.1. 150GE Cla-Val Cvs

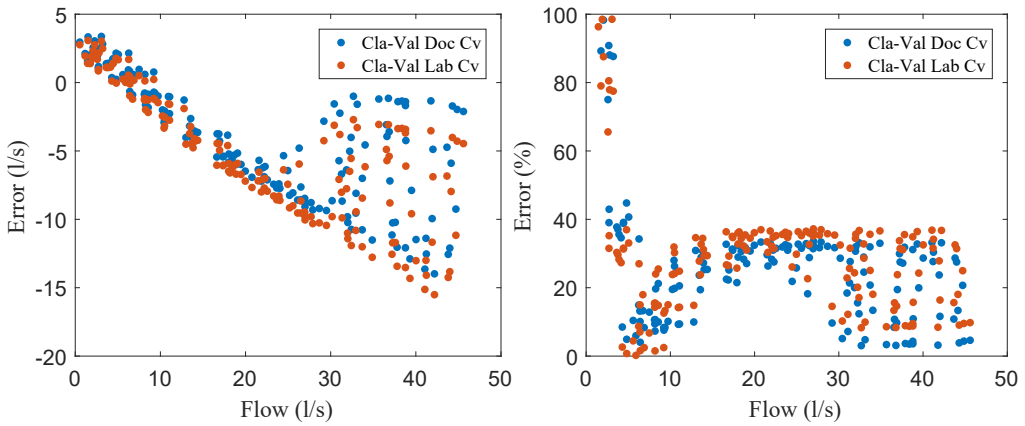

(a) 150GE absolute error (Cla-Val C_v) (b) 150GE relative error (Cla-Val C_v)

Figure 4.14: Accuracy of the 150GE flow estimation through the manufacturer's provided C_v

3.2. 150GE derived Cv

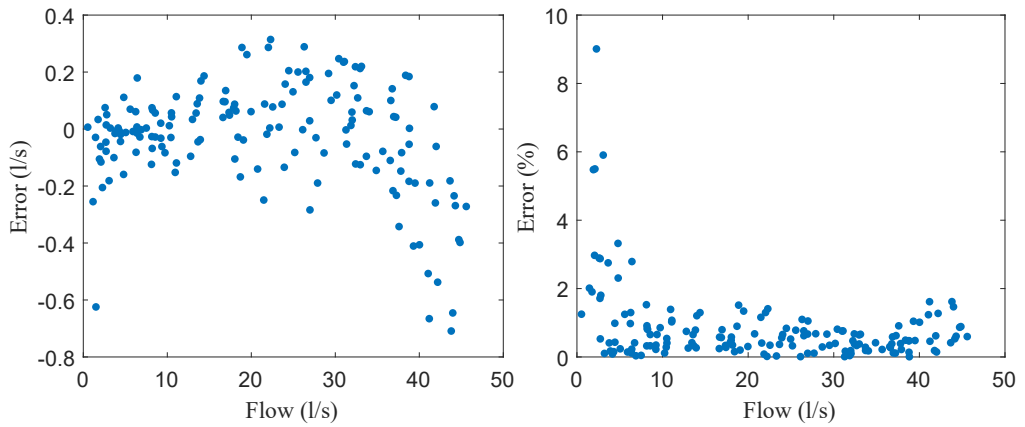

(a) 150GE absolute error (derived C_v) (b) 150GE relative error (derived C_v)

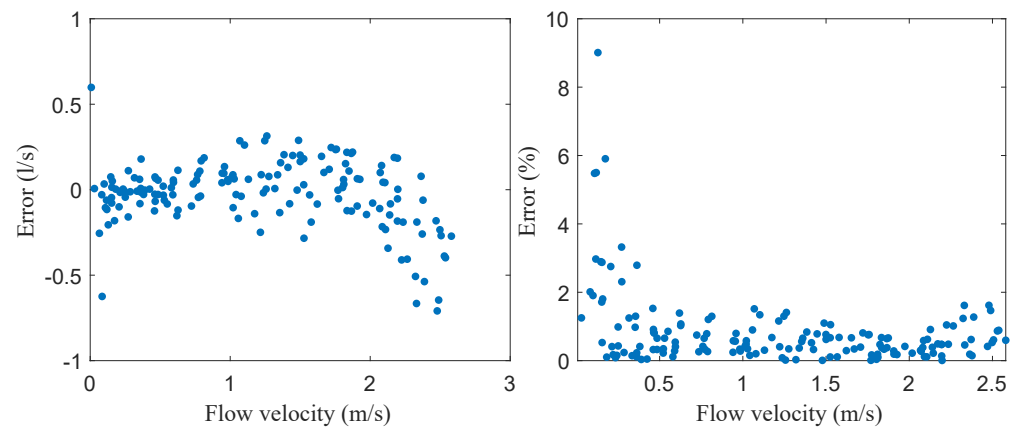

(c) 150GE absolute error (derived C_v) (d) 150GE standard error (derived C_v)

Figure 4.15: Accuracy of the 150GE flow estimation through the derived C_v

It should be noted that there will be a significant improvement in the accuracy of the flow estimation for a two pressure and a stem-position sensor when the C_v of a control valve is derived for a specific valve, as all valves, even those that are morphologically identical, do not have the same C_v. The variation of C_v values of the same valve size and type is shown in Figure 4.9. The accuracy of flow estimation was then compared to the accuracy of a mechanical, positive-displacement flowmeter. The initial error for very low flow velocities was mainly due to the fact that the velocity was below the measurement threshold of the electromagnetic flowmeter.

It can be concluded that each of a diaphragm-actuated globe valve has a C_v relationship corresponding to it. Although the pressure measurements were taken at a valve, which were different from the standard setting, the C_v relationship holds true for all values. A variation of C_v relationships of the same type of valves was observed and those are slightly different from the relationship provided by the valve manufacturer. This variation will affect the flow estimation either through the 2p&pos method or the 3p method. Hence, it is recommended to derive an accurate C_v relationship for a particular valve.

4.4 The SSM body part model validation part 2, the force balance equation

For the force balance equation of the SSM (Equation 4.12b), the difference between the measured pressure and the pressure in action under the diaphragm can affect the accuracy of the force balance equation. The measured pressure and the pressure in action under the diaphragm should be significantly different due to a high head loss at the bend of the valve body, i.e. minor loss. Pressure measurement points and action points are shown in Figure 4.16.

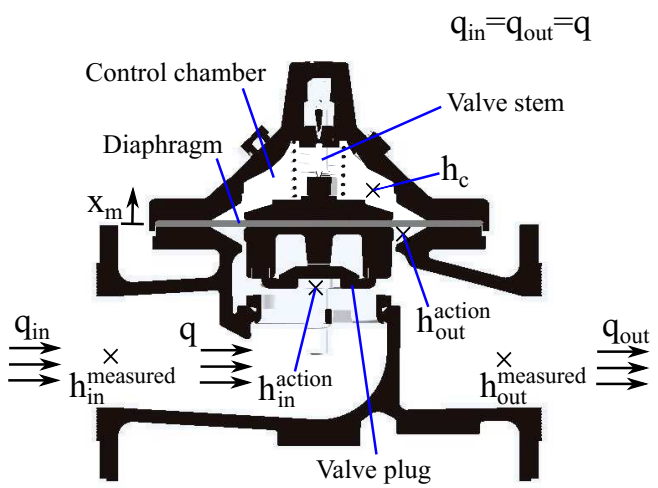

Figure 4.16: A diaphragm-actuated globe valve body; The control loop is not shown.

Equation 4.12b is rearranged to be:

$$x_m = \overbrace{\left(\frac{\rho g}{k_{mspr}} a_1\right)}^{b_1} h_{in} + \overbrace{\left(-\frac{\rho g}{k_{mspr}} a_2\right)}^{b_2} h_c + \overbrace{\left(\frac{\rho g}{k_{mspr}} (a_2 - a_1)\right)}^{b_3} h_{out} + \\ + \underbrace{\left(\frac{\rho}{k_{mspr} a_1}\right)}_{b_4} q_m^2 + \underbrace{\left(-x_0 - \frac{m_m g}{k_{mspr}}\right)}_{b_5}. \quad (4.14)$$

With this form, the valve stem position is a linear combination of other measured variables (h_{in}, h_c, h_{out}, q_m). Constants of the linear relationship only consist of constant valve parameters.

Two approaches to validate Equation 4.14 are employed. The first approach will perform the valve stem position estimation straight away through the force balance equation, Equation 4.14. The position estimate is expressed as $\tilde{x}_m = \tilde{x}_m(h_{in}, h_c, h_{out}, q_m)$. The position estimate will then be compared to the measured x_m. This approach is called **position estimate comparison** and will be investigated at valve 100GE due to the availability of the valve parameters. The second approach is to perform ordinary least squares (OLS) linear regression on an analogous linear equation of Equation 4.14, which is:

$$x_m = b_1 h_{in} + b_2 h_c + b_3 h_{out} + b_4 q_m^2 + b_5. \quad (4.15)$$

The regression coefficients will be compared to the parameterised coefficients, i.e. terms in

brackets from Equation 4.14. This approach is referred to as the **regression coefficients**.

4.4.1 Position estimate comparison

The steady-state data from experimental phase 1 were selected for investigation from 1 different PRV. The valve parameters were either measured directly or taken from the valve 3D model provided by the valve manufacturer. The valve parameters for the 100GE are given as: k_{mspr} = 1692.2 N/m, a_2 = 0.03317 m^2(diameter = 20.55 cm), a_1 =0.00855 m^2(diameter = 10.3 cm), m_m = 2.7 kg and x_0 = 39 mm. The position estimate is bound by a feasible range of the valve opening, [0mm,28mm]. By substituting the valve parameters, Equation 4.14 becomes:

$$x_m = 0.0495h_{in} - 0.1921h_c + 0.1426h_{out} + 69.12q_m^2 - 0.0546, \tag{4.16}$$

where x_m unit is metre, h unit is m$H_2O$and q unit is cubic metre per second. As a result, all of the position estimates are bound at the valve closed position (0mm) or at the valve maximum opened position (28mm). If the operational bounds are removed, the position estimates vary from 50 mm up to minus a few metres, which means errors up to 3 orders of magnitude are found. This result indicates that the force balance equation 4.14 underestimates the force below the valve diaphragm, or overestimates the force above the diaphragm, or the relationship is completely incorrect. It is concluded that Equation 4.14 is inaccurate and the position estimate is highly sensitive to pressure measurements.

4.4.2 Regression coefficients

In Equation 4.14, physical parameters of the valve are grouped into brackets. Each bracket is represented by a b_i coefficient. For each valve, the b_i coefficients are found through the OLS linear regression method. Linear regression is appropriate because the equation is a linear combination of the coefficients and the measurements (although measurement terms might not be linear, a new variable can be constructed from measurement only, for example q^2).

Firstly, data of the valve 100GE were selected to be analysed due to the availability of physical parameters. Table 4.3 shows the regression result of valve 100GE, with R-squared =0.844.

Variable	Estimated Coef	Standard Error	tStat	p-value
Intercept	0.007754	0.00067847	11.429	7.7728e-24
h_{in}	6.8577e-05	3.6845e-05	1.8612	0.06411
h_c	-0.00042385	7.2058e-05	-5.8821	1.5801e-08
h_{out}	0.0003281	4.802e-05	6.8326	8.8648e-11
q^2	7.9574	0.29237	27.216	8.5285e-71

Table 4.3: OLS regression of the 100GE valve

Although the p-values are small, which can reject the null hypothesis, coefficients for pressure are very small compared to the physical parameters in Equation 4.16. Further analysis has been performed by separating data into two groups: with $x_m > 10$mm and with $x_m < 10$mm. Table 4.4 and Table 4.5 show regression results for the valve stem position less than and higher than 10 mm , respectively. The estimated coefficients from the two cases are completely different and the coefficients for pressures are so small such that there is no meaningful interpretation. Forces due to pressures should come from the coefficients in a similar order to those in Equation 4.16.

Variables	Estimated Coef	Standard Error	tStat	p-value
Intercept	0.0039392	0.0012742	3.0914	0.0024856
h_{in}	0.00017561	9.3447e-05	1.8792	0.062685
h_c	-0.0003961	0.00017153	-2.3092	0.022671
h_{out}	0.00027853	0.00011187	2.4897	0.014177
q^2	0.34919	0.44157	0.7908	0.43065

Table 4.4: OLS regression of the valve 100GE ($x_m < 10$mm)

Variables	Estimated Coef	Standard Error	tStat	p-value
Intercept	0.014259	0.0022953	6.2124	1.7409e-08
h_{in}	0.00029477	0.00022405	1.3156	0.19175
h_c	-0.0004258	0.00043482	-0.97932	0.33014
h_{out}	0.0001061	0.00025355	0.41844	0.67666
q^2	0.5657	0.71682	0.78918	0.43215

Table 4.5: OLS regression of the valve 100GE ($x_m > 10$mm)

The same regression has been performed on the data of 80NGE and 150GE. The results are shown in Table 4.6 and Table 4.7. For both valves, coefficients for pressures are also small. The regression results indicate that the force balance equation needs to be reformulated.

Variable	Estimated Coef	Standard Error	tStat	p-value
Intercept	0.0082626	0.00087881	9.402	1.9431e-17
h_{in}	9.2924e-06	0.00010404	0.089312	0.92893
h_c	-0.00052439	0.00029008	-1.8077	0.072256
h_{out}	0.00051866	0.00018829	2.7546	0.0064569
q^2	24.486	1.3376	18.306	1.4693e-4

Table 4.6: OLS regression of the 80NGE valve

Variable	Estimated Coef	Standard Error	tStat	p-value
Intercept	0.0069748	0.00097384	7.1622	2.5439e-11
h_{in}	0.0016912	0.00027754	6.0933	7.6254e-09
h_c	-0.0037639	0.00054	-6.9702	7.3412e-1
h_{out}	0.0020771	0.00026391	7.8707	4.5355e-13
q^2	6.1196	0.19594	31.232	6.2401e-71

Table 4.7: OLS regression of the 150GE valve

4.5 Conclusions

The existing ACV models in the literature (PRV models in Prescott and Ulanicki (2003)) accurately represent behaviours of the ACVs. Further important applications of ACV models, which are the focus of this work, are flow estimation and fault diagnosis. This chapter focuses on a mechanistic model because it can provide an explanation for each valve component and interactions between them, which will facilitate fault diagnosis later. This chapter aims to assess the accuracy of an existing ACV model with minor modification (the steady-state model). Two flow estimation methods have been investigated: (i) through the valve stem position and 2 pressure measurements (2P&Pos) and (ii) through 3 pressure measurements (3P).

The 2P&Pos method employs the C_v characteristic relationship to calculate flow at any point of time, while it requires continuous measurements of the valve stem position, the valve inlet pressure and the valve outlet pressure (x_m, h_{in} and h_{out}). The C_v relationship was validated in this chapter through data from experiment phase 1 and phase 2. It was found that the C_v relationship is correct; however, the $C_v(x_m)$ (C_v curve) derived here is different from the C_v curve provided by the manufacturer (Cla-Val). Furthermore, the C_v curves of different valves of the same type have been derived and compared. The C_v relationships were found to be different although the valves were exactly the same. These two discrepancies ((i) between

the manufacturer C_v curve and the C_v curve derived through the experiment and (ii) between different valves of the same type) might not have an impact on some applications such as valve size selection, but it will have an impact on flow estimation accuracy. Therefore, it can be concluded that the C_v relationship is sufficiently accurate and can be used for flow estimation, but it will have to be derived individually for each valve to achieve maximum accuracy.

For the 3P flow estimation method, instead of using the directly measured stem position like in the 2P&Pos case, the valve stem position will be estimated through force balance relationship and the measurement of pressures balancing the valve position above and below the valve diaphragm. Control loop equations in the ACV steady-state model are unnecessary for flow estimation because the control loop provides a feedback control on the outlet pressure by adjusting the control chamber pressure which will be directly measured. However, control loop equations will play an important role in fault diagnosis.

The force balance equation has been validated in this chapter through two methods (i) direct position estimate from the current form of equation and (ii) rearranging all the physical terms into constants and perform Ordinary Least-Squared linear regression from experimental results and compare the physical values from the regression result. It was found that the current form of the force balance equation is not accurate enough for flow estimation. It has also been proved that the simple relationship for the force balance equation does not correctly represent the real phenomena. The force balance equation will need to be reformulated and validated in the next chapter (Chapter 5).

Chapter 5

Automatic Control Valves Model Development for Flow Estimation (Part 2: A derivation of force balance relationship for flow estimation)

This chapter proposes a data-driven parametric force balance relationship and the novel 3P flow estimation method. The force balance equation formulation is explained thoroughly via basic Physics principles. The 3P flow estimation method employs machine learning techniques. The method requires three relationships/models which are the force balance equation, the SVM classification model and the C_v characteristic relationship. All models, including those in different forms and orders, were trained through extensive experimental data from two laboratories. The training performance are compared and discussed. The justification for model selection is explained throughout the chapter.

To provide the idea of this chapter, the 3P flow estimation process is summarised in Figure 5.1 including the inputs and outputs of each process. Details of each process will be explained throughout this chapter

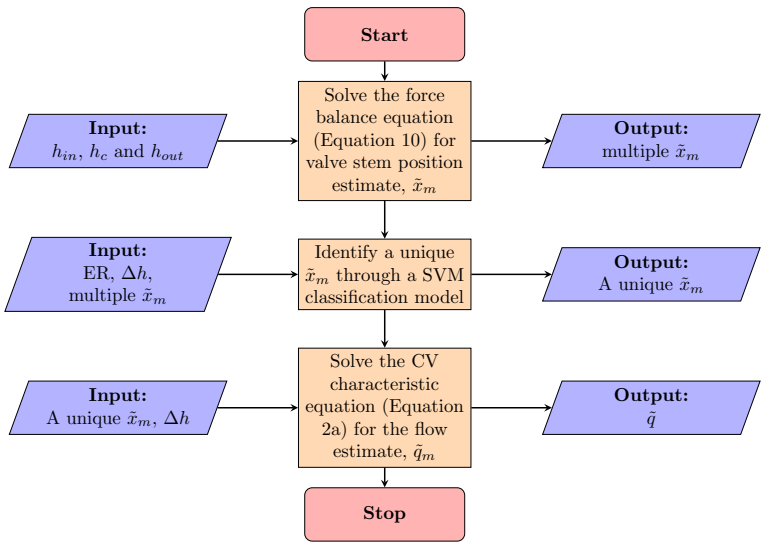

Figure 5.1: 3P Flow estimation process diagram; ER is the signal envelope range.

5.1 Introduction and analysis for improvement of the force balance equation

The validation results in Section 4.4 indicate that the force balance equation (Equation 4.12b) is not accurate enough for flow estimation and hence the force balance equation needs to be reformulated. To reformulate a more accurate force balance equation, the following aspects are considered.

(i) Scale analysis: The scale analysis includes the magnitude approximation of each term in Equation 4.12b. A typical set of operational variables for the valve 100GE is: $h_{in} = 50$m, $h_c = 30$m, $h_{out} = 20$m, $q_m = 20$l/s, $x_m = 10$mm. Each term is shown in Table 5.1. The scale analysis indicates that forces due to spring, flow and weight of the valve plug are small compared to forces due to pressure. Hence, those terms can be negligible in the formulation of a new force balance model.

Force due to	h_{in}	h_c	h_{out}	q_m	Spring	Weight
Expression	$\rho g h_{in} a_1$	$\rho g h_c a_2$	$\rho g h_{out}(a_2 - a_1)$	$\rho q_m^2 / a_1$	$k_{mspr}(x_m + x_0)$	$m_m g$
Value (N)	4189.5	9752	2412.8	11.7	82.9	26.5

Table 5.1: Scale analysis of the force balance equation (Equation 4.12b)

(ii) Pressure distribution at the diaphragm: In the literature, a number of computational

fluid dynamics (CFD) simulations have been performed to study pressure distribution inside the valve body. Pressure variation below the main valve is shown to have a distribution function of a complex non-uniformly distributed shape (An et al., 2008, Qian et al., 2014, Yang et al., 2011). Therefore, pressure acting below the diaphragm should be a form of effective pressure acting on the whole diaphragm area.

(iii) Minor loss and impacts of different opening: According to the Figure 4.16, pressure acting on the diaphragm is significantly different from the measured pressure at the valve inlet and outlet due to a minor loss. This minor loss should depend on the valve's geometry. Since the geometry of the valve changes at different openings, this minor loss should depend on the valve opening. Davis and Stewart (2002) showed that pressure contours are different for different valve openings.

In addition, a computational fluid dynamics (CFD) simulation was preliminarily performed in order to observe a pressure distribution and the pressure loss when the valve was in operation. The simulation was executed via the Simscale simulation package and an illustration of pressure distribution under the valve plug was observed. The simulation result shows that the force below the main valve was not partly affected by the inlet pressure or partly by the outlet pressure as Equation 4.12b suggests. Instead, the pressure under the main valve was not uniformly distributed and was ranging between the valve inlet pressure and outlet pressure.

The force balance equation (Equation 4.12b) validation results and the CFD results in the literature suggest that to have an accurate model for the valve force balance, a new force balance formulation is required. The newly formulated equation shall take into account that the pressure distribution function is non-linear and such a function varies at different valve openings.

Two main approaches can be explored to find an accurate force balance relationship of the diaphragm-actuated globe valve: the CFD analysis approach and the data-driven approach. If the CFD approach is chosen, it will require a large number of parameters as flow through the valve is expected to be highly turbulent and pressure distribution is expected to be non-linear. The accuracy of the CFD model is also sensitive to the chosen parameters which might not be a

good representation of the real world measurement. The data-driven approach, however, allows parameterisation of the non-linear distribution and the turbulence. Any hidden phenomena in the valve can be reflected through a number of measurements. The data-driven approach also allows scaling to different sizes and types of the control valve. Accordingly, the data-driven approach is selected to formulate a new force balance equation. In this chapter, a parametric force balance equation is constructed. A regression will be performed, followed by a residual analysis and a sensitivity analysis. The use of the model for flow estimation is also discussed.

5.2 Parametric force balance equation formulation

The valve stem position (x_m) depends on the balance of forces acting on the membrane (and the disc retainer) and pushing the valve stem downwards and upwards. The downward force, which acts on the top of the diaphragm, is defined by the control chamber pressure (h_c), the spring force and the combined weight of the stem, the disc retainer and the diaphragm. The upward force depends on the pressure beneath the valve diaphragm and the flow momentum change. The force from the flow momentum change is negligible compared to the force from the pressure acting beneath the disc retainer and the diaphragm (see Table 5.1). Furthermore, the pressure, which defines the upward force, is different from the pressure acquired at the inlet and outlet of the valve body (see Figure 5.2b). This pressure difference has a complex form relationship (See CFD results in Davis and Stewart (2002)). An "actuating" pressure beneath the valve diaphragm, h_b, is introduced as an effective pressure acting on the disc retainer and the valve diaphragm. An "actuating" pressure above the valve diaphragm, h_a, includes the pressure measured in the control chamber, the weight of the valve plug and the spring force. Figure 5.2b depicts a force balance principle within the valve body between actuating pressure above and below the diaphragm (h_a and h_b). An animation, which illustrates the operation of the investigated diaphragm-actuated globe valve, is presented by Cla-Val (2016).

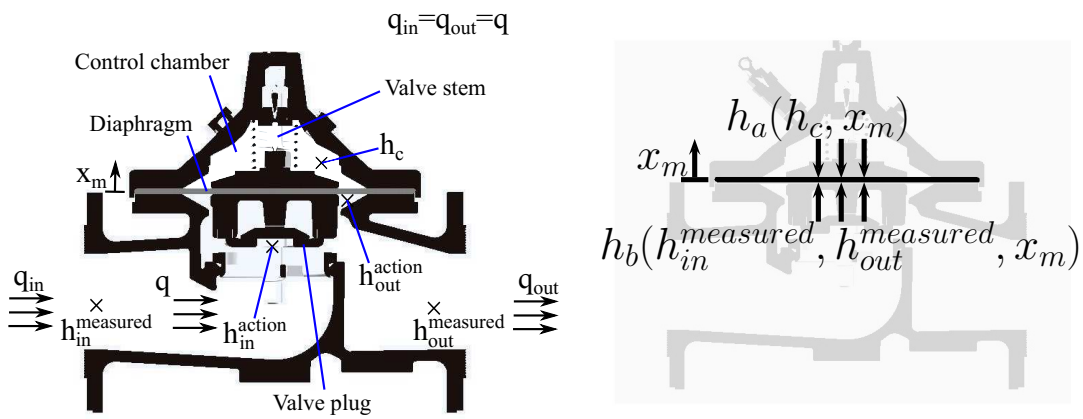

(a) A body of an automatic control valve in WSNs

(b) A depiction of force balance within the valve body

Figure 5.2: A diaphragm-actuated globe valve body is shown in 5.2a; The variables and points where they are measured are also shown. The diagram 5.2b depicts the force balance principles on the valve diaphragm.

Variables h_{in} and h_{out} are measured pressures. Pressure losses from h_{in} to h_b and from h_b to h_{out} are minor losses. Equations 5.1 are minor loss relationships between the inlet measurement point and a point under the diaphragm representative of an “effective pressure" and between the “effective pressure" point and the outlet measurement point.

$$h_{in} - h_b = K_1 \frac{V_1^2}{2g}, \tag{5.1a}$$

$$h_b - h_{out} = K_2 \frac{V_2^2}{2g}, \tag{5.1b}$$

where K_1, K_2 are minor loss coefficients, and V_1, V_2 are the velocities. V_1 and V_2 can be defined differently depending on contexts , i.e. before the change of geometry or the average velocity or the smaller pipe. Herein, flow velocities at a point can be related to another point through a mass balance principle.

Hence, let V_{in} be a velocity before the geometry change (at the inlet measurement point and V_{out} be a velocity after the geometry change (at the inlet measurement point). Then, K_1' and K_2' now become constants which combine both minor loss coefficients and constant responsible for mass balance. Due to the geometry of the inlet and the outlet of the valve and the mass conservation, flows are the same, $q_{in} = q_{out}$, and hence the flow velocities are the same, $V_{in} = V_{out} = V$ (see

Figure 5.2a).

Equations 5.1 become:

$$h_{in} - h_b = K_1' \frac{V^2}{2g}, \tag{5.2a}$$

$$h_b - h_{out} = K_2' \frac{V^2}{2g}, \tag{5.2b}$$

and are rearranged into:

$$h_b = \frac{1}{1 + \frac{K_1}{K_2}} h_{in} + \frac{K_1}{K_2(1 + \frac{K_1}{K_2})} h_{out}. \tag{5.3}$$

Since the loss coefficient is a function of geometry, Equation 5.3 holds true for all values at a particular opening. An additional constant is required to satisfy uncertainties due to hydraulic conditions and due to pressure distribution below the diaphragm. h_b at a certain opening is written in a form of:

$$h_b \mid_{x_m = const} = c_1 h_{in} + c_2 h_{out} + c_3, \tag{5.4}$$

where c_1, c_2 and c_3 are constants. Because the loss coefficients depend on the geometry, the coefficients c_1, c_2 and c_3 change at different openings. An alternative justification for Equation 5.4 is that an effective pressure below the diaphragm is a linear combination of inlet pressure and outlet pressure. The force below the valve diaphragm, h_b, is expressed as a function of the main valve stem position, x_m. Hence, the c_i coefficients are expressed as a function of x_m, $c_i(x_m)$: $c_1(x_m)$, $c_2(x_m)$ and $c_3(x_m)$. Expressions for effective pressure above and below the valve diaphragm are shown in Equation 5.5:

$$h_a = h_a(x_m, h_c) = h_c + \frac{k_{spr}(x_0 + x_m) + m_m g}{\rho g a_{top}}, \tag{5.5a}$$

$$h_b = h_b(x_m, h_{in}, h_{out}) = c_1(x_m) h_{in} + c_2(x_m) h_{out} + c_3(x_m). \tag{5.5b}$$

From the quasi-static approximation, the force balance principle holds true. Therefore, the

forces (and hence the pressure) above and below the diaphragm are equal, $h_a = h_b$,

$$h_c + \frac{k_{spr}(x_0 + x_m) + m_m g}{\rho g a_{top}} = c_1(x_m)h_{in} + c_2(x_m)h_{out} + c_3(x_m). \tag{5.6}$$

The force balance in a diaphragm-actuated globe valve is depicted in Figure 5.2b. The x_m dependent term and the constant term on the left side of Equation 5.6 can be included into $c_3(x_m)$. The force balance equation becomes:

$$h_c = c_1(x_m)h_{in} + c_2(x_m)h_{out} + c_3(x_m). \tag{5.7}$$

5.3 Regression fit of the c_i coefficients

A function $c_i(x_m)$ can be fitted through various function forms. According to a preliminary inspection of experimental results, the same combination of pressures, h_{in}, h_c and h_{out} corresponded to multiple valve stem positions x_m. This will be discussed in detail in Section 5.4. Due to this condition, the function $g(x_m) = h_c - c_1(x_m)h_{in} - c_2(x_m)h_{out} - c_3(x_m) = 0$ must have multiple solutions if the function is solved for x_m. If the function $g(x_m)$ is plotted where x_m is on the x-axis and $g(x_m)$ is on the y-axis, the function must intersect with the x-axis multiple times within the valve operational range. There can be a variety of choices to fit for the coefficients $c_i(x_m)$. The polynomial is selected because it provides both flexibility of model fit by varying polynomial orders and an ease of solving for the position estimate, $\tilde{x}_m$, which will be used for the 3P flow estimation method. The 3P flow estimation method will be discussed in detail in Section 5.4.

The coefficients $c_1(x_m)$, $c_2(x_m)$ and $c_3(x_m)$ are fitted through the ordinary least squares linear regression method. The force balance is most appropriately represented when the system is in equilibrium; therefore measurements of steady-state data to fit for the relationship are performed through experimental set-up 1. A steady state can also be an approximate of transient

states because any transient states are expected to oscillate around or moving toward steady states.

Initially, models for each valve were fitted through a polynomial of degrees 2-6. There are 5 valves to test: Imperial 100GE, 80NGE, 100GE, 150GE and 2nd 100GE. The experiment for the first valve, Imperial 100GE, was carried out in the hydrodynamic lab, Imperial College London, while experiments for the rest were carried out at Cla-Val Europe test lab, Lausanne, Switzerland. Experimental data to be used in regression are the phase 1 data up to about 75% of full opening. These data lie within a normal operational range of the control valve. Based on experience on analysing control valve data, most of the control valves in WSNs are oversized, and rarely operate at the opening higher than 75% because at high opening, volume of the control chamber is small and therefore the valve might lose its ability to control the opening.

The regression goodness-of-fit is shown in Table 5.2. Degrees of polynomials $c_1(x_m)$, $c_2(x_m)$ and $c_3(x_m)$ are equal for each regression. Error DoF is n - p, where n is the number of observations, and p is the number of coefficients in the model, including the intercept. RMSE is the root-mean-square error, which estimates the standard deviation of the error distribution. R-squared and Adjusted R-squared are the coefficient of determination and the adjusted coefficient of determination, respectively. F-stats vs. constant model is a test statistic for the F-test on the regression model. It tests for a significant linear regression relationship between the response variable and the predictor variables. The p-value is the p-value for the F-test on the model. All of the regression results show low RMSE, both R-squared values to be 1 or very close to 1, a very high F-stats value and a very low p-value. This means any forms of the model can be selected to represent the force balance relationship of various valves. However, additional analysis including residual analysis and analyses for model improvement will be performed in the next section.

Table 5.2: Goodness-of-fit of the regression; The regression values are not shown because only the goodness-of-fit of the regression is focused here. The * indicates a strange value of degree of freedom which could be caused by one of the polynomial coefficients is very close to 0.

Valve	Poly. Degree	Error DoF	RMSE (mH_2O)	R-squared	Adjusted R-squared	Fstats vs constant model	p-value
Lab 100GE	2	300	0.0809	1	1	2.59E+05	0
	3	297	0.0536	1	1	4.29E+05	0
	4	294	0.0521	1	1	3.57E+05	0
	5	291	0.0469	1	1	3.62E+05	0
	6	288	0.0456	1	1	3.26E+05	0
80NGE	2	117	0.122	1	1	3.50E+04	7.52E-194
	3	114	0.123	1	1	2.50E+04	2.68E-187
	4	111	0.118	1	1	2.13E+04	2.60E-183
	5	108	0.0984	1	1	2.54E+04	3.84E-186
	6	105	0.0723	1	1	4.00E+04	2.77E-194
100GE	2	170	0.109	1	1	1.48E+05	2.7e-322
	3	167	0.0932	1	1	1.47E+05	0
	4	164	0.0576	1	1	3.02E+05	0
	5	161	0.0565	1	1	2.58E+05	0
	6	158	0.0553	1	1	2.29E+05	0
150GE	2	153	0.0305	1	1	4.55E+05	0
	3	150	0.0255	1	1	4.75E+05	0
	4	147	0.0154	1	1	1.03E+06	0
	5	144	0.0148	1	1	9.05E+05	0
	6	142*	0.0147	1	1	8.28E+05	0
100GE 2nd	2	73	0.0926	0.999	0.999	1.81E+04	4.06E-117
	3	70	0.0926	1	0.999	1.32E+04	2.15E-111
	4	67	0.0805	1	1	1.37E+04	5.73E-110
	5	64	0.0504	1	1	2.84E+04	1.97E-117
	6	61	0.0499	1	1	2.49E+04	1.16E-111

5.3.1 Residual analysis

Residual is the difference between predicted values and real data. For a good model, the distribution of the residual must be stochastic. This property is ensured by performing residual analysis. There are two main approaches for residual analysis: graphical methods and numerical methods. Graphical methods have an advantage of being able to illustrate complex aspects of any relationships between residuals and variables. Numerical methods tend to focus on a particular aspect of relationships; however, they can quantify the goodness of different models. For graphical analysis, plots of the residuals against predictor variables, or potential predictors, can assess the sufficiency of the functional part of the model. The plot of the residual against

the predicted variable is also important, as it is also expected to be symmetrically distributed, to cluster toward 0 and to show no clear patterns. If any plots show any regular structures, the form of the function can be improved although the model could still be valid depending on applications.

Examples of unwanted patterns of residual plots are:

1. **Unbalanced residuals**: This means some of the prediction errors can be very high at one side and relatively low on the other side (over-predicted and under-predicted or vice versa). This suggests that the model could lack predictor(s) or the data require a transformation.

2. **Heteroscedasticity**: Residuals are larger at one side of the variables. Similar to the unbalanced residuals, the model could lack predictors or the data require a transformation.

3. **Non-linear pattern**: Residuals show non-linear patterns with some variables. This indicates that the regression is sub-optimal and the formulated terms can be improved. The cause of this could be missing variables or that it requires a new formulation of the model.

4. **Outliers**: Output outliers indicate that the model fails to predict some data points. It might come from measurement or data entry error, or it might be a legitimate outlier which requires impact assessment. Input outliers can affect model regression in a manner that reduces the error of an outlier point.

5. **Large residual data points**: On a residual plot against the predicted variable, residuals cluster around some other points which are not 0. The model will have prediction limitation. A likely cause for this is missing variables. Variable transformation could also resolve the issue.

6. **Unbalanced predicted variables**: Unbalanced predicted variables can be observed through a residual plot against the predicted variable. The feature is that the number of predicted variable data is much higher on one side than the other. Sometimes the model

is accurate despite this feature, but it is often the case that the model can be made more accurate.

The valve stem estimation functions were fitted with polynomials of varying degrees for x_m. These models had similar residuals defined by:

$$Res = h_c - (c_1(x_m)h_{in} + c_2(x_m)h_{out} + c_3(x_m)). \tag{5.8}$$

There is no definite method for the selection of the polynomial degree for each case. The model was fitted with various orders and a residual analysis was performed to obtain the most suitable degree of the polynomial, which depends on the valve size, hydraulic conditions and training datasets. Even though the most appropriate model order might not be selected, the model can still be applied to estimate the valve stem position, and therefore flow. High order polynomials can be selected when large training data sets are available with multiple flow combinations. Smaller training datasets could result in over-fitting, and consequently a failure in estimating the stem position reliably from new pressure data.

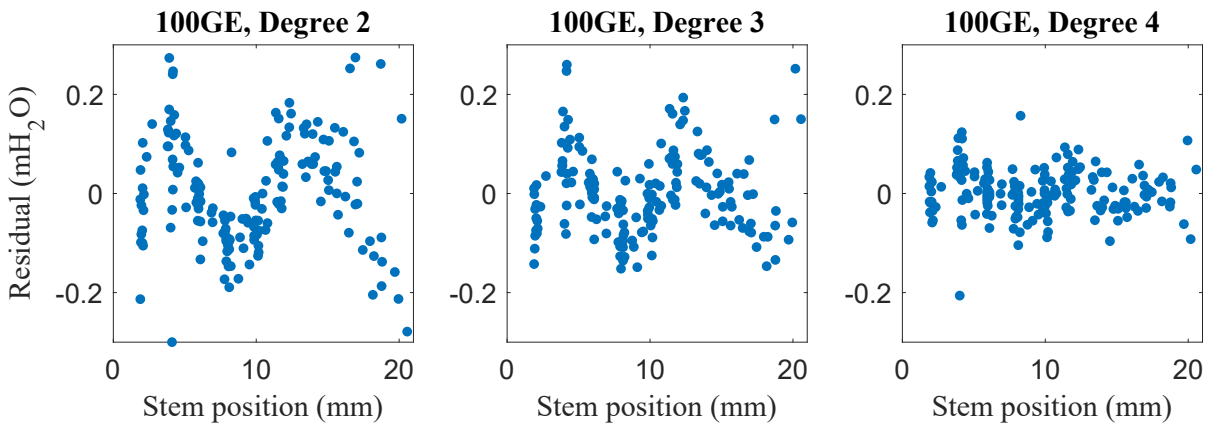

(a) Residual plots against valve stem position, 100GE

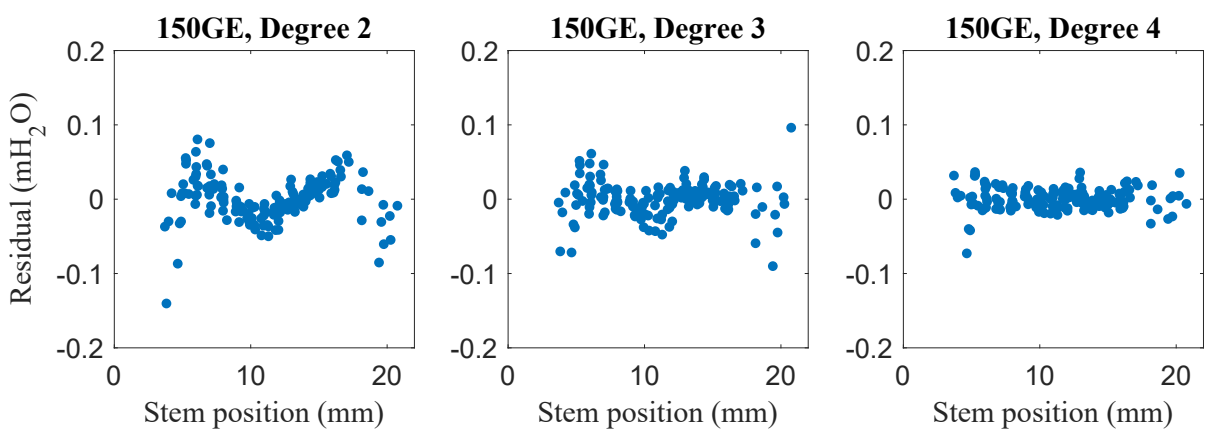

(b) Residual plots against valve stem position, 150GE

Figure 5.3: Example of residual plots against the valve stem position of two valves (100GE and 150GE); polynomial degree increases from 2-4

Figure 5.3a and Figure 5.3b show examples of the observed pattern on 100GE and 150GE, where residuals are plotted against the valve stem position. The polynomial degree increases from 2 to 4 and the non-linear pattern of M-shape reduces when the polynomial degree increases. When the polynomial degree is 4, the pattern is hardly observed.

The other two 100GE valves present similar results to the shown 100GE. However, the 80NGE shows a non-linear pattern even when the fitted polynomial degree is 6. If the polynomial degree is high, it risks overfitting and will also make the position estimation problem more difficult, as solving for the valve position estimate can lead to many solutions. Therefore, for most of the valves under test, models of degree 4 are the simplest models with no observed non-linear pattern.

For the experimental data sets, which were acquired from the control valves installed in a

laboratory pipe rig, the valve stem estimation functions were selected to be a fourth degree (quartic) polynomials for the three investigated valve sizes. Quartics have zero to four roots, and zero to three turning points (local extrema; or points, at which the derivative changes sign), and no general symmetry.

Since the model coefficients depend on valve sizes, hydraulic conditions and training datasets, the number of roots and the number of turning points within a feasible range depends on the completeness of the training datasets. According to our training datasets for the Cla-Val DN100 GE and Cla-Val DN150 GE, the valve stem estimation functions contain no more than two turning points within the full operational range. In comparison, and based on the experimental data, the valve stem estimation function contains no more than three turning points within the full operational range for the Cla-Val DN80 NGE. Consequently, the solution of a valve stem estimation function (Equation 5.10) results in no more than two solutions for Cla-Val DN100 GE and Cla-Val DN150 GE valves, and no more than three solutions for a Cla-Val DN80 NGE. It should be noted that the lowest stem position solution for a Cla-Val DN80 NGE is not a correct solution. This is because the polynomial is fitted with the same high order model using a smaller data range due to the narrow operational length of the valve stem movement. Furthermore, a typical operational range for diaphragm-operated globe valves is a valve stem position of up to 75% open. It is highly unusual for these control valves to operate as fully opened (or above 75%).

5.3.2 Analyses for model improvement

One way to look for improvement of a model is to make sure that all of the coefficients are significant. The software for this calculation is MATLAB statistics and machine learning toolbox Options for calculations available to investigate the significance level of each coefficient are:

1. Standard error: The standard error of the coefficient estimators.

2. t-statistic: t-statistic for each coefficient to test the null hypothesis that the corresponding

coefficient is zero against the alternative that it is different from zero, given the other predictors in the model. In this case, the t-statistic value is calculated from $t_{\tilde{\beta}} = \frac{\tilde{\beta}-\beta_0}{s.e.(\tilde{\beta})}$, where $\tilde{\beta}$ is an estimator of parameter β in some model, β_0 is a constant for the null hypothesis to be tested against (0 in this case) and $s.e.(\tilde{\beta})$ is the standard error of the estimator.

3. F-statistic p-value: The test for F-statistic of the hypotheses that the corresponding coefficient is equal to zero or not. In this case, it consists of a number of hypothesis tests which compare the model with and without the corresponding coefficient. The F-test compares the variances of the residuals with and without the particular coefficient. The test result comes in a form of probability that the similarity of the variance distribution happens by chance (p-value). The p-value helps to decide if the null hypothesis that the corresponding coefficient is 0 should be rejected. The analysis of F-statistic is sometimes referred to as the analysis of variance (ANOVA).

The F-statistic p-value was chosen for the analysis because it allows users to set the acceptable significant level and reject any terms with higher p-value. Typical values for acceptable p-value are 0.05, which means it has 5% that the result is obtained by chance.

According to the previous analysis in Section 5.3.1, the model with the 4th order polynomial terms of the valve stem position (the 4th order model) was selected for further analysis. As models of the same type of control valves are expected to be similar, analysis for model improvement was performed on models of three valve sizes, which are 80NGE, 100GE and 150GE. The other two models of 100GE (the 2nd 100GE and the lab 100GE) were expected to have similar results to the 100GE. Regression results of the 4th order model is presented in Table 5.3, Table 5.4 and Table 5.5.

From the 4th order model of the three valves as shown above, some of the p-values of the F-statistic show were higher than the acceptable value of 0.05. Those models were improved by adding/cutting terms and re-performing the regression multiple times. It is also important to perform a residual analysis for each model. As a result, a new version of models with acceptable

Table 5.3: 4th order model coefficients of the 80NGE; The RMSE obtained is 0.118 mH_2O. The expression terms on the leftmost of the table represent coefficients corresponding to each term.

	Estimate	SE	tStat	pValue
$h_{in}x_m^4$	6.61E-05	4.02E-05	1.642864	0.103241
$h_{in}x_m^3$	-0.00182	0.001038	-1.7553	0.081967
$h_{in}x_m^2$	0.019962	0.009501	2.100984	0.037906
$h_{in}x_m$	-0.09831	0.036193	-2.71634	0.007658
h_{in}	0.524894	0.048084	10.91612	2.76E-19
$h_{out}x_m^4$	2.32E-05	8.34E-05	0.277932	0.781581
$h_{out}x_m^3$	-0.00057	0.002095	-0.27114	0.786788
$h_{out}x_m^2$	0.002664	0.018592	0.143278	0.886331
$h_{out}x_m$	0.009966	0.068304	0.145903	0.884263
h_{out}	0.590727	0.086496	6.829547	4.77E-10
x_m^4	-0.00512	0.002368	-2.16121	0.032828
x_m^3	0.137462	0.060687	2.26509	0.025448
x_m^2	-1.31	0.551042	-2.37732	0.01915
x_m	5.192426	2.081356	2.494732	0.014078
Intercept	-8.11422	2.740591	-2.96076	0.003753

Table 5.4: 4th order model coefficients of the 100GE; The RMSE obtained is 0.0576 mH_2O. The expression terms on the leftmost of the table represent coefficients corresponding to each term.

	Estimate	SE	tStat	pValue
$h_{in}x_m^4$	-1.47E-05	9.89E-07	-14.9046	2.60E-32
$h_{in}x_m^3$	0.000497	3.59E-05	13.83287	2.45E-29
$h_{in}x_m^2$	-0.00396	0.000463	-8.54456	8.52E-15
$h_{in}x_m$	-0.00318	0.002494	-1.27425	0.204379
h_{in}	0.547864	0.00465	117.8142	2.08E-160
$h_{out}x_m^4$	1.56E-05	1.57E-06	9.91635	1.88E-18
$h_{out}x_m^3$	-0.00054	6.12E-05	-8.79994	1.83E-15
$h_{out}x_m^2$	0.004683	0.000821	5.703684	5.34E-08
$h_{out}x_m$	-0.0019	0.004374	-0.43462	0.664409
h_{out}	0.46317	0.007525	61.54907	3.01E-115
x_m^4	4.00E-05	2.73E-05	1.465208	0.144779
x_m^3	-0.00128	0.001205	-1.06169	0.289938
x_m^2	0.013946	0.018408	0.757577	0.449791
x_m	-0.04499	0.112448	-0.40006	0.689636
Intercept	-1.16874	0.225768	-5.17671	6.54E-07

Table 5.5: 4th order model coefficients of the 150GE; The RMSE obtained is 0.0154 mH_2O. The expression terms on the leftmost of the table represent coefficients corresponding to each term.

	Estimate	SE	tStat	pValue
$h_{in}x_m^4$	-9.39E-06	8.53E-07	-11.0187	5.85E-21
$h_{in}x_m^3$	0.000409	3.84E-05	10.65846	5.22E-20
$h_{in}x_m^2$	-0.00536	0.000622	-8.61649	9.97E-15
$h_{in}x_m$	0.019997	0.00423	4.727267	5.28E-06
h_{in}	0.521173	0.01006	51.80583	2.58E-96
$h_{out}x_m^4$	9.37E-06	7.81E-07	12.00916	1.40E-23
$h_{out}x_m^3$	-0.00041	3.47E-05	-11.8299	4.17E-23
$h_{out}x_m^2$	0.005463	0.000561	9.738281	1.34E-17
$h_{out}x_m$	-0.02152	0.003836	-5.61011	9.75E-08
h_{out}	0.484039	0.009215	52.52673	3.75E-97
x_m^4	2.76E-05	2.42E-05	1.144202	0.2544
x_m^3	-0.00119	0.001176	-1.01592	0.311336
x_m^2	0.017277	0.020191	0.855665	0.393576
x_m	-0.09012	0.143761	-0.62687	0.53172
Intercept	-0.8073	0.353553	-2.2834	0.02384

p-values was obtained. The new version of models is shown in Table 5.6, Table 5.7 and Table 5.8.

Although the p-value of each term was much lower, the RMSE was not very different from the 4th order model and sometimes even higher than the 4th order model. Therefore, the 4th order model was selected for further analysis. The 4th order model basis would then be the default basis for modelling a new test valve. Since the geometry of a new test valve can be completely different from the valves in this work, it is important to note that the residual analysis would have to be performed every time.

Table 5.6: An improved model of the 80NGE; The RMSE obtained is 0.0918 mH_2O. The expression terms on the leftmost of the table represent coefficients corresponding to each term.

	Estimate	SE	tStat	pValue
$h_{in}x_m^3$	1.37E-04	1.75E-05	7.822322	2.99E-12
$h_{in}x_m^2$	-0.00125	1.91E-04	-6.53596	1.89E-09
h_{in}	0.363616	0.00274	132.7116	6.75E-126
$h_{out}x_m^3$	-1.72E-05	4.84E-06	-3.55201	5.59E-04
h_{out}	0.646123	0.002361	273.6091	2.76E-161
x_m^7	-6.80E-05	2.21E-05	-3.07234	2.66E-03
x_m^6	0.003477	1.00E-03	3.4647	7.51E-04
x_m^5	-0.07376	0.018786	-3.92606	1.49E-04
x_m^4	0.836406	0.187575	4.459041	1.95E-05
x_m^3	-5.44098	1.074083	-5.0657	1.60E-06
x_m^2	2.02E+01	3.51E+00	5.744101	7.93E-08
x_m	-39.1952	6.05348	-6.47482	2.55E-09
intercept	29.65476	4.256781	6.966476	2.29E-10

Table 5.7: An improved model of the 100GE; The RMSE obtained is 0.982 mH_2O. The expression terms on the leftmost of the table represent coefficients corresponding to each term.

	Estimate	SE	tStat	pValue
$h_{in}x_m^4$	-4.31E-05	6.62E-06	-6.50297	8.65E-10
$h_{in}x_m^3$	0.001383	1.74E-04	7.972712	2.27E-13
$h_{in}x_m^2$	-0.01136	0.001246	-9.1147	2.32E-16
h_{in}	0.641334	0.018274	35.09535	2.99E-79
$h_{out}x_m^4$	0.00011	8.49E-06	12.98201	3.91E-27
$h_{out}x_m^3$	-3.68E-03	2.24E-04	-16.4395	8.18E-37
$h_{out}x_m^2$	0.031939	1.47E-03	21.79532	7.72E-51
x_m^4	-0.00076	0.000167	-4.56964	9.43E-06
x_m^3	0.026891	0.005496	4.893008	2.31E-06
x_m^2	-0.24631	0.047784	-5.15455	7.08E-07
intercept	3.25E+00	8.74E-01	3.714774	0.000277

Table 5.8: An improved model of the 150GE; The RMSE obtained is 0.018 mH_2O. The expression terms on the leftmost of the table represent coefficients corresponding to each term.

	Estimate	SE	tStat	pValue
$h_{in}x_m^4$	-4.49E-06	2.25E-07	-19.9439	2.11E-44
$h_{in}x_m^3$	0.000197	6.74E-06	29.22818	1.71E-64
$h_{in}x_m^2$	-0.00213	5.54E-05	-38.4827	1.40E-80
h_{in}	5.63E-01	9.59E-04	586.3918	2.46E-258
$h_{out}x_m^4$	4.35E-06	2.87E-07	15.15949	2.81E-32
$h_{out}x_m^3$	-1.93E-04	8.97E-06	-21.5178	3.94E-48
$h_{out}x_m^2$	0.002104	7.71E-05	27.27752	1.22E-60
h_{out}	0.436417	0.001449	301.278	3.98E-214
Intercept	-0.90971	0.010496	-86.6713	5.99E-132

5.4 Introduction to the 3P flow estimation method and multiple solutions problem

The purpose of the force balance model is to be able to solve for the valve stem position estimate ($\tilde{x}_m$) from 3 pressure measurements which are, h_{in}, h_c and h_{out}. The position estimate will be plugged into the C_v relationship with measured h_{in} and h_{out} to solve for the flow estimate $\tilde{q}$. This proposed method will be called the 3P flow estimation method.

A major benefit of building a model with polynomial bases is that it is straightforward and fast to achieve solutions. The force balance equation in a form of:

$$h_c = c_1(x_m)h_{in} + c_2(x_m)h_{out} + c_3(x_m). \tag{5.9}$$

can be rearranged into the position estimation defined by:

$$g(x_m; h_{in}, h_c, h_{out}) = c_1(x_m)h_{in} + c_2(x_m)h_{out} + c_3(x_m) - h_c = 0. \tag{5.10}$$

.

The estimation function, Equation 5.10, comes from the regression results that calculate the discrepancy between the force above the diaphragm and the force below the valve diaphragm at various valve stem positions. At the position that is corresponding to the force balance, the discrepancy should be 0. Therefore, one of the roots of the force balance equation should be the valve stem position estimate ($\tilde{x}_m$).

Equation 5.10 is a polynomial equation which can be solved through certain algorithms. One of the efficient algorithms to solve the polynomial equation is solving through the companion matrix. The companion matrix to a monoic polynomial:

$$a(x) = a_0 + a_1x + ... + a_{n-1}x^{n-1} + a_nx^n \tag{5.11}$$

is the $n \times n$ square matrix,

$$A = \begin{bmatrix} 0 & 0 & \dots & 0 & -a_0 \\ 1 & 0 & \dots & 0 & -a_1 \\ 0 & 1 & \dots & 0 & -a_2 \\ \vdots & \vdots & \ddots & \ddots & \vdots \\ 0 & 0 & \dots & 1 & -a_{n-1}, \end{bmatrix} \tag{5.12}$$

with ones on the subdiagonal and the last column given by the coefficients of $a(x)$. Sometimes, the companion matrix is defined as the transpose of the matrix in 5.12. The roots of the polynomial in 5.11 were calculated by computing the eigenvalues of the companion matrix, A. The results were the exact eigenvalues of a matrix within roundoff error of the companion matrix, A. However, this does not mean that they are the exact roots of a polynomial whose coefficients are within roundoff error of those in $a(x)$.

With this solving method, solving the estimation function $g(x_m; h_{in}, h_c, h_{out})$ can lead to multiple roots. According to the formulation and practical validation, one of them is a correct solution, which minimises the discrepancy between the position estimate, $\tilde{x}_m$ and the position measured, x_m.

Multiple roots can either come from the nature of the system, or from the regression. Further investigation is required to find causes of other roots.

5.4.1 Multiple solutions of the valve force balance equation

The valve stem position estimation function (Equation 5.10) can have multiple roots. Multiple roots result from the hydraulic conditions defined by the valve geometry and the control loop, and the resulting pressures/forces acting upon the valve membrane. To prove that the multiple roots arise from physical property of the valve, this research demonstrated experimentally that identical sets of pressures can correspond to different valve stem positions and therefore, to multiple roots (see Figure 5.4). The derivation of a parametric force balance equation, which is applied to the membrane of a valve, takes into account the various combinations of pressures

and valve stem positions. The control chamber is pressurised with water, and the volume of water within a control chamber discharges and recharges according to the differential pressure at the control loop connection (T-junction). As a result, it is feasible to have the same control chamber pressure at different valve stem positions (valve openings) as the hydraulic conditions change. It is also unnecessary to measure pressure at any other points in the control loop because the objective of the control loop is to control pressure in the control chamber which is directly measured.

As an illustration, Figure 5.4a shows multiple steady states for the Cla-Val DN80 NGE. With relatively constant h_{in} and h_{out}, h_c varies and reveals a non-monotonic behaviour as both the flow rate and valve stem position increase. In addition, two steady-state flows are presented with the same combination of pressure variables but different valve stem positions using a parallel coordinate plot (Figure 5.4b). The derivation of a parametric force balance equation takes into account the various combinations of pressure readings and valve stem positions that result from balancing the forces acting upon the membrane. Examples of valve stem estimation functions are plotted in Figure 5.5 for Cla-Val DN80 NGE and Cla-Val DN100 GE for a given set of three measured pressure variables.

From Section 5.3.1, the 4th order model was chosen. Therefore, the estimation functions for the three valve sizes are degree 4 polynomials, which can have up to four real solutions. For the valves DN100 GE and DN150 GE, the estimation functions contain no more than two turning points (a point at which the derivative changes sign) within a full operational range. For the valve DN80 NGE, the estimation function contains no more than three turning points within a full operational range. Within this operational range, solving an estimation function (Equation 5.10) will end up with no more than two solutions for DN100 GE and DN150 GE, and no more than three solutions for DN80 NGE. The operational range is determined to be the valve stem position of up to 75% of the fully opened position as it is not recommended for the valve to operate in a higher stem position range. Based on experience, most of the valves in networks are slightly oversized to avoid such a range. The shape of an estimation function is a property of the valve geometry fitted by data and therefore cannot be avoided. A detailed analysis of the method used to guide the correct solution is in Section 5.5.

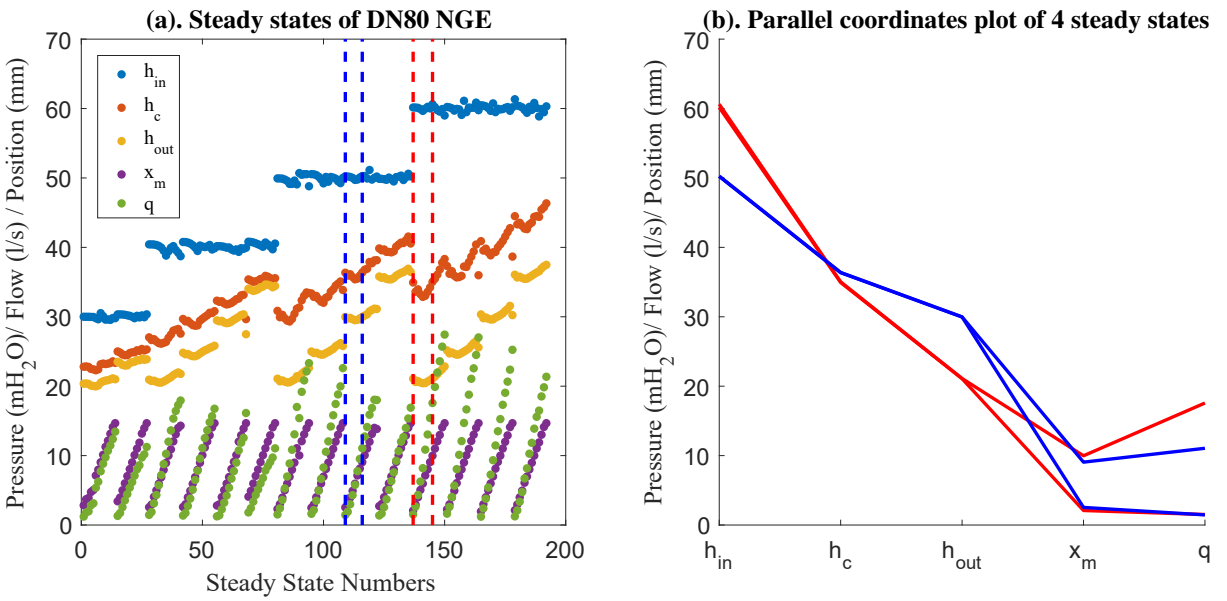

Figure 5.4: Figure (a) shows steady-state flow rates for a Cla-Val DN80 NGE. All variables are adjusted to be on the same scale. The x-axis represents the number of steady-state flows (individual experimental tests); each of which demonstrates a combination of measured pressures, flow and a valve stem position. Four steady states (experimental tests), which are identified in dash lines in (a), are also displayed across multiple dimensions using a parallel coordinate plot in (b). Figure (b) displays two sets of experimental tests with the same measured pressure data but different valve stem positions and flow rates.

(a.) Estimation functions of DN80 NGE with different orders (b.) Estimation functions of DN100 GE with different orders

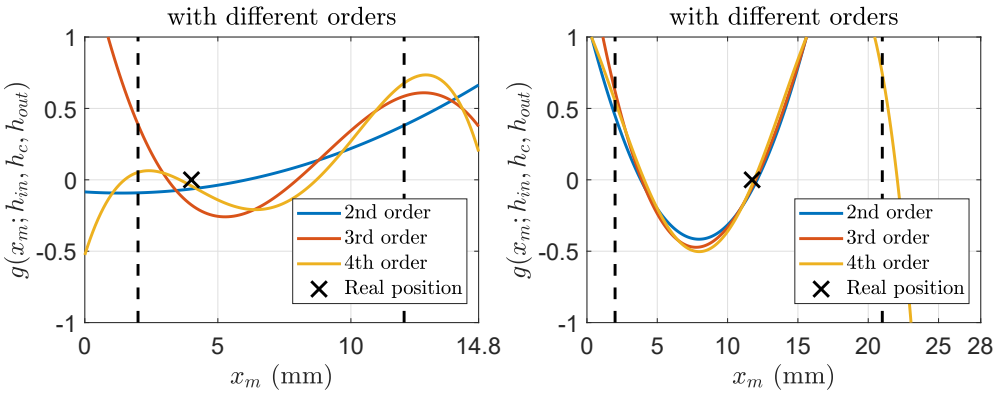

Figure 5.5: Examples of valve stem position estimation functions for (a.) Cla-Val DN80 NGE and (b.) Cla-Val DN100 GE; Each estimation function is subjected to a combination of three pressures. Corresponding stem position measurements are shown by the cross. The data range, which was used for model training, is bounded by the dash lines and it corresponds to the valve opening between 14% and 80% for the Cla-Val DN80 NGE and between 7% and 75% for the Cla-Val DN100 GE

The estimation function calculates the discrepancy between the forces above and below the diaphragm according to the derived model. Under normal circumstances, the discrepancy is minimised at a valve stem position that makes the estimation function 0, and therefore one of

the roots of the estimation function is the corresponding solution for the force balance equation. However, in some cases, the estimation function which tries to minimise the force discrepancy fails to provide the discrepancy of 0. Instead, within the operational range, the corresponding valve stem position only provides an optimal point which is the closest to 0. Therefore, it is necessary to add this optimal point into one of the candidates for the position estimate. A heuristic rule which adds those points into candidates is added on top of solutions to the estimation function. The rule selects a minima if the estimation function is higher than 0, and select a maxima if the estimation is lower than 0.

At this point, real solutions of the estimation function and an additional point from the heuristic rule within the valve stem position operational range are candidates for the valve stem position estimate ($\tilde{x}_m$).

5.4.2 Preliminary signal analysis for correct solution guidance

Sets of experiment for signal analysis were performed at Imperial Laboratory with the PRV DN100 GE with the sampling rate of 100 Samples/s. In the experimental pipe rigs, pressure signals were continuously measured. By making a step change on the gate valve downstream to the PRV, it was observed that the pressure signals oscillated more as the downstream gate valve was more opened, i.e. higher flow and higher valve stem position. The pressure dynamic range is therefore a good candidate to identify the correct solution to the estimation function because out of the two solutions, one is associated with higher valve opening and therefore a higher dynamic range, and the other with a lower opening and therefore with a lower dynamic range.

Bull and Lim (1968) shows that the wall-pressure fluctuation increases with the Reynolds number. Within the same operational rig, the Reynolds number is proportional to flow. This phenomenon has also been illustrated experimentally in the laboratories. This feature can be seen clearly in Figure 5.6. The step changes of flow indicate the step change of the downstream gate valve. For pressure dynamic range investigation, the outlet pressure is the most suitable among other pressure signals, as it has a higher dynamic range than the inlet pressure and

control chamber pressure. This dynamic range represents a high frequency signal dynamic (or oscillation of the signal measurement) which varies although the measured signal is relatively constant. Therefore, a variable that represents the level of pressure fluctuation can be used for classification.

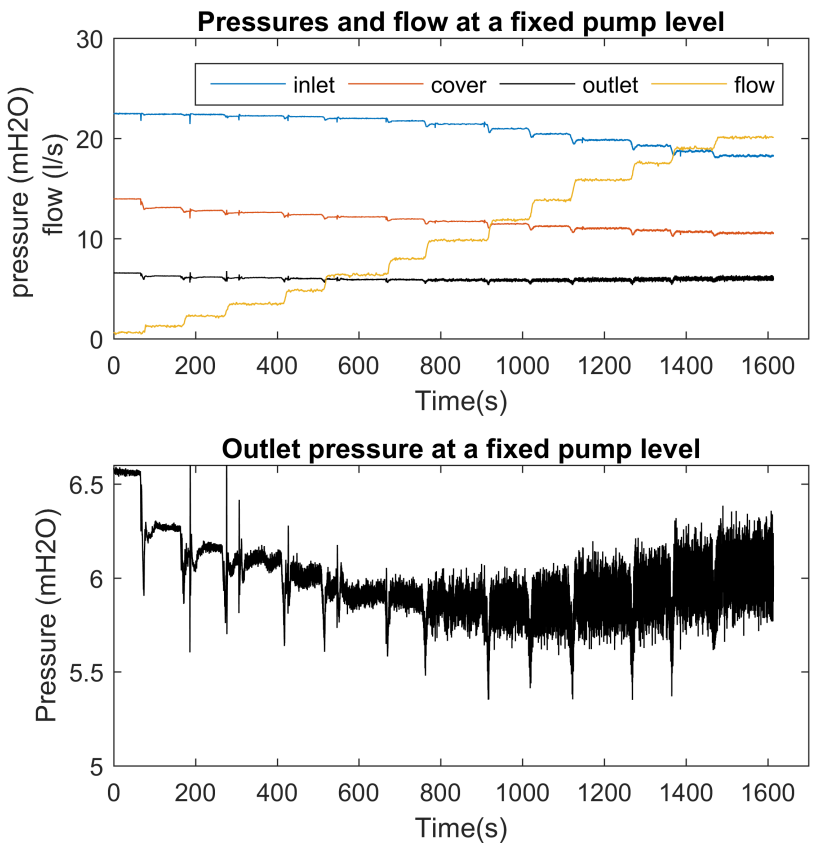

Figure 5.6: An example of the experiment showing pressures and flow signals at a fixed pump setting; The downstream gate valve was opened in steps. Spikes that occurred throughout the experiment were caused by pump circuit.

Frequency domain spectrum analysis of pressure signal

The frequency domain analysis is performed to find out if there is any predominant frequency responsible for the signal dynamic range. Both the fast Fourier transform (FFT) and the short time Fourier transform (STFT) methods were used for frequency domain analysis. For the FFT analysis, only steady states of the outlet pressure signal were analysed separately. As a result from the FFT, a periodogram power spectral density (PSD) estimate of the outlet pressure in 9 steady states is shown in Figure 5.7, where the valve position decreases from '1' to '9'. Since

the sampling rate is 100 Sample/s (100Hz), the PSD is shown up to 50 Hz (half of the sampling rate). The spectrogram is a result of the STFT analysis shown in Figure 5.8. Since the PSD shows that the PSD lies mostly between -30 to -70 dB/Hz, the spectrogram therefore shows the result shaded between -30 to -70 dB/Hz.

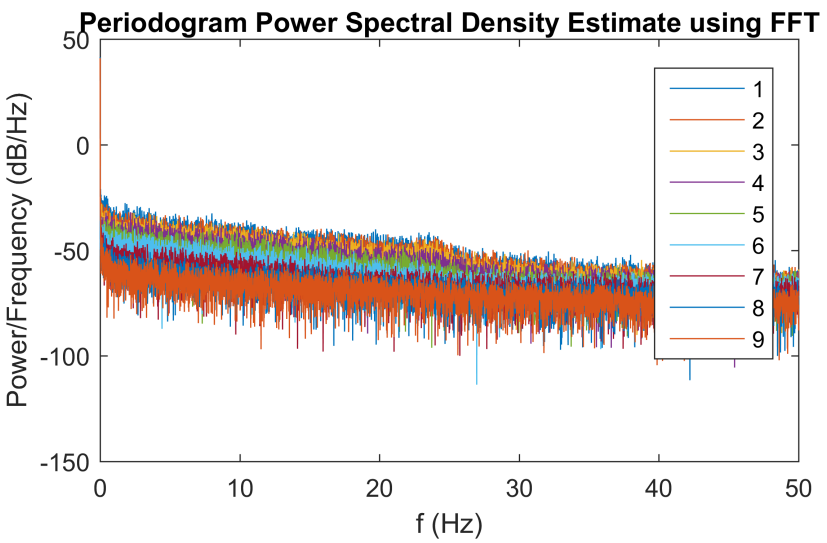

Figure 5.7: PSD of the outlet pressure in consecutive 9 steady states, where the valve opening decreases from 1 to 9.

Both Figure 5.7 and Figure 5.8 illustrate that the signal power is higher at higher valve opening throughout the whole frequency domain. No clear peak in the frequency domain is observed. The result implies pressure oscillation is random and caused by dynamics of the flow including turbulence. Although it can be seen that the power density of low opening signals fluctuates around a lower value than that of the high opening, it is still hard to compare them in frequency domain. In Figure 5.8, the STFT established a pattern in the time domain showing that the power throughout the whole range of frequency gradually changes over time.

Results of the frequency analysis show that higher signal oscillation when flow is higher indicates no specific frequency responsible for this oscillation. Signals with higher oscillation show higher power throughout the frequency domain. Therefore, a variable indicating the level of signal dynamic range should be extracted in the time domain.

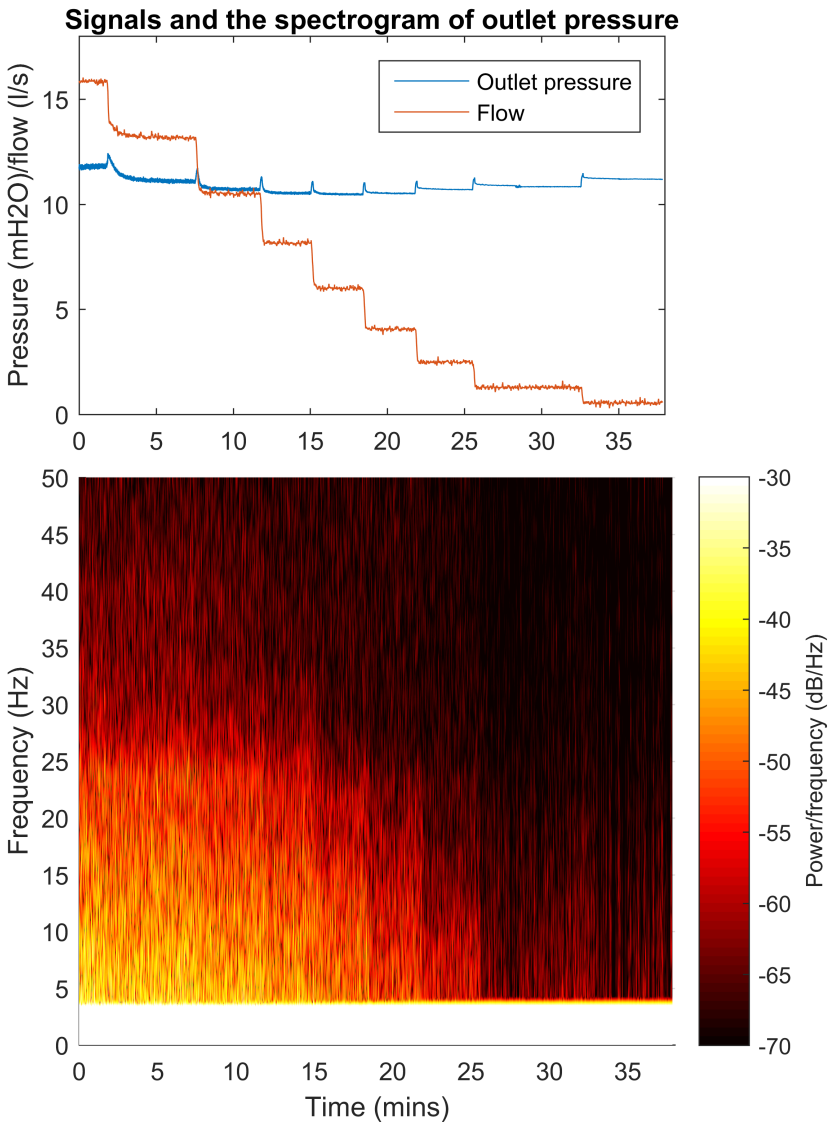

Figure 5.8: Outlet pressure and flow with a spectrogram of outlet pressure

Time domain spectrum analysis of pressure signals

This analysis particularly compares and discusses methods that return a variable indicating the signal dynamic range at a specific period of time. Signal envelope, which has been traditionally used for fault detection, has an interesting feature that makes the envelope a good measure of pressure fluctuation. Candidate methods of analysis are the signal envelope from analytic signal (Hilbert transformation), the RMS envelope and the peak envelope.

The analytic envelope and the RMS envelope are symmetrical with respect to the mean value of the signal, because both Hilbert transformation and the RMS of the signal return one value at a point of signal in the time domain. The envelope is therefore the mean plus/minus that value. In the control valve signal, the mean value can change when the control profile is changed. Both the analytic and the RMS envelope sizes are larger in a period of time when the pressure signal is increasing or decreasing. This feature makes the analytic envelope and the RMS envelope unsuitable for further analysis because when pressure is changing, those envelope values do not represent the pressure dynamic range.

On the other hand, the peak envelope is calculated from spline interpolation over local maxima and minima separated by a number of samples which can be specified. In MATLAB, the peak envelope tool utilises MATLAB findpeaks routine, which makes use of max and imregionalmax to detect local maxima. The peak envelope value does not increase when pressure is changing and therefore well represents the pressure dynamic range.

Figure 5.9 compares 3 types of envelope of the continuously decreasing signal. All types were calculated using the same size of the sliding window of 2000 samples. The sample rate was 1200 Hz.

Alternatively, the moving standard deviation can also represent the pressure dynamic range. It indicates how much the signal spreads out from the moving average. However, the value of the moving standard deviation will be high when the steady state changes. For example, in Figure 5.9, the value of the moving standard deviation would rise at time points 610s and 650s.

In conclusion, since the peak envelope is a good measure for the dynamic range of signals, further investigation will be carried out based on the peak envelope. A variable extracted from the peak envelope will be detailed in Section 5.5.1.

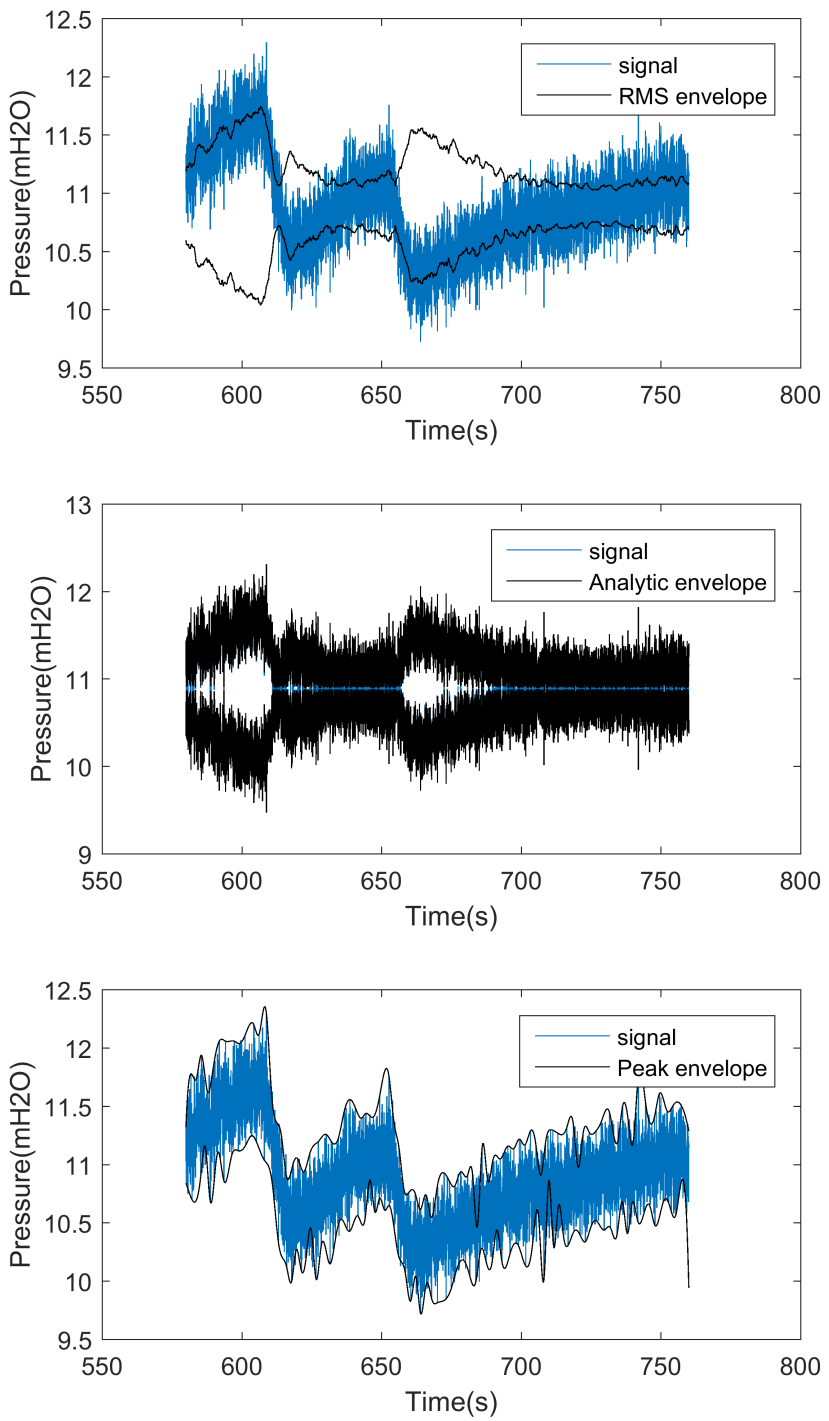

Figure 5.9: A comparison of different types of envelope of a part of the PRV outlet signal

5.5 Multiple solutions classification for the 3P flow estimation

The presence of multiple solutions in solving the position estimation function, $g(x_m; h_{in}, h_c, h_{out})$, indicates that an extra variable is required to identify solutions. Instead of having an extra sensor, the data acquisition system with high frequency can provide an additional variable through signal sampling. In this section, a method to identify a correct estimate out of multiple solutions is proposed. The method includes an analysis of the pressure signals and a classification process.

5.5.1 The definition of pressure envelope range, ER

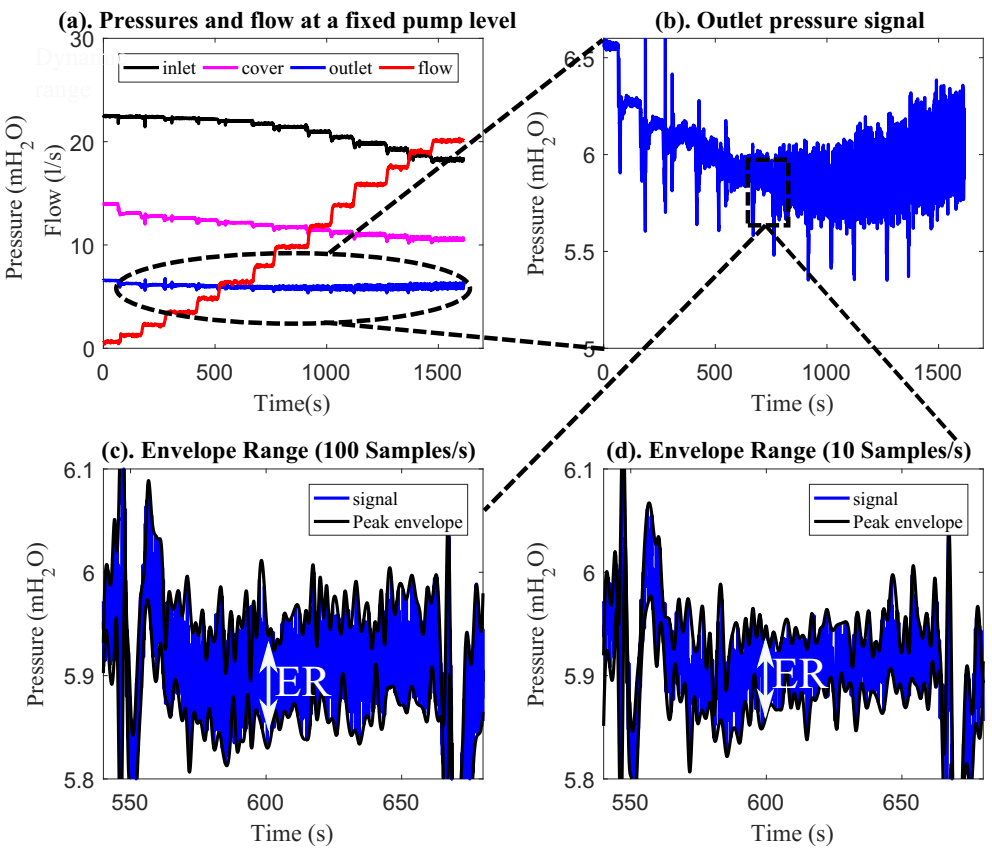

Figure 5.10: The definition of pressure envelope range, ER, from an experimental result of the DN100 GE valve; Figure (a) shows pressure and flow measurements; Figure (b) shows a magnified outlet pressure signal. ERs of data at two sampling rates are shown in Figure (c) and (d). Envelopes are smoothed over an interval of 1s.

The pressure envelope range variable, ER, is defined as the difference between the upper and the lower peak envelope of pressure signals. Envelopes are calculated by spline interpolation over local maxima/minima separated by a range of data points. Figure 5.10 shows the definition of the pressure envelope range and also shows how the pressure envelope range increases as flow increases.

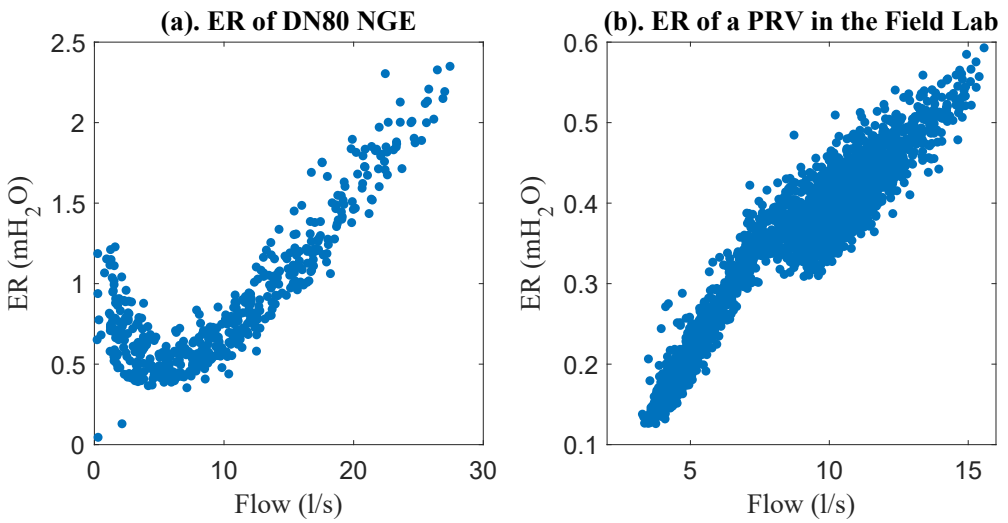

Figure 5.11: Plots of flow against ER; Laboratory conditions (a.) shows high ER at low flow. Since ER alone cannot distinguish low flow and high flow, flow below the turning point cannot be estimated. (b.) Operational networks: this phenomenon was observed.

The ER can be high while the flow is low because the valve at low opening can create high cavitation conditions. Further signal analysis is required to distinguish low and high flow corresponding to the same value of ER. For the purpose of flow estimation, flow is plotted against ER and data with flow below the turning point being taken out. An example of this turning point is shown in Figure 5.11 (a.) for the DN80 NGE valve. For the DN80 NGE valve, flow less than 5l/s is not in a feasible range for flow estimation. Similarly, the estimation flow range is higher than 5l/s for DN100 GE and higher than 7l/s for DN150 GE. However, this feature has only been observed in laboratory valves and not in operational valves in the real WSN (shown in Figure 5.11 (b.)). It is suspected that the high ER at low flow in the laboratory came from turbulent or cavitation from the experimental rig.

5.5.2 Correlation between ER and flow at various sampling rates

A preliminary analysis of the ER has been performed to ensure that it is a suitable variable in the correct solution guidance process. ER is expected to have a strong correlation with flow rate and if this is the case, it will be a perfect choice of variables. The statement is confirmed by the transformation of the C_v characteristic relationship as:

$$q = C_v(x_m)\sqrt{h_{in} - h_{out}} \Longrightarrow q(ER) = C_v(x_m) \cdot f(DP) \tag{5.13}$$

$$\therefore \;\; x_m = C_v^{-1}\left(\frac{q(ER)}{f(DP)}\right) \tag{5.14}$$

, where f represents the square root and DP is a differential pressure. As long as $C_v(x_m)$ is a monotonic function, the C_v^{-1} function can be found. If an accurate measure of ER and an accurate relationship $q(ER)$ were found, one would be able to determine x_m through a measurement of ER and DP. Unfortunately, there is no way to find an accurate measure of ER, and the upper and lower envelopes are defined on random peaks over a range of signals. This measure of ER, however, should be enough to roughly estimate the position as long as q has a strong correlation with ER. The turning point of the estimation function is relatively constant. To be able to guide for the correct solution, the ER only has to be accurate enough to distinguish two solutions to the estimation function. The turning point of the estimation function is relatively constant such that the boundary between two data classes can be constructed. Statistical classification techniques will be employed in constructing the boundary.

Due to the above arguments, the feasibility of using ER as a predictor variable in classification models depends on the correlation between ER and q. The relationship between ER and q does not have to be linear; therefore, the Spearman's rank correlation was used to establish how good the relationship is. The assessment of the ER will be performed in this section while ER is derived in various sampling rates.

According to high sampling rate measurement of the pressure signals, the maximum component frequency is around 50-60 Hz therefore, the sampling rate of higher than about 120 Samples

Table 5.9: Spearman correlation coefficient at various sampling rates of valve 80NGE

Case No.	Sampling Rate (S/s)	np (points)	Window width (s)	Spearman Correlation Coefficient
1	100	100	1	0.8009
2	60	60	1	0.7846
3	10	10	1	0.6772
4	1	10	1	0.3693
5	100	100	10	0.8834
6	60	60	10	0.8803
7	10	10	10	0.844
8	1	10	10	0.3848
9	100	100	30	0.8802
10	60	60	30	0.8723
11	10	10	30	0.85
12	1	10	30	0.4437

per second (or 128 Samples per second for analog sensors), which is the Nyquist rate, becomes unnecessary in terms of detecting useful information. The measurement of the pressure envelope range, ER, also depends on the chosen sampling rate. Signals with higher sampling rates oscillate wider compared to signals with lower sampling rates (See Figure 5.10(c.) and 5.10(d.)). However, high sampling rate measurement consumes lots of energy, which is a limited resource in WSNs. Therefore, it is important to assess the impacts of various sampling rates before using them to guide for a solution. If the characteristics of higher sampling rates are similar to that with lower sampling rates, the lower sampling rates will be chosen for further analysis. Results of the Spearman's correlation analysis between ER and q at various sampling rates are shown in Table 5.9, Table 5.10 and Table5.11 for 80NGE, 100GE and 150GE, respectively. The correlation was performed on various separations between peaks (np) and various sizes of window width used to average the ER. The results indicate that higher sampling rates correspond to higher correlation coefficients. The ER with 100 S/s has the Spearman's coefficient in the range of 0.80-0.97, The 60 S/s and 10S/s have the coefficients between 0.7 and 0.9, while the 1 S/s has the coefficient as low as 0.3-0.7. The coefficient value implies how well the ER can be used to identify the correct solution out of multiple solutions.

Table 5.10: Spearman's correlation coefficient at various sampling rates of valve 100GE

Case No.	Sampling Rate (S/s)	np (points)	Window width (s)	Spearman Correlation Coefficient
1	100	100	1	0.8337
2	60	60	1	0.8258
3	10	10	1	0.7431
4	1	10	1	0.5342
5	100	100	10	0.8909
6	60	60	10	0.8898
7	10	10	10	0.8578
8	1	10	10	0.5575
9	100	100	30	0.8997
10	60	60	30	0.8981
11	10	10	30	0.8636
12	1	10	30	0.6621

Table 5.11: Spearman's correlation coefficient at various sampling rate of valve 150GE

Case No.	Sampling Rate (S/s)	np (points)	Window width (s)	Spearman Correlation Coefficient
1	100	100	1	0.9244
2	60	60	1	0.9221
3	10	10	1	0.8695
4	1	10	1	0.6410
5	100	100	10	0.9583
6	60	60	10	0.9585
7	10	10	10	0.9321
8	1	10	10	0.6587
9	100	100	30	0.9660
10	60	60	30	0.9668
11	10	10	30	0.9433
12	1	10	30	0.6962

5.5.3 Identification of the correct position estimate through the Support Vector Machine (SVM) technique

This section highlights a technique which will be used to identify a correct solution out of the multiple solution mentioned in previous sections. The turning points of the estimation functions are located at about the same point on the x-axis (x_m)(see examples in Figure 5.5). Solutions of the estimation function are candidates for a position estimate ($\tilde{x}_m$). The correct position estimate is defined by an estimate that is closest to the position measurement. The data are divided into two classes depending on the location of the correct position estimate with respect to the estimation function. For the case of DN100 GE and DN150 GE, Class 1 is when the correct estimate is below the first turning point and Class 2 is when the correct estimate is higher than the first turning point. For DN80 NGE, the first turning point is around 1-3 mm and there is no correct position estimate in a feasible range before this turning point. Instead, correct solutions are before and after the second turning point. Therefore, for DN80 NGE, there are 2 classes of solutions, of which class 1 can be obtained when the correct estimate is before the second turning point and class 2 obtained when the correct estimate is after the second turning point. At this point, there are no more than two feasible solutions for all valve sizes (80NGE, 100GE and 150GE) in the experiment (i.e. no more than 2 classes of solution).

Two variables are predictors, which are the pressure envelope range (ER) and the differential pressure ($DP = h_{in} - h_{out}$) (See Equation 5.14).

In laboratories, the sampling rate of the data was 1200 Samples/s and it was downsampled to 1-100 samples/s because it is more practical to achieve on valves in real WSNs (a high-speed analog sensor in WSNs can provide up to 128 Samples/s). Data for validation of this method were collected through both experimental phase 1 and 2.

Here, a classification technique to identify the correct position estimate is discussed. The support vector machine (SVM) technique, which is a non-linear, non-parametric classification process is selected. The SVM technique includes the transformation of predictor variables through kernel functions and derives an optimal separating hyperplane between data classes.

The SVM classifier firstly defines a margin, which is a "distance" between data points at the boundary between two classes. An SVM algorithm essentially defines and solves a convex optimisation problem to maximise this margin. The best hyperplane therefore contains the largest margin between two classes. The SVM is appropriate when the data have exactly two classes and they already show good results in image recognition (Chapelle et al., 1999, Cuingnet et al., 2011, Moser and Serpico, 2013, Pontil and Verri, 1998, Tong and Chang, 2001), bioinformatics (Brown et al., 2000, Jaakkola and Haussler, 1999) and other fields (Herrera et al., 2014, Joachims, 1998). The SVM also performs well in a preliminary classification test compared to other techniques such as the k-nearest neighbours algorithm (k-nn), decision tree learning and linear discriminant analysis. The SVM has the main advantage that it easily avoids overfitting through the use of a regularisation parameter. The Kernel trick includes a non-linear transformation that will make classes linearly separable; therefore, it works well for cases with no prior assumption or knowledge about the separating boundary. The boundary can also be highly non-linear.

5.5.4 Classification models training and validation

Both steady-state and non-steady-state datasets were used to train for the classification models. To obtain an accurate hyperplane for SVM models, as many data points as possible along the boundary between the two classes are required. The value of the ER can vary from random noises and in order to reduce the variability of the ER. The time-series data were processed through non-overlapped moving windows where all variables were averaged within the window to obtain a single value. The width of a sliding window was chosen to be 30 seconds for training and validation. This was based on the response time of the flow modulation control and a sampling rate for the ER of 100S/s. The envelopes were determined using spline interpolation over local maxima separated by at least a number of samples in 1 second. Alternative sampling rates were also successfully explored such as sampling rates of 10S/s and 1S/s.

Six SVM kernel functions were evaluated for the classification analysis; namely, Linear SVM (LSVM), Quadratic SVM (QSVM), Cubic SVM (CSVM), Fine Gaussian SVM (FGSVM),

Medium Gaussian SVM (MGSVM) and Coarse Gaussian SVM (CGSVM). The SVM models were validated with the 50-fold model validation method. Different sampling rates were also studied to to assess their impact on classification. The results are shown in Table 5.12. All SVM kernels demonstrated a good classification performance. The data subset of 100S/s consistently achieved the best classification performance.

Table 5.12: Accuracy of the SVM classification kernels applied to pressure tuples that were acquired (sub-sampled) with different sampling rates; The accuracy is calculated as a percentage of correctly classified data. The sampling rate with the best classification accuracy are labelled in red.

	Cla-Val DN80 NGE			Cla-Val DN100 GE			Cla-Val DN150 GE		
Model	100 S/s	10 S/s	1 S/s	100 S/s	10 S/s	1 S/s	100 S/s	10 S/s	1 S/s
LSVM	**94.4%**	91.9%	84.2%	**95.8%**	94.7%	80.2%	90.5%	**91.2%**	83.1%
QSVM	**93.9%**	92.8%	84.2%	**96.2%**	94.6%	81.7%	**94%**	92.9%	58.2%
CSVM	**94.4%**	92.2%	36.7%	**96.2%**	94.7%	59.4%	**93.8%**	93.3%	62.8%
FGSVM	**93.1%**	91.1%	83.3%	**95.2%**	94.4%	81.7%	**94.2%**	**94.2%**	85.5%
MGSVM	**93.6%**	90.8%	84.2%	**94.9%**	94.7%	82.5%	**93.8%**	93.7%	83.2%
CGSVM	**85.3%**	84.7%	84.2%	**94.3%**	93.8%	81.6%	87.1%	**97.8%**	83.1%

For the training process, tuples with a sampling rate of 100S/s were used (e.g. discrete periods of steady-state conditions; or quasi unsteady-state conditions). The selected window widths were 30s (a tuple) for the lab-based experimental programme, and both 10s and 60s for the experimental programme in operational networks. Figure 5.12 shows two classes of data for the three investigated control valves. The classification models used for the flow estimation were trained using the datasets plotted in Figure 5.12.

The number of training data tuples should be specified to define the boundary between the two classes. In order to achieve this, the turning point of the estimation function shown in Figure 5.5 needs to be determined. Tests were conducted to collect data at every 1mm of the valve stem position for the full range of operational hydraulic conditions as part of the experimental investigation. The current models were trained by 188 data tuples for the Cla-Val DN80 NGE, 258 data tuples for the Cla-Val DN100 GE and 319 data tuples for the Cla-Val DN150 GE. The experimental validation in operational networks was based on a 24-hour training dataset (1440 tuples) and validated with datasets of which window widths are 10s (3P) and 60s (2P&Pos). Since the boundary between the two classes is expected to be similar for the same valve type, the amount of data to train a classification model could be reduced if the data were only

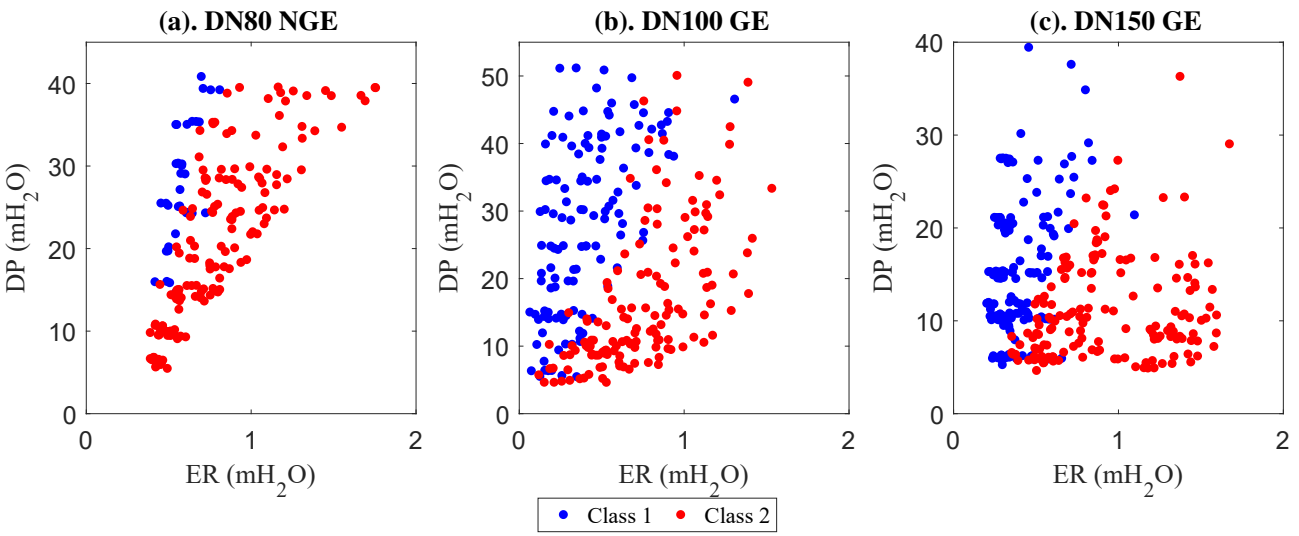

Figure 5.12: Data categorised by an estimation function turning point; Data of three valves are shown separately in Figure (a), (b) and (c).

collected along the expected boundary area (e.g. the turning point of the valve stem position estimation function). An illustrative example based on Figure 5.5(b.) shows a turning point of around 7mm for the stem position estimation function for the DN100 valve. Consequently, the classification model can be successfully trained with data within 7mm (±2 mm).

5.5.5 Additional option for solution classification: 1 Sample/s with max/min value

It was illustrated in Section 5.5.4 that the correct position estimate (out of multiple solutions) could be selected with the use of Support Vector Machine Classification models. Signals with high sampling rates are required to obtain the best classification performance (100 S/s). Such sampling rates are achievable and the sampling rate of 128 S/s is already available at ACVs in the “Field Lab". However, high sampling rate data collection requires resources in storage capacity and it is computationally expensive to extract the signal envelope range from high sampling rate data.

Only the information obtained from high sampling rate data was the signal envelope range. Therefore, an alternative method for signal collection was investigated. This method is called **1 S/s with max/min**. Data were collected in high sampling rates, but only some values would

Table 5.13: Classification performance of 1 S/s with max/min including the 50-fold cross validation

Models	80NGE	100GE	150GE
LSVM	94	91.7	96.3
QSVM	94.8	93.4	95.3
CSVM	93.6	93.7	96.3
FGSVM	92.3	93.4	95.6
MGSVM	93.1	93.9	94.9
CGSVM	83.7	91.2	96.6

be stored, which are the mean value, the maximum value and the minimum value within the window width of 1 second. The ER is defined by the difference between the max value and the min value.

The classification performance including the 50-fold cross validation is shown in Table 5.13 and a comparison between classification through the ER defined by the max/min values within the 1 second window and the ER defined by the peak envelope of 100 Samples/s data is shown in Figure 5.13 The result clearly shows that the classification using the ER defined by the max/min values does not provide any significantly different result from that using the ER defined by the peak envelope of 100 Samples/s data. Therefore, the ER defined by the max/min values is a good option for future work on correct position estimate identification (the classification part of the validation results in Chapter 6 was performed through the ER defined by the peak envelope of 100 Samples/s data).

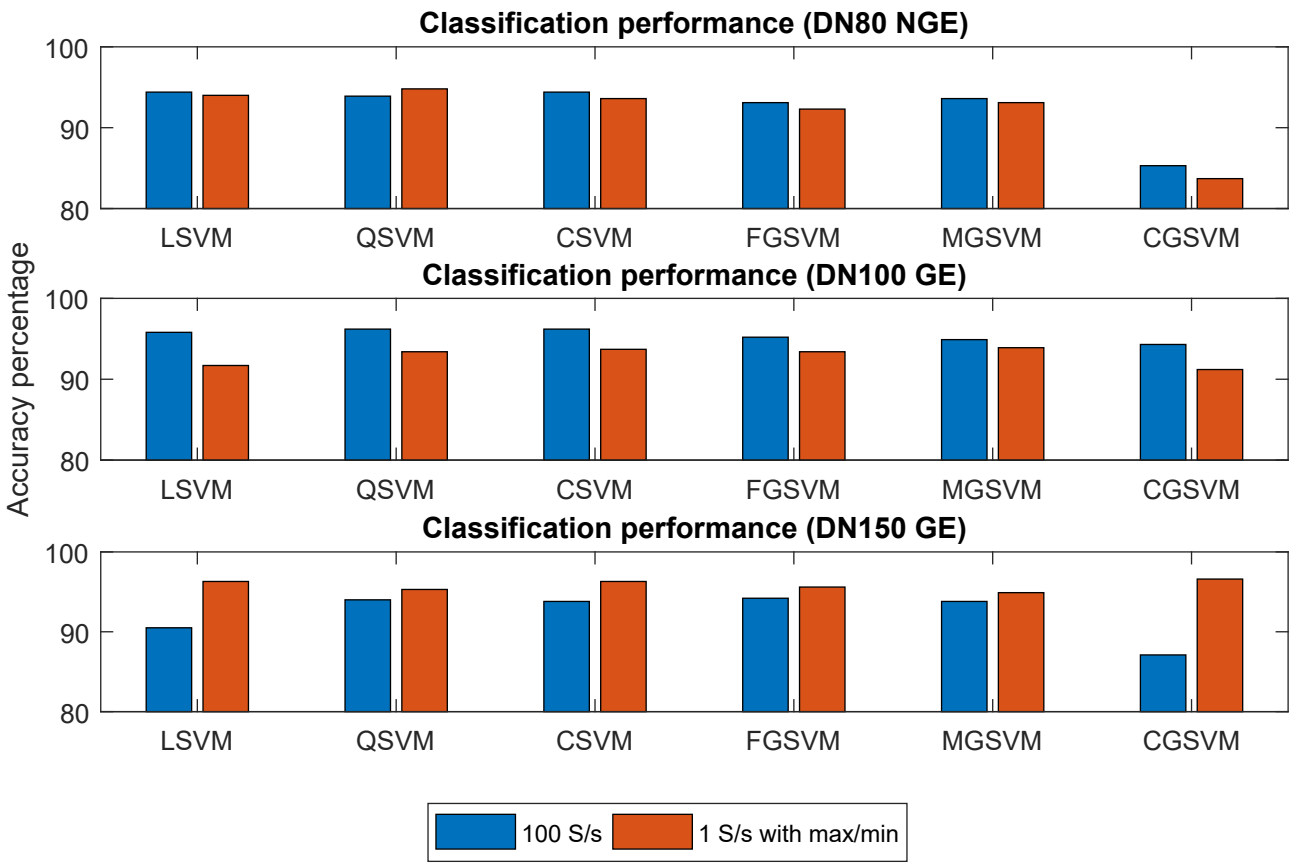

Figure 5.13: A comparison between classification through the ER defined by the max/min values within the 1 second window and the ER defined by the peak envelope of 100 Samples/s data

5.6 Conclusions

An accurate force balance relationship is necessary for the 3P flow estimation method. The required level of accuracy is high such that the valve stem position can be estimated from pressure measurements. A parametric force balance relationship has been proposed and validated. The relationship consists of coefficients which are polynomial functions of the valve stem position. These coefficients were derived through experimental data collected in various hydraulic conditions. The process of fitting the coefficients is called the "model training process".

The parametric force balance relationship was rearranged into the valve stem position estimation function, which can be solved for the valve stem position estimate. However, it was found that multiple solutions occur. According to the experimental data, the occurrence of multiple valve stem positions with the same pressure combinations is an intrinsic property of the valve. Normally, an outlet pressure signal with high flow tends to have a higher signal envelope. The

signal envelope range (ER) was defined, providing that the signal was measured at high sampling rates. With the use of ER and the differential pressure (DP), the SVM classification model was trained and validated through the k-fold cross-validation method. The accuracy of the classification of multiple valve types at given different sampling rates of h_{out} was also assessed and compared. The overall result indicates that a correct position estimate can be guided with high accuracy.

Combining all the proposed relationships, a novel method of flow estimation from 3 pressure measurements at ACVs has been successfully derived (the 3P method). The method requires three relationships/models which are the force balance relationship, the C_v characteristic relationship and the SVM classification model. All of the three relationships require the model training process in a priori. Validation of the 3P method and the comparison to the 2P&Pos method are performed in Chapter 6.

Chapter 6

Validation of flow estimation methods

This chapter validates the novel 3P flow estimation method. The validation is separated into two phases: (i) through laboratory data and (ii) through the “Field Lab" data. For the laboratory validation, the models used were derived earlier in Chapter 5 and were validated through separately collected data sets. For the “Field Lab” validation, the models were trained through a continuous 24-hour data set and validated through a different data set, which is also a continuous 24-hour data.

6.1 Introduction and specifications for flow estimation

Flow estimation through the 3P method requires a continuous measurement of the inlet pressure, the control chamber pressure and the outlet pressure. The 3P method includes estimating a position from three pressure measurements through the force balance equation, classifying a unique position estimate through an SVM classification model and estimating the flow through the C_v curve. The process diagram for 3P flow estimation method is shown in Figure 5.1 including the inputs and outputs of each process. Since all the SVM classification models provide a similar level of accuracy, the Linear SVM was selected because it requires the least resources in both training and utilising. Details of requirements in terms of measurements and model training will be highlighted again for clarity.

Three models/relationships are required to perform the 3P flow estimation which are the C_v relationship, the force balance relationship and the SVM classification model. Requirements for each model derivation (model training) are listed as follows:

- C_v **characteristic relationship:** The C_v requires q, h_{in}, h_{out} and x_m. These variables are best measured in steady states when they are constants. While the steady-state condition can be generated in laboratories, the quasi-steady states when the variables gradually change are acceptable. The C_v curves of three valves were derived using the measured steady-state data from experimental phase 1 because the real C_v characteristic of each valve was slightly different from the C_v curves provided by the manufacturer (See Section 4.3).

- **Force balance relationship:** The force balance relationship requires three pressures, h_{in}, h_c and h_{out}, and valve stem position, x_m. Similar to the C_v, this requires steady-state data, whereas quasi-steady states are acceptable.

- **SVM classification model:** The variable ER, DP, the correct position estimate and the class of the position estimate are required to train the classification model. The ER was obtained from the high sampling rate measurement of h_{out}. The DP was obtained through the inlet and outlet pressure measurement at the valve. The correct position estimate is one of the solutions to the estimation function which is closest to the stem position measurement. The class of the position estimate is defined by which position estimate is the correct position estimate (1 for lower solution and 2 for higher solution).

Once these three models have been trained, the 3P flow estimation can be performed at the same sampling rate to the lowest sampling rate of the three pressure measurements. Similarly, the 2P&Pos flow estimation requires continuous measurements of two pressures and a stem position. While the model training process is much easier as only the C_v relationship is sufficient for the 2P&Pos, position sensors installation requires operational disruption. Also, stem position sensors consume a lot of energy compared to pressure sensors with the same sampling rate and energy is limited in WSNs. Currently, in the "Field Lab", for each valve, the sampling rate for

the position sensor is 1 sample/min. This chapter aims to show the validated results for flow estimation and to compare errors between the pioneered 3P method and the existing 2P&Pos method.

6.2 Flow estimation validation of laboratory valves

As it is mentioned in Chapter 3, the experiments were developed in two stages: Stage 1 was carried out at Imperial College London, and Stage 2 was carried out at Cla-Val headquarter, Lausanne, Switzerland. At Imperial College London, the experiments were carried out on only one valve, which is 100GE, while at Cla-Val Switzerland, data of 3 valves were collected from 80NGE, 100GE and 150GE.

6.2.1 Flow estimation validation from Imperial Laboratory

A set of experiments at Imperial College London Laboratory was carried out as the initial proof of concept for the proposed 3P flow estimation. Only steady-state data were taken in two phases of experiment. The first phase collected data for model training and the second phase collected data for validation. The first phase included various steady state openings, while the pump setting and the valve set outlet pressure were constant. The process was repeated for different pump settings and outlet pressure settings. The training data sets were collected at every 1 mm opening until 75% of full opening, whereas the validation data sets were collected in 6 groups at 12.5%, 25%, 37.5%, 50% and 62.5% and 75% of full opening.

The validation of this experiment is regarded as an initial validation of the methodology as the position sensor is less accurate ($\pm$0.5mm) than those at Cla-Val laboratory, and also the variable speed pump is less adjustable (10 speeds). On this set of experiments, the sampling rate was selected to be 100 samples/s and the selected classification model, the Cubic SVM, was the best performance on training. The validation result is shown in Figure 6.1.

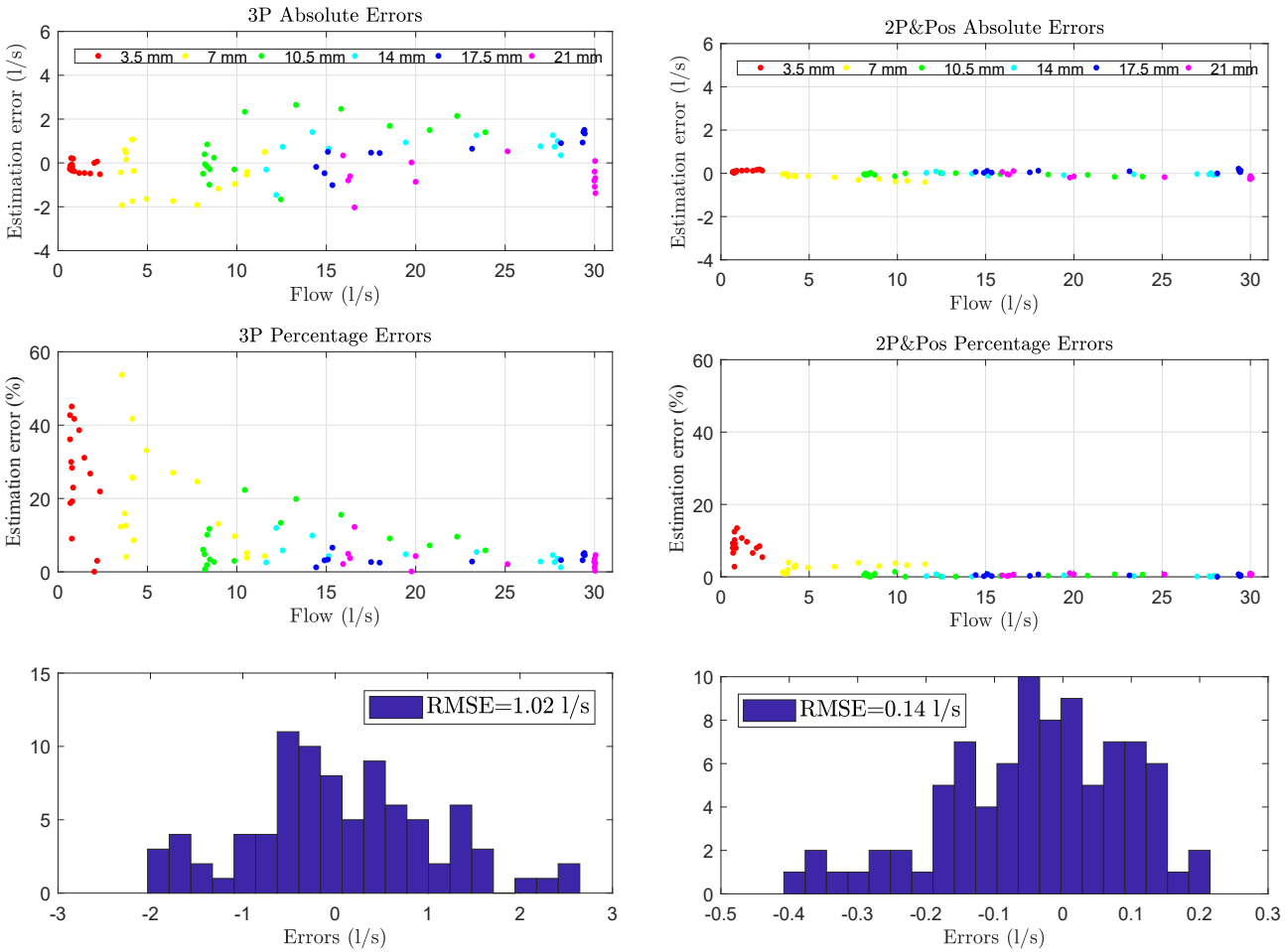

(a) 3P flow estimation validation results (b) 2P&Pos flow estimation validation results

Figure 6.1: Flow estimation validation at Imperial College Laboratory; It is worth reminding that although the 2P&Pos method obtains higher accuracy compared to the 3P method. A major drawback of the 2P&Pos method is that it has constraints to implement on valves in networks (disruption).

6.2.2 Flow estimation validation from Cla-Val Laboratory

At Cla-Val laboratory, three valve sizes were installed for the experiment. The position sensors for stem position measurement are accurate to ±0.1mm. The variable speed pump has a wide range of speed adjustments such that it can adjust the pressure of around 0.2 mH_2O. Similar to the set of experiments at Imperial Laboratory, the pump and the downstream flow control valve were adjusted until a particular steady state was obtained. The steady-state data were used to derive models (Experimental phase 1 as mentioned in Chapter 3). However, these sets of experiments aimed to use dynamic data sets for validation to observe impacts if pressures and flow are relatively unsteady. Dynamic data sets came from two types of experiment. The

first type consisted of separate experiments, which continuously varied flow and pressures. The second type included experiments searching for steady states, whereas the steady-state data that would be used in model training were deleted from the data. Since each experiment always started with the valve stem position of 0 mm and the flow of 0 l/s, the data were connected to represent a single time-series data set. The time-series data set was then divided into multiple time-windows. Within a window width, pressures, flow, stem position and ER were averaged. The preliminary result shows that too small window widths do not accurately represent ER for the classification model because spikes of the pressure signal can cause high ER. On the other hand, too large window widths will make flow estimation hard to be implemented in the "Field Lab" because the control signal will need to be sent to the valve every minute (current stage). The window size was chosen to be 30 seconds.

Flow estimation was validated in 2 ways:

1. **Discrete data points:** The first validation aimed to assign a higher accuracy classification model which requires a high number of data along the boundary between two classes. Hence, the time-series data were broken and half of the data would be used to train the classification model.

2. **Time-series data:** The second validation aimed to preserve the time-series data for visualisation purposes and the flow estimation was performed throughout the time-series.

Cla-Val laboratory flow estimation validation 1 (discrete data points)

Errors of the 3P flow estimation with the experimentally derived C_V curves are shown in Figure 6.2. For each valve, they are shown in flow values and box plots of flow groups in the range of 5 l/s. Errors of the 2P&Pos flow estimation are shown in Figure 6.3.

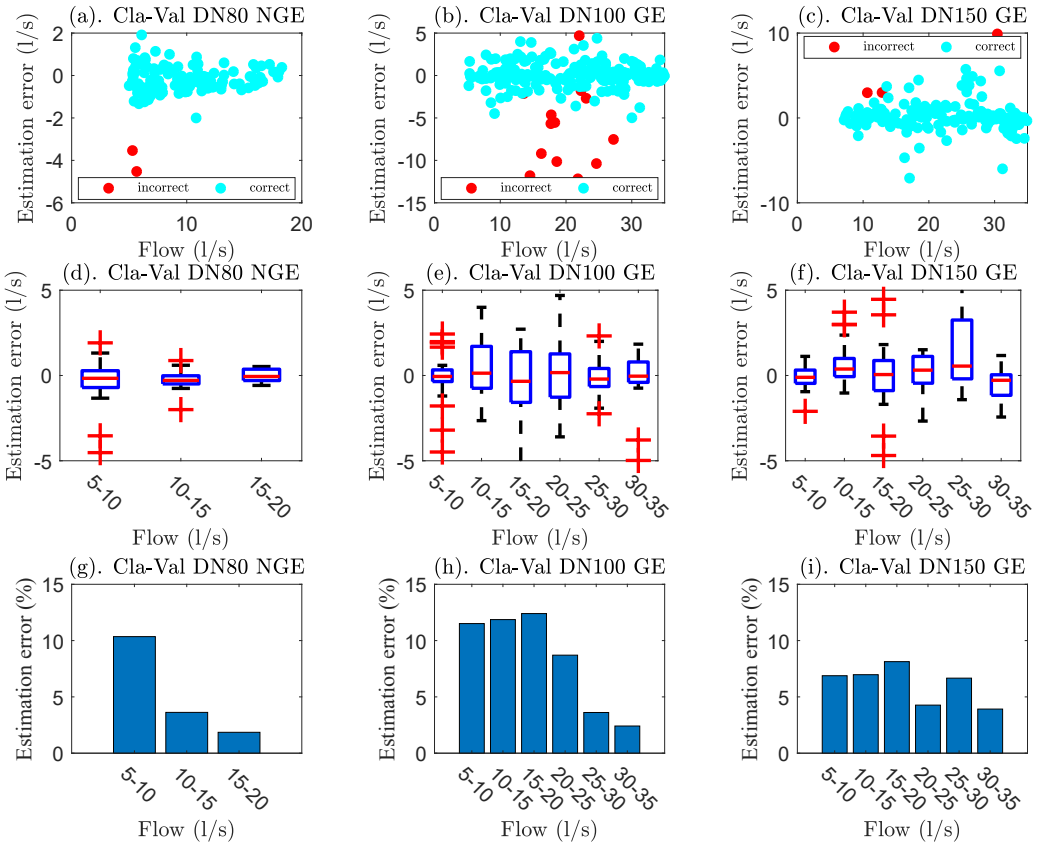

Figure 6.2: Performance assessment of the **3P flow estimation method** for the three control valves tested under laboratory conditions (DN80, DN100 and DN150); Figure (a), (b) and (c) show the absolute flow estimation errors, and also the correctly and incorrectly classified flows. Figure (d), (e) and (f) utilise box plots for comparing the range and distribution of the absolute flow estimation errors shown in Figure (a), (b) and (c). Figure (g), (h) and (i) show percentage errors.

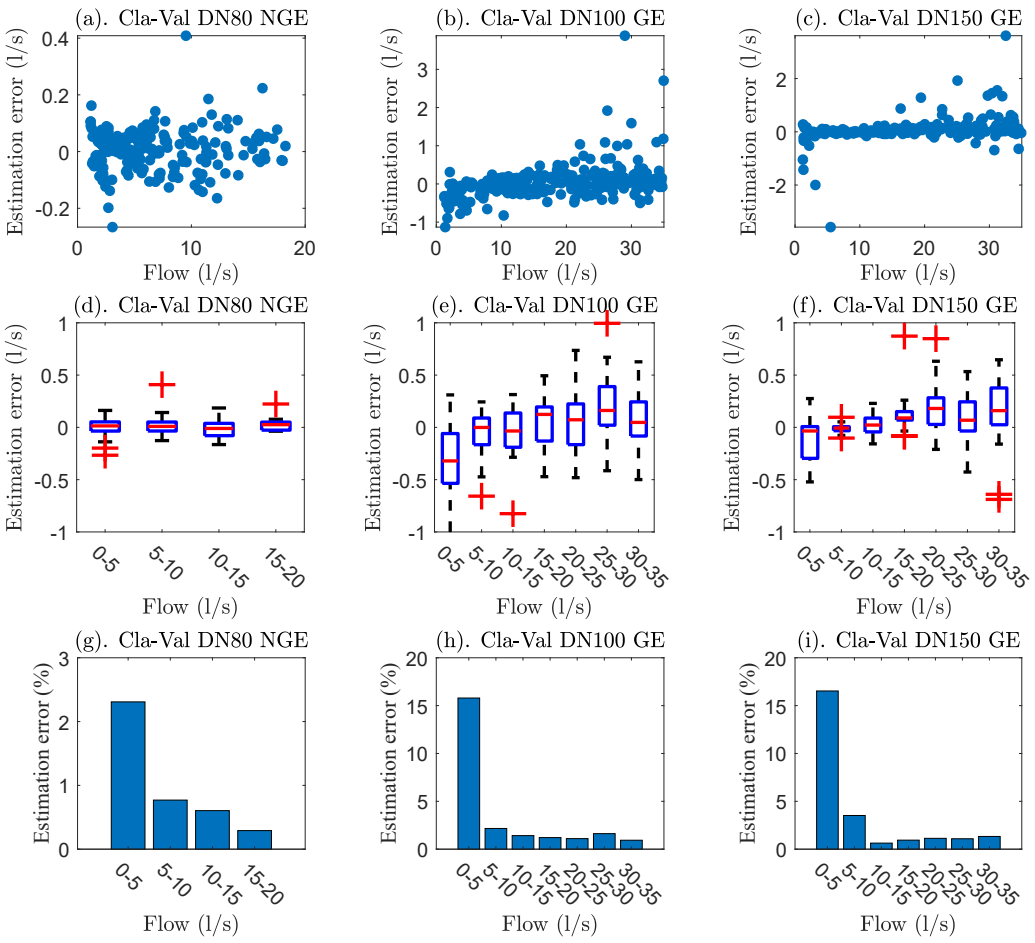

Figure 6.3: Performance assessment of the **2P&Pos flow estimation method** for the three control valves tested under laboratory conditions (DN80, DN100 and DN150). Figure (a), (b) and (c) show the absolute flow estimation errors, and also the correctly and incorrectly classified flows. Figure (d), (e) and (f) utilise box plots for comparing the range and distribution of the absolute flow estimation errors shown in Figure (a), (b) and (c). Figure (g), (h) and (i) show percentage errors.

Cla-Val laboratory flow estimation validation 2 (time-series data)

It was mentioned previously that for each valve, validated data sets were connected to create a single time-series. Validation results of the two methods, the 3P and the 2P&Pos methods, are shown next to each other and will be labelled as (a.) and (b.). Each validation consists of 5 plots, (i). 3 Pressure measurements (h_{in}, h_c and h_{out}). (ii). Valve stem position measurement and position estimate in the 3P case. (iii). Flow estimate and flow measurement. (iv). Errors of flow estimate. and (v). Histogram of flow estimation errors. Sub-figures (i). to (iv) are shown with the same time on the x-axis. Time-series validation results for valves 80NGE, 100GE and 150GE are shown in Figure 6.4, Figure 6.5 and 6.6, respectively. The validation will be shown in a 5-figure format, while the 3P and the 2P&Pos methods are compared next to each other. All of them are shown in time-series. The five figures include:

1. Three pressure measurements h_{in}, h_c and h_{out}.

2. Position measurement and position estimate for the 3P method and only position measurement for the 2P&Pos method.

3. Flow measurement and flow estimate through the 3P and the 2P&Pos methods.

4. Errors of the flow estimation through both methods. The errors are the difference between the measured flow and the flow estimate. Since flow variables are directly measured with electromagnetic flowmeters with an accuracy of 0.02% error, the flow measurement is used as a benchmark.

5. Histogram of flow estimation errors with the root-mean-squared error (RMSE).

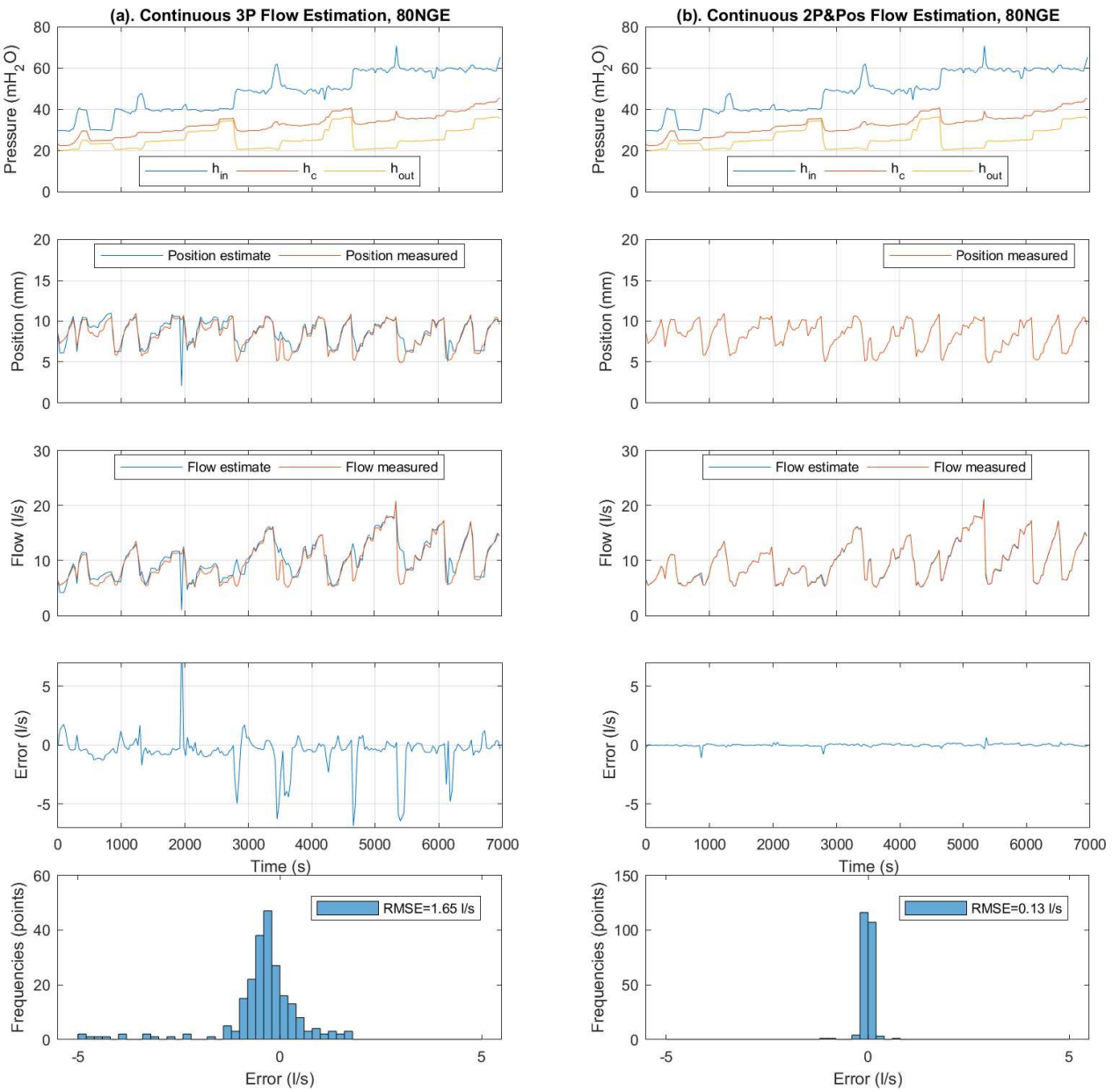

(a) 3P flow estimation validation results

(b) 2P&Pos flow estimation validation results

Figure 6.4: Flow estimation validation at Cla-Val Laboratory, 80NGE

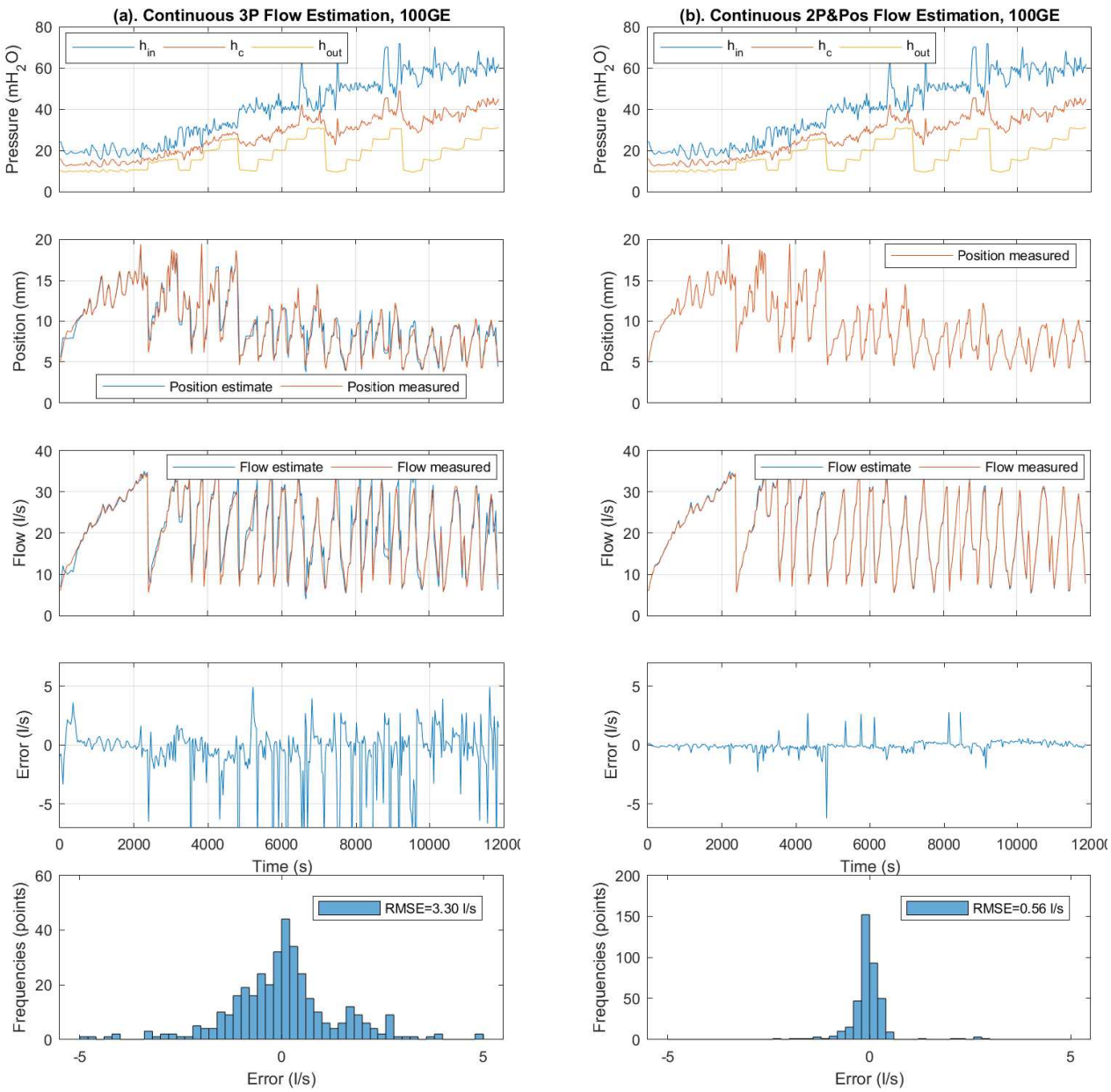

(a) 3P flow estimation validation results

(b) 2P&Pos flow estimation validation results

Figure 6.5: Flow estimation validation at Cla-Val Laboratory, 100GE

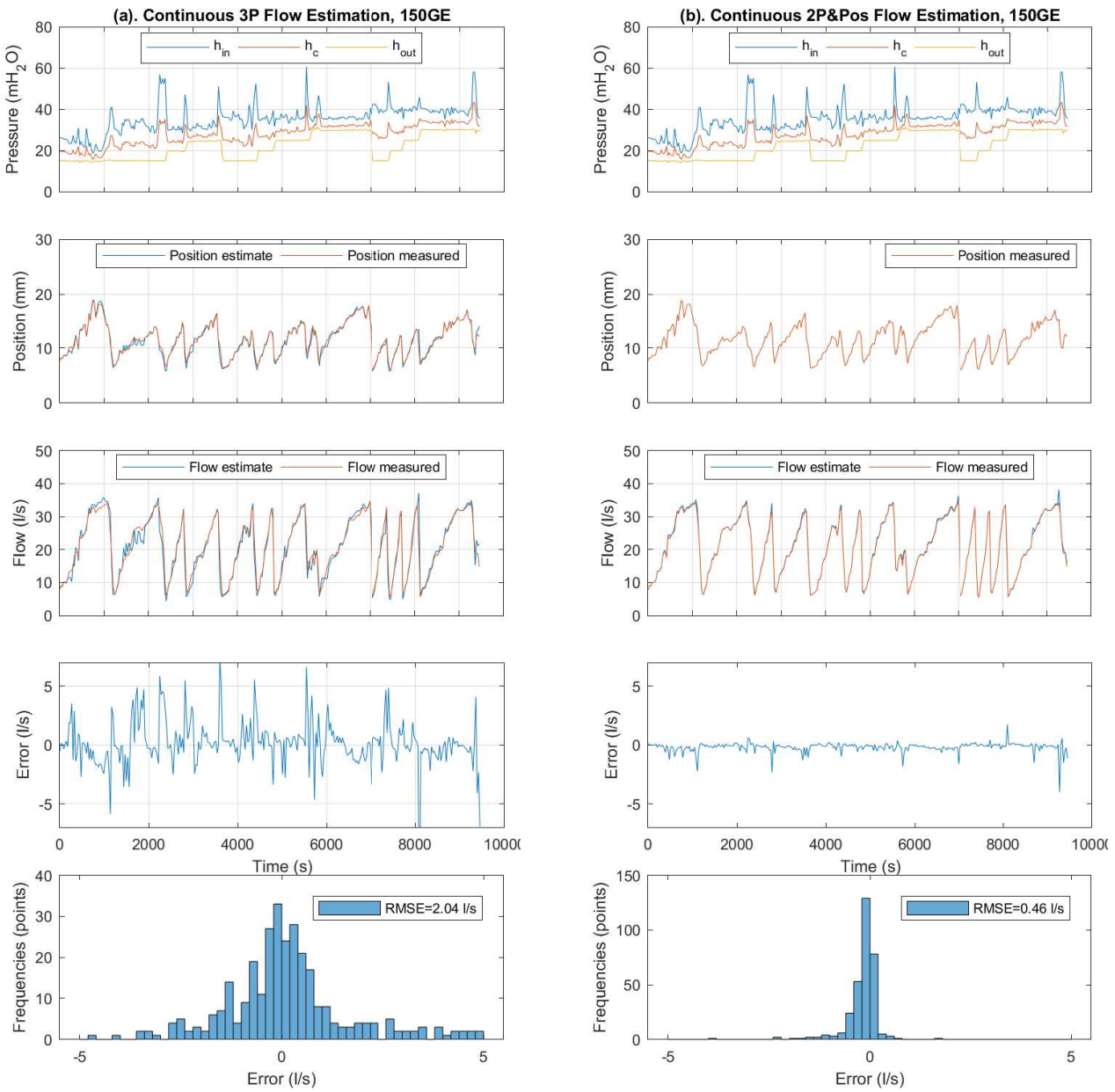

(a) 3P flow estimation validation results

(b) 2P&Pos flow estimation validation results

Figure 6.6: Flow estimation validation at Cla-Val Laboratory, 150GE

6.3 Flow estimation validation of the "Field Lab" data

Details of the "Field Lab" were described in Chapter 3. Flow estimation validation in the "Field Lab" was performed using the data which were continuously collected on 3 valves. The three valves are located at Stoke Lane (Cla-Val DN100 GE), Woodland Way (Cla-Val DN150 GE) and Lodge Causeway (Cla-Val DN100 GE), referred to as SKL, WLW and LCW, respectively. All of the valves are controlled by the flow modulation scheme (FM), which has their own control profiles. The analysis included three control profiles implemented for each valve, which have been set as a target pressure at a particular flow reading from electromagnetic flow meters. Control profiles (CP) with real data are illustrated in Figure 6.7. The first control profile (CP#1) was implemented between 26th January 2018 and 4th February 2018. The second control profile (CP#2) was implemented between 4th February 2018 and 23rd February 2018. This primarily included a change of the upstream PRV (Stoke Lane) control profile, which caused higher flow through this PRV and a change of demand pattern at the other two valves, while the control profiles of the other two valves were relatively the same. During this period, step changes during the night time were introduced for an experiment on leakage detection at Stoke Lane (out of scope for this work). Data at low flow were away from the control profile due to this change. The third control profile (CP#3) was implemented on 23rd February 2018. During this period at Woodland Way, there was a discrepancy between the data and the control profile at high flow as there was insufficient inlet pressure for the set outlet pressure.

Validation was performed in the following steps:

1. Three dates, namely 27th January 2018, 5th February 2018 and 25 February 2018, which correspond to each control profile were selected for the training process.

2. Another three dates corresponding to each control profile were selected for validation. They were 29th January 2018, 6th February 2018 and 26 February 2018. These are called validation data sets.

3. For each of them, 6-dimensional time-series data were downloaded. The six dimensions consisted of h_{in}, h_c, h_{out}, x_m, q and ER. All variables except x_m were sampled with

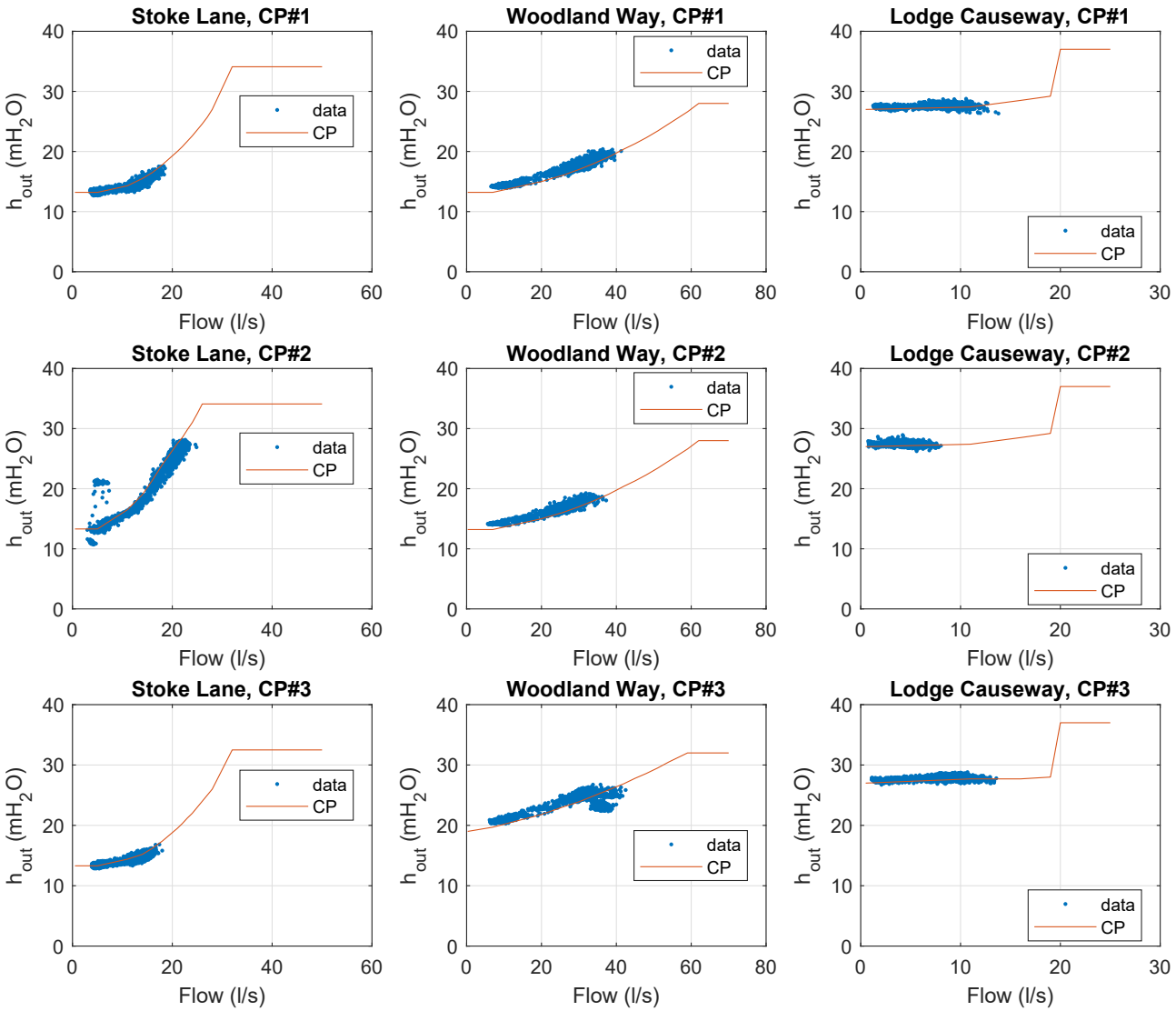

Figure 6.7: Control Profiles compared with 24-hour data; Title formats include "Field Lab" cites (Stoke Lane, Woodland Way and Lodge Causeway) and control profile orders (CP#1, CP#2 and CP#3).

the rate of 128 Samples/s, which then were averaged through a non-overlapped moving window with a one-minute width. The sampling rate of the x_m was 1 sample per minute.

4. Since each variable was collected through various devices with different time stamps, the synchronisation process was required. The synchronisation process is extremely important. From experience, missynchronised data can result in a completely incorrect model with high error rates. Apart from the time-stamp that each data acquisition device provides, synchronisation can be cross-checked through the variable measured in common, here the outlet pressure. This cross-check can be done by cross-correlation.

5. The training data sets were trained for the force balance relationship, the C_v relationship and the Classification model (if required). Different orders of the force balance model were tested and it was found that the 2nd order models provided a similar level of estimation accuracy to the 4th order model. The lower order model also had a lower risk of over-fitting because the training data sets contained a limited range of pressure combinations. Pressures and flow at the "Field Lab" valves had a daily pattern. However, this was not the case for laboratory experiments where a wide range of hydraulic conditions were created and hence the 4th order models could be explored.

6. The 3P flow estimation method was implemented in non-overlapping moving windows with a fixed time interval of 10s for all valves and experiments presented in this section. The pressure is continuously sampled at 128S/s. The 2P&Pos flow estimation was done every 1s for the laboratory experimental set-up and every 60s for the valves in the operational network. The 60s time interval was because of sampling constraints for the stem position sensor for the valves installed in the operational network.

7. There is **no stem position sensor at Lodge Causeway** due to logistic limitation. The installation of the stem position sensor would interrupt both road transport and water supply services. A workaround had been implemented. It is assumed that the manufacturer's C_v relationship is strongly held and therefore the "virtual valve stem position" has been derived through the relationship. The force balance model was trained normally from pressure and flow measurements and the virtual valve stem position.

8. As a result, out of 9 cases, 8 cases did not require the classification model because the lowest solution is always the correct solution. Only 1 case required the classification model, and it was Woodland Way, CP#3, which operated up to 70% of maximum opening.

9. The validation will be shown in a 6-figure format, while the 3P and the 2P&Pos methods are compared next to each other. All of them are shown in time-series. The five figures include:

   (a) Three pressure measurements h_{in}, h_c and h_{out}.

(b) Position measurement and position estimate for the 3P method and only position measurement for the 2P&Pos method.

(c) Flow measurement and flow estimate through the 3P and the 2P&Pos methods.

(d) Errors of the flow estimation through both methods. The errors are the difference between the measured flow and the flow estimate.

(e) Histogram of flow estimation errors with the root-mean-squared error (RMSE).

(f) Histogram of flow estimation percentage errors with the mean absolute percentage error (MAPE).

Discussion is provided separately for each "Field Lab" location.

6.3.1 SKL valve

Flow estimation at Stoke Lane is shown in Figure 6.8, Figure 6.9 and Figure 6.10 (SKL#1, SKL#2 and SKL#3). In all three cases, the 2P&Pos method provided highly accurate flow estimation with the RMSE of only about 0.3 l/s. The 3P method provided a decent accuracy in the case SKL#1 and SKL#3 with the RMSE of 0.70 l/s and 0.56 l/s , respectively. The RMSE in the case of SKL#2 was 1.54l/s, which is higher than the other two because it involves higher flow. Most of the high errors occurred when flow was as high as 20 l/s. The RMSE in the case of SKL#2 was 1.54 l/s, a value still much lower than the laboratory validation of the same valve size (RMSE of 3.30 l/s) because laboratory validation includes more various hydraulic conditions.

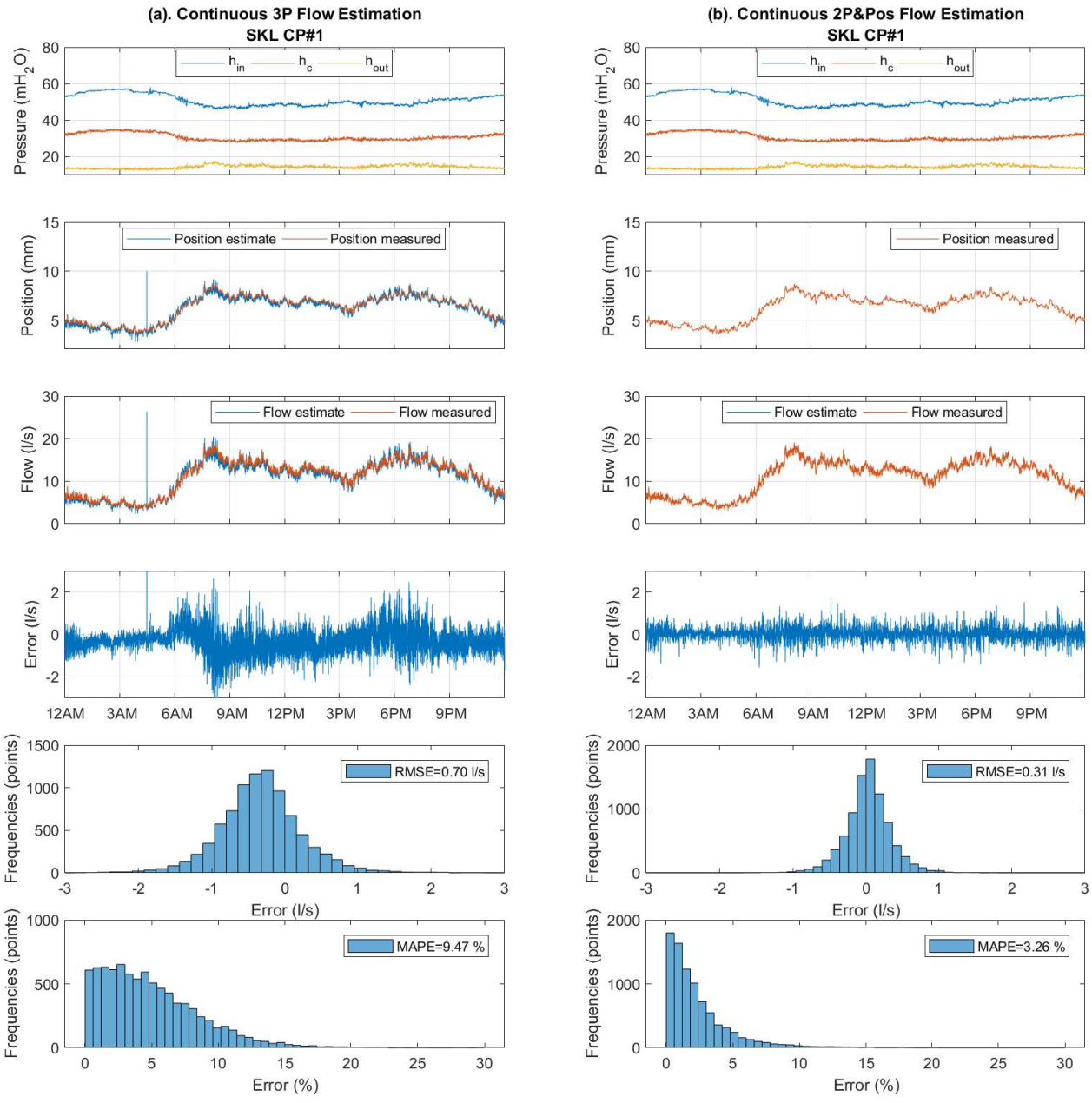

(a) 3P flow estimation validation results

(b) 2P&Pos flow estimation validation results

Figure 6.8: Flow estimation validation at the "Field Lab", Stoke Lane

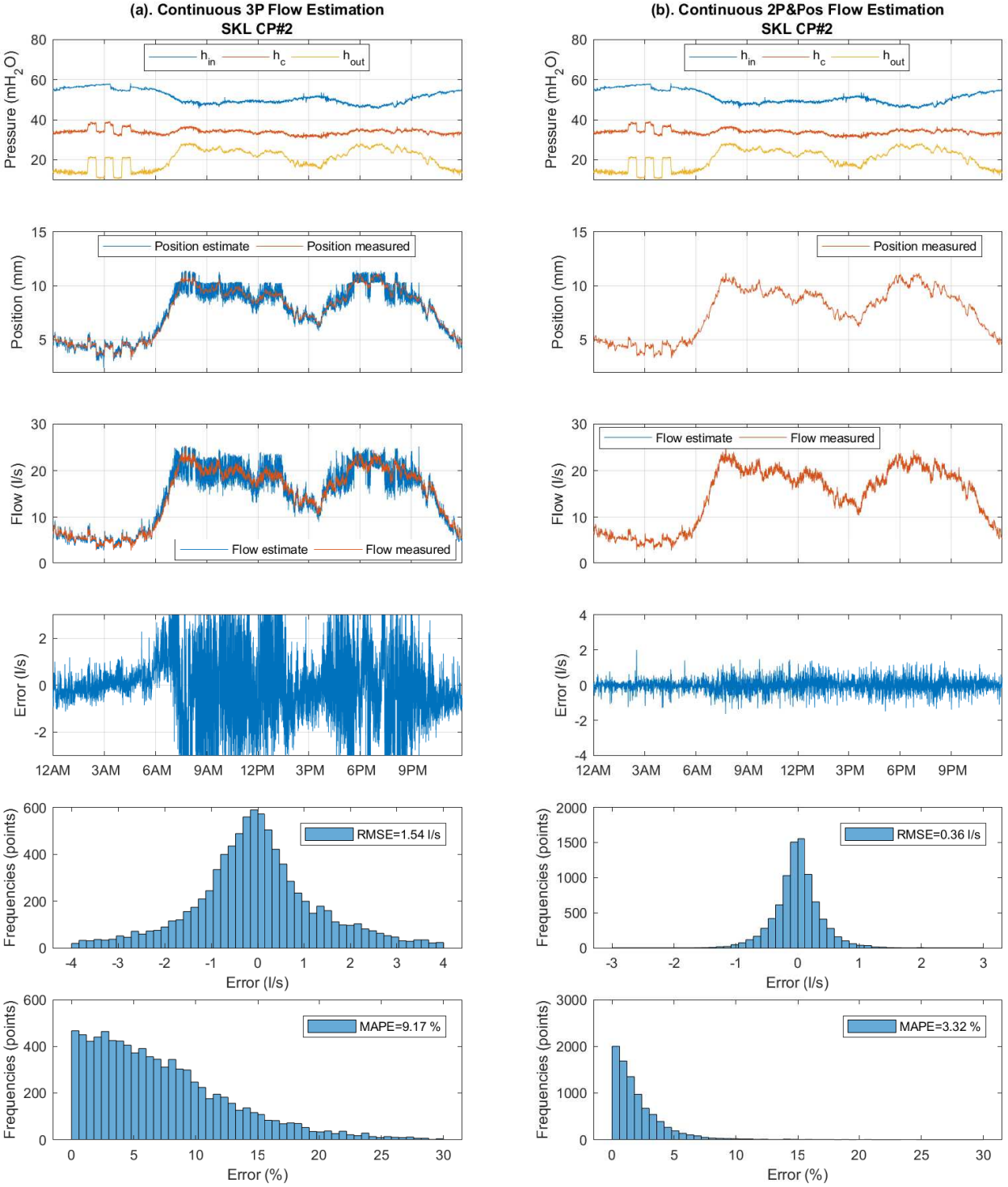

(a) 3P flow estimation validation results

(b) 2P&Pos flow estimation validation results

Figure 6.9: Flow estimation validation at the “Field Lab”, Stoke Lane

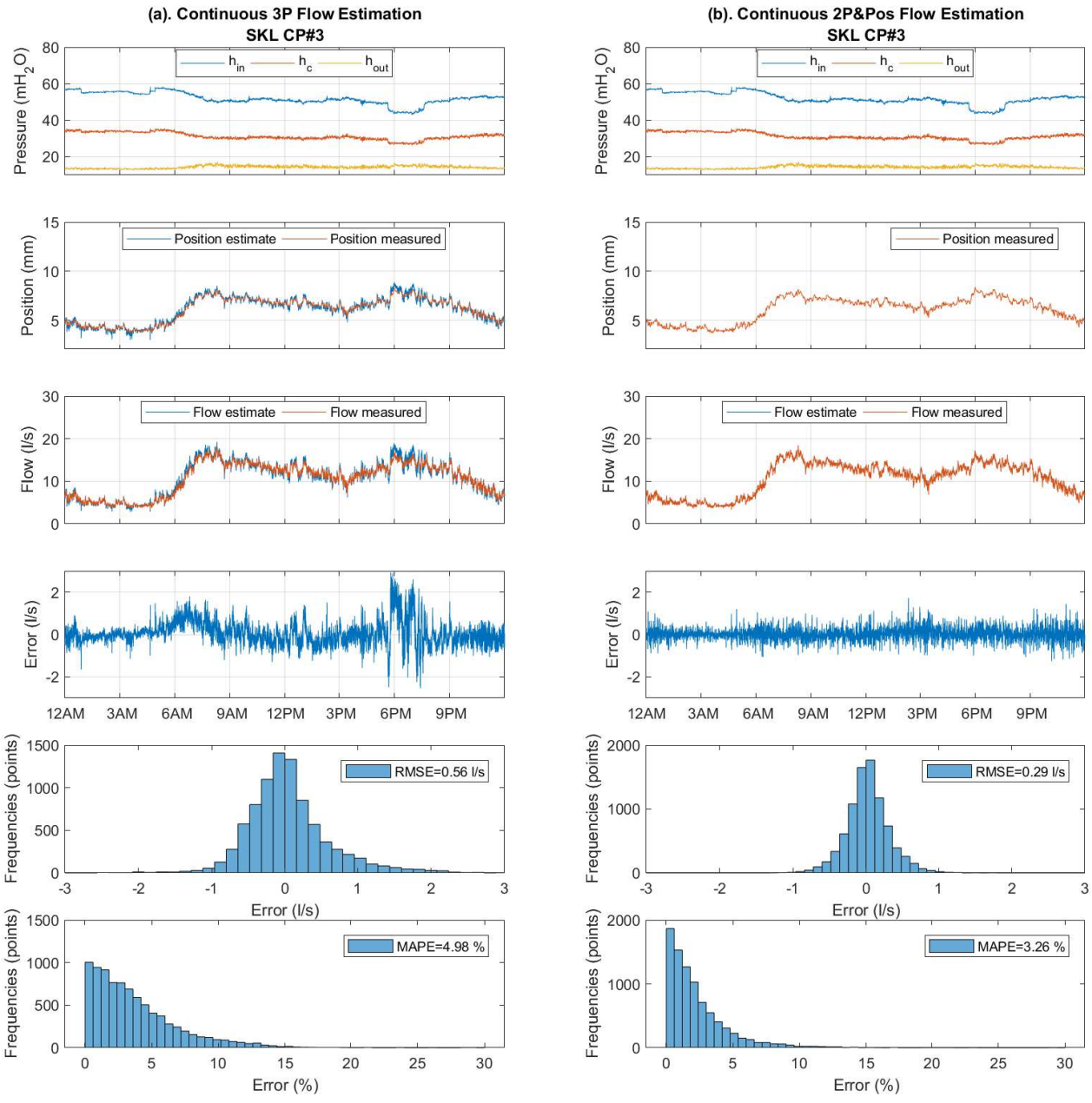

(a) 3P flow estimation validation results

(b) 2P&Pos flow estimation validation results

Figure 6.10: Flow estimation validation at the "Field Lab", Stoke Lane

6.3.2 WLW valve

Flow estimation at Woodland Way is shown in Figure 6.11, Figure 6.12 and Figure 6.13. Generally, the errors are higher because the valve is large (DN150 GE) and the differential pressure is small (less than 10mH_2O). The 2P&Pos method achieve accurate flow estimate for all control profile cases with RMSE less than 1 l/s or MAPE around 3-4%. Flow estimation is less accurate with the 3P method. For the WLW#1 and WLW#2, the estimation RMSE is slightly less than 4 l/s or MAPE of 17%. For the WLW#3 case, flow estimation obtains very high errors. The RMSE is 14 l/s or the MAPE is 53%. The high error in the WLW#3 case is due to the differential pressure with this control profile is small (less than 5 mH_2O). For the low differential pressure case, a slight change of pressure leads to a large change of the valve stem position and hence the valve stem position is very sensitive to pressure measurement. This is considered to be a limitation of the 3P flow estimation method.

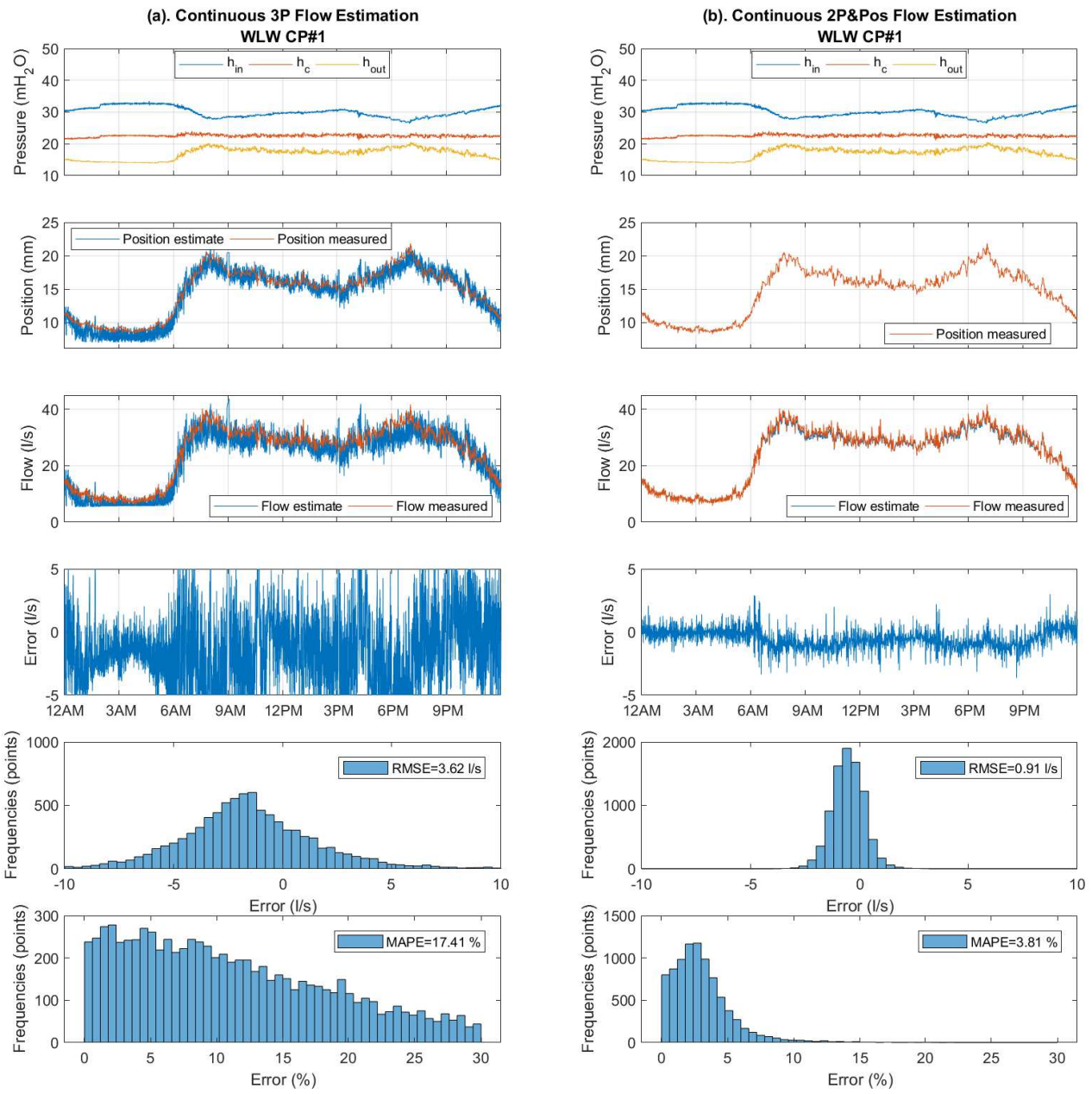

(a) 3P flow estimation validation results

(b) 2P&Pos flow estimation validation results

Figure 6.11: Flow estimation validation at the "Field Lab", Woodland Way

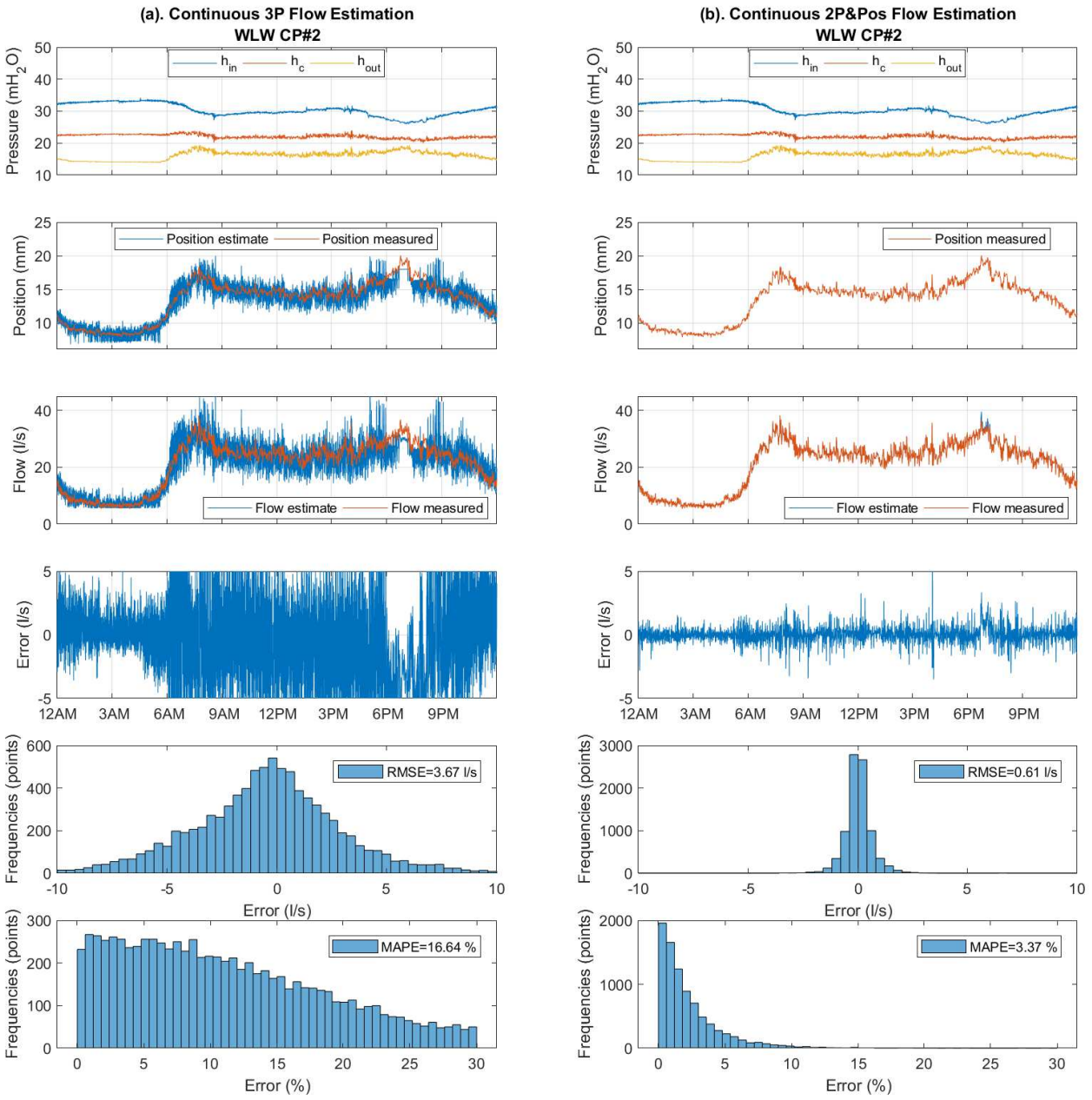

(a) 3P flow estimation validation results

(b) 2P&Pos flow estimation validation results

Figure 6.12: Flow estimation validation at the “Field Lab”, Woodland Way

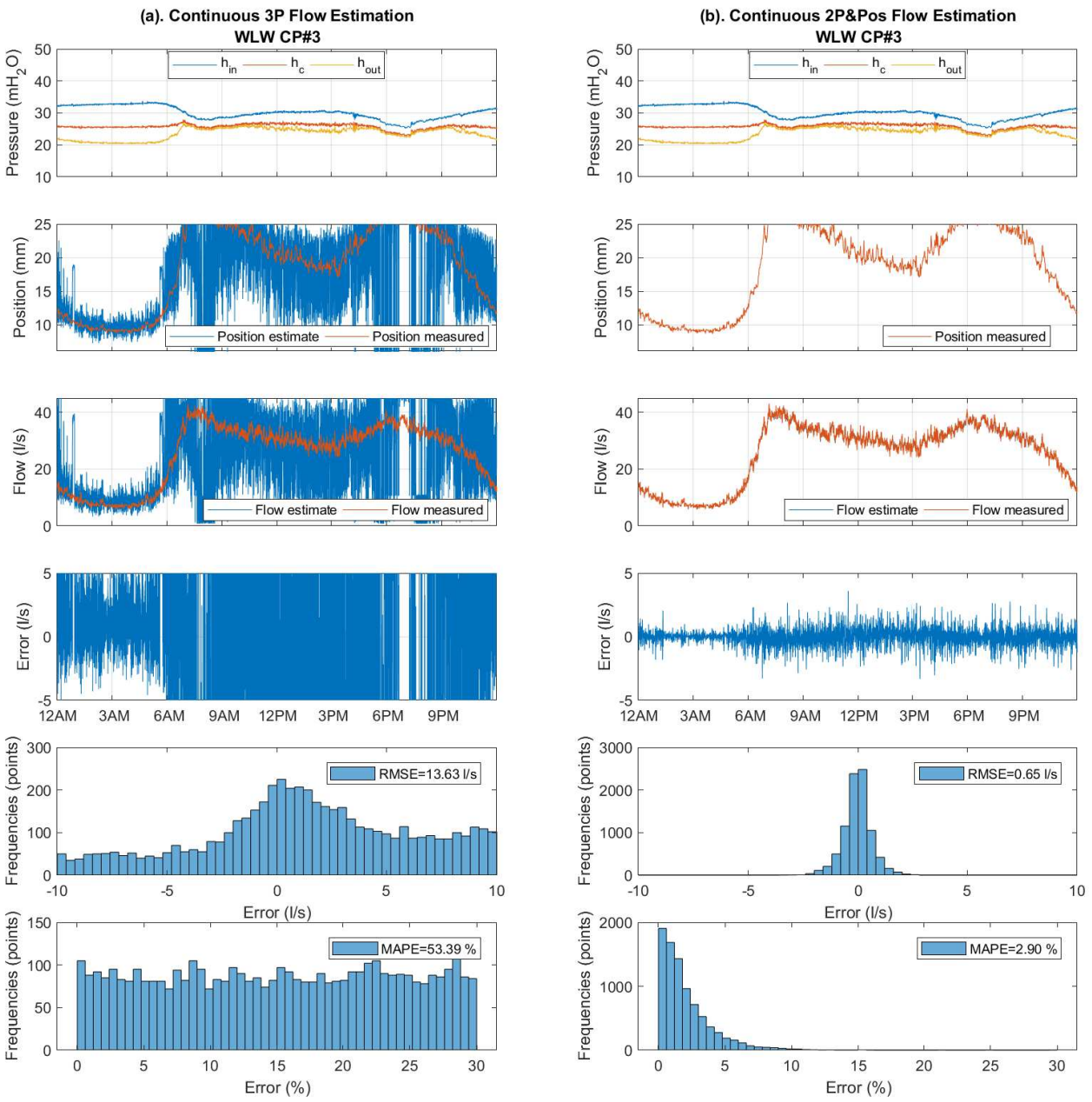

(a) 3P flow estimation validation results

(b) 2P&Pos flow estimation validation results

Figure 6.13: Flow estimation validation at the "Field Lab", Woodland Way

6.3.3 LCW valve

The LCW valve is DN100 GE. Due to restriction of the valve location, there is no valve stem position measurement on this valve. The workaround on this case is to assume the manufacturer's C_v relationship is strongly hold. The valve stem position is derived through that C_v relationship. One this is done, the force balance relationship is trained through the "virtual valve stem position". Only the 3P method can be performed at this site. Typical flow rate of LCW valve is low (less than 10l/s). Flow estimation results for LCW valve are relatively accurate compared to the other two valves. RMSE for 3 control profiles are 0.73 l/s, 0.22 l/s and 0.57 l/s respectively and the percentage errors are less than 10% for all CPs.

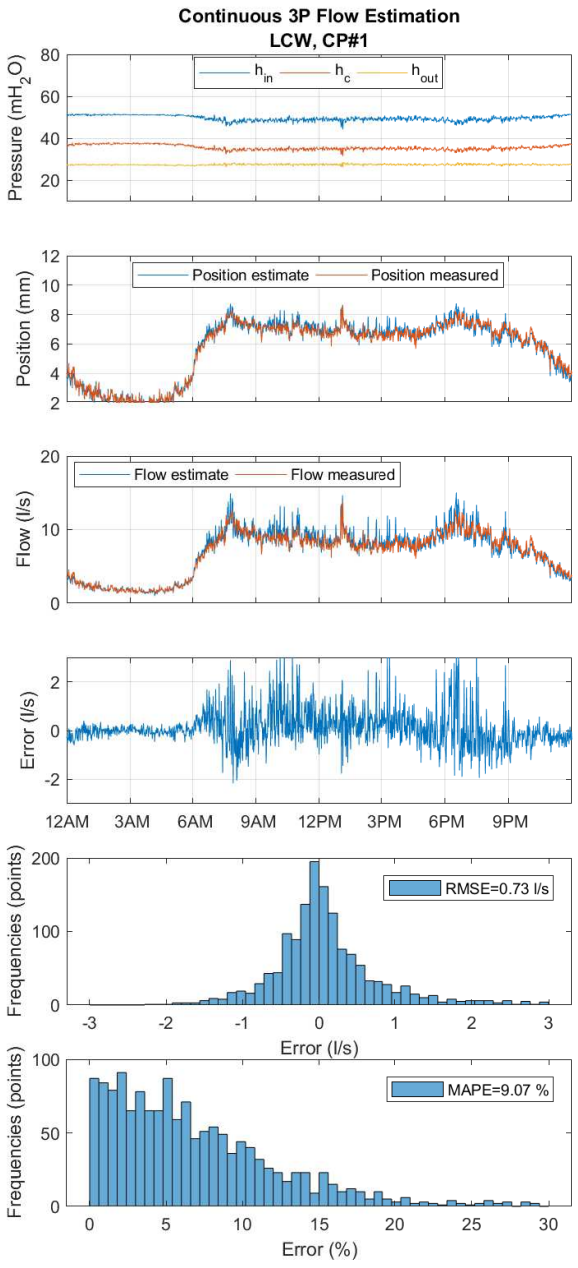

Figure 6.14: Flow estimation validation at the "Field Lab", Lodge Causeway

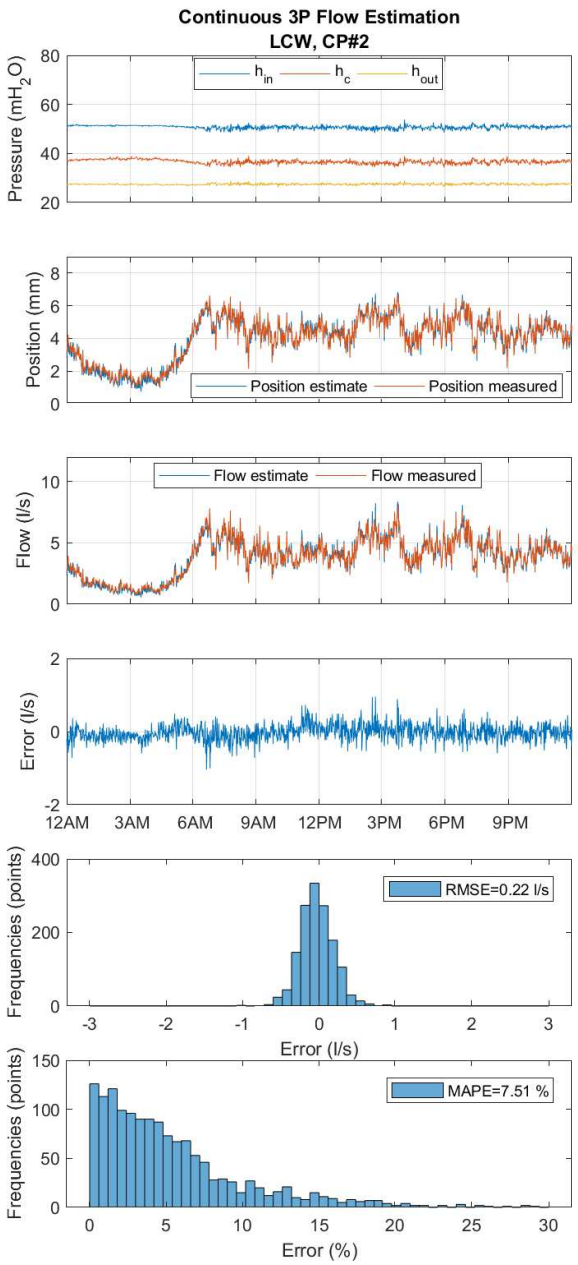

Figure 6.15: Flow estimation validation at the “Field Lab”, Lodge Causeway

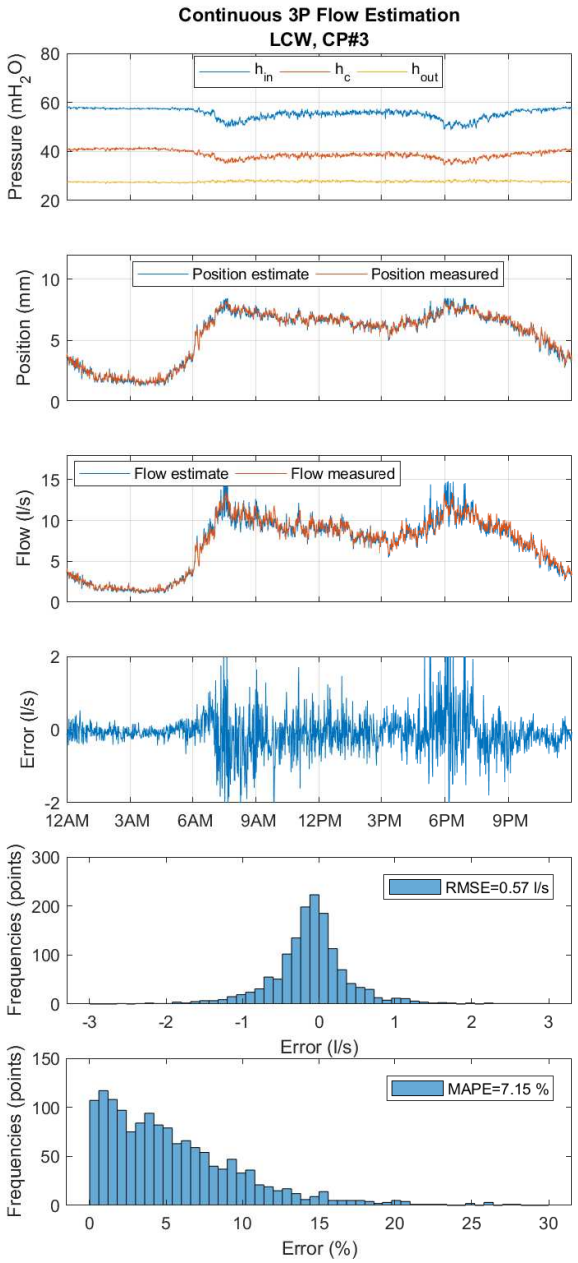

Figure 6.16: Flow estimation validation at the "Field Lab", Lodge Causeway

6.4 Conclusions and applicability of the result

The 3P flow estimation method was validated and compared with the 2P&Pos method. The validation was performed on all the 3 phases of experimental results. For application purposes, the validation accuracy of the phase 3 experiment (the "Field Lab" validation) is summarised in Table 6.1, The "expected" implementation of flow-modulating control profiles from flow measurement and flow estimation methods is calculated. An ACV reads the flow from either direct measurement or estimation and sets the pressure control according to the received flow. An illustration of this calculation is shown in Figure 6.17, where the valve is SKL (Cla-Val DN100 GE).

Errors are then calculated from the difference between the pressure according to the control profile and the pressure that the valve sets according to the received flow reading. The impact of those errors onto control profiles is shown in Figure 6.18.

With the availability of flow measurement, deviations from the control profile only come from control devices. With flow estimation, flow estimation errors were added to errors due to devices to obtain predicted data. Results obtained through both estimation methods were compared with the direct flow measurement. Overall, the valve SKL and LCW achieved a more accurate 3P flow estimation result compared to the valve WLW. This could be because the WLW valve is large and operates at low differential pressure conditions. Consequently, the key variable for 3P flow estimation, the control chamber pressure (h_c), oscillates at high frequency (unstable) and only varies by a few meters which limits the model training range. These conditions are suspected to affect the 3P flow estimation performance. The impact of the 2P&Pos method was almost identical to the case with a flowmeter. The 3P method provided similar variations in most cases. Cases where the 3P method did not perform well were the SKL#2 where the variation was high even with the flowmeter and the WLW#3, where the DP was very low most of the time (less then 5 mH_2O).

Table 6.1: The Root-Mean-Squared Errors (RMSE) for the control valves installed in an operational network (the “Field Lab"); Errors are shown in l/s and percentage (%)

		RMSE(l/s)		MAPE(%)	
Valve ID	Valve Model and size	3P	2P&Pos	3P	2P&Pos
SKL#1	Cla-Val DN100 GE	0.7	0.3	9	3
SKL#2	Cla-Val DN100 GE	1.5	0.4	9	3
SKL#3	Cla-Val DN100 GE	0.6	0.3	5	3
WLW#1	Cla-Val DN150 GE	3.6	0.9	17	3
WLW#2	Cla-Val DN150 GE	3.7	0.6	17	3
WLW#3	Cla-Val DN150 GE	13.6	0.6	53	3
LCW#1	Cla-Val DN100 GE	0.7	-	9	-
LCW#2	Cla-Val DN100 GE	0.2	-	8	-
LCW#3	Cla-Val DN100 GE	0.6	-	7	-

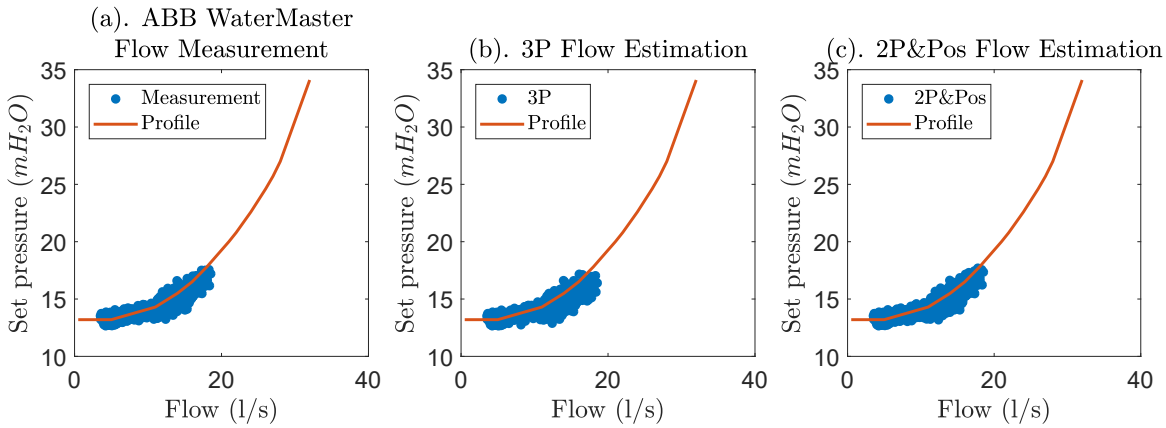

Figure 6.17: A comparison of the “expected” implementation of a flow-modulating control profile for the Cla-Val DN100 GE valve (Valve ID:SKL) in the “Field Lab" based on (a.)flow measured by ABB WaterMaster DN100 electromagnetic flowmeter, the flow was sampled at 1S/s; (b.)flow estimated using the 3P method; (c.)flow estimated using the 2P&Pos method. The red line shows the pre-determined (calculated) flow modulation control profile and the blue dots show the implemented control profiles from the acquired flow and pressure measurements.

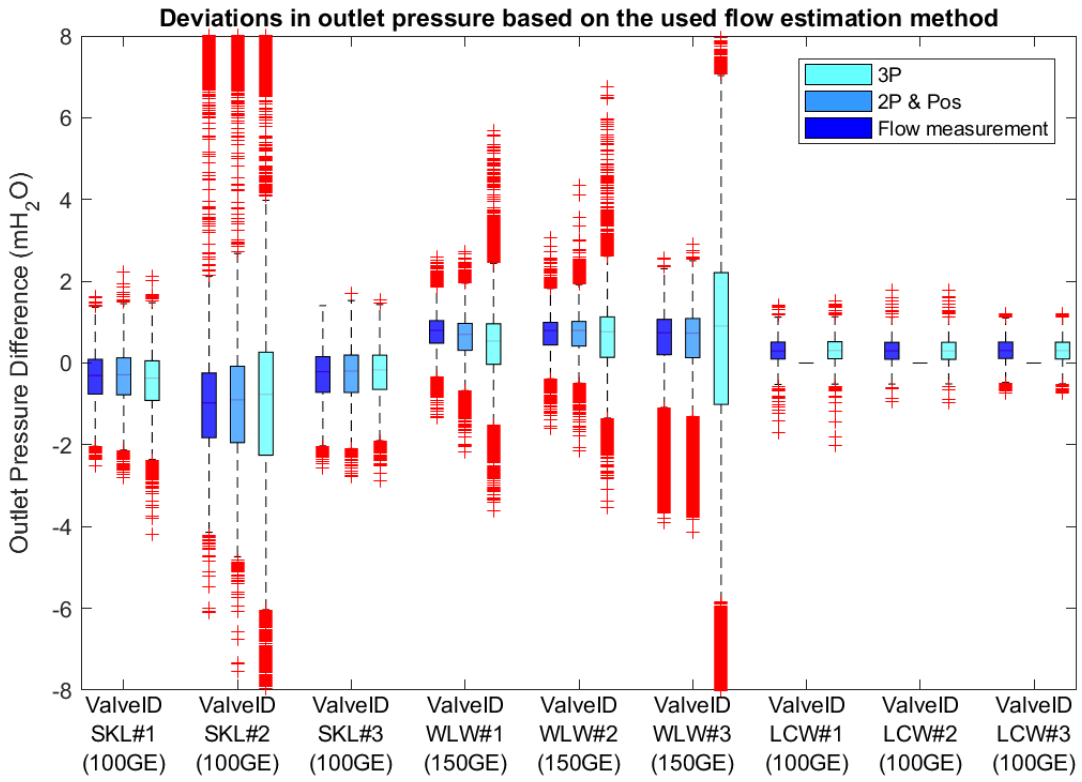

Figure 6.18: A comparison of the application of the investigated flow estimation methods on the performance of the flow modulating control; There are no valve stem position measurements for LCW due to on-site physical constraints. Red "+" indicates outliers lower than Q1-1.5*IQR or higher than Q3+1.5*IQR, where Q1, Q3 and IQR are first quartile, third quartiles and interquartile range respectively. Outliers in WLW#3 are caused by low inlet pressure (lower than the calculated flow modulating control curve). This was caused by excessive energy losses upstream of the control control valve (sediments and particles in the strainer of the ABB flow meter).

Chapter 7

Fault Detection and Diagnosis for automatic control valves in WSNs

This chapter derives a novel fault detection and diagnosis scheme for ACVs. Relationships derived in the previous chapters for flow estimation directly support the fault detection and diagnosis scheme. Accurate relationships, required for flow estimation, allow a detailed simulation of ACV operations at various hydraulic conditions. The simulation can be performed for both fault-free cases (normal ACV parameters) or for fault cases (ACV parameters indicative of fault). The simulation supports studies of fault conditions, and data generation (both fault and fault-free cases).

The proposed scheme will be able to identify when a fault occurs and define the type of fault. Common faults are reviewed and collected through either sets of experiment or computer simulations. Data for fault-free cases and fault cases are compared and observed. Feature for each fault is then engineered (designed and extracted). Machine learning techniques are applied for the detection and diagnosis process. Based on the level of sophistication of the FDD method, various monitoring options and variables are utilised such as: (i) flow and outlet pressure; (ii) inlet, outlet and cover chamber pressures; (iii) inlet and outlet pressures, and stem position. The detection and diagnosis scheme for some faults is validated through data collected from ACVs in real operational networks (the “Field Lab").

7.1 Introduction

A robust control of a water supply network relies upon multiple factors such as knowledge of the hydraulic dynamics of the system (both steady and unsteady state), the optimal definition of control requirements such as pressure reducing and/or sustaining that can tolerate uncertain parameters or disturbances for compact operational bounds, the selection of control valves, their installation, commissioning and maintenance. The scalable installation of a large number of pressure control valves with advanced control functionalities requires methods and tools for (i) the continuous monitoring of their performance for detecting and diagnosing incipient and sudden valve control faults (Fault Detection and Diagnosis, FDD), and differentiating these faults from system (network) related failures; and, (ii) the derivation of a cost-effective condition-based maintenance solution to replace the current practice of time-based maintenance for critical control assets.

The ACV faults will be investigated in the following steps:

1. **Faults collections and fault tree derivation:** Common faults have been collected from ACV users, which are a valve manufacturer company (Cla-Val), water utilities (Bristol Water, Welsh Water, Anglian Water, Severn Trent Water) and a PRV maintenance subcontractor (RPS Water). Details for each fault have been gathered from companies' reports, presentations and interviews. The faults are then categorised in groups.

2. **Fault Study/Model calibration**

   - Derive model of ACV under normal conditions (the nominal fault-free model of the hydraulic performance of an ACV), which include parameters tuning and model validations, particularly for the Imperial lab valve.
   - Use the fault-free model to simulate the operation of an ACV under normal operational conditions.
   - Use the fault-free model to simulate fault conditions by changing the model parameters.

- Carry out experiments with faults conditions and collect data under fault conditions.
- Validate the model of an ACV under fault conditions through experimental results.

3. **FDD scheme proposition:** Engineer a feature indicative of fault and propose a method to extract the feature.

4. **FDD scheme validation:** Validate the fault scheme through experimental data if possible and through simulation data when experimental data are not available.

5. **The “Field Lab" Case Studies:** Investigate the developed FDD scheme in a part of an operational WSN (the “Field Lab"). Sets of fault data are extracted from particular dates in the “Field Lab". Features corresponding to particular faults are tested for consistency.

7.2 ACV fault studies, fault data collection and fault detection scheme

7.2.1 Control Valve Fault Tree

A fault tree analysis has been derived for a set of potential faults gathered from interviews with control valve technicians from a valve manufacturer company (Cla-Val), water utilities (Bristol Water, Welsh Water, Anglian Water, Severn Trent Water) and a PRV maintenance subcontractor (RPS Water). The fault tree consists of categories of faults and the faults, symptoms and/or expected signal measurements, and potential causes for each fault. The fault tree is shown in Figure 7.1. Faults are divided into 3 main types which are hydraulic instabilities, control profile deviation and cavitation. This work investigates the first 2 types, including the detection scheme and the diagnosis scheme through the features indicative of fault. Details of faults from the fault tree are summarised in Table 7.1.

Table 7.1: Details of faults, expected observations and potential causes; Pressure sensor faults are not included as they can be detected and diagnosed through redundant measurement

Fault	**Observation**	**Potential Cause**
Control loop blockages	$h_{set} \neq h_{out}$	Particle blockages in the control pilot rail (control loop)
Stem movement constraints	$h_{set} \neq h_{out}$ for a specific stem position range	Object trapped in the valve plug/valve stem
Speed control	$h_{set} \rightarrow h_{out}$ for a short period of time when the hydraulic condition changes	-Improper setting of the speed control valve -Additional friction for the valve stem movement
Insufficient inlet pressure	$h_{out} < h_{set}$ when h_{in} is close to h_{out}	Insufficient inlet pressure so that the valve cannot deliver the set outlet pressure
High frequency instability	High-frequency oscillation of h_{out}	- Low flow condition - Incorrect setting of the control pilot so interactions between small valves/orifice/spring in the control loop occur
Low frequency instability	Low-frequency oscillation of h_{out}	Incorrect valve sizing for the specific location and hydraulic conditions
Cavitation	Vibration, loud noise and high cavitation index	- Too high differential pressure - Incorrect valve sizing

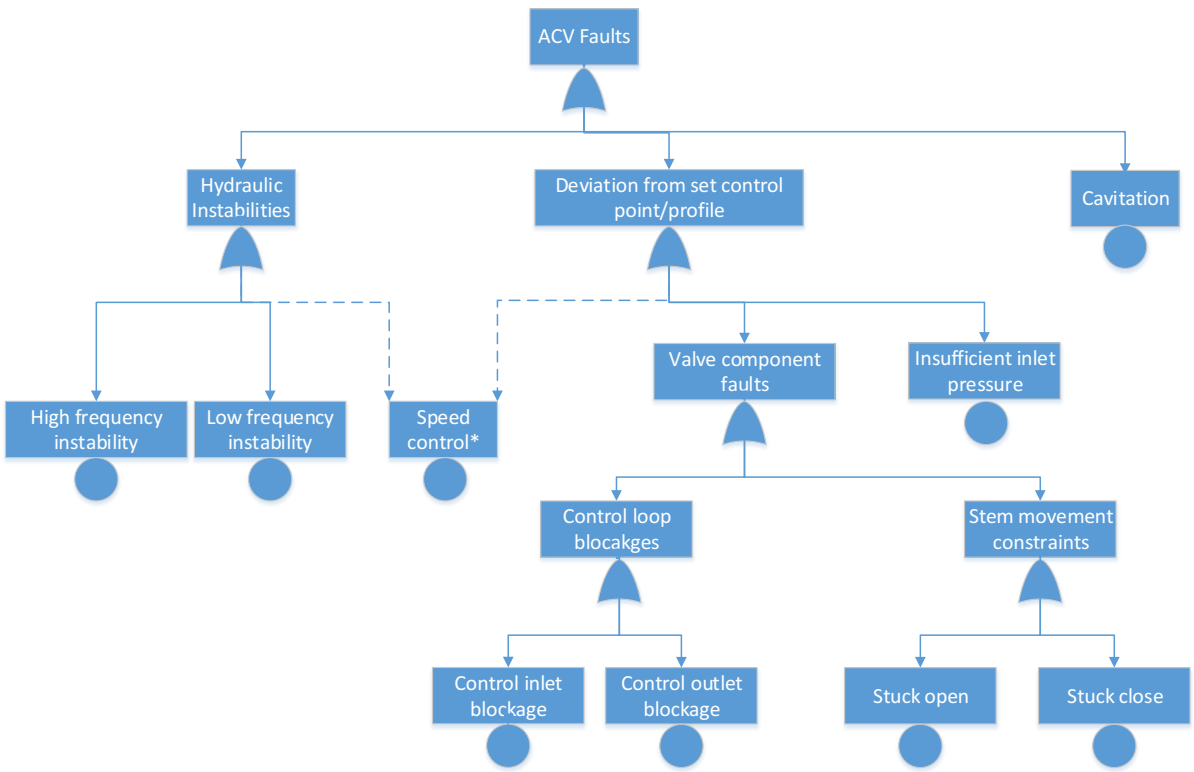

Figure 7.1: An ACV fault tree: Faults relating to speed control valve can trigger both detection scheme belonging to hydraulic instabilities and the control profile deviation.

7.2.2 Control valve model for data generation through computer simulation

In Chapter 6, flow estimation through the use of force balance equation and C_v characteristic equation were illustrated. A typical ACV, particularly a PRV, consists of a control loop (pilot rail). Equation describing the control loop has been shown in Prescott and Ulanicki (2003). In Chapter 4, a steady state simplification of the PRV model, especially the control loop, was presented. Combining the steady state-equations of the PRV control loop, the force balance equation and the C_v characteristic equation, the steady-state nominal fault-free model of a PRV is:

$$h_c = c_1(x_m)h_{in} + c_2(x_m)h_{out} + c_3(x_m) \tag{7.1a}$$

$$q = C_{vm}(x_m)\sqrt{h_{in} - h_{out}} \tag{7.1b}$$

$$C_{vfo}\sqrt{h_{in} - h_c} = C_{vp}(x_p)\sqrt{h_c - h_{out}} \tag{7.1c}$$

$$k_{spr}(P_{sp} - x_p) - \rho g h_{out} a_d + m_p g = 0. \tag{7.1d}$$

where h_{in}, h_c and h_{out} are pressure heads for the control valve inlet, control chamber and outlet [mH_2O]; x_m is the opening of the valve [%]; x_p is the opening of the CRD pilot valve [%]; q is flow through the main valve [l/s]; $c_1(x_m)$, $c_2(x_m)$ and $c_3(x_m)$ are polynomial functions for calculating the minor losses between the pressure measurement points within a globe control valve and the force-balance axis (stem axis); C_{vm}, C_{vfo} and $C_{vp}(x_p)$ are the flow coefficients (valve/orifice capacities) [l/s per m$^{0.5}$]; K_{spr} is the CRD pilot valve spring constant [N/m]; P_{sp} is the set point of the CRD pilot valve [m]; a_d is the area of the CRD pilot valve diaphragm [m^2] and m_p is the mass of the CRD pilot valve element [kg].

The steady-state model, shown in Equations 7.1, consists of a force balance relationship, a main valve flow characteristic, a pilot control loop flow characteristic and a CRD pilot valve force balance equation, respectively. With the applied steady-state model, dynamic states are represented by quasi-steady states for which the time derivative part and flow between the valve control chamber and the control loop are neglected.

For an initial FDD analysis and simulation, data were taken from a pipe rig at Imperial College London (InfraSense Labs). The valve is Cla-Val PRV GE9001 DN100 and details of the lab were presented in Chapter 3. A model will be calibrated for this valve, including parameters and relationships. After the model is calibrated, a simulation will be performed to confirm that the model accurately represents the valve behaviour.

7.2.3 Control valve model calibration, parameters tuning and model simulation under normal conditions (no faults)

The model Equations 7.1a and 7.1b have already been calibrated previously for flow estimation. The $C_{vp}(x_p)$ characteristic was validated experimentally in Prescott and Ulanicki (2003). Since the CRD pilot valve is the same, the relationship $C_{vp}(x_p)$ is assumed to be the same, which is:

$$C_{vp}(x_p) = 0.0000753(1 - e^{-1135x_p}). \tag{7.2}$$

Other variables such as m_p, a_d and k_{spr} are also assumed to be the same as those in Prescott and Ulanicki (2003), which are $m_p = 0.1$ kg, $a_d = 0.00196$ m^2, $k_{spr} = 70{,}000$ N/m. The only variables that can be different to those in Prescott and Ulanicki (2003) are C_{vfo} and P_{sp}. The C_{vfo} is unique to the Imperial pipe rig as the control loop is extended to a control panel which includes pipe bends, connectors and extra length introducing an additional head loss. Although there is also additional head loss at the control loop outlet, it is not accounted for because its effect would only result in a different pilot valve opening, which will not be measured. The P_{sp} was determined by a CRD pilot setting, which does not change for each experiment if the setting is fixed.

The C_{vfo} and the P_{sp} were found through regression of experimental data. 10 sets of experiments were conducted, each of them included a constant pump setting (inlet control) and a constant CRD pilot valve setting (outlet control). The flow was varied by adjusting the demand valve downstream to the PRV. Each experiment included either "step opening" or "step closing" of the demand control valve. Steady-states data which contained constant pressures and flow were taken. The values of C_{vfo} and the P_{sp} were found using the non-linear least squares method. The method solves non-linear least-squares curve fitting problems in the form:

$$\min_x ||f(x)||_2^2 = \min_x(f_1(x)^2 + f_2(x)^2 + ... + f_n(x)^2). \tag{7.3}$$

Settings for the routine were 'OptimalityTolerance' = 10^{-10}; 'StepTolerance' =10^{-10} and 'Func-

tionTolerance' $=10^{-10}$. The regression result is shown in Table 7.2. For experiment sets 9 and 10, the solver did not converge to the solution for P_{sp}. The solver reported that it found "local minimum" for those two cases. The results also show that hydraulic conditions also had an impact on the value of C_{vfo}. If one wants to find a more accurate representation of the behaviour, hydraulic condition factors will need to be included.

Table 7.2: Least-squares non-linear regression for C_{vfo} and P_{sp}

Experiment No.	Experiment			Regression result	
	Action	h_{in}[mH_2O]	h_{out}[mH_2O]	C_{vfo} [l/s per m$^{0.5}$]	P_{sp}[m]
1	step opening	13.7	5.7	0.0026	3.63E-05
2	step closing	13.6	5.8	0.0026	3.52E-05
3	step opening	15.3	5.9	0.0024	3.20E-05
4	step closing	15.2	5.9	0.0023	2.94E-05
5	step opening	21	6	0.0023	3.32E-05
6	step closing	20.9	6	0.0023	3.08E-05
7	step opening	41.6	12.3	0.0042	4.14E-05
8	step closing	41.5	12.4	0.0043	4.21E-05
9*	step opening	39.7	25.4	0.0040	0
10*	step closing	39.7	25.6	0.0040	0

After the C_{vfo} and P_{sp} were found for each experiment, model simulation was performed to validate that Equations 7.1 can accurately represent the valve behaviours. The simulation took h_{in}, q and P_{sp} as inputs and computed h_c, h_{out}, x_m and x_p as outputs. The outputs were then compared with measurements, showing that the model accurately represents the valve behaviours under normal conditions. Any normal condition data sets representing the Imperial ACV can be generated through a computer simulation using a specific set of valve parameters. Input values for the simulation at a time point were h_{in}, q and P_{sp}, and the output were h_{out}, h_c, x_m and x_p.

7.2.4 Fault data collection from model simulation and the experimental investigation of an ACV with deliberately induced physical faults.

Data have been collected from both computational simulation and experiments. Identical to the simulation under normal conditions, the inputs for the simulation at a point in time were

h_{in}, q and P_{sp}, and the outputs were h_{out}, h_c, x_m and x_p. For each set of fault data simulation, a normal condition data set was generated aside. The flow was varied in steps of 2l/s from 2l/s to 30l/s through the time range of 150s. Gaussian white noise of 10 dB was also added to the flow signal. The following data sets with fault conditions were generated from a computer simulation:

1. **Control loop blockages**: Control loop blockage conditions were generated by adjusting the head loss coefficients, C_{vfo} and C_{vp}, in the control loop in the model in Equation 7.1c. Two types of faults were generated according to the following conditions:

   (a) **Control inlet blockage**: The coefficient, C_{vfo} was adjusted because it represents a loss coefficient in the control loop between the ACV inlet and the control chamber. In total, there were 48 sets of simulation consisting of 4 inlet pressure combinations (30, 40, 50, 60 mH_2O), 4 CRD settings (corresponding to *hout* of 5, 10, 15, 20 mH_2O) and 3 blockage levels of the C_{vfo} (25%, 50%, 75%).

   (b) **Control outlet blockage**: The coefficient, $C_{vp}(x_p)$ was adjusted because it represents a loss coefficient in the control loop between the control chamber and the ACV outlet. In total, there were 48 sets of simulation consisting of 4 inlet pressure combinations (30, 40, 50, 60 mH_2O), 4 CRD settings (corresponding to *hout* of 5, 10, 15, 20 mH_2O) and 3 blockage levels of the $C_{vp}(x_p)$ (25%, 50%, 75%).

2. **Valve stem position blockage**: Valve stem position blockage conditions were generated by adjusting the operational range of the valve stem position. When the simulated position value reached the bound, h_{out} was calculated through the C_v characteristic equation because with the blockage, the force balance equation no longer holds true for all values.

   (a) **Valve stem stuck open**: The minimum operational range of the stem position was limited. In total, there were 48 sets of simulation consisting of 4 inlet pressure combinations (30, 40, 50, 60 mH_2O), 4 CRD settings (corresponding to *hout* of 5, 10, 15, 20 mH_2O) and 3 minimum opening limits (5mm, 10mm, 15mm).

(b) **Valve stem stuck close**: The maximum operational range of the stem position was limited. In total, there were 64 sets of simulation consisting of 4 inlet pressure combinations (30, 40, 50, 60 mH_2O), 4 CRD settings (corresponding to *hout* of 5, 10, 15, 20 mH_2O) and 4 maximum opening limits (10mm, 15mm, 20mm, 25mm).

Particular faults were experimentally generated for a PRV at Imperial College London (InfraSense Labs), through a Cla-Val DN100 GE. The following data sets were generated from a laboratory experiment at Imperial College London:

1. **Control inlet blockage:** The control valve inlet blockage condition was experimentally simulated by partly blocking the control loop inlet stopcock. 12 sets of experiment were conducted, which included 6 inlet-outlet combinations and 2 blockage levels on each combination. Flow was adjusted in steps throughout each experiment.

2. **Control outlet blockage:** The control valve inlet blockage condition was generated by partly blocking the control loop outlet stopcock. 12 sets of experiment were conducted, which included 6 inlet-outlet combinations and 2 blockage levels on each combination. Flow was adjusted in steps throughout each experiment.

3. **Speed control settings:** There were 9 sets of experiment including 3 inlet-outlet combinations. On each combination, the SCV was adjusted to be 0 turn, 5 turns and 10 turns.

4. **Instability:** An instability in the laboratory valve was generated by getting a low flow with high differential pressure. There was one set of experiment consisting of inlet pressure changes.

5. **Insufficient inlet:** Since this fault was straightforward and occurred relatively often, one set of experiment including this fault was selected for analysis.

7.2.5 Fault detection scheme

For pressure control ACVs, faults occur when they fail to control pressure set by the control profile. In other words, there is an unacceptable level of discrepancy between the measured pressure and the pressure according to the control profile. A residual which is this discrepancy can be analysed for fault detection. Table 7.3 shows examples of signals indicating faults, consisting of 3 subfigures: Pressure and flow signals, outlet pressure vs set pressure, and residuals (the difference between the outlet pressure and the set pressure). Example signals were collected from laboratory experiment phase 1 (insufficient inlet, control loop blockages, instability), a previous experiment (Borotoulas, 2009) (improper speed control valve setting) and simulations (valve stem restriction). The residuals of particular faults establish certain characteristics. These characteristics will be quantified as "features". The residual features will be extracted and investigated separately on each type of fault in Section 7.3 (feature engineering and fault diagnosis).

According to fault examples on Table 7.3 and other collected signals indicative of faults, during fault conditions, the ACVs delivers significantly different outlet pressure compared to the desired pressure (set pressure). The residual was defined to be the discrepancy between the regulated pressure and the set pressure as $Res = h_{out} - h_{set}$ where h_{set} is set pressure from the control profile. Herein, a fault detection scheme was therefore constructed that if the residuals reached the acceptable threshold, fault was detected and further a fault diagnosis scheme was required. Two main types of residuals and their threshold for fault detection are:

1. **Control profile deviation:** The deviation occurs at a presence of most types of fault except for instabilities. The offsets occur in different patterns depending on the type of faults. Fault is detected when the residual size is larger than an acceptable level (decided by users), which could be set differently on different valves. For example, in this research, fault was detected when the residual was higher than 1 mH_2O for lab ACVs and 2 mH_2O for "Field Lab" ACVs.

2. **Instabilities:** With instabilities, signal oscillation occurs at various amplitudes and char-

Table 7.3: Plots of signals indicating faults. Plots for each fault include pressure and flow signals, set vs measured pressure and residuals plot.

Fault	Plots
Insufficient inlet	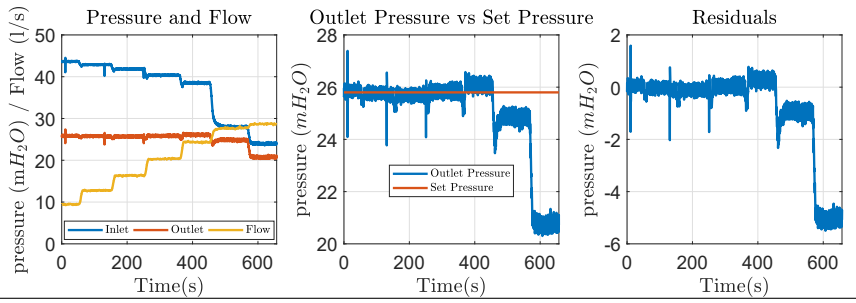
Stem restriction	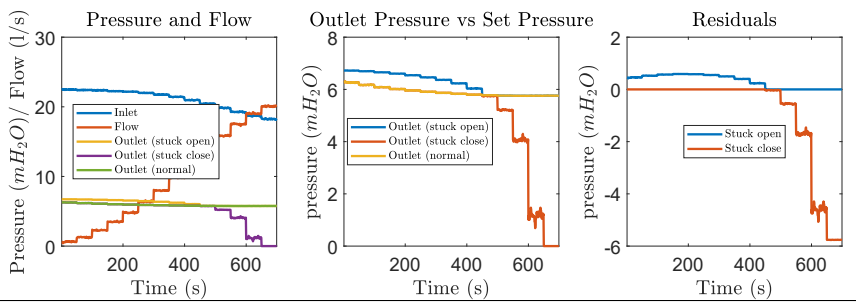
Control inlet blockage	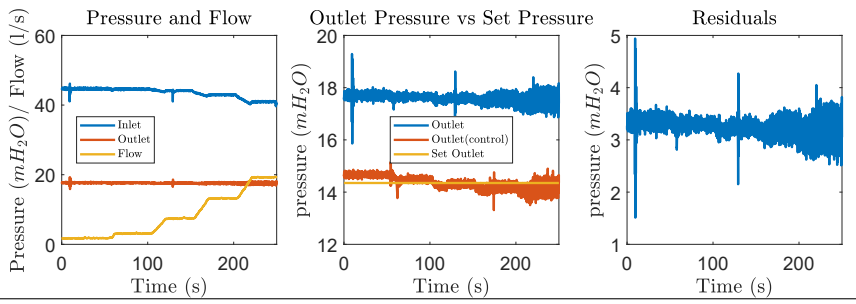
Control outlet blockage	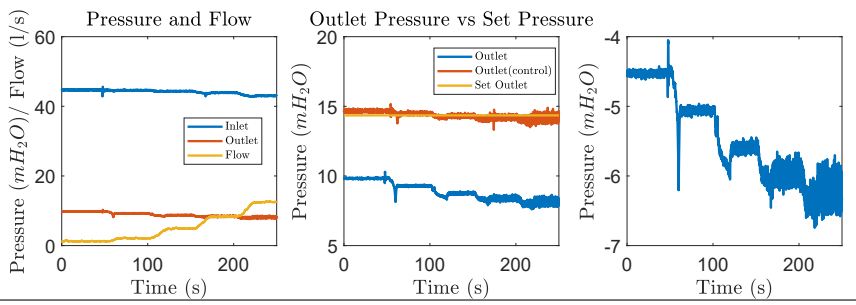
Improper speed control valve setting	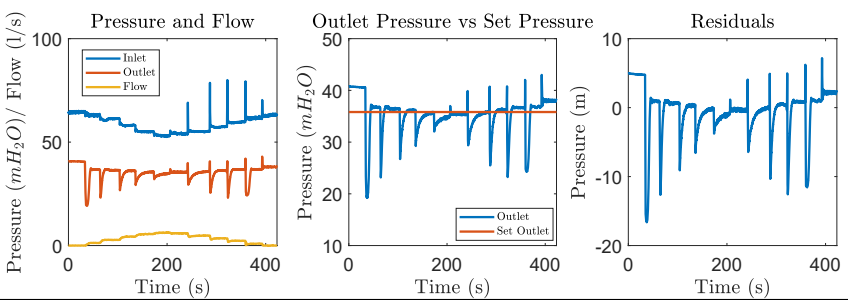
Instability	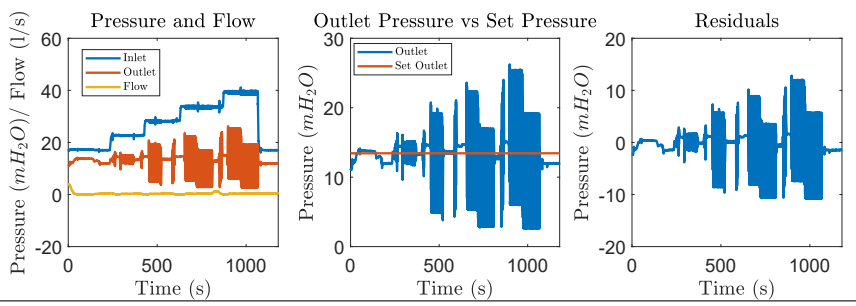

acteristics. It is different from the Control Profile Deviation because the signal might present a small deviation but fluctuate around the set pressure instead. Therefore, there needs to be a continuous monitoring scheme, especially for instabilities. The scheme will be determined from instability features which will be discussed in Section 7.3.4. The length of time for performing the monitoring scheme can be set differently. For example, for the “Field Lab" valves, the monitoring scheme for instabilities aimed to operate every hour.

As a result of the residual types, one can design their own fault detection scheme by setting a certain threshold for the case of the Control Profile Deviation and by setting the oscillation parameter thresholds for instabilities. A major benefit of having the fault detection scheme is that the further fault diagnosis scheme does not have to be run all the time as it will only be run once fault is detected.

7.3 Feature engineering and fault diagnosis

The proposed FDD method is intended to be computationally efficient so it can be implemented in low power electronic systems, which manage in-situ the operation of automatic control valves. Furthermore, the developed FDD methods rely upon recent advances in continuous high-resolution pressure sensing with sampling rates ranging from 1 Sample/s to 128 Samples/s, based on the desired accuracy in representing the waveform of the hydraulic dynamics. For pressure control valves, faults are defined when a valve fails to regulate pressure according to the set pressure in the control profile. Features will be defined based on the residual variable, Res. Features indicative of faults are designed and extracted in the following sub-sections. The processes are called together as “feature engineering”. Feature engineering is sometimes referred to as feature extraction and is an important process in machine learning. The quantitative features facilitate computers in distinguishing data sets with expected characteristics. This research makes use of feature engineering to identify data indicative of faults. This section discusses fault characteristics and potential features, which are designed to

represent those characteristics. Feature variables extracted from data sets indicative of faults must be distinguishable from those feature variables extracted from data sets under fault-free conditions.

7.3.1 Systematic control profile discrepancy

For this fault category, the steady-state outlet pressure differs from the set pressure. Two common faults are considered: a blockage in the pilot control system and restriction in the valve stem movement. This can also be referred to as the valve component fault because faults occur from malfunction valve components (control loop blockage or valve stem position movement restriction).

Control loop blockage

When a blockage in the inlet pilot control loop occurs, C_{vfo} decreases as described by Equation 7.1c, causing an increase in h_{out} in order to balance the P_{sp} setting. In the case of a blockage in the outlet pilot control loop, $C_{vp}(x_p)$ decreases together with h_{out} in order to balance P_{sp}.

Valve stem movement restriction

Valve stem movement restriction can be caused by the entrapment of large items such as solid formations from sediments to corrosion scales in the body of a control valve. As a result, the valve cannot operate in its full range; it fails to fully close (stuck open) or to fully open (stuck close).

Features formulation for systematic control profile discrepancy

The relationship between h_{out} and q were considered under both normal control and fault conditions. The considered faults, which are shown in Figure 7.2, had distinctive characteristics which could easily be detected and diagnosed by inspection. To detect and diagnose through

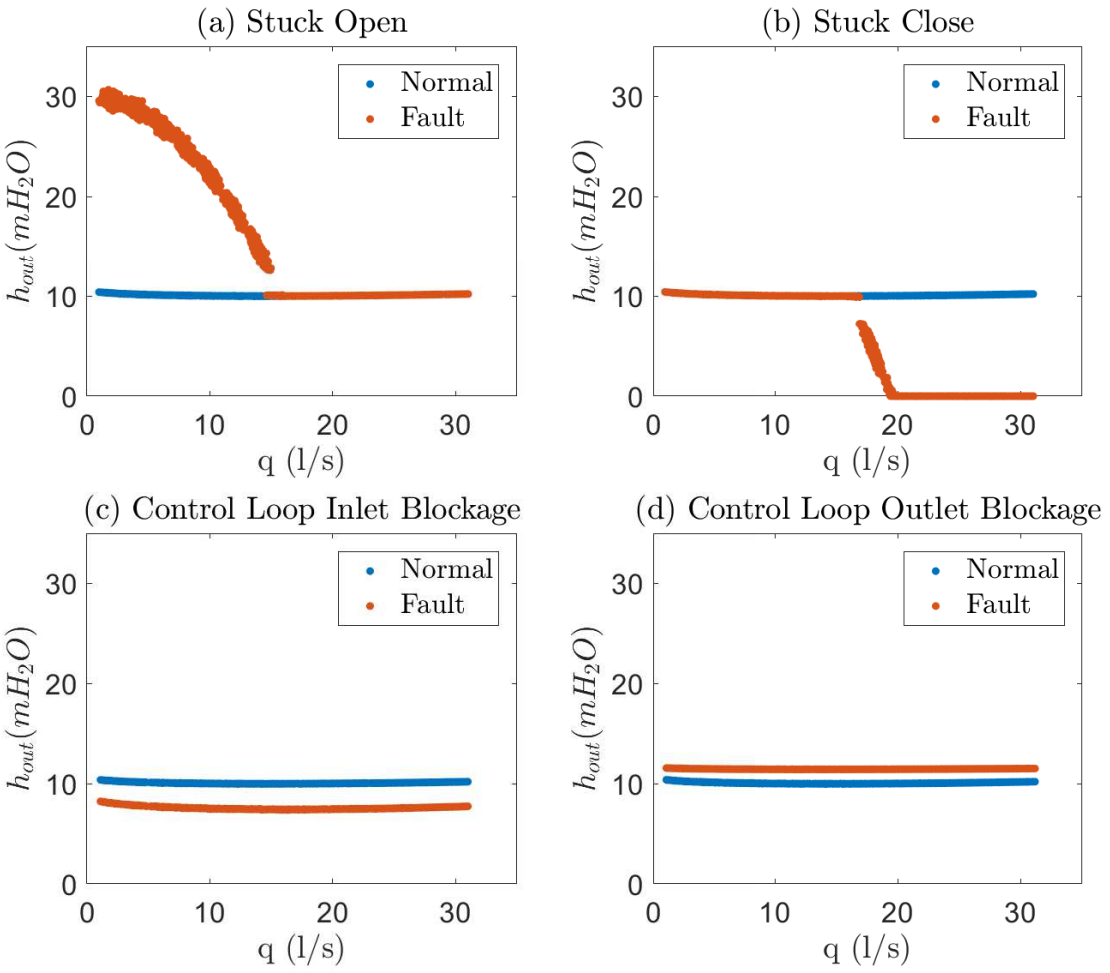

Figure 7.2: Example signals of systematic control profile discrepancy faults; Signals were generated from computer simulation. h_{out} was plotted against q for both normal and fault conditions.

a computer, feature variables representing this observation are required. To begin with, the feature variables will be a function of the residual, Res which is the difference between the outlet pressure and the set pressure. In this case, the set pressure is assumed to be pressure under normal conditions (fault-free). Four faults showed different Res characteristics. If one plots Res on the y-axis against q on the x-axis, the "Average" value and "Gradient" value should be able to distinguish four faults as follows:

1. **Valve stem stuck open:** Positive average of Res and negative gradient of Res against q

2. **valve stem stuck close:** Negative average of Res and negative gradient of Res against q

3. **Control loop inlet blockage (FO blockage):** Positive average of Res and approximately zero gradient of Res against q

4. **Control loop outlet blockage (PV blockage):** Negative average of Res and approximately zero gradient of Res against q

Therefore, the variable A is introduced, which represents an average of Res for the whole data set with any time period. Similarly, the variable M representing gradient or Res against q is introduced. However, the gradient variable cannot be obtained directly. With continuous measurements, more data can lie in a particular range of pressure targets than the rest. This will cause a bias depending on which flow region has more data points and therefore the directly calculated gradient will be different from what is observed. To prevent this issue, the variable M was calculated with Res accumulated into consecutive non-overlapping flow windows.

For example, within this work, the flow window width was set to be 5 l/s. The flow range was between 0-30 l/s; therefore, there were 6 flow windows of equal range. On each flow window, the Res variables were averaged into 1 data point in the middle of the flow window. The gradient variable, M, was calculated by linear regressions on those 6 points.

Consequently, the proposed variables A and M were extracted from simulation data sets with fault conditions. Extracted variables were then plotted in fault groups as shown in Figure 7.3. It can be seen that with the extracted feature variables, A and M, data sets indicative of different faults are well separated.

Further investigation to separate these 4 faults was performed. The investigation aimed to train and validate the use of classification models to classify 4 faults in this fault category. Models were trained and validated from 208 simulated datasets. The predictors were A and M as shown in Figure 7.3 and the target variable contained 4 faults. The classification results with 50-fold cross validation are in Table 7.4. The classification model type which achieved the best performance was the decision tree. The Fine tree and the Medium tree achieved 99.5% and the Coarse tree achieved 99%.

After the classification models had been trained through simulation data, the best performance

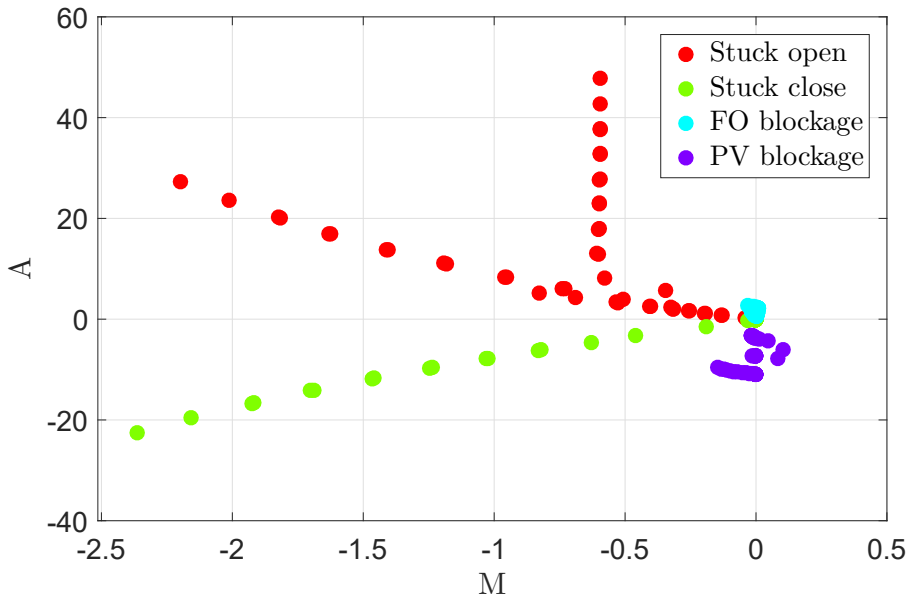

Figure 7.3: Variable A against M from control valve simulation data with faults

Table 7.4: Accuracy of classification through various classification models; The results include 50-fold validation.

Model	Accuracy
Fine Tree	99.5 %
Medium Tree	99.5 %
Coarse Tree	99 %
Linear Discriminant	62 %
Quadratic Discriminant	76 %
Linear SVM	96.2 %
Quadratic SVM	97.1 %
Cubic SVM	96.6 %
Fine Gaussian SVM	97.6 %
Medium Gaussian SVM	93.8 %
Coarse Gaussian SVM	61.5 %

Model	Accuracy
Fine kNN	98.1 %
Medium kNN	97.6 %
Coarse kNN	28.8 %
Cosine kNN	95.7 %
Cubic kNN	97.6 %
Weighted kNN	30.8 %
Boosted Trees	99.0 %
Bagged Trees	51.9 %
Subspace kNN	84.6 %
RUSBoosted Trees	39.4 %

model, the Fine tree model, was selected for further validation through laboratory data. The experiment was carried out at the Imperial pipe rig. Due to the limitation of the pipe rig, only two faults could be experimentally generated. These were the control loop inlet blockage and the control loop outlet blockage. 24 sets of experiment had been conducted (12 sets of control loop inlet blockage and 12 sets of control loop outlet blockage). A plot of variables A and M extracted from the experiments is shown in Figure 7.4. The trained fine tree classifier has successfully identified the fault condition with an accuracy of 95% (23 out of 24 datasets).

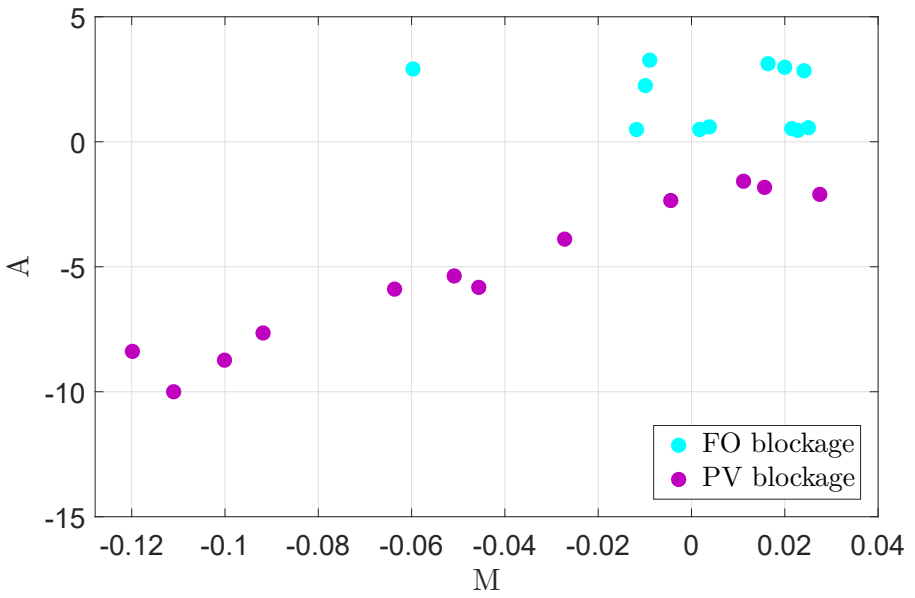

Figure 7.4: A against M from control valve experimental data with faults

7.3.2 Response time of control valves (speed control setting)

The stochastic nature of demand and rapid changes in the hydraulic conditions in water supply networks together with an increased level of complexity of the control functions (pilot control loops) and a number of control valves could induce suboptimal response and/or hydraulic instabilities from automatic control valves. A speed control valve (SCV, also referred to as the CV control valve) is used to control the opening and/or closing speed of a pressure modulating valve. It combines a needle valve and a check valve depending on the direction of the flow through the pilot system. The SCV reduces the risk of hydraulic instabilities as it slows down the control response. However, if the SCV setting is too conservative (closed) and the response time of the control valve is too slow, a sub-optimal hydraulic response to rapid changes in demand and hydraulic oscillations due to interactions with electronic control pilots might occur. On the other hand, if the SCV setting is too relaxed (opened), it will fail to suppress unwanted instabilities. Figure 7.5 shows a comparison of the control response of a valve with extreme settings of the SCV (too closed and too opened). The variations in the valve response require careful tuning for control valves with more elaborate pilot control systems and functions. The characteristics of a potential control speed fault depend on the discrepancy between the measured and set outlet pressures, Res, and the duration of this discrepancy.

When the SCV is set tight (closed), it limits flow into the control chamber. As a consequence, the valve takes time to equalise pressure in the control chamber with the pressure underneath the diaphragm. In terms of signal observation, when the hydraulic condition changes, the outlet pressure will slowly move toward the set pressure.

From experiments and published results (Prescott and Ulanicki, 2003), when hydraulic condition changes, the outlet pressure will move toward the set pressure exponentially. Hence, the ideal response feature should include both time factors and the difference between the set pressure and the outlet pressure during the response time. A slow control response feature parameter, F_{SR} is introduced. It is an integration of Res over a specific time interval, providing that the measured regulated pressure is moving towards the set pressure:

$$F_{SR} = \frac{1}{(t_2 - t_1)} \int_{t_1}^{t_2} Res \ \mathrm{d}t \quad \text{, given} \quad \frac{\mathrm{d}|Res|}{\mathrm{d}t} < 0, \tag{7.4}$$

where the selected time period is from $t = t_1$ to $t = t_2$. The Savitzky-Golay filter is used as it has a peak shape preservation property and an area under function preservation property.

The parameter F_{SR} as formulated in Equation 7.4 should be able to quantify the level of closeness of the SCV because when the SCV is set tight (closed), it limits flow into the control chamber and hence it takes a longer time to reduce Res to 0.

A set of experiments was carried out to illustrate various response times for a control valve; for example, the settings of the SCV were closed, 5 turns and opened (10 turns), and used to validate the feasibility of using F_{SR} to identify the SCV setting. There were 27 sets of experiment; 9 sets of experiment for each SCV setting with 3 different DPs. In this case, the SCV was installed to manage the speed of the opening of the control valve; however, SCVs could be installed for managing both the speed of opening and closing of the control valve. Figure 7.6 shows that the control speed feature variable, F_{SR}, can be a measure of the response rate of the control valve opening (and closing).

To use the feature variable, F_{SR}, one can define an acceptable bound for this variable at a given differential pressure (DP). A sub-optimal control is detected when a coordinate of F_{SR} and

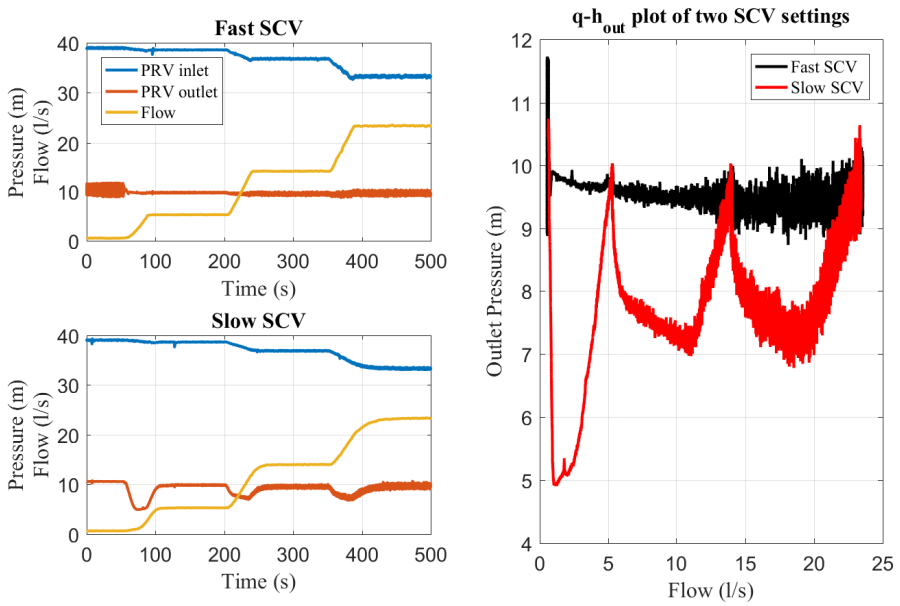

Figure 7.5: Comparison of slow and fast settings of the speed control valve

DP at a given valve is outside the acceptable level. For example, the application of the F_{SR} in assessing the performance of a control valve with large variations in the outlet pressure (Figure 7.5) is presented with one of the red dots in Figure 7.6.

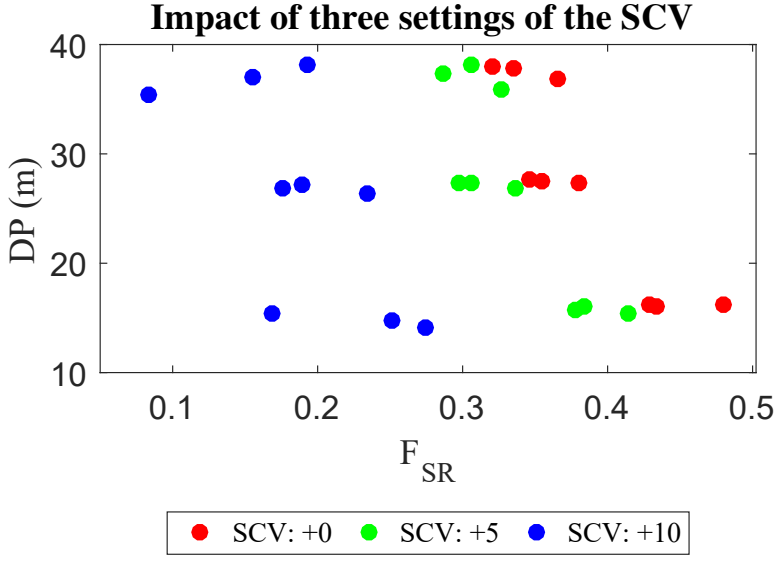

Figure 7.6: A Comparison of 3 speed control valve settings

Furthermore, for a given ACV, one can train a classification model to identify the setting of the SCV. As an example, assuming that an optimal setting of an SCV in this case is +5, the classification model will be able to distinguish the two extreme cases, SCV+0 and SCV+10. Decision trees were applied to classify experimental data based on the SCV setting in order

to characterise a slow control response. A slow control response was also observed in cases of valve stem stiction, which would result in a slow control response for both valve opening and closing.

If one aims to distinguish the acceptable level with the less extreme sub-optimal setting (for example, distinguish +5 from +3 and +7), more data to train for the classification model will be required although the boundary between different SCV settings might not be as clear as Figure 7.6. It is important to note that for an advanced control pilot such as flow modulation or time-based modulation, it is likely that a sub-optimal setting of the SCV will result in an instability because the electronic pilot would set a new target pressure while the current outlet pressure is moving toward the previous target pressure (interactions between the electronic pilot and the SCV).

7.3.3 Insufficient Upstream Pressure

The active sectorisation of water supply networks with the introduction of District Metering Areas (DMAs) together with aggressive pressure reduction for leakage management lowers the pressure in water supply systems while it increases hydraulic energy losses. Consequently, control valves might experience insufficient inlet pressure during peak diurnal or incident related demands in order to modulate a set outlet pressure. Novel pilot control systems allow for diaphragm-actuated globe valves to fully open (e.g. automatically vent the cover chamber) in order to reduce minor energy losses (Wright et al., 2015). This network-related fault condition is characterised as: $h_{in} < h_{set} + \left(\frac{q}{max(C_v(x_m))}\right)^2$. An alarm variable, F_{LH}, is defined as:

$$F_{LH} = h_{in} - h_{set} - \left(\frac{q}{max(C_v(x_m))}\right)^2. \tag{7.5}$$

If F_{LH} is positive, the valve inlet pressure is sufficient for the pre-set modulation profile and if F_{LH} is negative, the valve inlet pressure is insufficient for the control to be implemented.

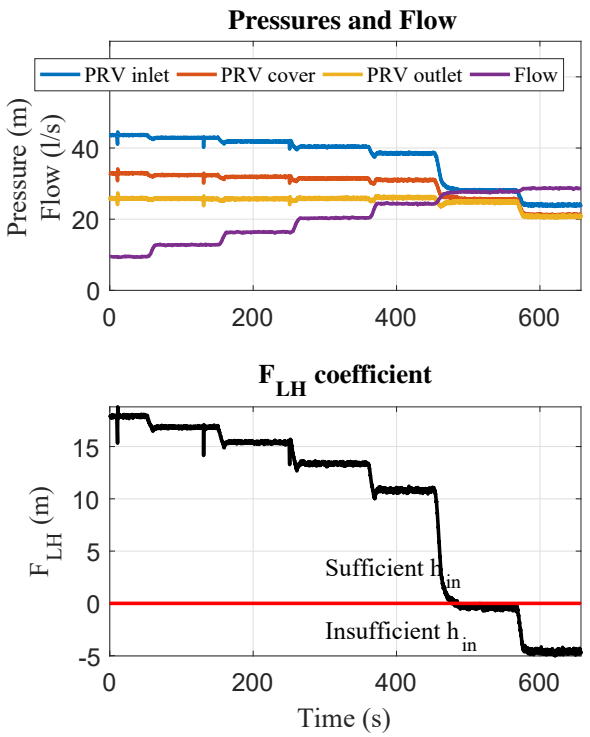

Figure 7.7: An illustration of insufficient upstream pressure; The coefficient F_{LH} is calculated using pressure and flow signals

7.3.4 Hydraulic Instabilities

Hydraulic instabilities are oscillatory changes in pressure that may have a period ranging from sub-seconds to minutes. These oscillatory changes may originate from various network control assets and users, and/or from control valves. The main causes of hydraulic instabilities due to control valves include their control behaviour under low-flow conditions and particularly for over-sized design choices, poor understanding of the network hydraulic conditions under which the control valves operate, cavitation, and advanced control options, which are not properly commissioned and managed. Instabilities can also be caused by improper settings of the SCV (as discussed in Section 7.3.2) as the SCV tends to have interactions with advanced control pilots.

Since hydraulic instabilities are characterised by short-term oscillatory pressure variations, this research extends the method for characterising complex pressure waveforms as described in Stoianov and Hoskins (2015) and applies it to diagnose hydraulic instabilities in ACVs. Three features indicative of instabilities have been proposed as follows:

1. **Cycle count:** The pressure waveforms are converted into a series of straight segments and inflexion points for a moving count-based window by applying hysteretic quantisation. The maximum edge cycle counting algorithm is applied to characterise and âĂIJcountâĂİ the hydraulic instabilities based on their amplitude and frequency (counts) and the mean pressure under which the pressure oscillations occur. Normally, the cycle count requires a sampling rate of 1 Sample/s with a low-pass filter, as cycles at higher frequency are related to noises. A major benefit of the cycle count method is that it can capture low-frequency instabilities very well (instabilities with an order of magnitude of 1 cycle/s). Those instabilities are normally associated with control pilots of an ACV. Furthermore, the cycle count gathers complex loading information which enables the estimation of fatigue-induced stress on critical components and failures of control valves. The cycle count index is defined by the summation of the product of cycle numbers and cycle ranges.

2. **Pressure Envelope Range (PER):** The ER is essential for identifying the correct solution in the 3P flow estimation method. Since instabilities normally result in high-pressure oscillation, which will cause high values of ER, the ER can be obtained through either peak envelope or max/min values (similar to the flow estimation). The PER method is suitable for high-frequency instabilities (with an order of magnitude lower than 1 cycle/s). The ER is beneficial owing to the fact that it requires very little computational power as only the subtraction between the max and min values is needed. A main disadvantage of the PER method is that it does not provide any insight into the instability.

3. **Short Time Fourier Transform (STFT):** The STFT provides a full spectrum analysis of the signal which will be useful for further analysis to find the cause of the instability for each case. The STFT depends on a few parameters which are window sizes, samples of overlap, and sampling points to calculate Fourier Transform. The STFT method provides details of any periodic oscillations but users are expected to customise the frequency ranges to see details. The result of the STFT is a spectrogram which will require further complex criteria to separate instability events, although they are easily distinguished from inspection.

For hydraulic instability, a fault detection scheme can be built by monitoring any of the three features regularly. The routine can be varied from using 15-minute data to using 24-hour data depending on sites and availability. A validation of these three features will be shown in Section 7.4.1.

7.4 Validation of the FDD scheme through the “Field Lab" case studies

7.4.1 A hydraulic instability

In this case, the hydraulic instability was observed around 14:00 on Apr 12, 2018 due to improper commissioning of the SCV. The valve was controlled with the flow modulation scheme. Figure 7.8 shows a comparison between the normal condition and the instability condition. Each case consists of 4 subplots:

1. **The outlet pressure signal:** Under an instability condition, outlet pressure fluctuates a lot more compared to under a fault-free condition.
2. **The cycle count index:** The cycle count index is defined by the summation of the product of cycle numbers and cycle ranges. The cycle count index is high when instability occurs.
3. **The pressure envelope range:** The outlet pressure envelope range is high when instability occurs.
4. **The STFT:** The spectrogram is distinguishable between the case with and without instabilities.

The plots illustrate that all the three features indicative of instability can be used to detect a fault right when it occurs.

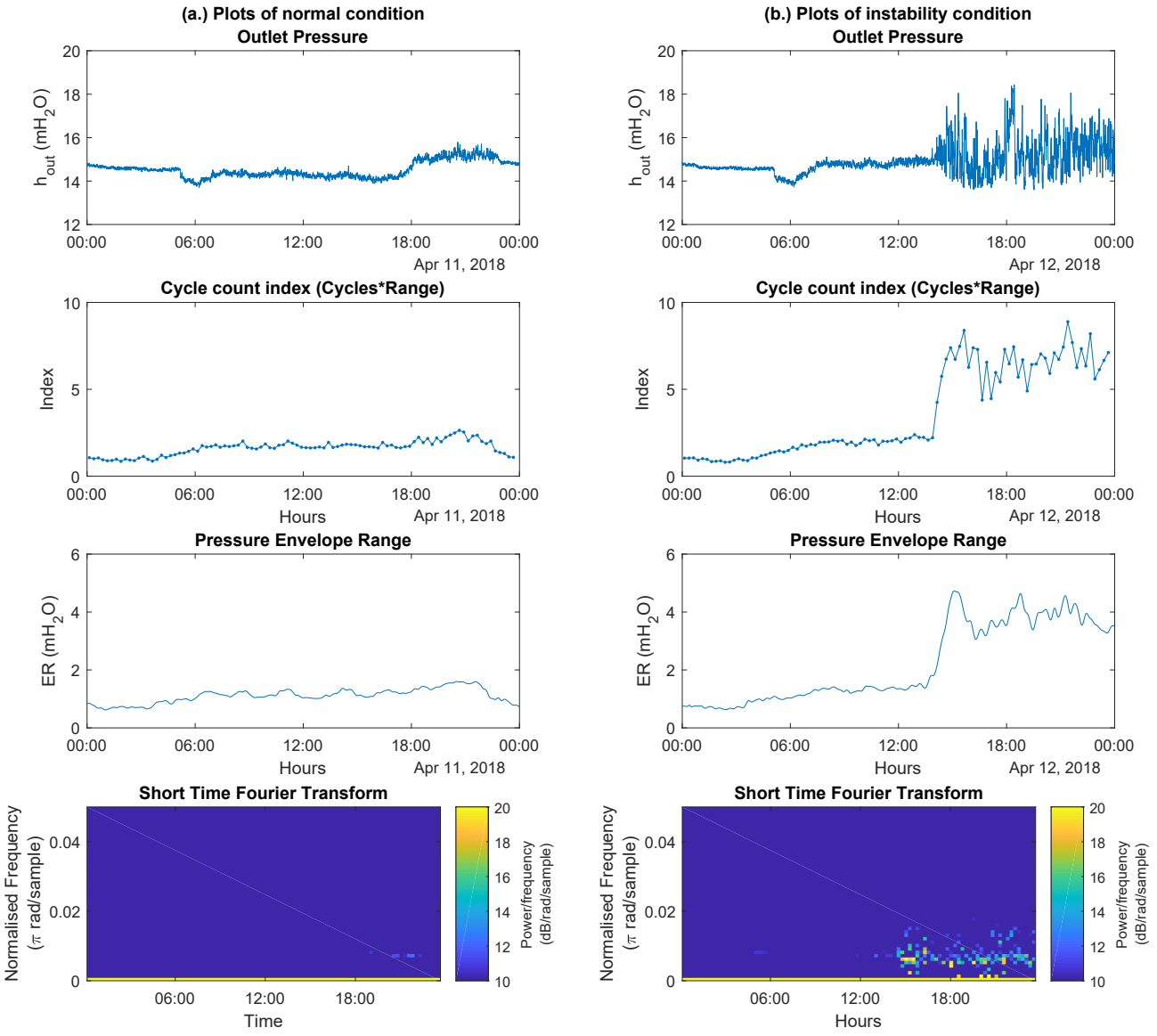

Figure 7.8: Features validation through data with and without instabilities; Data were taken from an operational valve in the “Field Lab" for 24 hours.

7.4.2 A test of feature indicative of systematic control profile discrepancy under normal conditions (fault-free)

So far, there has never been a reported fault on systematic control profile discrepancy from the “Field Lab." It is important to make sure that the derived feature variables do not activate a fault alarm (false positive). Therefore, the variables A and M were calculated from 24-hour data with the normal conditions of 3 valves, each with 3 control profiles. The result is shown in Figure 7.9. Compared to fault cases from laboratory data (Figure 7.4), a span of area including

points extracted from “Field Lab" data was smaller that plots with fault points in Figure 7.4. Hence, one can define a span of area in an $A-M$ coordinate as a threshold area for the normal condition. If the value of A or M is outside this area, the alarm for systematic control profile discrepancy is triggered and the case will be classified using the trained classification model for the sub-category fault. The monitoring of A and M can be an alternative to the fault detection scheme using Res.

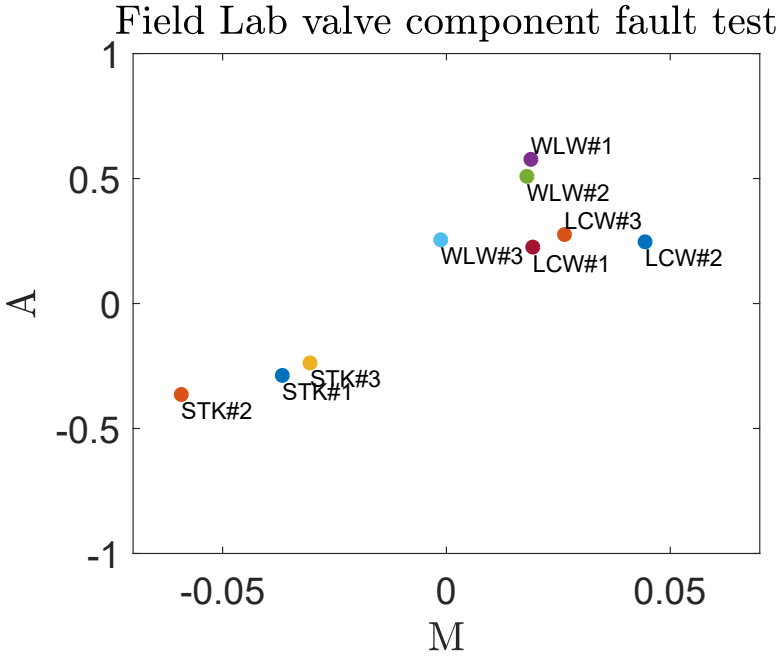

Figure 7.9: The “Field Lab" valve component fault test under normal conditions (fault-free); Each dot represents test result of each “Field Lab" valve on variable A and M coordinates.

7.4.3 Validation of feature indicative of insufficient inlet pressure in a “Field Lab" valve

In this case, a significant discrepancy from the control profile was detected. It was found that the reason behind this is insufficient inlet pressure. An insufficient inlet pressure feature, F_{LH} was continuously calculated throughout the time series signals as shown in Figure 7.10. The calculation also included the proposed flow estimation methods. It was found that the proposed insufficient inlet pressure feature, F_{LH}, could detect the insufficient inlet fault.

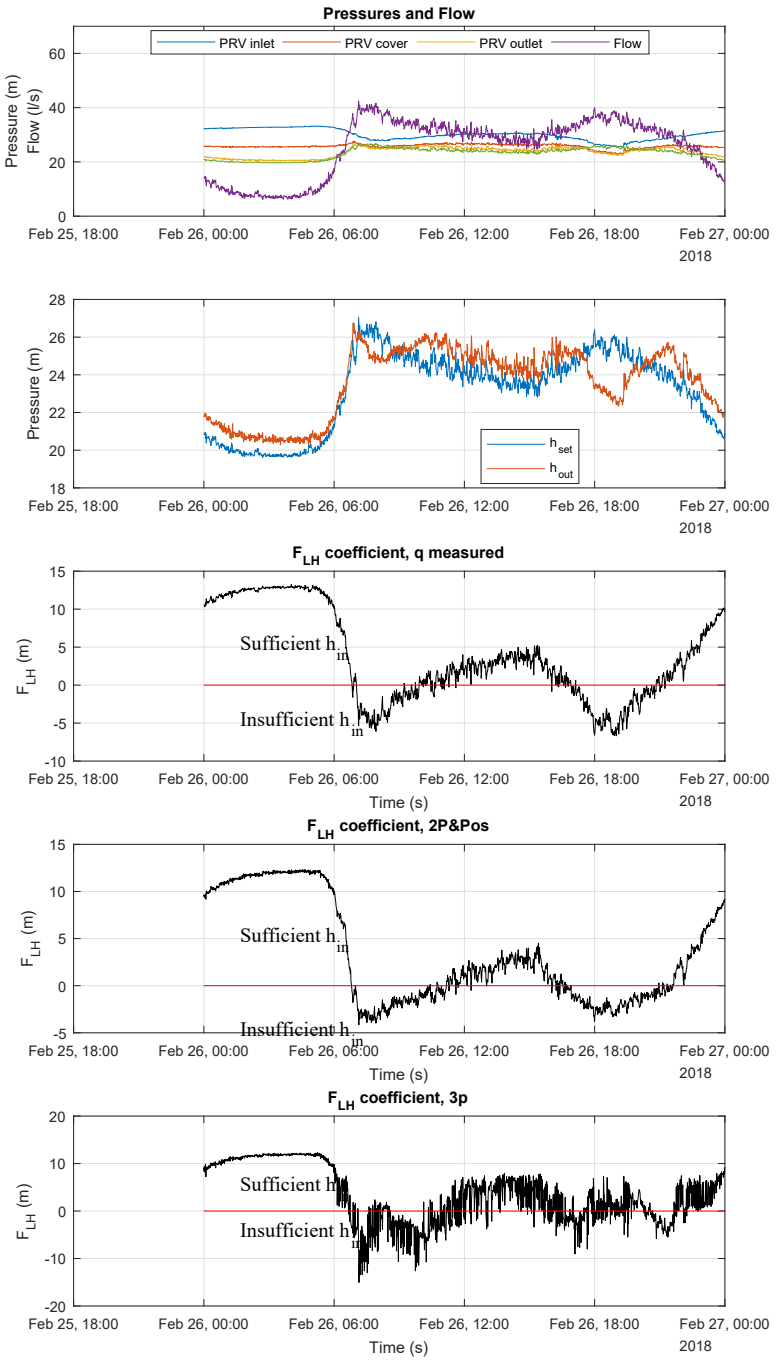

Figure 7.10: Insufficient inlet pressure test in the “Field Lab"

7.5 Conclusions

The optimal control of water supply networks requires good knowledge of the hydraulic dynamics and the implementation of sophisticated but complex control solutions and technologies. Possible faults in control valves were reviewed and a fault detection and diagnosis method was proposed. Faults-related data were collected through experiments and mathematical modelling.

Features indicative of specific faults have been engineered and validated. The proposed FDD facilitates the implementation of condition-based predictive maintenance and supports the robust and implementation of advanced control solutions in complex water supply networks.

A combination of flow estimation and the FDD scheme was also investigated. Requirements, specifications and applicability of the FDD scheme are concluded in Table 7.5.

Table 7.5: Requirements, Specifications and Applicability of FDD scheme

Faults Diagnosis method	Flow estimation method			Sampling rate requirement
	No estimation (q, h_{out})	$2P\&Pos$	$3P$	
Systematic CP discrepancies 1 (Control loop blockages)	Yes	Yes, because the C_v characteristic stays the same	No, because the force balance equation would change with the blockage	Any
Systematic CP discrepancies 2 (Valve stem blockages)	Yes	Yes, because the stem position is directly measured	No, because the force balance equation would change with the blockage	Any
Insufficient inlet	Yes	Yes as the flow estimate can be used	Yes, as the flow estimate can be used	Any
Improper Speed Control Valve	Yes	Yes	Yes	High enough to capture the drop period (higher than 10 Samples/minute)
Instabilities (Cycle count method)	Yes, because only outlet pressure is continuously measured			∼1 Samples/s
Instabilities (Envelope range)				1 Sample/s with max/min for high-freq instablity and without max/min for low-freq instability
Instabilities (STFT)				Any, preferably high sampling rate as the spectrogram will be clear

Chapter 8

Conclusions

8.1 Summary of Thesis Achievements

8.1.1 Flow estimation

In the era of the ever-increasing demand for economically efficient allocation of water resources worldwide, reliable and effective pressure management in Water Supply Networks (WSNs) is of paramount concern. Automatic control valves (ACVs) are recognised as important control devices for pressure management in WSNs. In this thesis, technologies and studies that have contributed to greater uses of ACVs have been explored. Advances in low-powered electronic pilots, which allow a range of control functions of ACVs, are coupled by concerted efforts to develop accurate valve modelling strategies. The flow-based pressure control (Flow-Modulation or FM) has emerged as one of the most effective control schemes. The FM scheme decides the set pressure from demand (flow) and therefore very much relies on accurate flow measurement. Hence, a redundancy on flow measurement is crucial to ensure a full serviceability.

To overcome the research gap on robust and accurate modelling approaches for flow measurement, this thesis has developed a novel 3P flow estimation method, where the flow through an ACV is estimated by three pressure measurements located at the valve inlet, the valve control chamber and the valve outlet. Comprehensively built on experimental data sets and refined by

machine learning techniques, the 3P approach encompasses an extensive toolkit of mathematical models of control valves for flow estimation and design principles for fault detection and diagnosis. One of the core strengths of this unified framework is that it is highly sensitive and supports accurate simulation on valve operation and surveillance. The 3P method development process has led to the following key achievements:

- **The parametric force balance equation of an ACV**: The force balance equation formulated from physically measured parameters is not accurate enough for flow estimation. An analogous relationship, of which coefficients were obtained through regression are also insufficient because the constant coefficients do not represent the actual phenomenon of pressure loss. In this thesis, a new formulation of force balance equation has been proposed and validated. The formulation takes into account the hydraulic head loss between the measurement points and the actuating points and also allows variability of the head loss coefficients at different valve openings. This formulation requires experimental data to fit for the relationship, hence the adoption of the model-training process in machine learning. It was found that the force balance relationships of two valves with the same type were slightly different.

- **The C_v characteristic relationship of an ACV**: From an experiment, the C_v relationship provided by the valve manufacturer did not reach a sufficient level of accuracy for flow estimation. The C_v relationship for flow estimation needed to be derived individually for a particular valve as they are slightly different although the valve type, size and control pilots are the same.

- **Multiple solutions on valve stem position estimation**: Once the force balance relationship was trained through data, the valve stem position could be estimated by solving the relationship for the position. It has been found that multiple solutions can occur and it is the nature of the ACV as cases of which two valve stem positions with the same pressure measurements were found experimentally. It is also found that there exists no more than two feasible solutions (dual solutions).

- **Predictor variables to identify the correct position estimate**: High flow correlates

with high signal envelopes. One can make use of signal envelopes at high sampling rates (to represent flow) together with differential pressure to roughly find the valve stem position. Since multiple solutions normally occur across a specific valve stem position point, the two variables (the signal envelope range and the differential pressure) have become predictors to identify a correct position estimate.

- **The SVM classification model**: Support vector machine is a popular classification technique. This thesis has employed the technique to discriminate between the correct stem position estimate and the incorrect stem position estimate. Various SVM models have been trained and validated for further use of correct valve stem position estimate identification.

Three relationships/models are required for flow estimation (trained through experimental data): (i) Parametric force balance relationship, (ii) C_v characteristic relationship and (iii) The SVM classification model. Once the relationships are trained, the 3P flow estimation processes are summarised as:

1. **Position estimation**: The position estimate(s) are obtained by solving the valve stem position estimation function (a rearranged version of the parametric force balance equation) which requires measurements of the valve inlet pressure, the valve control chamber pressure and the valve outlet pressure.

2. **Correct position estimate identification**: Classification was performed through the selected SVM classification model. The model requires the outlet pressure signal envelope range and the differential pressure (the difference between the valve inlet and the outlet pressure). An output of the classification model is either lower class or upper class which allows user to select the lower position estimate or the upper position estimate. Most of the time, position estimates were dual-solutions.

3. **Flow estimation**: The selected position estimate together with differential pressure can be used to calculate flow through the C_v characteristic relationship.

Once the 3P method was established, the method was performed on validated data sets and compared against the 2P&Pos method, which estimated flow through a direct measurement of the valve stem position and differential pressure. Overall validation results are concluded as follows:

- **Imperial lab**: The valve in the laboratory was DN100 GE. The RMSE for the 3P flow estimation was 1.04 l/s whereas the RMSE for the 2P&Pos was 0.14 l/s.
- **Cla-Val lab**: The valves in the laboratory were DN80 NGE, DN100 GE and DN150 GE. The RMSE was calculated in time-series validation. On the DN80 NGE, the RMSE for the 3P flow estimation was 1.65 l/s whereas the RMSE for the 2P&Pos was 0.13 l/s. On the DN100 GE, the RMSE for the 3P flow estimation was 3.30 l/s whereas the RMSE for the 2P&Pos was 0.56 l/s. On the DN150 GE, the RMSE for the 3P flow estimation was 2.04 l/s whereas the RMSE for the 2P&Pos was 0.46 l/s.
- **The "Field Lab"**: There were 3 valves in the "Field Lab", labelled as SKL (Cla-Val DN100 GE), WLW (Cla-Val DN150 GE) and LCW (Cla-Val DN100 GE). Impacts of the accuracy of the 3P method were also simulated using the current device performance with respect to control profiles. Deviation from control profiles are shown in Figure 6.18, and in 7 out of 9 cases (SKL#1, SKL#3, WLW#1, WLW#2, LCW#1, LCW#2 and LCW#3), the deviation was below 2 mH_2O, which is the standard measure for calibration. For SKL#2, errors from the FM device itself were already high and they were magnified by the estimation. For WLW#3, the valve differential pressure was very low, which limits the accuracy of the force balance relationship.

The "Field Lab" result illustrates the feasibility of using continuously measured data to train for the relationships (force balance relationship, C_v relationship and classification model). The method was successfully adopt on a site with no valve stem position data available to train (Lodge Causeway). Also, the method still works when there is no high sampling rate data available as long as the operational range of the valve does not vary too much. One major drawback of using 24-hour data to train for relationships is that the method will fail to estimate

flow when the valve operates out of the training range or when a new hydraulic condition occurs. In practice, the derivation process can be done before commissioning a valve in a real WSN.

With the achieved level of accuracy, one can obtain a flow measurement for FM control purposes at locations where flowmeters are not installed. Impacts of using the flow estimates in the real network control will be investigated in future work. A direct potential application from this work is to support the concept of adaptive WSNs (Wright et al., 2014). Based on this concept, the PMAs can be aggregated and segregated, i.e. the permanently closed boundary valves are replaced by the control valves called dynamic boundary valves (DBVs) (Wright et al., 2015). Typically, the DBVs are opened and closed at a certain time of the day; therefore, the networks will not respond effectively to unexpected changes of demand. The flow estimation will facilitate the demand-based valve setting and hence improve the network resilience. For example, the flow estimation can signal the DBVs to open if there is a fire-flow event during their closed period.

8.1.2 Fault detection and diagnosis

After the formulated parametric force balance equation was validated for flow estimation purposes, the equation facilitates an improved understanding of valve behaviours. The force balance equation was used with the C_v characteristic equation and control loop equations to study valves under both fault and normal conditions. Laboratory experiments have also improved an understanding of ACV faults. The fault tree and characteristics of common ACV faults have been summarised in this thesis.

Faults data were collected through both sets of simulation and laboratory experiments. The "fault detection" scheme was defined through the threshold of the residuals between the fault conditions and the expected fault-free conditions.

Features indicative of faults were designed and extracted (feature engineering). Once a fault was detected, the signal proceeded to the "fault diagnosis " scheme, which included various tests of feature variables for specific faults. For a special case of instability, the fault was detected

immediately from fault parameter monitoring.

Ultimately, the proposed FDD facilitates the implementation of condition-based predictive maintenance and supports the robust and implementation of advanced control solutions in complex water supply networks.

8.2 Applications

Direct applications achieved from this thesis include:

- **A ready-to-use set of codes for the 3P and 2P&Pos flow estimation**: The codes contain "the model-training part", which takes time-series data to train for necessary models for flow estimation and "the prediction part", which imports the trained model for flow estimation.

  This flow estimation directly supports an implementation of a robust FM scheme. The FM scheme can then obtain a redundancy of flow signal measurement, and also can be implemented on a valve location without a flowmeter. The achieved engineering reliability on FM can improve WSNs toward more robust operational networks.

- **An FDD scheme:** includes a fault diagnosis scheme to separate fault data conditions from normal data conditions. It also includes sets of tests to diagnose specific faults.

  The conventional time-based maintenance of ACVs can be replaced by the condition-based maintenance from the proposed FDD scheme. The achieved engineering reliability on ACV operation holds significant promise for WSN refinement toward a variety of control forms, which will allow more controllability in networks.

8.3 Future Work

Suggestions for future work include:

- **Improvement of the parametric force balance equation by fitting with functions other than polynomial function**: The parametric force balance equation is highly non-linear and it is fitted with data through ordinary least square regression into the polynomial form. The polynomial form has a major advantage on the simplicity of root finding. It is suggested by the author that more sophisticated functional forms other than polynomial be fitted, as they might be more accurate than the polynomial form. This improvement could provide a more accurate 3P flow estimation.

- **Effects of the 3P and 2P&Pos on the real FM scheme**: This thesis has investigated the impact of the FM scheme if the 3P and 2P&Pos are to be implemented. The author suggests future experiments on the real implementation of the flow estimation scheme. This will allow practitioners to assess issues on the implementation side, ranging from computational power and real-time signal reliability to controller devices.

- **Modelling of FM control pilots**: From the control perspective, if the complex FM control pilots are accurately modelled, one can include an additional controller on the FM control pilots, which will prove suitable for the implementation of the flow estimation scheme. The flow estimation function might be included in the FM control pilots.

Bibliography

H. Abdelmeguid and B. Ulanicki. Pressure and leakage management in water distribution systems via flow modulation PRVs. In *Water Distribution System Analysis 2010*, Tucson, AZ, USA, 2010.

Y. J. An, B. J. Kim, and B. R. Shin. Numerical analysis of 3-D flow through LNG marine control valves for their advanced design. *Journal of Mechanical Science and Technology*, 22 (10):1998–2005, 2008. ISSN 1738-494X. doi: 10.1007/s12206-008-0745-6.

A. Atmanand and M. Konnur. A novel method of using a control valve for measurement and control of flow. In *Quality Measurement: The Indispensable Bridge between Theory and Reality (No Measurements? No Science! Joint Conference - 1996: IEEE Instrumentation and Measurement Technology Conference and IMEKO Tec*, volume 2, pages 813–816 vol.2, June 1996. doi: 10.1109/IMTC.1996.507281.

I. Borotoulas. Experimental evaluation of the dynamic performance of pressure reducing valves. Master's thesis, Department of Civil and Environmental Engineering, Imperial College London, 2009.

M. P. Brown, W. N. Grundy, D. Lin, N. Cristianini, C. W. Sugnet, T. S. Furey, M. Ares, and D. Haussler. Knowledge-based analysis of microarray gene expression data by using support vector machines. In *Proceedings of the National Academy of Sciences of the United States of America*, volume 97, pages 262–267. National Academy of Sciences, 2000. ISBN 0027-8424 (Print)\r0027-8424 (Linking). doi: 10.1073/pnas.97.1.262.

M. Bull and K. Lim. Effects of Reynolds Numbers on Wall-Pressure Fluctuations in Constant-

Perssure Turbulent Boundary Layers. In *Conference on Hydraulics and Fluid Mechanics*, pages 143–150, 1968.

A. R. Burrows. Controller and control system for a pressure reducing valve, 2010. URL `http://www.google.com/patents/US20100168927`.

J. C. Butcher. *Numerical methods for ordinary differential equations*. John Wiley & Sons, 2008.

A. Campisano, C. Modica, and L. Vetrano. Calibration of Proportional Controllers for the RTC of Pressures to Reduce Leakage in Water Distribution Networks. (August):377–384, 2012. doi: 10.1061/(ASCE)WR.1943-5452.0000197.

M. Chandrashekar. Extended set of components in pipe networks. *Journal of the Hydraulics Devision, ASCE*, 106(HY1):133–152, 1980.

O. Chapelle, P. Haffner, and V. N. Vapnik. Support vector machines for histogram-based image classification. *IEEE transactions on Neural Networks*, 10(5):1055–1064, 1999. ISSN 1045-9227. doi: 10.1109/72.788646.

B. Charalambous and S. Kanellopoulou. Applied pressure management techniques to reduce control leakage. In *IWA Int. Specialized Conf. Leakage*, Sao Paolo, Brazil, 2010.

J. Choi. Flow control system design without flow meter sensor. *Sensors and Actuators A: Physical*, 185:127–131, oct 2012. ISSN 09244247. doi: 10.1016/j.sna.2012.07.010.

Cla-Val. Cla-val position controller, 2015. URL `http://www.cla-val.co.uk/products/Datasheets/138-01/Position%20control.pdf`.

Cla-Val. Cla-val 90-01 pressure reducing valve 3d animation, April 2016. URL `https://www.youtube.com/watch?v=XhOqm6T5CcE`.

M. Collins. Pitfalls in pipe network analysis techniques. *Transportation Engineering Journal, ASCE*, 106(TE5):507–521, 1980.

E. Creaco and M. Franchini. A new algorithm for real-time pressure control in water distribution networks. *Water Science & Technology: Water Supply*, 13(4):875, Aug. 2013.

ISSN 1606-9749. doi: 10.2166/ws.2013.074. URL http://www.iwaponline.com/ws/01304/ws013040875.htm.

R. Cuingnet, C. Rosso, M. Chupin, S. Lehéricy, D. Dormont, H. Benali, Y. Samson, and O. Colliot. Spatial regularization of SVM for the detection of diffusion alterations associated with stroke outcome. *Medical Image Analysis*, 15(5):729–737, 2011. ISSN 13618415. doi: 10.1016/j.media.2011.05.007. URL http://dx.doi.org/10.1016/j.media.2011.05.007.

J. a. Davis and M. Stewart. Predicting Globe Control Valve PerformanceâĂŤPart I: CFD Modeling. *Journal of Fluids Engineering*, 124(3):772, 2002. ISSN 00982202. doi: 10.1115/1.1490108.

J. Gessler. Analysis of Pipe Networks. In Yevjevich and Chaudhry;, editors, *Closed-Conduit Flow*, chapter 4. Water Resourses Publications, Colorado, USA, 1981.

B. Greyvenstein and J. van Zyl. An experimental investigation into the pressure - leakage relationship of some failed water pipes. *Journal of water supply: Research and Technology-AQUA*, 56(2):117–124, 2007. doi: 10.2166/aqua.2007.065.

S. Guo, T.-q. Zhang, W.-y. Shao, D. Z. Zhu, and Y.-y. Duan. Two-dimensional pipe leakage through a line crack in water distribution systems. *Journal of Zhejiang University SCIENCE A*, 14(5):371–376, 2013. ISSN 1673-565X. doi: 10.1631/jzus.A1200227.

J. Hardy, J. Hylton, T. McKnight, C. Remenyik, and F. Ruppel. *Flow Measurement Methods and Applications*. A Wiley-Interscience publication. Wiley, 1999. ISBN 9780471245094. URL https://books.google.co.th/books?id=kkP10wYCfpsC.

R. Heron and A. Burrows. Pilot valve for a pressure reducing valve, May 27 2010. URL http://www.google.com/patents/US20100126601. US Patent App. 12/532,566.

M. Herrera, A. Guglielmetti, M. Xiao, and R. Filomeno Coelho. Metamodel-assisted optimization based on multiple kernel regression for mixed variables. *Structural and Multidisciplinary Optimization*, 49(6):979–991, 2014. ISSN 16151488. doi: 10.1007/s00158-013-1029-z.

HWM. Si-clops intelligent control, 2011. URL http://www.hwm-water.com/products/palmer-environmental-products/pressure-control/si-clops-intelligent-control/.

R. Isermann. *Fault-Diagnosis Systems: An Introduction from Fault Detection to Fault Tolerance*. Springer-Verlag GmbH, 2011. ISBN 9783642108082. URL https://books.google.co.th/books?id=5dxFQgAACAAJ.

T. S. Jaakkola and D. Haussler. Exploiting generative models discriminative classifiers. In *Advances in neural information processing systems*, pages 487–493, 1999.

R. Jeppson. *Analysis of Flow in Pipe Networks*. Ann Arbor Science, 1976.

R. Jeppson and A. Davis. Pressure reducing valves in pipe network analyses. *Journal of the Hydraulics Division*, 1976.

T. Joachims. Text categorization with support vector machines: Learning with many relevant features. In *European conference on machine learning*, pages 137–142. Springer, 1998. ISBN 3540644172.

L. Khezzar, S. Harous, and M. Benayoune. Modeling of pressure reducing valves revisited. In *WRPMD'99: Preparing for the 21st Century*. ACSE, 1999.

L. Khezzar, S. Harous, and M. Benayoune. Steady-State Analysis of Water Distribution Networks Including Pressure-Reducing Valves. *Computer-Aided Civil and Infrastructure Engineering*, 16(4):259–267, July 2001. ISSN 1093-9687. doi: 10.1111/0885-9507.00231. URL http://doi.wiley.com/10.1111/0885-9507.00231.

A. Lambert. What do we know about pressure: leakage relationships in distribution systems? In *Iwa Conference 'System Approach To Leakage Control and Water Distribution Systems Management'*, pages 1–9, Brno, Czech Republic, 2000. ISBN 8072041975.

A. Lambert and M. Fantozzi. Recent Developments in the Pressure. In *Proceedings of the IWA International Specialised Conference Water Loss 2010*, volume 25, pages 7–20, 2009.

A. Lambert and J. Thornton. Pressure : Bursts Relationships : Influence of Pipe Materials , Validation of Scheme Results , and Implications of Extended Asset Life. In *IWA Int. Specialized Conf. Water Loss 2012*, Hague, the Netherlands, 2012.

T. Leephakpreeda. Flow-sensorless control valve: Neural computing approach. *Flow Measurement and Instrumentation*, 14(6):261–266, 2003. ISSN 09555986. doi: 10.1016/S0955-5986(03)00029-3.

P. Li, L. Postlethccwaite, E. Prempain, and B. Ulanicki. Delivery of 30 Ml/d Leakage Reduction Through Intelligent Pressure Control. In *10th In. Conf. on Computing and Control for the Water Industry. Integrated Water Systems, Boxall J. and Maksimovic, C.*, 2010.

Mathworks. Equation Solving Algorithms. `https://uk.mathworks.com/help/optim/ug/equation-solving-algorithms.html`, 2018. [Online; accessed 10-August-2018].

G. Moser and S. B. Serpico. Combining support vector machines and Markov random fields in an integrated framework for contextual image classification. *IEEE Transactions on Geoscience and Remote Sensing*, 51(5):2734–2752, 2013. ISSN 01962892. doi: 10.1109/TGRS.2012.2211882.

M. Nicolini and L. Zovatto. Optimal Location and Control of Pressure Reducing Valves in Water Networks. (June):178–187, 2009.

P. Papalambros and D. Wilde. *Principles of Optimal Design: Modeling and Computation*. Cambridge University Press, 2000. ISBN 9781316101865.

O. Piller and B. Bremond. Modeling of Pressure Regulating Devices: A Problem Now Solved. In *Bridging the Gap, ACSE*, number 1, pages 1–10, Reston, VA, May 2001. American Society of Civil Engineers.

O. Piller and J. van Zyl. Modeling Control Valves in Water Distribution Systems Using a Continuous State Formulation. *Journal of Hydraulic Engineering*, pages 1–9, 2014.

M. Pontil and A. Verri. Support Vector Machines for 3D Object Recognition. *IEEE transactions on pattern analysis and machine intelligence*, 20(6), 1998.

S. Prescott and B. Ulanicki. Modelling the dynamic behaviour of pressure reducing valves. In *Proc. Int. Conf. Computing and Control for Water Industry*. Research Studies Press Ltd., 2001.

S. Prescott and B. Ulanicki. Dynamic modeling of pressure reducing valves. *Journal of Hydraulic Engineering*, 129(10):804–812, 2003.

S. Prescott, B. Ulanicki, and N. Shipley. Analysis of district metered area (dma) performance. In *Advances in Water Supply Management: Proceedings of the CCWI '03 Conference, London, 15-17 September 2003*, London, UK, 2003. A.A. Balkema Publishers. ISBN 90-5809-608-4.

J.-y. Qian, L. Wei, Z.-j. Jin, J.-k. Wang, H. Zhang, and A.-l. Lu. CFD analysis on the dynamic flow characteristics of the pilot-control globe valve. *Energy Conversion and Management*, 87:220–226, 2014. ISSN 01968904. doi: 10.1016/j.enconman.2014.07.018. URL `http://linkinghub.elsevier.com/retrieve/pii/S0196890414006499`.

B. Ratcliffe. *The Performance and Selection of Pressure Reducing Valves: The PRV performance atlas*. Number pt. 2 in Engineering TR. Water Research Centre, 1986. ISBN 9780902156425. URL `https://books.google.co.th/books?id=MyHzugAACAAJ`.

L. Rossman. *Epanet 2 Users Manual*. Water Supply and Water Resources Division, National Risk Management Research Laboratory, Cininnati, OH, USA, 1st edition, 2000.

G. Sanz, R. Perez, and R. Sánchez. Pressure control of a large scale water network using integral action. In *IFAC Conference on Advances in PID Control*, 2012. doi: 10-3182/20120328-3-IT-3014.00046. URL `http://www.recercat.net/handle/2072/185833`.

A. Shirzad, M. Tabesh, and R. Farmani. A comparison between performance of support vector regression and artificial neural network in prediction of pipe burst rate in water distribution networks. *KSCE Journal of Civil Engineering*, 18:941–948, 2014. ISSN 1226-7988. doi: 10.1007/s12205-014-0537-8. URL `http://link.springer.com/10.1007/s12205-014-0537-8`.

A. R. Simpson. Modeling of pressure regulating devices: The last major problem to be solved in hydraulic simulation. In *WRPMD'99: Preparing for the 21st Century*. ACSE, 1999.

A. Sotoudeh. Pressure control apparatus and method, Feb. 2 2000. URL `https://www.google.co.uk/patents/EP0977102A2?cl=en`. EP Patent App. EP19,990,306,097.

I. Stoianov and A. Hoskins. Monitoring fluid dynamics, 2015. Patent Application GB1517901.3.

J. Thornton. Managing Leakage by Managing Pressure: A Practical Approach. *Water 21*, October 20:1–2, 2003. ISSN 15619508.

J. Thornton and A. Lambert. Progress in practical prediction of pressure: leakage, pressure: burst frequency and pressure: consumption relationships. In *IWA Special Conference 'Leakage'*, pages 1–10, 2005. URL `http://www.leakssuite.com/ResearchPapers/2005_ThorntonLambertIWAHalifax.pdf`.

E. Todini and S. Pilati. A gradient algorithm for the analysis of pipe networks. *Computer Applications in Water Supply*, 1—system:1–20, 1988.

S. Tong and E. Chang. Support Vector Machine Active Learning for Image Retrieval. In *Proceedings of the ninth ACM international conference on Multimedia*, pages 107–118. ACM, 2001.

B. Ulanicki, P. Bound, J. Rance, and L. Reynolds. Open and closed loop pressure control for leakage reduction. *Urban Water*, 2(2):105–114, June 2000. ISSN 14620758. doi: 10.1016/S1462-0758(00)00048-0.

B. Ulanicki, H. S. AbdelMeguid, P. Bounds, and R. Patel. Pressure control in district metering areas with boundary and internal pressure reducing valves. In *10th Int. Water Distribution System Analysis Conf*, pages 691–703, Kruger National Park, South Africa, 2008. ASCE. ISBN 978-0-7844-1024-0. doi: 10.1061/41024(340)58. URL `http://hdl.handle.net/2086/4370`.

J. van Zyl and C. Clayton. The effect of pressure on leakage in water distribution systems. (June):109–114, 2007. doi: 10.1680/wama.2007.160.2.109. URL `http://dx.doi.org/10.1680/wama.2007.160.2.109`.

V. Venkatasubramanian. A review of process fault detection and diagnosis part i: Quantitative model-based methods. *Computers & Chemical Engineering*, 27:293 – 311, 01 2003.

V. Venkatasubramanian, R. Rengaswamy, and S. N Kavuri. A review of process fault detection and diagnosis part ii: Qualitative models and search strategies. *Computers & Chemical Engineering*, 27:313–326, 03 2003a.

V. Venkatasubramanian, R. Rengaswamy, S. N. Kavuri, and K. Yin. A review of process fault detection and diagnosis part iii: Process history based methods. *Computers & Chemical Engineering*, 27:327–346, 03 2003b.

D. J. Vicente, L. Garrote, R. Sánchez, and D. Santillán. Pressure Management in Water Distribution Systems : Current Status , Proposals , and Future Trends. *Journal of Water Resources Planning and Management*, 142(2):1–13, 2016. ISSN 0733-9496. doi: 10.1061/(ASCE)WR.1943-5452.0000589.

J. Watton. *Modelling, Monitoring and Diagnostic Techniques for Fluid Power Systems*. Springer-Verlag London, 2007.

R. Wright, I. Stoianov, P. Parpas, K. Henderson, and J. King. Adaptive water distribution networks with dynamically reconfigurable topology. *Journal of Hydroinformatics*, pages 1280–1301, 2014.

R. Wright, E. Abraham, P. Parpas, and I. Stoianov. Control of water distribution networks with dynamic DMA topology using strictly feasible sequential convex programming. *Water Resources Research*, 51(12):9925–9941, 2015. ISSN 19447973. doi: 10.1002/2015WR017466.

G. Wyeth and R. Chalk. Delivery of 30 Ml/d Leakage Reduction Through Intelligent Pressure Control. In *IWA Int. Specialized Conf. Water Loss*, Manila, Philippines, 2012.

Q. Yang, Z. Zhang, M. Liu, and J. Hu. Numerical simulation of fluid flow inside the valve. *Procedia Engineering*, 23:543–550, 2011. ISSN 18777058. doi: 10.1016/j.proeng.2011.11.2545.

C. Yonnet. Water distribution pressure control method and apparatus, Aug. 17 2004. URL `https://www.google.co.uk/patents/US6776180`. US Patent 6,776,180.

M. Zarghamee. Mathematical model for water distribution systems. *Journal of the Hydraulics Division, ASCE*, 97(HY1):1–14, 1971.

Appendix A

Parametric force balance equation sensitivity analysis

The accuracy of flow estimation depends significantly on accuracy of the valve stem position estimate. The estimation function (Equation 5.10) is another form of the parametric force balance equation (Equation 5.7), which receives pressure measurements as inputs. Since pressure measurements contain an accuracy limitation and fluctuation of signals, a sensitivity of the valve stem position with respect to pressure variables is important to assess an accuracy of the stem position estimate.

The analysis investigates a change of x_m with respect to one pressure variable at a time. The analysis is performed on an analytical formulation of a parametric force balance relationship obtained from regression of the valve at Imperial Laboratory (Infrasense Labs) which is DN100 GE. The model is fourth order polynomial function of x_m. A local method is employed to calculate the sensitivity index defined by:

$$\phi_{x_m,h_{i\neq j}} = \frac{\delta x_m}{x_m} \Big/ \frac{\delta h_i}{h_i} \mid_{h_j=const} \tag{A.1}$$

where h_i and h_j can be h_{in}, h_c or h_{out}. The sensitivity index, ϕ_{x_m,h_i}, illustrates how an uncertainty of the stem position estimate, x_m, is apportioned into an uncertainty from a pressure

measurement, h_i. **The magnitude of the sensitivity index shows how much an uncertainty of the estimate is amplified on one variable with respect to another variable**. In this variable space of $\mathbf{X}(x_m, h_{in}, h_c, h_{out})$, by rearranging the force balance equation (Equation 5.7), any pressure can be written as a function of other pressures and the position, i.e. $h_{in}(x_m, h_c, h_{out})$ etc. Therefore, knowing two pressures and position always confines another pressure. Given there are three pressure measurement variables, the sensitivity index of position with respect to the first pressure **(respective pressure)** is calculated, where the second pressure is fixed **(fixed pressure)** and the third pressure is varied **(varied pressure)**. Results of all sensitivity indices for the Infrasense Labs valve (DN100 GE) are shown in Figure A.1, which presents the sensitivity index of stem position with respect to one pressure measurement at a time. The sensitivity index is visualised through contour plots of which axes are the stem position and the varied pressure. Colors indicate 3 levels of sensitivity which are less than 10, between 10 to 20 and more than 20. The stem position is limited to its recommended operational range of 75% (the range is shown from 0-22 mmwhich is 74%). There are 6 subplots which show

(a). A sensitivity of x_m with respect to h_c (Φ_{x_m,h_c}). h_{in} is varied from 30 to 50 mH_2O and h_{out} is fixed at 15 mH_2O.

(b). A sensitivity of x_m with respect to h_c (Φ_{x_m,h_c}). h_{out} is varied from 10 to 20 mH_2O and h_{in} is fixed at 40 mH_2O.

(c). A sensitivity of x_m with respect to h_{out} ($\Phi_{x_m,h_{out}}$). h_c is varied from 20 to 32 mH_2O and h_{in} is fixed at 40 mH_2O.

(d). A sensitivity of x_m with respect to h_{out} ($\Phi_{x_m,h_{out}}$). h_{in} is varied from 30 to 50 mH_2O and h_c is fixed at 25 mH_2O.

(e). A sensitivity of x_m with respect to h_{in} ($\Phi_{x_m,h_{in}}$). h_c is varied from 20 to 40 mH_2O and h_{out} is fixed at 15 mH_2O.

(f). A sensitivity of x_m with respect to h_{in} ($\Phi_{x_m,h_{in}}$). h_{out} is varied from 10 to 20 mH_2O and h_c is fixed at 25 mH_2O.

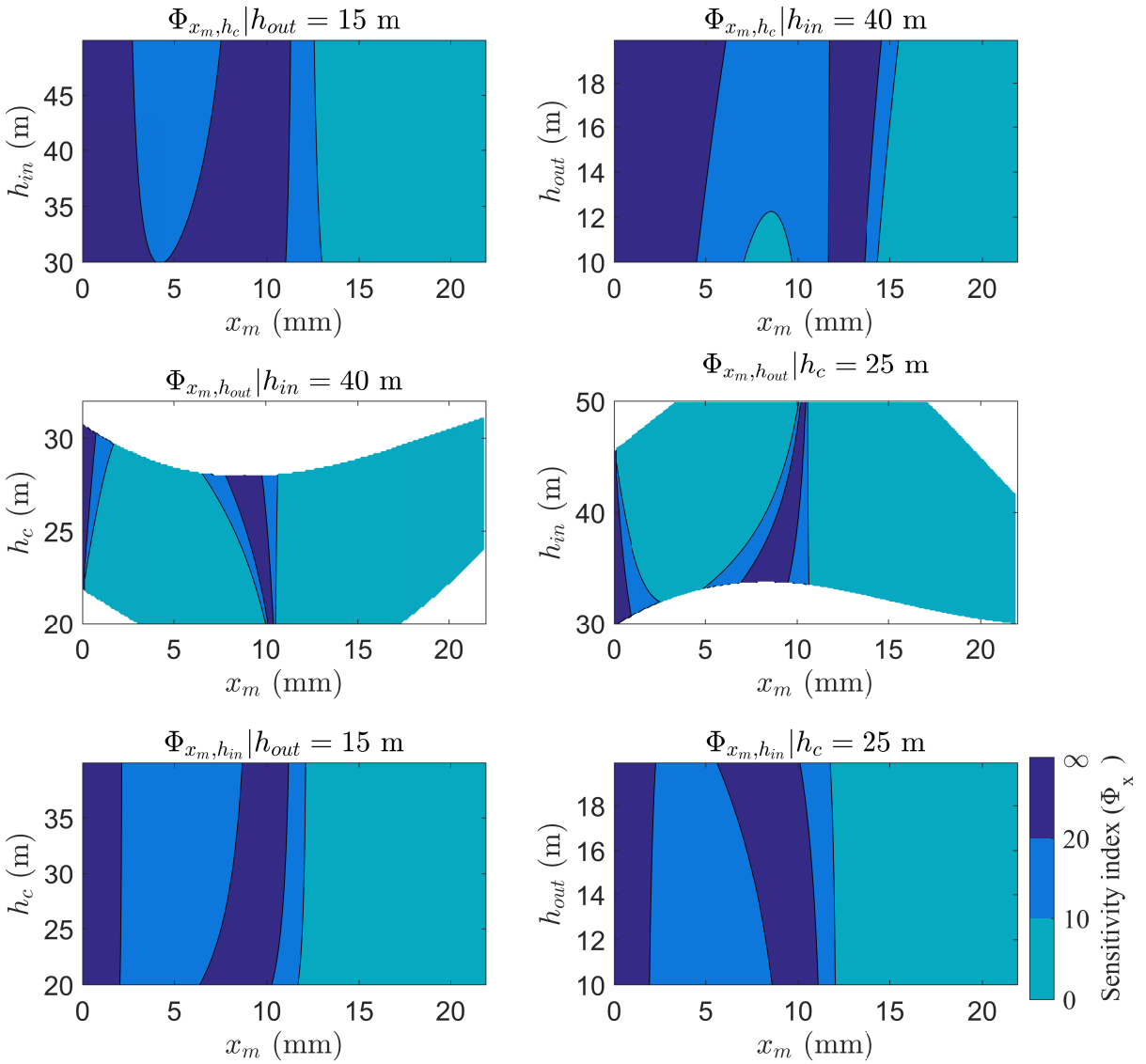

Figure A.1: Sensitivity index of the valve stem position with respect to the change of pressures

The sensitivity analysis result shows that the valve stem position is "generally sensitive to all pressure measurements". The sensitivity index is less than 10 at any valve stem position higher than 15 mm. This index plota indicate an accuracy limitation of the position estimation. Index of higher than 1 magnifies uncertainty from pressure measurement to the position estimate. The uncertainty of pressure measurement does not necessarily come from instruments, it can also come from its fluctuation. High sensitivity regions are generally found at a low position (i.e. small orifice area) and around a position of 8-9 mm for this particular valve. The high

sensitivity at low position comes from the fact that the absolute value of the valve stem position is low. The high sensitivity at 8-9 mm comes from the shape of the estimation function as the estimation function is a polynomial which has a turning point at around 8-9 mm.

Appendix B

The “Field Lab” flow estimation through second order models

The “Field Lab" model is trained on site instead of in laboratory and therefore pressure combination is limited. Since the model is highly non-linear, fitting high order model with a small range of pressure could take a risk of overfitting. Hence, the validation in chapter 6 is repeated here with 2nd order parametric force balance equation. Errors for the 3P flow estimation through 2nd order model and 4th order models are summarised in Table B.1 , while the full validation results are shown in sections afterward.

The estimation results show that in most cases, the 2nd order model and the 4th order model

Table B.1: A comparison between the 3P flow estimation using 4th order force balance equation and 2nd order force balance equation; RMSE and MAPE are shown in l/s and percent (%)

	RMSE (l/s)		MAPE (%)	
	4th order	2nd order	4th order	2nd order
SKL#1	0.70	0.49	9.47	5.11
SKL#2	1.54	1.60	9.17	8.97
SKL#3	0.56	0.45	4.98	4.10
WLW#1	3.62	3.12	17.41	15.17
WLW#2	3.67	2.06	16.64	8.80
WLW#3	13.63	6.25	53.39	21.98
LCW#1	0.73	0.66	9.07	8.77
LCW#2	0.22	0.24	7.51	11.08
LCW#3	0.57	0.56	7.15	9.40

achieve similar level of accuracy. Especially, the estimation accuracies on SKL valve and LCW valve are indifferent. However, for the case WLW#2 and WLW#3, the 2nd order model achieve much lower errors. It is suspected that is because the pressure variability of WLW is low and therefore, it is slightly overfitted to train the 4th order model. It can be concluded here that the selection of model order should depends on the availability of training data range. If the data sets spread widely, it is safe to train the model with high order polynomial degrees. On the other hand, if the data range is limited, trying a model with lower order is recommended.

B.1 SKL valve

Flow estimation at Stoke Lane is shown in Figure B.1, Figure B.2 and Figure B.3.

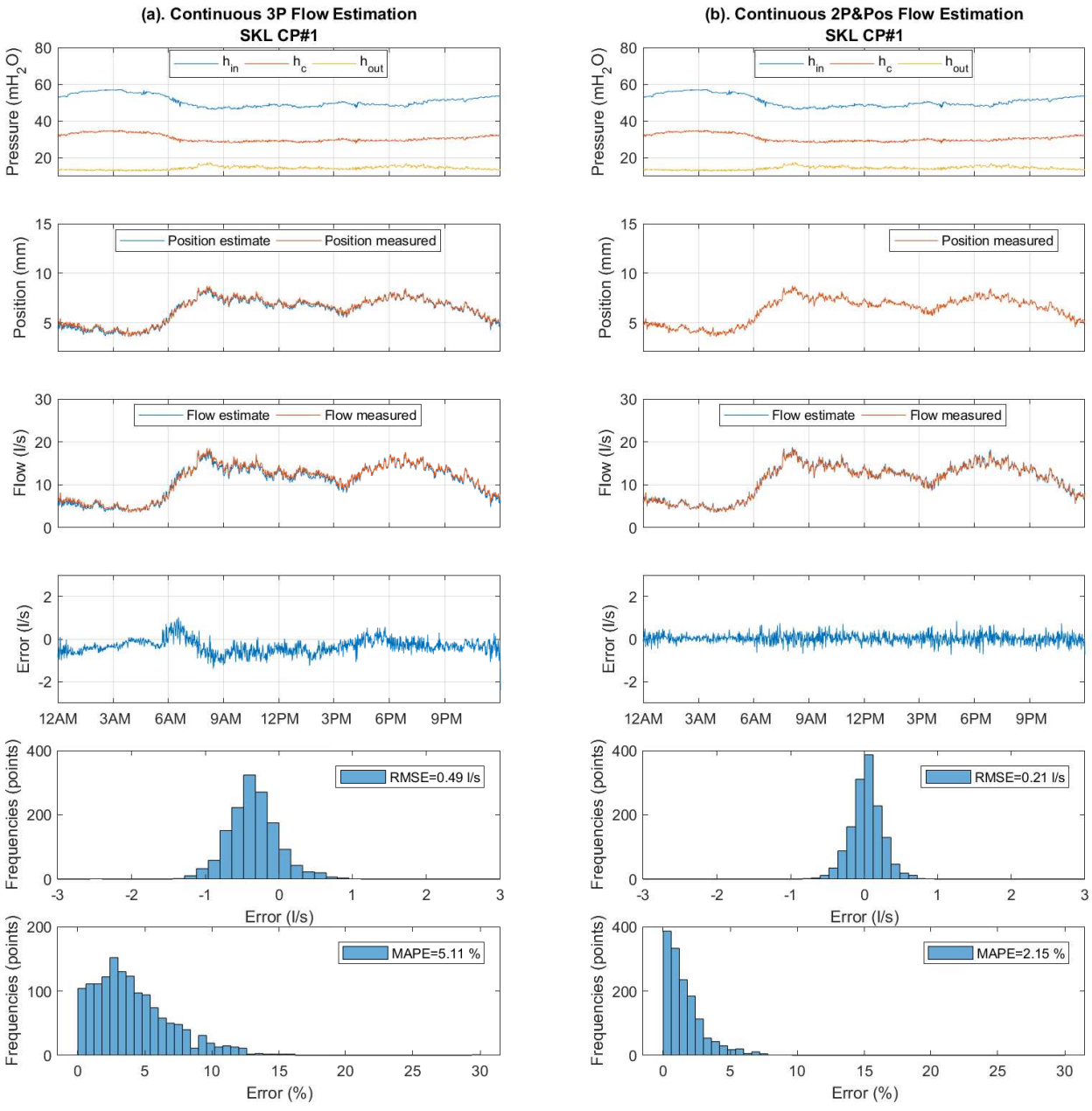

(a) 3P flow estimation validation results

(b) 2P&Pos flow estimation validation results

Figure B.1: Flow estimation validation at the "Field Lab", SKL #1

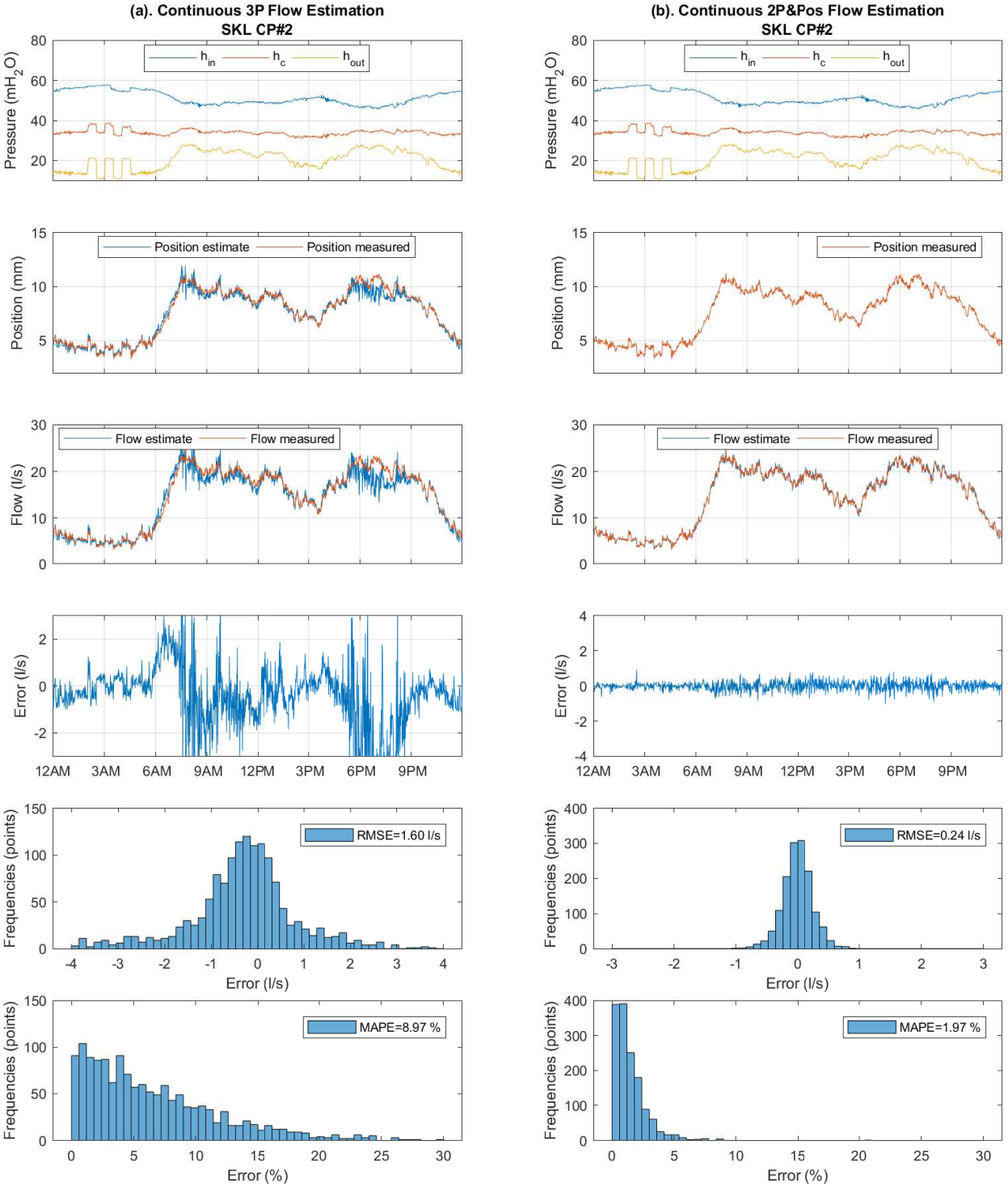

(a) 3P flow estimation validation results

(b) 2P&Pos flow estimation validation results

Figure B.2: Flow estimation validation at the “Field Lab", SKL #2

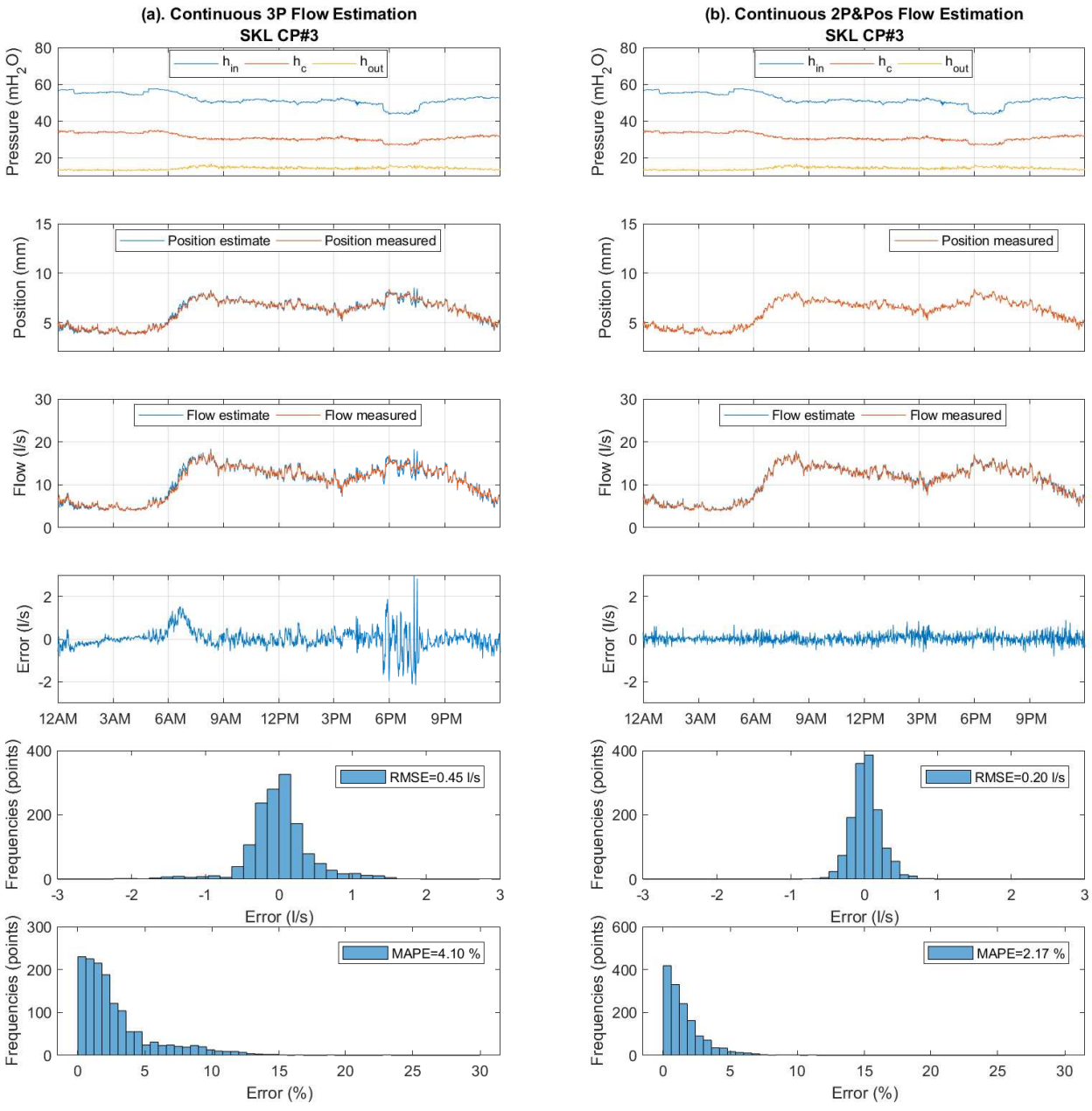

(a) 3P flow estimation validation results

(b) 2P&Pos flow estimation validation results

Figure B.3: Flow estimation validation at the "Field Lab", SKL #3

B.2 WLW valve

Flow estimation at Woodland Way is shown in Figure B.4, Figure B.5 and Figure B.6.

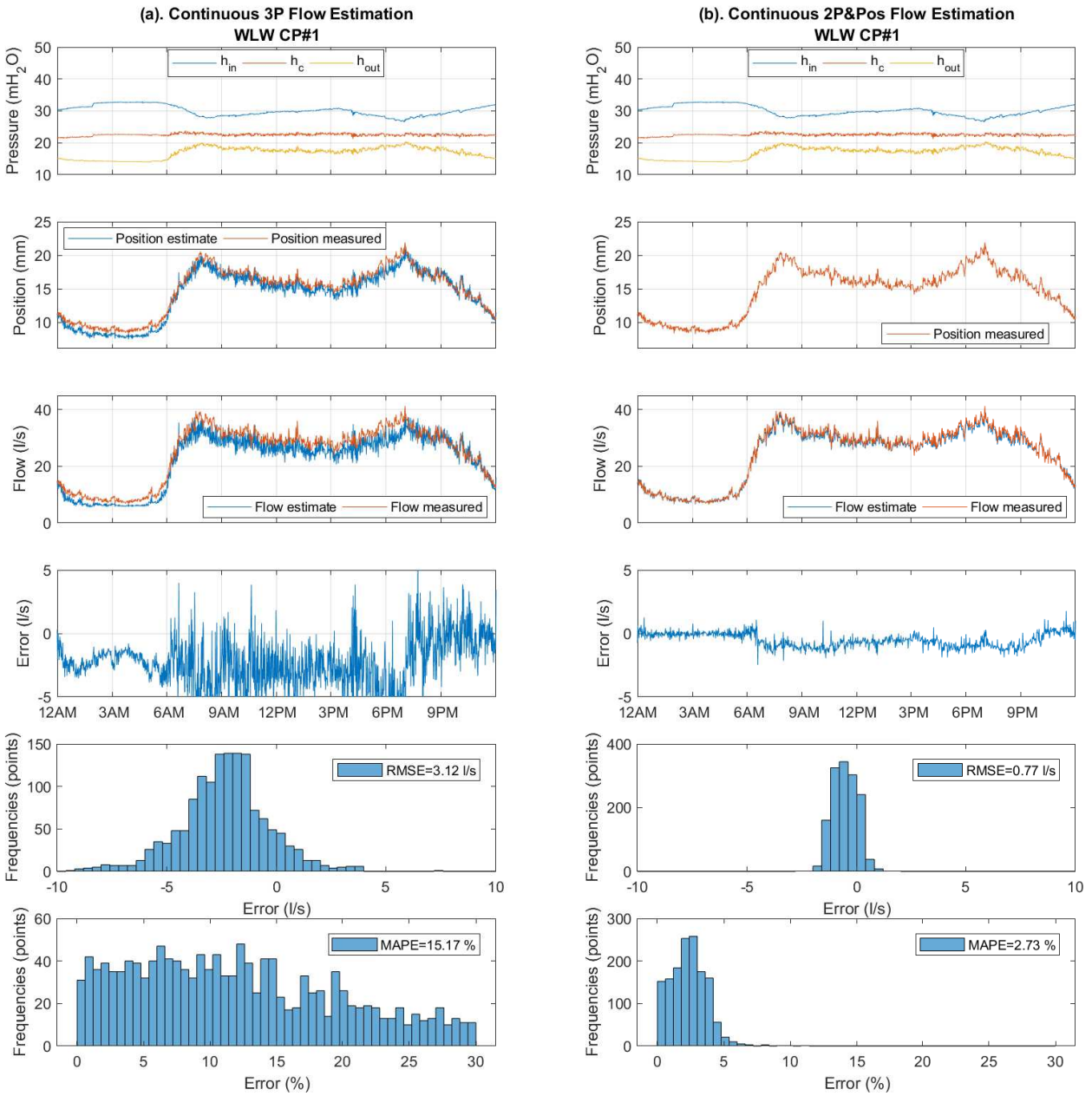

(a) 3P flow estimation validation results

(b) 2P&Pos flow estimation validation results

Figure B.4: Flow estimation validation at the “Field Lab", WLW #1

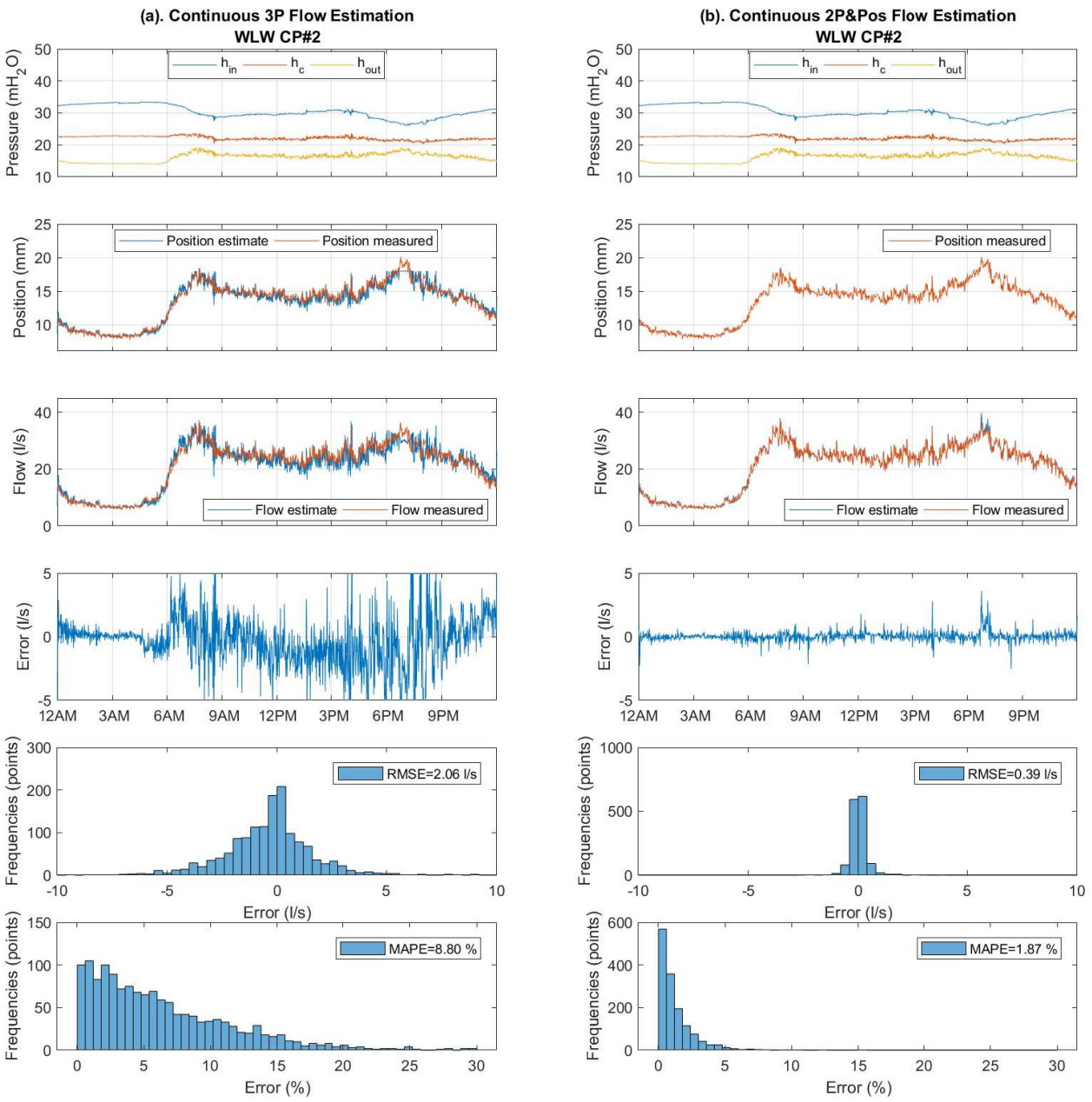

(a) 3P flow estimation validation results

(b) 2P&Pos flow estimation validation results

Figure B.5: Flow estimation validation at the "Field Lab", WLW #2

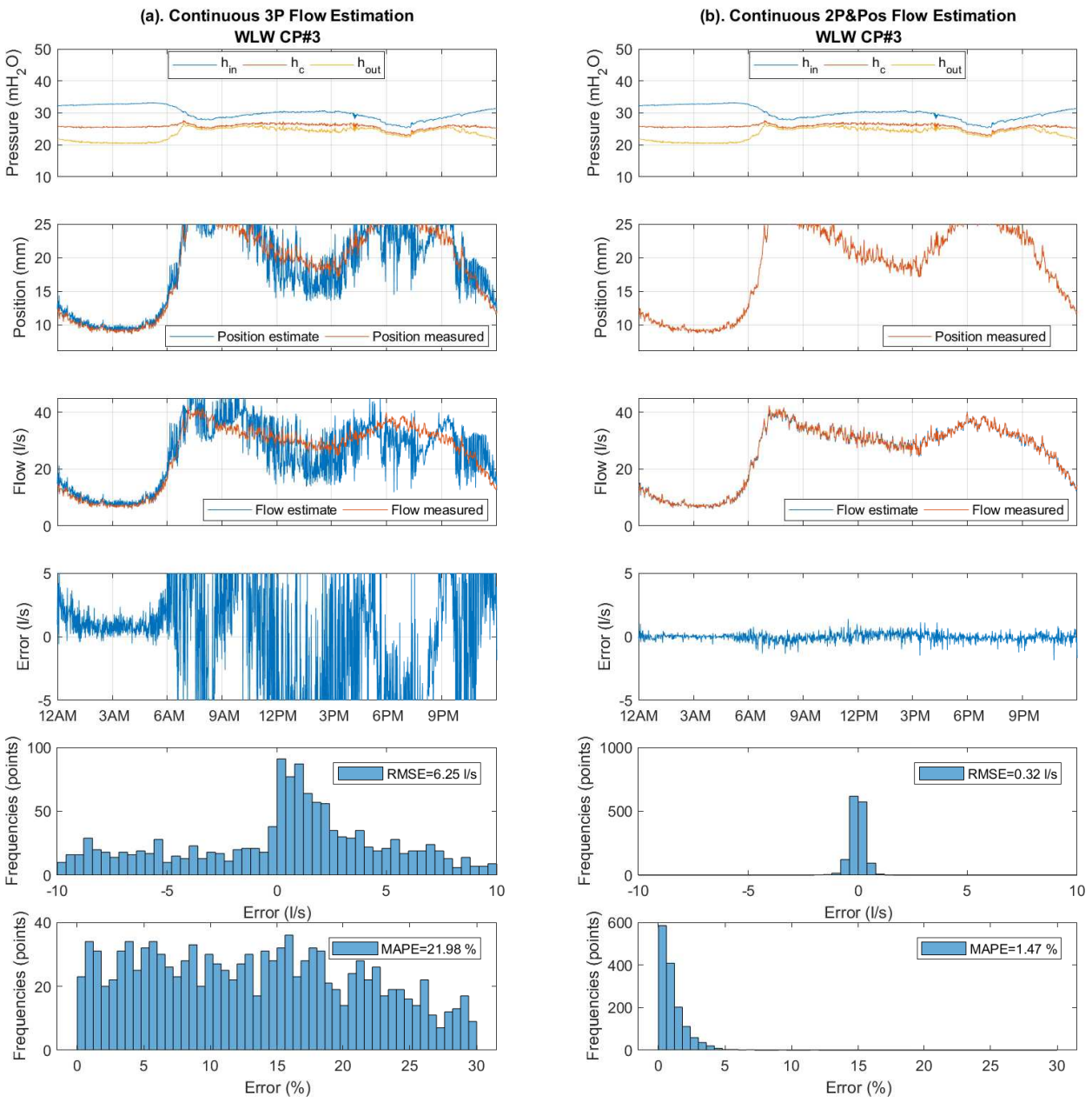

(a) 3P flow estimation validation results

(b) 2P&Pos flow estimation validation results

Figure B.6: Flow estimation validation at the “Field Lab", WLW #3

B.3 LCW valve

Flow estimation at Lodge Causeway is shown in Figure B.7, Figure B.8 and Figure B.9.

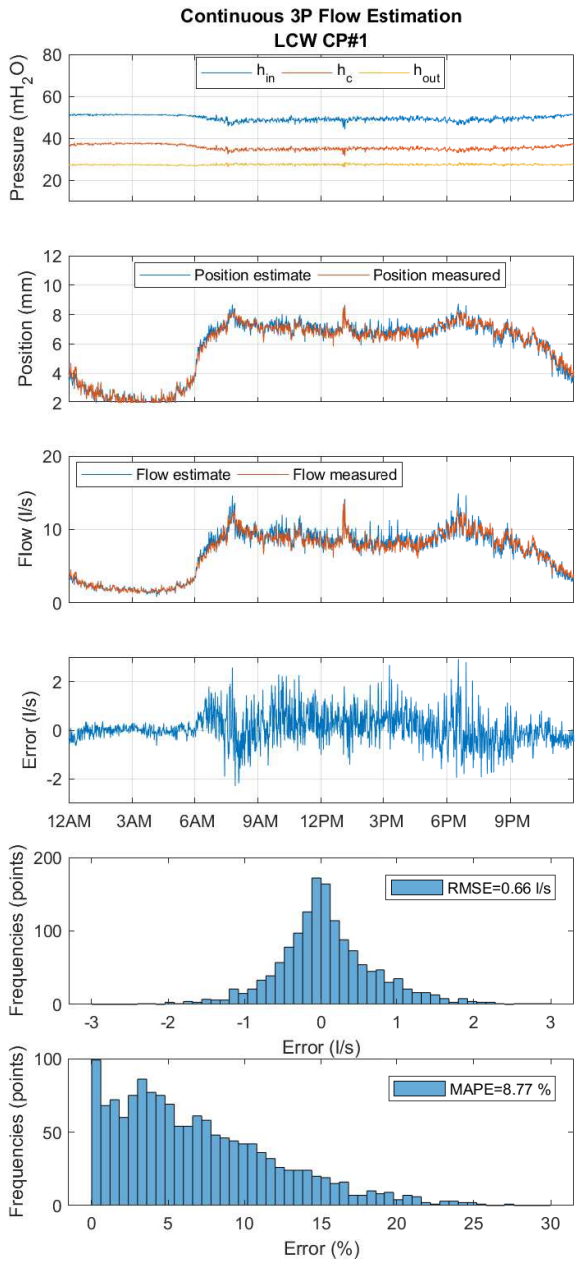

Figure B.7: Flow estimation validation at the "Field Lab", LCW#1

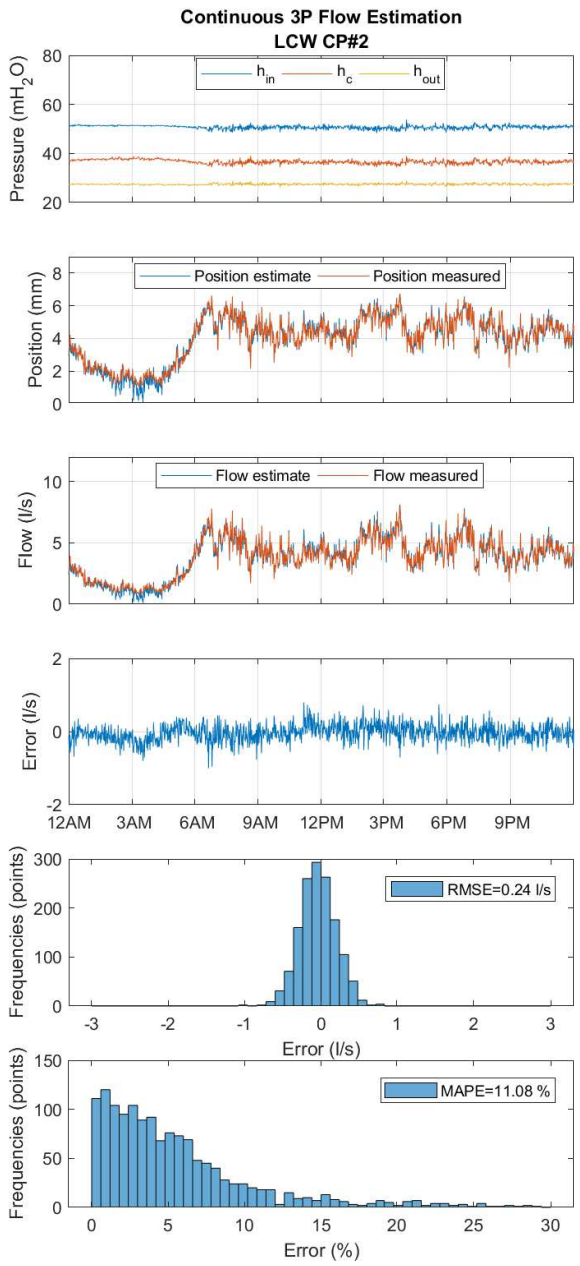

Figure B.8: Flow estimation validation at the “Field Lab", LCW#2

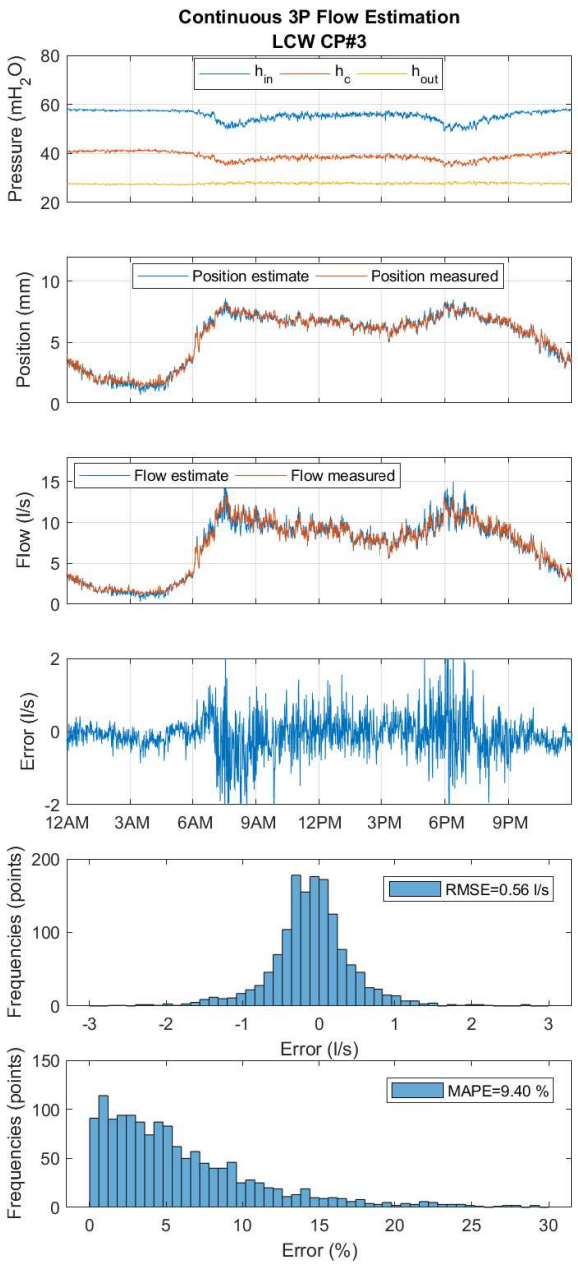

Figure B.9: Flow estimation validation at the "Field Lab", LCW#3